PNL-3700 PT3
UC-11

Pacific Northwest Laboratory Annual Report for 1980 to the DOE Assistant Secretary for Environment

Part 3 Atmospheric Sciences February 1981

Prepared for the U.S. Department of Energy
under Contract DE-AC06-76RLO 1830

Pacific Northwest Laboratory
Operated for the U.S. Department of Energy
by Battelle Memorial Institute

Battelle

PACIFIC NORTHWEST LABORATORY
operated by
BATTELLE
for the
UNITED STATES DEPARTMENT OF ENERGY
Under Contract DE-AC06-76RLO 1830

Printed in the United States of America
Available from
National Technical Information Service
United States Department of Commerce
5285 Port Royal Road
Springfield, Virginia 22151

Price: Printed Copy $_____*; Microfiche $3.00

*Pages	NTIS Selling Price
001-025	$4.00
026-050	$4.50
051-075	$5.25
076-100	$6.00
101-125	$6.50
126-150	$7.25
151-175	$8.00
176-200	$9.00
201-225	$9.25
226-250	$9.50
251-275	$10.75
276-300	$11.00

PNL-3700 PT3
UC-11

Pacific Northwest Laboratory Annual Report for 1980 to the DOE Assistant Secretary for Environment

Part 3 Atmospheric Sciences

C. E. Elderkin and Staff Members
of Pacific Northwest Laboratory

February 1981

Prepared for
the U.S. Department of Energy
under Contract DE-AC06-76RLO 1830

Pacific Northwest Laboratory
Richland, Washington 99352

PREFACE

Pacific Northwest Laboratory's (PNL) 1980 Annual Report to the Department of Energy (DOE) Assistant Secretary for Environment describes research in environment, health, and safety conducted during fiscal year 1980. The report again consists of five parts, each in a separate volume.

The five parts of the report are oriented to particular segments of our program. Parts 1 to 4 report on research performed for the DOE Office of Health and Environmental Research. Part 5 reports progress on all other research performed for the Assistant Secretary for Environment, including the Office of Environmental Assessment and the Office of Environmental Compliance and Overview. Each part consists of project reports authored by scientists from several PNL research departments, reflecting the interdisciplinary nature of the research effort. Parts 1 to 4 are organized primarily by energy technology.

The parts of the 1980 Annual Report are:

Part 1:	Biomedical Sciences Program Manager - H. Drucker	D. L. Felton, Editor
Part 2:	Ecological Sciences Program Manager - B. E. Vaughan	B. E. Vaughan, Report Coordinator C. M. Novich, Editor
Part 3:	Atmospheric Sciences Program Manager - C. E. Elderkin	R. L. Drake, Report Coordinator M. F. Johnson, Editor
Part 4:	Physical Sciences Program Manager - J. M. Nielsen	J. M. Nielsen, Report Coordinator I. D. Hays, J. L. Baer, Editors
Part 5:	Environmental Assessment, Control, Health and Safety Program Managers - D. L. Hessel S. Marks W. A .Glass	W. J. Bair, Report Coordinator R. W. Baalman, I. D. Hays, Editors

Activities of the scientists whose work is described in this annual report are broader in scope than the articles indicate. PNL staff have responded to numerous requests from DOE during the year for planning, for service on various task groups, and for special assistance.

Credit for this annual report goes to many scientists who performed the research and wrote the individual project reports, to the program managers who directed the research and coordinated the technical progress reports, to the editors who edited the individual project reports and assembled the five parts, and to Ray Baalman and Irene D. Hays, editors in chief, who directed the total effort.

W. J. Bair, Manager
S. Marks, Associate Manager
Environment, Health, and Safety Research Program

Previous Reports in this series:

Annual Report for

1951	W-25021, HW-25709
1952	HW-27814, HW-28636
1953	HW-30437, HW-30464
1954	HW-30306, HW-33128, HW-35905, HW-35917
1955	HW-39558, HW-41315, HW-41500
1956	HW-47500
1957	HW-53500
1958	HW-59500
1959	HW-63824, HW-65500
1960	HW-69500, HW-70050
1961	HW-72500, HW-73337
1962	HW-76000, HW-77609
1963	HW-80500, HW-81746
1964	BNWL-122
1965	BNWL-280, BNWL-235, Vol. 1-4, BNWL-361
1966	BNWL-480, Vol. 1, BNWL-481, Vol. 2, Pt. 1-4
1967	BNWL-714, Vol. 1, BNWL-715, Vol. 2, Pt. 1-4
1968	BNWL-1050, Vol. 1, Pt. 1-2, VNWL-1051, Vol. 2, Pt. 1-3
1969	BNWL-1306, Vol. 1, Pt. 1-2, BNWL-1307, Vol. 2, Pt. 1-3
1970	BNWL-1550, Vol. 1, Pt. 1-2, BNWL-1551, Vol. 2, Pt. 1-2
1971	BNWL-1650, Vol. 1, Pt. 1-2, BNWL-1651, Vol. 2, Pt. 1-2
1972	BNWL-1750, Vol. 1, Pt. 1-2, BNWL-1751, Vol. 2, Pt. 1-2
1973	BNWL-1850, Pt. 1-4
1974	BNWL-1950, Pt. 1-4
1975	BNWL-2000, Pt. 1-4
1976	BNWL-2100, Pt. 1-5
1977	PNL-2500, Pt. 1-5
1978	PNL-2850, Pt. 1-5
1979	PNL-3300, Pt. 1-5

FOREWORD

The goals of atmospheric research at Pacific Northwest Laboratory (PNL) are to assess, describe and predict the nature and fate of atmospheric pollution and to study the impacts of pollutants on local, regional and global climates. The pollutants being investigated are those resulting from the development and use of four energy resources: coal, gas, oil and nuclear power. In the course of this research, investigative tools are also being developed and atmospheric assessments are being made that will contribute to the development of environmentally acceptable oil shale, solar and fusion energy resources.

Coal, Gas and Oil Combustion

The behavior of air pollution resulting from fossil-fuel power plants is being examined. Involved in making this examination are these factors: the type of pollutants emitted, their transport and diffusion in the air, their physical and chemical transformations during transport, their removal by wet and dry deposition processes, and their impacts on climate, bodies of water and living species. Since a result of the current and projected coal and oil utilization is the release of large quantities of particulate matter and sulfur and nitrogen compounds, current research is being conducted primarily in the Atmospheric Studies in Complex Terrain (ASCOT), DOE's Carbon Dioxide Program, and a Long Range Transport Modeling Study.

Fission and Fusion

Concern about long-lived particulates (i.e., plutonium and other radionuclides) released to the environment from fission and fusion plants indicates that the deposition and resuspension of these substances must be studied. For example, because the primary hazard from plutonium is inhalation, its residence in the atmosphere must be clearly defined. Current research is evaluating the removal of particulates from the atmosphere by deposition (which limits initial exposure) and any future resuspension from the surface (which continues the potential for inhalation).

Oil Shale

The mountainous oil shale regions of Colorado, Utah and Wyoming present a particularly difficult air pollution problem because air may be trapped in the valleys of these regions for extended periods of time under certain meteorological conditions. Therefore, especially stringent siting requirements must be fulfilled to meet state and federal air quality standards. Adequate models and field measurements of the complex airflow and dispersion conditions in this complex area are not available; they must be developed to assure acceptable siting of oil shale facilities. PNL has undertaken the assessment of the requirements for proper modeling activities and field measurement programs that will contribute to this important area of research, and to the development of solar and geothermal energy.

The description of atmospheric research at PNL is organized in terms of energy technologies:

- Coal, Gas and Oil
- Fission and Fusion
- Oil Shale

This report describes the progress in FY 1980 for each of these technologies. A divider page summarizes the goals of each area and lists, as bulleted items, project titles that fund research in each technology.

R. L. Drake
Program Coordinator

CONTENTS

1 Coal, Gas and Oil

COAL, GAS AND OIL

- **Atmospheric Diffusion in Complex Terrain**
- **Atmospheric Boundary Layer Studies**
- **Radiative Effects of Clouds and Aerosols**
- **Pollutant Transformation in the Atmosphere**
- **Atmospheric Carbon Dioxide - An Archival Study of Spectroscopic Data**
- **Meteorological Effects of Thermal Energy Releases (METER)**
- **Long Range Transport Modeling**
- **Theoretical Studies and Applications**

As the use of fossil fuels as an energy source increases, so too will air pollutants, such as sulfur, nitrogen compounds and trace metals, produced by the combustion and conversion of these fuels. The analysis of the fate of these pollutants from source to receptor is most urgent so that the nation's energy plan can proceed efficiently and be environmentally sound.

The research activities at PNL are basically related to four interlaboratory programs: the ASCOT, METER, Carbon Dioxide, and Long Range Transport Modeling Programs. The ASCOT Program is currently concerned with the Geysers Geothermal Site in California, but future studies will be centered at other complex terrain sites in the west. The METER Program is studying the effects of cooling towers on local climate, while the Carbon Dioxide Program concentrates on the effects of fossil fuel burning on global climate. The Long Range Transport Modeling Program is concerned with the assessment of the air quality impacts of different energy scenarios on the regional and national scales.

The field activities in the ASCOT Program include the micrometeorological description of drainage winds, radiation measurements, and tracer experiments. Field activities in the METER Program include air chemistry, meteorological and scavenging measurements in and around cooling tower and pollutant plumes from a very large coal-fired power plant.

• Atmospheric Diffusion in Complex Terrain

Objectives of this study are:

- Defining and developing a long-range technical plan for studying the transport and diffusion of pollutant particles and gases over complex landforms.
- Reviewing past theoretical, numerical and field studies pertinent to diffusion in complex terrain.
- Assisting a multilaboratory program studying diffusion in complex terrain by providing methodologies and techniques of analyses for transport and diffusion over a variety of complex landforms.

Project ASCOT--Pacific Northwest Laboratory's Contribution to the Department of Energy's Multi-Laboratory Complex Terrain Field Program, September 1980

M. M. Orgill, T. W. Horst, R. I. Schreck, N. S. Laulainen, P. W. Nickola, D. W. Glover, O. B. Abbey, J. S. Wetzel, and C. D. Whiteman

This report gives a general overview of Pacific Northwest Laboratory's (PNL) contribution to DOE's Atmospheric Studies in Complex Terrain (ASCOT) field project from September 7 to 27, 1980. This was the second relatively intensive multilaboratory effort to collect field data on drainage winds and tracer experiments in the Anderson Creek area of The Geysers-Calistoga Geothermal Resource Area (GCGRA). The GCGRA is being investigated for future expansion of electrical generation operations now existing west of the Anderson Creek area near Middletown, California (Orgill et al. 1980).

PNL's field effort in September consisted of the following tasks:

- Instrumenting a 61-m tower at eight levels at Unit 19. This site is 823 m Mean Sea Level (MSL) in elevation on the slope of Anderson Creek Valley.
- Collecting wind, turbulence, temperature, and radiation data from the tower; soil temperatures and near-surface solar and net radiation measurements curve also obtained at this site.
- Collecting temperature, humidity, pressure, and wind data up to about 600 m with two Tethersonde® systems, one located at Unit 19, and the other at a ridge site at about 1128 m MSL.
- Collecting data on the height and structure of temperature inversions and thermals by a monostatic acoustic sounder at Unit 19.
- Collecting solar and net radiation data at five locations in the Anderson Creek Valley area in conjunction with NCAR's Portable Automated Mesonet (PAM).
- Assisting with the establishment and documentation of a multiple tracer sampling network in the Putah and Anderson Creek drainages.
- Taking rawinsonde ascents in the Healdsburg area in order to obtain upper-level data on temperature, humidity, and winds.

The location of these various field operations is shown in Figure 1.1. It is not feasible to indicate and discuss all field operations from the various laboratories. PNL's two Tethersonde locations were part of a seven-Tethersonde network in the Putah and Anderson Creek Valleys. PNL's rawinsonde was part of an upper-level sounding network providing data on the sub-synoptic

® Tethersonde--Registered Trademark of Atmospheric Instrumentation Research, Inc., Boulder, Colorado.

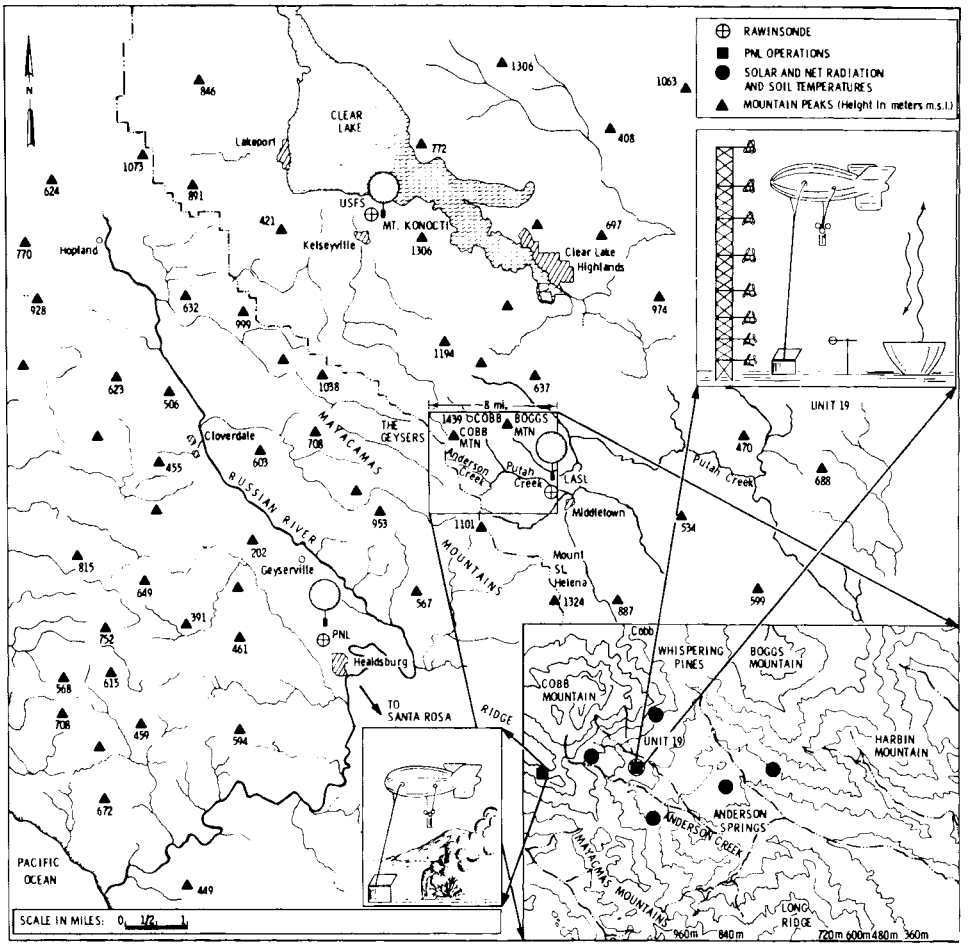

Figure 1.1. Topography Surrounding Geysers-Calistoga Geothermal Resource Area and Rawinsonde Locations. Inset 1 (lower right-hand corner of figure): Topography of Anderson Creek Area and Location of PNL Operations. Inset 2 (upper right-hand corner): Equipment used at Unit 19, left to right, 61-m Tower, Tethersonde, Radiation Sensors and Acoustic Sounder

scale surrounding the GCGRA. PNL's radiation and soil temperature sensors were integrated with the NCAR's PAM system that collects and displays mesoscale meteorological data from a surface (height ~4 m) array of remote sampling stations.

Some of the main objectives of the field effort in September were to define the nocturnal drainage windcycle--including initiation, perpetuation, and dissipation; the temporal and spatial characteristics of the drainage flow; the pooling of drainage flows; evaluation of the exchange of mass between the nocturnal drainage flows and the overlying transition layer; and the effect of drainage flows on transport and dispersion of tracers injected in these flows.

All the experimental periods were conducted during the nighttime and early morning hours between 1700 PDT and 0800 PDT. Table 1.1 lists the dates of the experimental periods. Generally, five fairly clear nights with little synoptic wind interference were good for tracer releases. Experiments one night were cancelled because of inclement weather, and during two other nights the tracer experiments were cancelled because of marginal wind conditions.

PNL's preliminary evaluation of its data set from the tower measurements, solar and net radiation, Tethersondes, acoustic sounder, and tracer experiments are presented in following articles in this Annual Report. All data will be processed, edited, and put on magnetic tapes to be

Table 1.1. Experimental Periods for Ascot During September 1980 at Anderson Creek Valley

Experiment	Date	Remarks
1	Sept. 11 - 12	Some tethersonde problems; two tracer releases in the valley.
2	Sept. 15 - 16	Easterly winds on ridge; two tracer releases in the valley.
	Sept. 17 - 18	Experiment cancelled due to cloudiness and light rain showers
3	Sept. 18 - 19	Experiment terminated around 5:00 a.m. Gusty winds and cloudiness; one tracer release.
4	Sept. 19 - 20	Two tracer releases.
	Sept. 21 - 22	Strong NE winds at ridge level; tracer experiment cancelled.
	Sept. 22 - 23	NE winds increasing in speed on ridge; tracer experiment cancelled
5	Sept. 24 - 25	Tethersonde problems; one tracer release.

sent to the ASCOT data bank at Lawrence Livermore Laboratory.

Reference

Orgill, M. M., T. W. Horst, R. I. Schreck, D. W. Glover, P. W. Nickola, O. B. Abbey, and J. C. Doran. 1980. Project ASCOT--Pacific Northwest Laboratory's Contribution to the Department of Energy's Multi-Laboratory Complex Terrain Field Program, July 1979. PNL-3300 Pacific Northwest Laboratory Annual Report from 1979, Part 3, Atmospheric Sciences, pp. 1-8.

Tethersonde Data at the Geysers Geothermal Site Project ASCOT, September 1980

R. I. Schreck

Seven portable tethered-balloon meteorological data acquisition systems (Tethersonde)® were operated in the Anderson Creek area near Middletown, California, during the September 1980 ASCOT field experiment. Two of the Tethersondes were from the Pacific Northwest Laboratory (PNL) and one each from the Lawrence Livermore Laboratory (LLL), Wave Propagation Laboratory (WPL), Los Alamos Scientific Laboratories (LASL), Savannah River Laboratory (SRL), and the Oak Ridge National Laboratory (ORNL).

On the afternoon of September 9, the seven Tethersonde units were run simultaneously in the same proximity to test for interference of telemetry signals and intercomparison of indicated wet and dry bulb temperatures and wind direction. The telemetry frequency of each sonde was at least 100 kHz, different from any other sonde, and there were no significant interference problems. Dry bulb temperatures agreed within 1°C and wet bulb depressions agreed within 0.5°C except for the WPL system, which indicated a depression 2° to 3°C higher than the other units. The WPL data will be corrected for this offset.

The wind directions were all found to be satisfactory. In addition to these parameters the Tethersonde airborne package also measures the wind speed and pressure, but no intercomparison was done on these parameters since no facilities were available to compare wind speeds (e.g., wind tunnel or constant RPM calibration motors). The indicated pressures depend upon the potentiometer setting.

Beginning on the evening of September 11, the Tethersonde systems were operated at the sites shown in Figure 1.2. Profile criteria were to start the ballon ascent at the beginning of each hour, ascend and descend through the first 100 m at a very slow rate (about 0.5 m/sec), and ascend only to 600 m with the rate of ascent and descent in the upper 500 m being about 1 m/sec. Experimental nights were September 11, 15, 18, 19, 21, 22 and 24. The intent was to make one profile per hour between 7:00 p.m. and 7:00 a.m. (PDT). High winds on the nights of the 21st and 22nd resulted in those two experiments being aborted around midnight.

Telemetry data from the Tethersonde airborne packages were received by the seven respective Tethersonde ground stations and recorded on a printing calculator and on an audio cassette recorder. The calculator was an HP-97, modified to receive the raw Tethersonde data from the ground station and programmed to calculate and print the clock time, barometric pressure, height, dry bulb temperature, relative humidity, mixing ratio, true wind direction, wind speed, and potential temperature. The

® Tethersonde--Registered Trademark of Atmospheric Instrumentation Research, Inc., Boulder, Colorado.

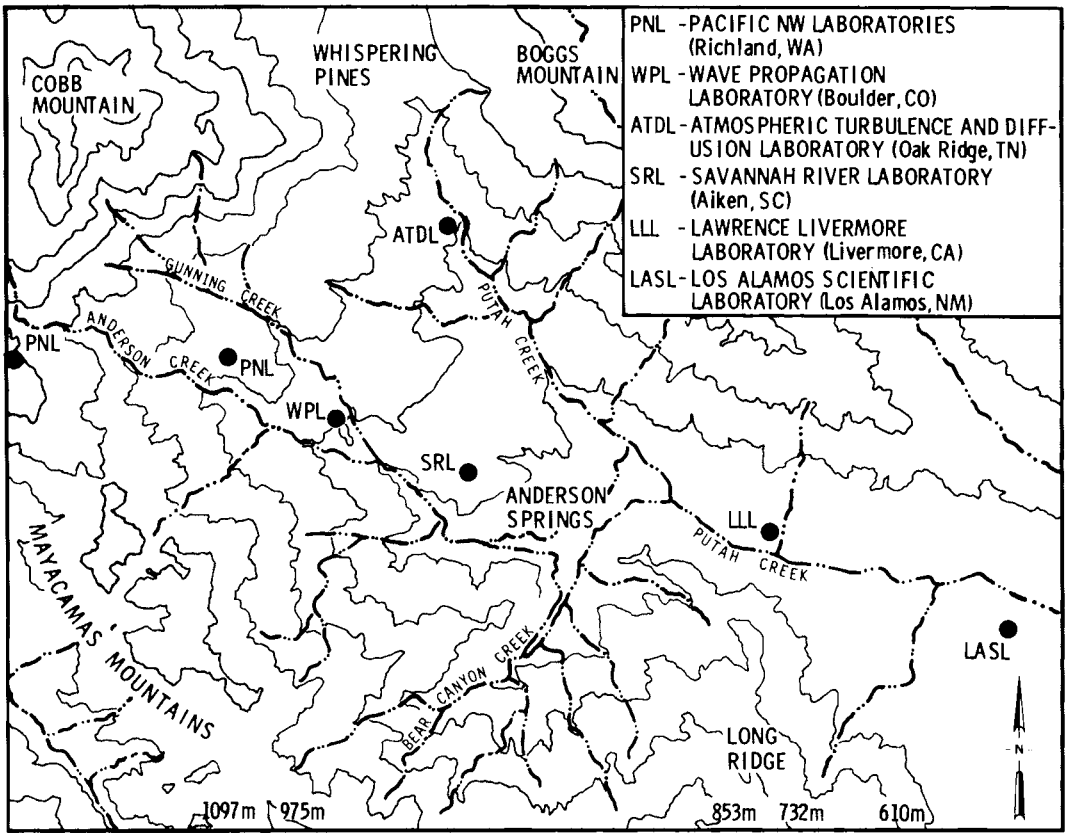

Figure 1.2. Tethersonde® Sites in the Geysers Area During the September, 1980, ASCOT Field Experiment

audio cassette recorder received the raw data and recorded it as a frequency-shifted keyed tone. The data frame rates of each of the airborne packages were set a approximately one frame per ten seconds. Every data frame was recorded on the audio cassette whereas every third frame was sent to the printing calculator.

The HP-97 data is useful in making real-time profiling decisions and provides a backup for the cassette data. At a later time the audio data is replayed into the Tethersonde ground station, which decodes it and puts out digital data to a digital cassette, nine track tape, or computer disc file. Each laboratory is responsible for digitizing its own cassette data and editing out any strange characters and shifted scans. The digital data will then be sent to PNL where it will be computer-edited, converted to engineering units, and plotted utilizing computer graphics. These plots and digital tapes of the engineering units will then be sent to the LLL data bank.

Acoustic Sounder Data--Project ASCOT, September 1980

P. W. Nickola and M. M. Orgill

An array of 10 acoustic sounders was operated on a near-continuous basis during the Atmospheric Studies in Complex Terrain (ASCOT) 1980 program. These sounders, located in the Anderson and Putah Creek Valleys were intended primarily as an aid in defining the spatial and temporal characteristics of the drainage flow. The easternmost sounder was operated in Middletown, California, about 5 km downstream from the point where the Anderson and Putah Creek Valleys merge and open into the much broader Collayomi Valley. The westernmost sounder (farthest up-valley) was deployed about 5 km up the Anderson/

Gunning Creek Valley from the head of Collayomi Valley.(a) This westernmost sounder was operated by PNL.

The analog strip charts generated by this PNL monostatic acoustic sounder have not been reduced. They have, however, been examined and found to be of good quality for the bulk of the 14 days of continuous operation during ASCOT 1980.

There were five 1-hour periods of multi-tracer releases during the September ASCOT experiments. Four of these periods were associated with relatively strong drainage flows. The other tracer release period (Release No. 3) occurred during a marginal drainage flow--at least at the PNL acoustic sounder site. Figures 1.3a and 1.3b show the sounder records for two of the experimental periods.

Figure 1.3a reproduces the PNL acoustic sounder record for the 1-hour Tracer Release Period No. 5, which occurred during one of the most stable atmospheric test periods. The sounder trace suggests the height of the inversion remained below 50 m during most of the depicted 1-hour release. Figure 1.4a plots potential temperature versus height from a tethered balloon (Tethersonde) ascent made within 100 m of the sounder site. The temperature profile shows a strong surface inversion up to an elevation of 40 m.

Elevation of the Tethersonde sensor package as a function of time is

(a) Universal Transverse Mercator (UTM) coordinates 524.10, 4293.33.

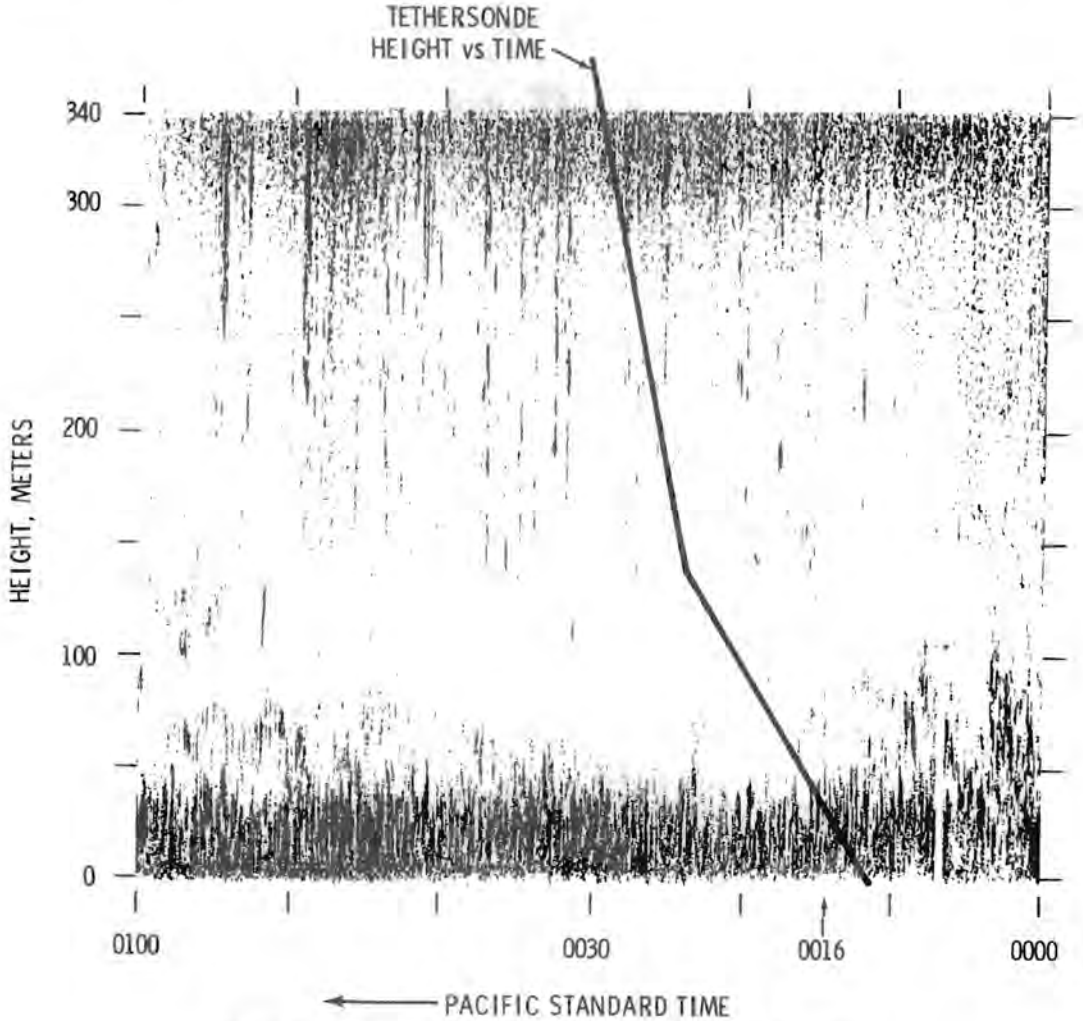

Figure 1.3a. Acoustic Sounder Record During Tracer Release No. 5

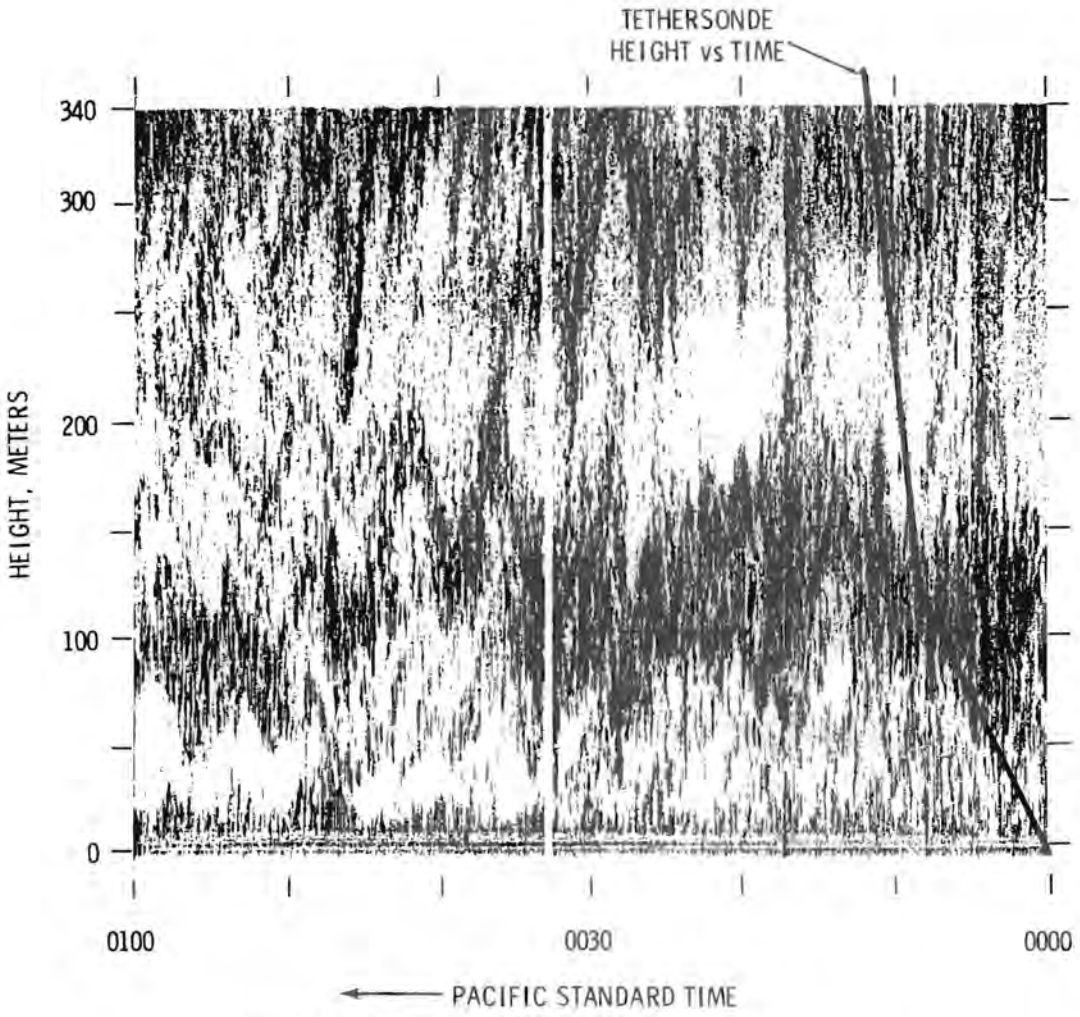

Figure 1.3b. Acoustic Sounder Record During Tracer Release No. 3

superimposed on the acoustic sounder graphics for Release No. 5 (Figure 1.3a). Note that at 0016 PST, the time the Tethersonde sensor was at 40 m, the acoustic sounder confirmed the existence of a surface inversion of about 40 m in depth.

The sounder record for the less dramatic drainage flow of Release No. 3 shows a more complex vertical atmospheric structure (Figure 1.3b). There is a suggestion of a very shallow surface inversion fluctuating from 15 to 40 m, although there may well be some mixture of near-surface background noise in this trace. There is also a layer of strong temperature gradient fluctuating between roughly 75 and 175 m, and the suggestion of a weaker thermal discontinuity fluctuating at about the 300-m elevation. The Tethersonde ascent shown in Figure 1.4b presents a temperature structure with inversions compatible with the layering depicted by the acoustic sounder. As with Release No. 5, the Tethersonde package height as a function of time is superimposed on the Release No. 3 sounder record of Figure 1.3b.

The agreement between acoustic and tethered balloon soundings bodes well for the prospect of better quantifying the vertical atmospheric structure in the experimental regions from the continuous acoustical sounder records.

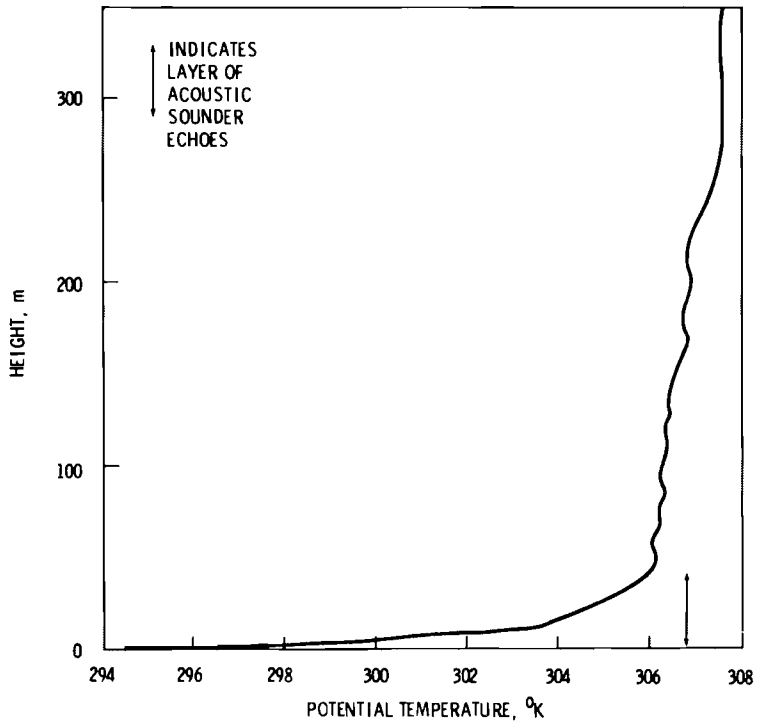

Figure 1.4a. Potential Temperature Versus Height from Tethered Balloon Ascent During Tracer Release No. 5

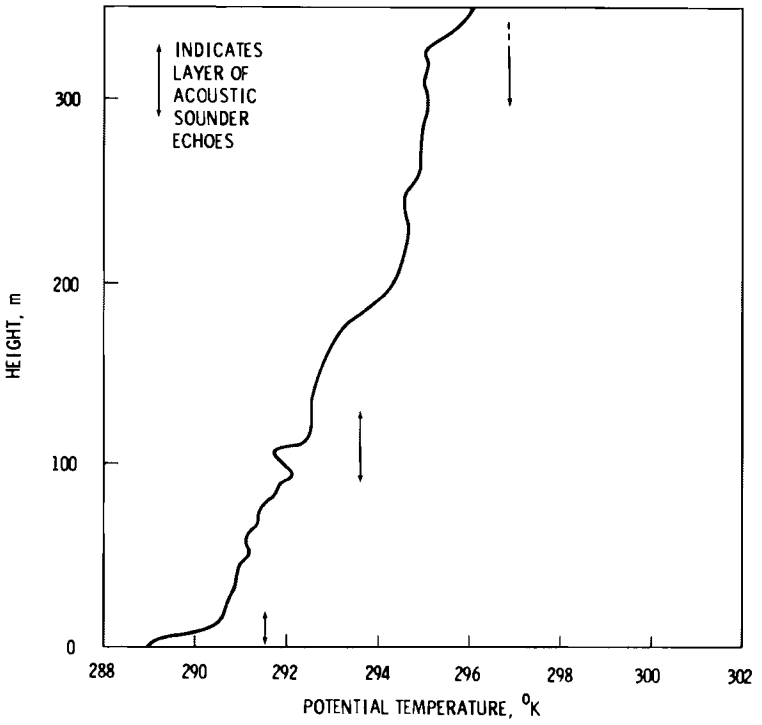

Figure 1.4b. Potential Temperature Versus Height from Tethered Balloon Ascent During Tracer Release No. 3

Selection and Documentation of Tracer Release and Sampling Locations--Project ASCOT, September 1980

P. W. Nickola

A general goal of the ASCOT program is the study of the effect of nocturnal drainage flow on the transport and dispersion of pollutants injected into these flows. Thus, the release and sampling of atmospheric tracers in and near the Anderson Creek and Putah Creek Valleys in California during drainage conditions was an important facet of the September 1980 field program. Although Pacific Northwest Laboratory (PNL) was not directly involved in the tracer release and sampling operations during their implementation, PNL personnel were heavily involved in the selection and documentation of tracer sampling sites.

In May 1980, Dr. Paul Gudikson, director of the 1980 ASCOT field program, requested that PNL generate proposed tracer sampling arrays for a specified number of samplers for each of the three types of non-visible tracers to be employed. These arrays, combined with Dr. Gudikson's similar planned arrays, formed the basis for the field marking of sampling locations in late August 1980. The precise physical location of sampling sites (a labeled stake driven in the ground) was made at each site by a team composed of personnel from the Lawrence Livermore Laboratory, PNL, and Environmental Systems and Services. Modest departures from the paper-planned sampling arrays were dictated by such uncontrollable local factors as terrain, vegetation, and accessibility (legal or logistical). The final array of sampling and release sites is illustrated by Figure 1.5.

During the three-week September 1980 experimental period, terrain and vegetation were documented by motion pictures taken facing north, east, south, and west from each of the 70 tracer sampling and release sites. During the site visits, locations also were carefully documented on a 1/12,500 topographic map. Elevations and Universal Transverse Mercator (UTM) coordinates were derived from the marked map and were incorporated into the ASCOT '80 data bank.

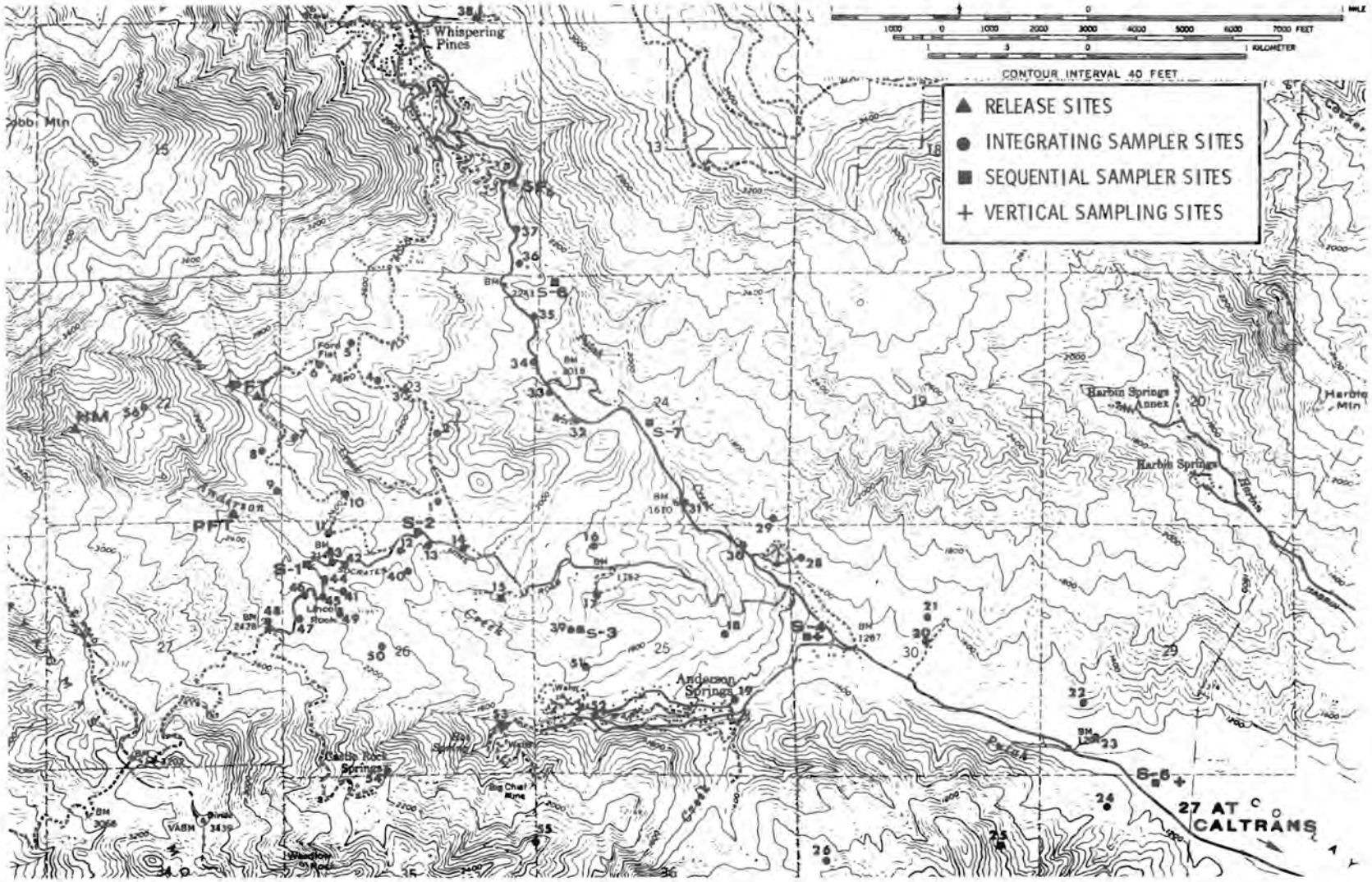

Figure 1.5. Project ASCOT 1980 Tracer Release and Sampling Locations. Triangles indicate release sites; circles indicate integrating sampler sites; squares indicate sequential sampler sites; and crosses indicate balloon supported vertical sampling sites.

Time Variation of Wind and Temperature from Tethersonde Data--ASCOT July 1979

M. M. Orgill

This report briefly describes a preliminary analysis on the time variation of winds and temperatures from Tethersonde data taken during the Atmospheric Studies in Complex Terrain (ASCOT) July 1979 field project. This material was abstracted from a report given at the ASCOT meeting in Gettysburg, Pennsylvania, April 15-18, 1980 (Orgill et al. 1980).

Two mobile Tethersonde units were utilized in the Anderson Creek area near Middletown, California, during the July 1979 ASCOT field effort. One unit was from Pacific Northwest Laboratory (PNL) and the other from the Wave Propagation Laboratory (WPL) in Boulder, Colorado. On the evening of July 16, a cooperative effort between the two groups obtained Tethersonde data at the Diamond D Ranch site for 18 hours. After that period, the PNL Tethersonde was located at the PDC-1 well site in the northwestern part of the Anderson Creek drainage (840 m) for the duration of the project. WPL's Tethersonde was located near the Thorne 7 well site (height, 600 m) around 1.1 km southeast of the PDC-1 well site.

Data were obtained from both Tethersonde sites for six nighttime and early morning periods. Vertical profiles of wind, temperature and humidity were taken about every hour except when strong winds, equipment malfunction or inclement weather prevented it. Ground stations received the data remotely, where it was printed on a paper tape.

The PNL and WPL Tethersonde data volume was edited and computer-plotted as well as being placed on punch cards and a magnetic data tape. The edited, nonaveraged data were processed by a computer plotting routine for incorporation into the ASCOT Data Summary (1980) and for preliminary assessment and analysis.

A number of operational problems were encountered in using the Tethersonde system, yet the data volume as a whole made an important contribution to the field project by showing the time and height variation of the winds, temperature and humidity structure over the Anderson Creek area. Generalized temperature and wind speed vertical profiles for afternoon and nighttime hours, as deduced from the Tethersonde data volume, is depicted in Figure 1.6. Figures 1.7 and 1.8 are a preliminary presentation of the time variation of temperature structure and winds for experiments

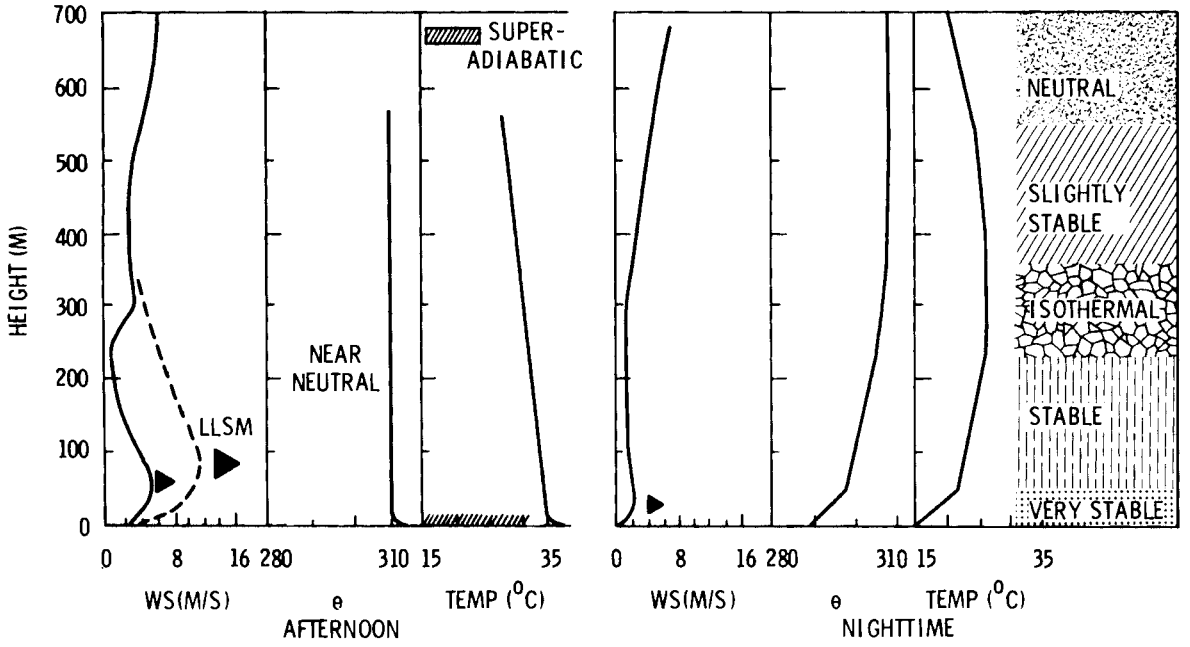

Figure 1.6. Generalized Temperature and Wind Speed Vertical Profiles for Afternoon and Nighttime Hours as Deduced from the Tethersonde Data Volume. LLSM -Low Level Speed Maxima (ms^{-1}).

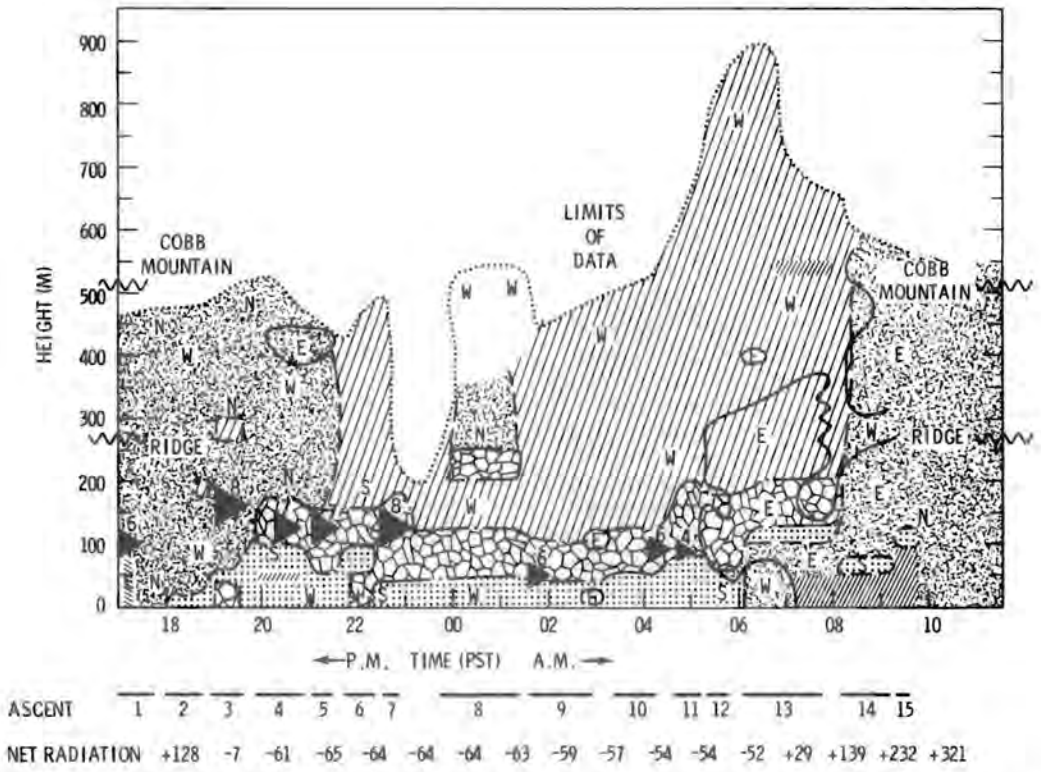

Figure 1.7. Time Variation of Temperature Structure and Wind Profiles PDC #1, July 22-23, 1979. 1707 to 0925 PST. See right-hand side of Fig. 1.6 for stability key.

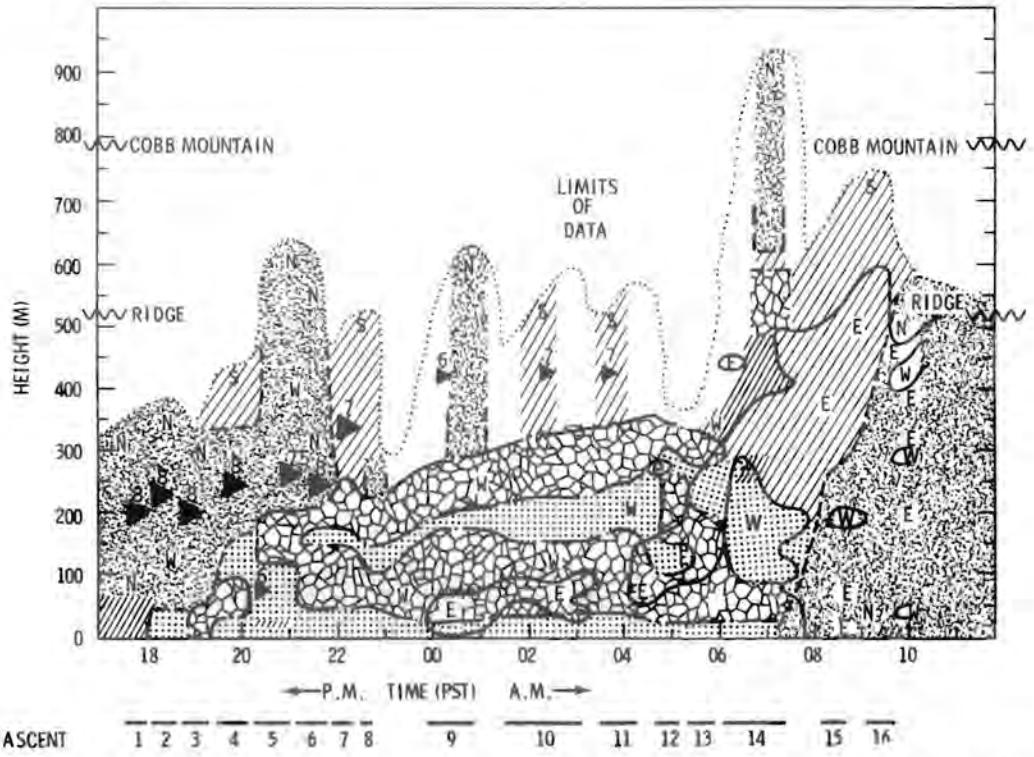

Figure 1.8. Time Variation of Temperature Structure and Wind Profiles Thorne 7, July 22-23, 1979. 1739 to 0947 PST. See right-hand side of Fig. 1.6 for stability key.

conducted during the night of July 22-23. Similar analysis is available for July 16-17 (Diamond D), 18-19, 24-25, and 26-27. In Figures 1.7 and 1.8 wind data are only marked by west (W) and east (E) components. Temperature structure was divided into six different stability classes, as depicted in Figure 1.6.

Generally, during the experimental periods, late morning easterly upslope winds were replaced by westerly downslope winds early in the afternoon (~1200 to 1500 PDT). These afternoon westerly winds were apparently related to the combined monsoonal-sea breeze and west-side valley-slope wind that is apparently common in this area in the summertime (Schroeder 1961). The afternoon westerly winds exhibited peaked vertical wind speed profiles with low-level (50 to 400 m above ground) wind maxima Low Level Speed Maximum (LLSM) varying from 3 to 11 m s^{-1}. These wind speed maximas usually decrease in magnitude by midnight for most experimental nights.(a) The atmospheric stability in the lower 500 to 600 m was usually neutral or unstable during these afternoon westerly downslope winds.

Time variation of vertical profiles of wind and temperature was strongly influenced by the diurnal net radiation cycle. With sunset and the onset of negative net radiation the lower atmosphere in the Anderson Creek area quickly cooled, forming as many as four distinct, stable layers (Figure 1.6). Generally, these were: 1) a shallow (50 to 100 m), very stable layer near the ground (+0.1 to 0.2°C/m); 2) a primary stable layer (~+0.02 to +0.03°C/m); 3) an isothermal layer (bottom and top of temperature inversion); and 4) a slightly stable layer. Quite frequently a near neutral (adiabatic) layer was found above the temperature inversion or the slightly stable layer.

On first examination of Tethersonde data the nocturnal drainage winds were shallow and poorly defined. Possibly one reason for this was the superposition of the decaying, afternoon westerly wind. Best evenings for apparent drainage wind phenomena appeared to be July 16-17, 18-19, 24-25, and 26-27. Depth of the drainage layer on the slope varied with time, rarely exceeding 100 m. Drainage wind speed maxima were 2 to 4 m s^{-1}. Periods of easterly winds above the low-level nocturnal westerly downslope winds were frequent on most nights. The night and early morning of July 26-27 was exceptional in this regard. Some of these easterly winds may be anti-mountain winds as defined by Buettner and Thyer (1966) and some may be related to upper-level gradient flow.

On those experimental mornings when observations were taken 3 to 4 hours beyond sunrise, the nocturnal stable conditions and the westerly drainage layer were observed to quickly (1 to 2 hours) dissipate with the onset of positive net radiation (daytime). Stability conditions on the slopes were unstable and neutral during daytime hours, and easterly upslope winds were observed.

Any conclusions made now are tentative since detail analysis of all the data volume should present a more coherent picture of the meteorological and dispersion phenomena of this period. However, this preliminary analysis has indicated that Tethersonde soundings showed that the winds and temperatures over the Anderson Creek area were strongly influenced by the net radiation cycle. Although nocturnal drainage winds were apparently observed on the slopes and in the valley, they were shallow and, at times, apparently influenced by the synoptic monsoonal-sea breeze airflow pattern present in this area during summertime. Fluorescent Particle Tracer experiments also revealed the presence of nocturnal drainage winds although the experimental test of July 22-23 appeared to be influenced by the prevailing westerly synoptic winds.

(a) July 22-23, 1979, was an exception.

References

ASCOT Program 1980. ASCOT Data--July 1979. Lawrence Livermore Laboratory, Livermore, California.

Buettner, K. J. K. and N. Thyer, 1966. "Valley Winds in Mt. Rainier National Park." Arch. Met. Geoph. Biobl., Series B Bd 14 H.2:125-147.

Orgill, M. M., R. I. Schreck, P. W. Nickola, T. W. Horst, D. W. Glover, J. C. Doran, O. B. Abbey, W. D. Neff, and R. F. Larson. 1980. "Net Radiation, Vertical Profiles of Wind and Temperature, and Cross-Valley FP Tracer Sampling in the Anderson Creek Valley Area July 1979." Presented at ASCOT 1979 Field Study Review Meeting, (April 15-18, 1980), Gettysburg, Pennsylvania.

Schroeder, M. J. 1961. "Down-Canyon Afternoon Winds." Bull. Amer. Meteor. Soc. 42(8):527-542.

A Planning Guide for Future Studies--ASCOT

M. M. Orgill

This report briefly summarizes the contents of an ASCOT planning document that will be published in FY 1981. This document will provide a preliminary basis for future planning and selecting both the technical aspects and the location of field experiments for relevant DOE research related to airflow and dispersion in complex landforms.

In 1978, the DOE Assistant Secretary for the Environment developed a program aimed specifically at Atmospheric Studies in Complex Terrain (ASCOT). The ASCOT program is designed to develop the technology needed to assess atmospheric properties and the imact of new energy sources on air quality in areas of complex landforms.

The initial research focus of ASCOT was nocturnal drainage winds within the Geysers-Calistoga Geothermal Resource Area of Northern California. However, the ASCOT participants recognized the need for program planning beyond the drainage wind study in the Geysers area. The Atmospheric Sciences Department of Pacific Northwest Laboratory was asked to prepare a document summarizing past research, surveying potential study sites and recommending future research sites and topics for the ASCOT program.

The planning guide is divided into three parts: 1) a review and discussion of terrain-induced airflow phenomena and their importance in transport and dispersion in complex landforms; 2) an assessment of future candidate research sites; and 3) discussion and recommendations on various research options for ASCOT. The review content of the report surveys the past observational, theoretical, laboratory, and numerical work relative to complex landforms. It defines and reviews as many airflow and dispersion phenomena as possible that are important to questions and problems regarding air quality in complex terrain. Some of these phenomena are:

- channeling of plumes
- impaction of elevated plumes on terrain surfaces
- stagnation of air pollutants in basins and valleys
- effects of local terrain-induced winds on plumes, such as drainage, anabatic, valley-mountain, and lake breezes
- trapping and fumigation of elevated plumes or pollutant layers
- effects of streamline deformation, terrain-induced eddies, turbulence and gravity waves on plumes.

Many or all of these terrain-related airflow problems influence decisions on siting of plant locations, establishing stack height requirements and emission controls and evaluating air quality in complex terrain area.

Assessing candidate sites for future reserch was limited to the alternative energy resource areas of oil shale, geothermal, and coal gasification/liquefaction. In the oil shale area, approximately 13 sites in the Green River oil shale region (Colorado-Utah- Wyoming) were examined on the basis of complexity of terrain, meteorology, air quality, and expansion of operations. A number of research options are available from Federal Oil Shale Lease Sites and other sites in Utah and Colorado. Complexity of terrain varies from the stream-eroded plateau of eastern Utah to the large valley-basin of the Piceance Basin (Colorado) to the rugged canyons of the Roan Plateau (Colorado). The variety of terrain-induced airflow phenomena in such terrain could require the efforts of one or more research projects in order to understand and assess the air quality.

In relation to the geothermal areas, about ten or more geothermal areas are considered as potential sites for ASCOT. Of these sites, the more promising areas of interest are The Geysers (California), Lake City-Surprise Valley (California), Raft River (Idaho), Valles Caldera (New Mexico), and Roosevelt Hot Springs (Utah). With respect to complexity of terrain, the more interesting sites would probably be The Geysers, Mono-Long Valley, and the Valles Caldera.

In the near future (5 to 10 years) coal gasification and liquefaction projects could offer a selection of complex terrain sites. Presently, future development in the west appears directed toward the San Juan River Region (New Mexico), Powder River Region (Wyoming and Montana), and Fort Union Region (North Dakota). In the

east, some development is occurring in the Appalachian Region. In general, the current potential sites for development are not located in very complex terrain except for the Appalachian Region.

The major recommendations to ASCOT as a result of this study are:

- The airflow and diffusion characteristics of a particular landform are a result of the topographic details and terrain-induced airflow patterns. Taking terrain uniqueness into consideration, it is recommended that the ASCOT program study a range of different landform types.

- The study recommends more emphasis be placed on the quantification of the basic components of terrain to help understand the various interactions between landforms and meteorology.

- On the basis of the first recommendation, we suggest that ASCOT seriously consider the option of conducting future studies at other energy development areas. Some possible current options for candidate sites are: 1) Oil shale resource areas of Utah and Colorado; 2) Mono-Long Valley Geothermal Resource Area (California); and 3) the Valles Caldera Geothermal Resource Area (New Mexico). Other options could develop in the next five years because of new energy developments and political, economic, and energy policy decisions.

- A long-term (5 to 10 years) but flexible research plan should be adopted by the ASCOT program. A principal objective of this plan would be to use field programs and model development toward constructing a validated operational model that can be utilized for different landforms and meteorology.

• Atmospheric Boundary Layer Studies

Objectives of these studies are:

- Investigating the meteorological characteristics of the planetary boundary layer that pertain to pollutant transport and dry removal.
- Analyzing the transport and diffusion of pollutants in complex terrain, particularly in the Geysers Geothermal Area of California.
- Constructing simple models for the prediction of the depth, speed and direction of gravity-controlled drainage flows and pollutant dispersion within these flows.

Wind and Temperature Oscillation in Drainage Winds

J. C. Doran and T. W. Horst

As part of the ASCOT measurements program in 1979, wind speeds and temperatures were recorded on a 30-m tower located in the Geysers area of California. Located near the end of a valley, the tower was subject to the outflow from several major drainage regions as well as a number of smaller ones.

In 1968, Tyson reported observations of velocity fluctuations in the mountain winds in valleys in South Africa. Similar fluctuations were believed likely at the Geysers and the tower data were therefore examined for evidence of this effect. For this analysis, winds and temperatures from the 22.9-m level on the tower were averaged in 20-second blocks and 2048 such blocks were then analyzed with a fast Fourier transform routine. Each period analyzed lasted approximately 11.5 hours, nominally extending from sunset to sunrise for nighttime runs and from sunrise to sunset for daytime runs.

Wind data from 30 nights were examined. In 26 of these, a peak in the logarithmic spectral energy density was found in the frequency range 10^{-4} to 3.3 x 10^{-3} Hz, corresponding to periods of approximately 1 to 3 hours. The spectra were normalized to the peak average value. The results are shown in Figure 1.9. There is a well-defined peak at a period of about 1.5 hours. For comparison purposes, 14 days were chosen from the time periods during which the nighttime spectra were determined and a similar analysis was made. Again, a well-defined peak in the spectrum was observed, but at a frequency almost 20 times higher than that of the nighttime peak. The location of the daytime peak agrees well with values reported in the literature (e.g., Kaimal et al. 1972) while the nighttime peak occurs within the frequency range often associated with the "spectral gap" (Lumley and Panofsky 1964).

Temperature spectra also were obtained in a manner similar to that described above. For 14 nights selected from the 26 used for the wind spectra, the spectrum of temperature fluctuations showed a low frequency peak at a frequency close to where the wind spectrum exhibited its peak.

Discussion

Simple models cannot be expected to predict the details of wind fields in topography and conditions as complex as those found in the Geysers area. However, they may account for some of the observed qualitative features. Fleagle (1950) proposed a model wherein the forces acting on a cooled layer of air adjacent to the slope produce oscillations in the velocity of this layer. He showed that as the air accelerates down the slope, adiabatic heating results in a reverse pressure gradient which retards the flow. As the air decelerates, radiational cooling increases the pressure gradient and the cycle is

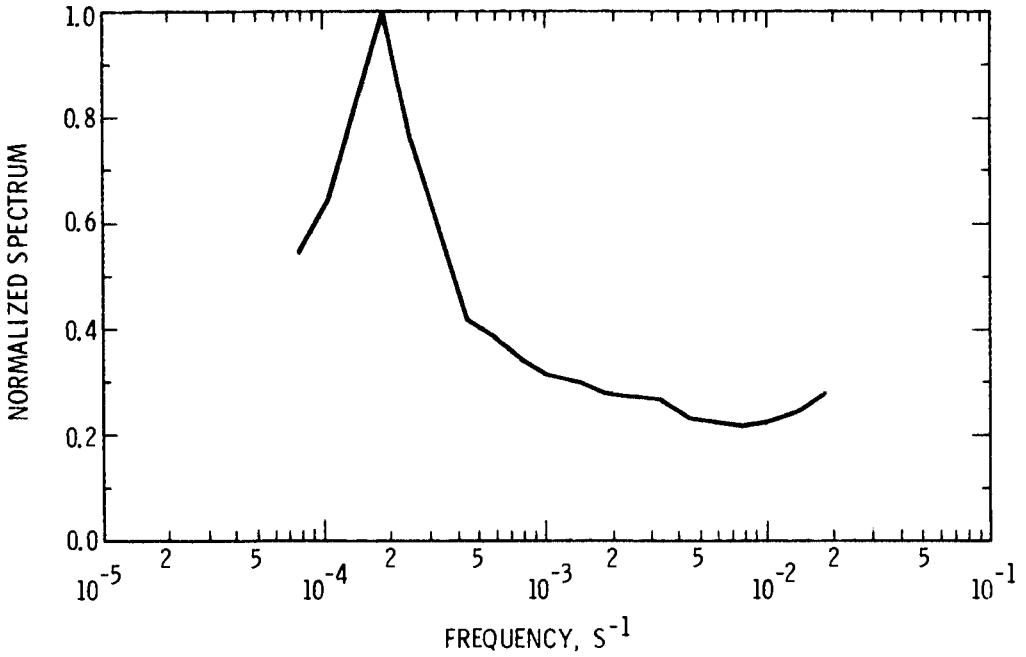

Figure 1.9. Averaged Normalized Logarithmic Velocity Spectra for 26 Nights

repeated. Frictional drag will eventually damp out the oscillation.

Following the approach of Petkovsek and Hocevar (1971), and Manins and Sawford (1979), we may write, for a layer-averaged model

$$\frac{\delta V}{\delta t} = \frac{-gD \sin\alpha}{\theta_o} - Fr \qquad (1)$$

$$\frac{\delta D}{\delta t} - V_\gamma \sin\alpha = \frac{Q}{H} \qquad (2)$$

where V and D are the bulk velocity and temperature deficit for the cooled layer, respectively, α is the slope angle, γ is the ambient potential lapse rate, H is the depth of the layer, θ_o is the potential temperature and Q is the net vertical temperature flux into the cooled layer. The term Fr refers to a general frictional force which may include surface drag and entrainment effects.

Numerical solutions of (1) and (2) lead to damped oscillatory solutions for both V and D. For reasonable estimates of the input parameters the period of oscillation is found to be ~1.5 to 2 hours. While this agrees with the observations at the Geysers, additional measurements, particularly in regions with simpler topography, are necessary before this simple model can be adequately tested.

References

Fleagle, R. G. 1950. "A Theory of Air Drainage." J. Meteor. 7:227-232.

Kaimal, J. C., J. C. Wyngard, Y. Izumi, and O. R. Cote. 1972. "Spectral Characteristics of Surface Layer Turbulence." Quart. J. Roy. Meteor. Soc. 98:563-589.

Lumley, J. L. and H. A. Panofsky. 1964. The Structure of Atmospheric Turbulence. New York, Interscience--Wiley.

Manins, P. C. and B. L. Sawford. 1979. "A Model of Katabatic Winds." J. Atmos. Sci. 36:619-630.

Petkovsek, A. and A. Hocevar. 1971. "Night Drainage Winds." Arch. Meteor. Geophys. Bioklim. A20:353-360.

Tyson, P. D. 1968. "Velocity Fluctuations in the Mountain Wind." J. Atmos. Sci. 25:371-384.

A Comparison of Observed and Predicted Slope Winds

T. W. Horst and J. C. Doran

Introduction

Nocturnal drainage winds begin when air adjacent to an inclined surface flows down the slope because it is cooler than the free air at some distance horizontally from the surface. The topography channels and merges these slope winds to form larger-scale drainage or mountain winds. This paper discusses the slope flow phase of the drainage wind. The predictions of a simple model for flow down a two-dimensional slope are compared to observations of the drainage wind obtained during the July 1979 Atmospheric Studies in Complex Terrain (ASCOT) field study near Middletown, California.

A Simple Model of Slope Winds

Manins and Sawford (1979) following Elison and Turner (1959) have developed a simple model for katabatic flow down a plane surface inclined at an angle α above the horizontal. Coriolis effects are neglected and the ambient air is assumed to be at rest, so the cross-slope wind is zero and the katabatic flow equations are functions only of time, the down-slope coordinate s and the coordinate n normal to the slope. The dynamic equations are further simplified by integration over the normal coordinate n, from the surface to a height unaffected by the katabatic flow. The closure problem for the Reynolds fluxes of heat and momentum reduces to specifying the fluxes at the surface. Entrainment at the top of the mixed layer is assumed proportional to the average velocity of the layer, multiplied by an empirical function E of the layer Richardson number Ri. The resulting equations predict the layer-averaged wind V, the depth of the cooled layer h, and the temperature deficit D.

An analytical prediction of the slope flow follows from assuming a steady-state and zero ambient stratification,

$$h = 0.75\ Es$$

$$V^3 = \frac{s}{Ri}\left[\frac{g}{\theta_o} Q\right] \cos \alpha$$

$$D = Qs/Vh$$

where $\rho C_p Q$ is the net heat flux out of the drainage layer. The layer Richardson number is found to be independent of s and a function only of the slope angle, a surface drag coefficient C_d, and the functional relationship between E and Ri.

The authors have extended the analytical solution to account for a change of slope angle by assuming that Ri immediately adjusts to the new slope angle and by conserving either the mass or momentum flux through the slope change. For a decrease in the slope angle this produces an immediate deceleration, thickening and cooling of the drainage layer. Numerical calculations within the complete equations show that this solution is only qualitatively correct near the slope change, but improves rapidly with distance downslope from the change.

Observations of Slope Winds

Pacific Northwest Laboratory measured profiles of wind speed, wind direction and temperature with a Tethersonde located at the PDC-1 site, at an elevation of 850 m Mean Sea Level (MSL) on the south-southeast slope of Cobb Mountain. The summit of Cobb Mountain is 1440 m, and the slope angle is roughly 22° down to an elevation of 900 m and 6.5° thereafter.

The best drainage wind observations were made on the night of July 24-25, 1979, particularly after midnight PST. Values of h, V, D, and Ri were determined from the data for seven profiles made from 8:00 p.m. July 24 to 5:00 a.m. July 25. The downslope direction was defined for each profile by the wind direction at the height of the maximum wind speed, and the wind data were resolved into downslope and cross-slope components. For most of the profiles this direction was south-southeast, the direction of a line between the top of Cobb Mountain and PDC-1.

Table 1.2 shows the observed values for three of the seven profiles. These profiles were selected because they have downslope winds with maxima of 3 to 4 m/s, which decrease above the drainage layer to 1 m/s or less, and cross-slope winds below 1 m/s. Profiles of wind and temperature for the 0309 sounding are shown in Figures 1.10 and 1.11. Table 1.2 also lists the predictions of the simple slope flow model. Since C_d and Q were not directly measured, reasonable values have been chosen for these parameters.

Considering that the model assumptions of cross-slope homogeneity and a neutral ambient atmosphere are not satisfied by the observations, this initial comparison is

Table 1.2. Slope Wind Observations at PDC-1, July 25, 1979. Model Predictions Assume $C_d = .047$ and $\rho C_p Q = 40$ watts/m^2

t (PST)	h (m)	V (m/s)	D (C°)	Ri
0011	60	1.92	1.19	0.62
0309	72	2.35	1.40	0.55
0500	67	2.14	1.01	0.47
Average	66	2.14	1.20	0.55
Model	36	1.51	1.10	0.55

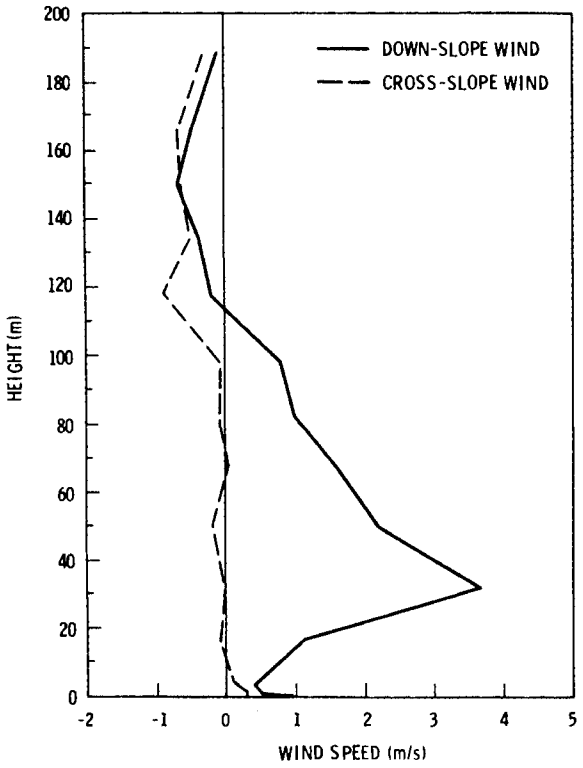

Figure 1.10. Drainage Wind Profiles at PDC-1, 0309 to 0316 PST, July 25, 1979

encouraging. Two approaches are being taken for improvement. First, a numerical solution is being developed to include the effects of slope change, ambient stratification, and ambient winds. Second, more detailed slope flow measurements have been made, both at Richland, Washington, at a site which more nearly approximates the two-dimensional assumptions of the model, and again at Cobb Mt. using both instrumented towers and a Tethersonde to better define the structure of the drainage flow (Horst et al. 1980).

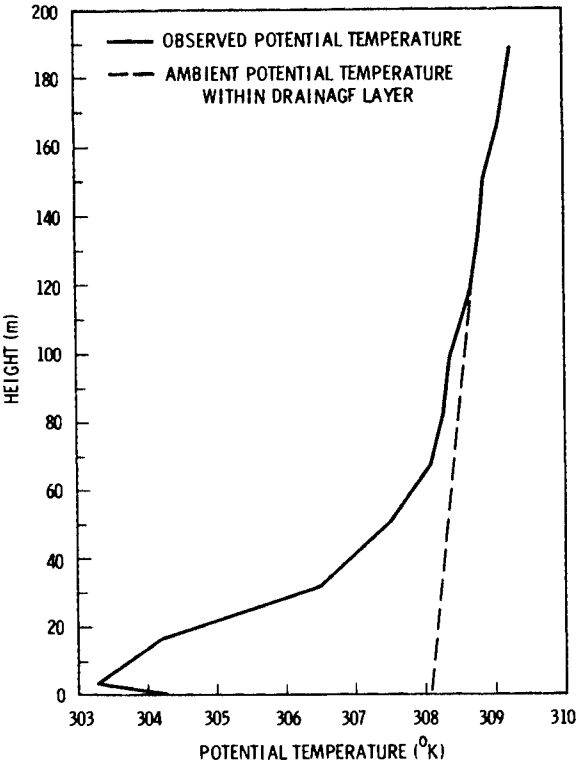

Figure 1.11. Potential Temperature Profile at PDC-1, 0309 to 0316 PST, July 25, 1979

References

Ellison, T. H. and J. S. Turner. 1959. "Turbulent Entrainment in Stratified Flows." J. Fluid Mech. 6:423-448.

Manins, P. C. and B. L. Sawford. 1979. "A Model of Katabatic Winds." J. Atm. Sci. 36:619-630.

Horst, T. W., J. C. Doran, and O. B. Abbey. 1980. "Observations of Nocturnal Slope Winds." This Annual Report.

Observations of Nocturnal Slope Winds

T. W. Horst, J. C. Doran, and O. B. Abbey

Introduction

Preliminary measurements of nocturnal drainage winds were made during the July 1979 Atmospheric Studies in Complex Terrain (ASCOT) field study near Cobb Mountain in northern California. Analysis of these data (Horst and Doran 1980, and Doran and Horst 1980) showed the need for

additional observations to better define the structure of drainage winds. These additional data were collected locally on Rattlesnake Mountain and again near Cobb Mountain during the September 1980 ASCOT field study.

Rattlesnake Mountain

The northeast slope of Rattlesnake Mountain on the Hanford reservation was selected for measurements of slope flow in the simplest possible geometry, a tilted plane. Rattlesnake Mountain is a ridge extending for 15 km from northwest to southeast. The measurement site, on the southeast end of the ridge, is uniform in the cross-slope direction for about 2.5 km and has an elevation drop from 595 m MSL to 365 m MSL. There is a distinct change in slope at 430 m from 20° to 8°.

To determine the growth of the drainage layer with distance down the slope, wind and temperature profile towers were erected near the top and bottom of the steep slope (520 m and 445 m) and at 365 m on the shallow slope. The towers were designed to extend through the drainage layer, increasing from 6 m at 520 m, to 10 m at 445 m, and 18 m at 365 m. Temperature was measured at four heights on the top tower; wind and temperature were both measured at five heights on the lower towers. In addition, net radiation and a soil temperature profile were measured at the lowest tower to determine the surface energy budget, and regular soundings were made with a Tethersonde to an altitude of 700 m to 900 m MSL to define the ambient wind and temperature profiles. During June and July 1980, data were collected on three nights that met the experimental requirements of clear skies and low wind speeds above the drainage layer.

Cobb Mountain

As part of the September 1980 ASCOT field study (Orgill, et al. 1980), a site called Unit 19 was selected for detailed measurements of slope flow in a more complex topography than the Rattlesnake site. Unit 19 is at an elevation of 770 m on 1440-m cobb Mountain and is near the PDC-1 site used for Tethersonde ascents during July 1979 (Horst and Doran 1980).

A 60-m tower was erected amidst 10-m to 15-m trees to provide a more complete record of the development of the drainage layer and a better definition of its structure than can be had with Tethersonde soundings. Wind and temperature were measured at eight levels from 5 m to 60 m, net radiation was measured at 1 m and 60 m, and soil temperatures were measured at four depths from 1 cm to 20 cm. Tower data were recorded continuously on digital magnetic tape from 1700 PST on September 11 to 0800 PST on September 25, with each parameter sampled at a rate of 0.5 Hz. In addition, hourly Tethersonde ascents were made to altitudes of 1100 m to 1400 m MSL from 1800 PST to 0600 PST on five nights selected for favorable drainage conditions.

Data Analysis

These two data sets are being analyzed simultaneously. The Rattlesnake Mountain data will be used to test and further develop simple models of nocturnal slope flow. The application of these models to more complex topography wil then be tested with the Cobb Mountain data.

References

Doran, J. C. and T. W. Horst. 1980. "Wind and Temperature Oscillations in Drainage Winds." (This Annual Report.)

Horst, T. W. and J. C. Doran. 1980. "A Comparison of Observed and Predicted Slope Winds." (This Annual Report.)

Orgill, M. M., et al. 1980. "Project ASCOT--Pacific Northwest Laboratories' Contribution to the Department of Energy's Multilaboratory Complex Terrain Field Program, September 1980." (This Annual Report.)

• Radiative Effects of Clouds and Aerosols

Objectives of this study are:

- Measuring energy-related aerosol radiative properties and relating them to aerosol physical and chemical properties.
- Measuring upwelling and downwelling short- and longwave radiation at various levels within the planetary boundary layer.
- Determining radiative effects of clouds, particularly those that have been influenced by energy-related pollutants.
- Modeling radiative transfer in the planetary boundary layer using measured aerosol radiative properties and fluxes.

Insolation, Net Radiation and Soil Temperature Measurements During the ASCOT-1980 Field Study

N. S. Laulainen

Introduction

Net radiation measurements were made at the Geysers Geothermal Site during the ASCOT-1979 field study to quantify the rate of surface cooling--an important factor in establishing valley drainage flow. These measurements provided an interesting but incomplete record of the radiation balance at the earth's surface for the 1979 study.

With inclusion of the National Center for Atmospheric Research (NCAR) PAM System (Brock and Govind 1977) into the ASCOT-1980 field study, special sensors were added to the existing meteorological sensors. This was done at a limited number of individual PAM (Portable Automated Mesonet) stations to provide more complete spatial and temporal coverage of radiation balance over the study area. This report describes the experimental design and a few preliminary results illustrating the relationships between air and soil temperature, net radiation and insolation.

Experimental Design

Pacific Northwest Laboratory deployed net radiometers,(a) pyranometers,(b) and soil temperature sensors(c) at four soil depths at five PAM stations and at the PNL 60-m tower site within the Geysers Geothermal Site study area. A reference pyranometer(d) was included at one of the PAM sites to verify calibrations.

The radiation sensors were mounted on 1-m booms approximately 1 m above the surface. The soil temperature sensors were

(a) Temperature-compensated miniature net radiometer (Model MNR) manufactured by Micromet Instruments, Bothell, Washington.
(b) Cosine-corrected silicon cell pyranometer (Model LI-200S) manufactured by Lambda Instruments Corp., Lincoln, Nebraska.
(c) YSI-10K thermisters manufactured by Yellowsprings Instruments Inc., Yellowsprings, Ohio.
(d) Temperature-compensated Precision Spectral Pyranometer (Model PSP) manufactured by Eppley Laboratory, Inc., Newport, Rhode Island.

installed at soil depths of 1, 3, 7, and 20 cm, respectively. At the PNL tower an additional net radiometer was mounted at the top of the 60-m tower and an upward and downward-looking pyranometer pair was mounted at about the 9-m level on the tower. The latter pyranometer pair can be used to estimate surface albedo. A measure of incident-diffuse short wave radiation also was provided by this pair by means of a motorized shadow band which occluded the direct beam periodically (about every 5 min).

Sensor output signals were processed differently for the NCAR and PNL systems. Special interface cards were provided by NCAR to amplify and digitize the added sensor outputs. These data, along with the other meteorological parameters monitored at each PAM site, were telemetered to the PAM base station where they were recorded on 9-track magnetic tape. The PAM computer/data acquisition system was able to store up to 18 hours of previous data, which could be examined tabularly or graphically from a video terminal console. With preliminary sensor calibration values, the raw data were coverted to engineering units before displaying. Hard copies of the video display were produced by a copy unit.

Sensor outputs at the PNL tower also were amplified, digitized and recorded on 9-track magnetic tape. In addition, two 2-channel chart recorders were used to record the amplified output signals of the 1-m and 9-m radiometers.

After completing calibration checks of the sensors, the calibration values for each sensor were sent to NCAR for incorporation into the data archiving process. Reduction of the PNL data is in progress.

Preliminary Results

Examples of graphical results obtained during the course of the field study from the video terminal are shown in Figures 1.12 through 1.16. In Figure 1.12, soil temperatures at the four depths, 1, 3, 7, and 20 m, respectively, are shown. The 1-cm depth is most sensitive (as expected) to changes in the surface heating (or cooling) rate. Cloudiness, both during daylight hours and during the night, affects the net radiation transfer. At the 3-cm depth the temperature response is smaller than and lags behind the response at 1-cm, while at the 20-cm depth only a slow diurnal variation occurs.

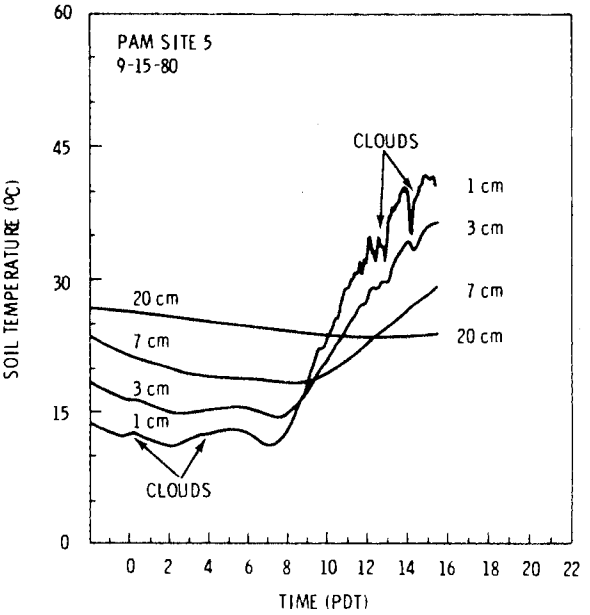

Figure 1.12. Soil Temperature at 1, 3, 7 and 20 cm Depths, Respectively, at PAM Site 5 on 9/15/80, 0000 to 1600

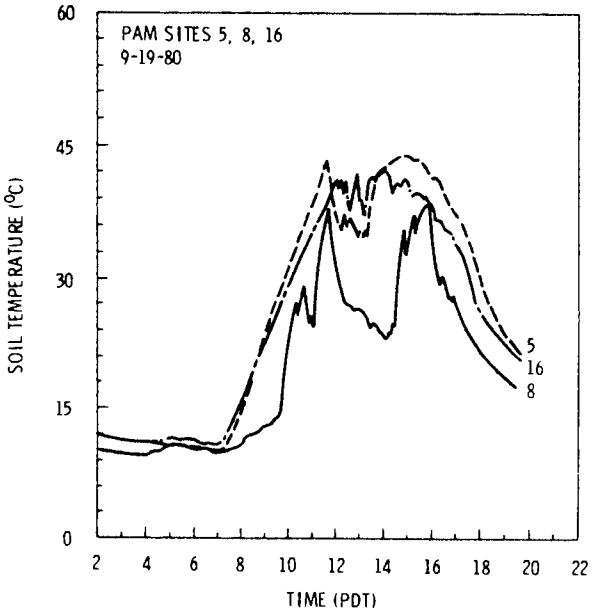

Figure 1.13. Soil Temperature at 1-cm Depth at 3 PAM Sites on 9/19/80, 0200 to 2000

Figure 1.13 compares soil temperature variations during daylight hours at the 1-cm level on 9/19/80 for 3 PAM sites. PAM Site 5 (UTM 523.40, 4293.58, elev. 914 m) had a southeasterly exposure and was at the

highest elevation, while PAM Site 16 (UTM 524.88, 4292.00, elev. 658 m) had an easterly exposure. PAM site 8 (UTM 525.02, 4292.51, elev. 774 m) was located within a forest canopy. PAM Site 5 and 16 show variations as a result of cloudiness while PAM Site 8 shows variations as a result of shading by trees. The soil at PAM Site 8 was cooler than the other sites for all hours.

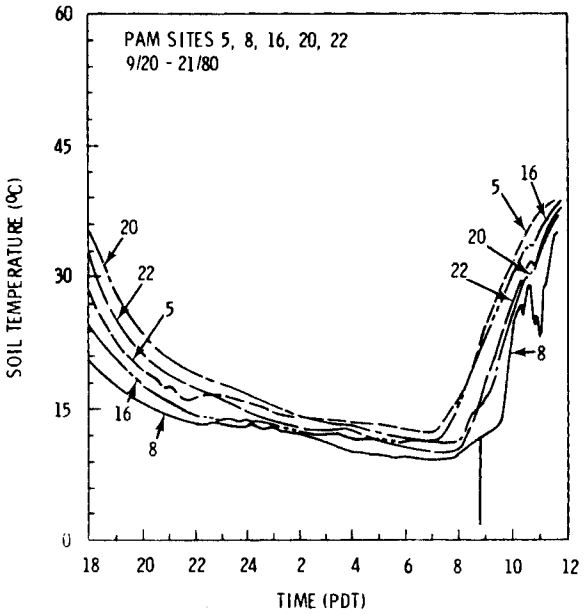

Figure 1.14. Soil Temperature at 1-cm Depth at the 5 PAM Sites on 9/20 (1800) through 9/21 (1200)

A similar comparison of soil temperature variations at the 1-cm level during the nighttime hours on 9/20 and 9/21 for all PAM sites is shown in Figure 1.14. Again, PAM Site 8 was cooler than the other sites for all hours. Differences between the other sites can be partially accounted for by differences in topography and sunrise/ sunset relationships, e.g. ridge shadows or vegetation.

The response of the 1-cm soil temperature to insolation and net radiation on a clear day is shown in Figure 1.15 for PAM site 4 on 9/21/80. Peak insolation and peak net radiation occurred shortly after 1300 PDT and at 1320 PDT, respectively, while the peak soil temperature occurred at ~1410 PDT. Although the insolation curve is symmetric about solar noon, the curves for net radiation and soil temperature are shown (in addition to lagging behind solar noon). A similar response of 1-cm soil temperature and the dry bulb air temperature to net radiation is shown in Figure 1.16 for PAM Site 5 on 9/17/80. Correlation between these quantities is quite striking.

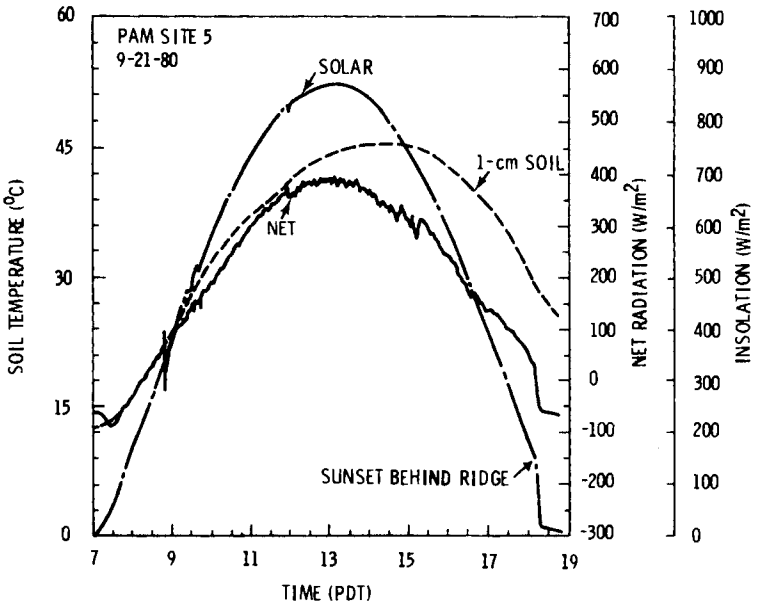

Figure 1.15. Soil Temperature at 1-cm Depth Net and Solar Radiation at PAM Site 5 on 9/21/80, 0700 to 1900 PDT

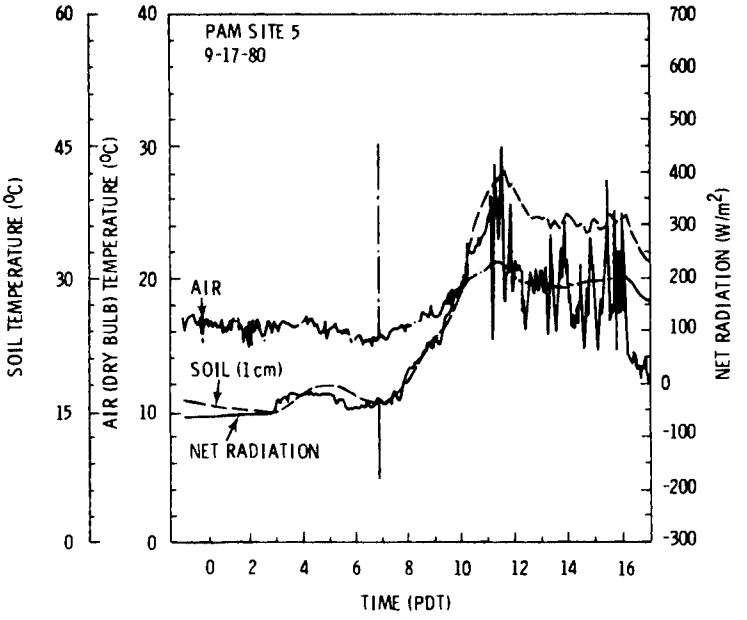

Figure 1.16. Dry Bulb Air Temperature, Soil Temperature at 1-cm Depth and Net Radiation at PAM Site 5 on 9/17/80, Midnight to 1700 PDT

Conclusions

The addition of special soil, insolation and net radiation sensors to the PAM system during the Geysers-ASCOT-1980 field study provided a valuable contribution to the data set for the analysis of conditions necessary for establishing valley drainage flow. Sensor calibrations, which have been redetermined after the study program, have been provided to NCAR for the conversion of the raw data to engineering units. Further analysis of the data will proceed upon completion of the archival process.

Analysis of the data acquired at the PNL is also in progress.

Reference

Brock, F. V. and P. K. Govind. 1977. "Portable Automated Mesonet in Operation." J. Appl. Meterol. 16:299-310.

Optical Properties of Mt. St. Helens Ash Over Eastern Washington

N. S. Laulainen and A. J. Alkezweeny

Introduction

Considerable volcanic ash was deposited on the ground in Eastern Washington as a result of the May 18, 1980, eruption of Mt. St. Helens. Much of this ash is very fine and, when dry, is easily resuspended in the atmosphere. During late May and early June, numerous dust devils were observed. These dust devils appeared to be one of the primary mechanisms for vertical transport and mixing of St. Helens ash from the surface.

It has been conjectured that volcanic ash or other aerosol particles originating from volcanic eruptions may cause a shift in the heat balance at the earth's surface through redistribution of solar radiation in the atmosphere, and, perhaps thereby, lead to a cooling. The actual effects of volcanic aerosol depend upon the optical properties of the aerosol particles. During June 1980, several flights were made with the Pacific Northwest Laboratory (PNL) Cessna-411 research aircraft equipped with aerosol and solar radiation instrumentation. A summary of the experiments is described in this report.

Experiments

Instrumentation used during the experiments is shown in Table 1.3, and summary of the flights is given in Table 1.4. One of the goals of the flights was to characterize the optical, chemical and physical properties of the aerosol over Eastern Washington after the May 18 eruption. A second goal was to examine the effect of the aerosol particles on shortwave

Table 1.3. Cessna-411 Instrumentation Used During the June 1980 Eastern Washington Measurements of Aerosol Optical Properties and Solar Radiation

Measurement Type	Instrument	Manufacturer Model	Comment
Particles			
Total particle concentration	Aitken Nuclei Counter	General Electric/ CNC-II	
Aerosol light scattering	Interating Nephelometer	MRI/Model 1560	0 - 1 x 10^{-4} m^{-1} scale
Particle Size Distribution	Forward Scattering Spectrometer	PMS/Model FSSP-100	1 - 7.5 μm range
Aerosol light absorption	Filter sampler		0.4 and 0.8 μm pore size nuclepore filters
Particle composition	High Volume Filter Sampler	Staplex	IPC or Teflon coated fiber glass filter
Radiation			
Total Shortwave	Silicon cell pyranometer	Licor/LI-200S	
Spectral Shortwave	Modified Silicon-cell pyranometer	Licor/LI-200S	Interference filters at 429, 550, 648, 853, and 990 nm, respectively.
Ultraviolet	uv radiometer	Eppley/TUVR	
Infrared/temperature	ir radiometer	Barnes/PRT-5	
State			
Altitude	pressure transducer	Metrodata/M8	
Temperature		Metrodata/M8	
Dew Point	dew cell	EG&G/Cambridge	
Coordinates	VLF System	GNS	

radiative transfer in the planetary boundary layer (up to about 5000 to 6000 ft). Finally, the interaction/redistribution of shortwave radiation by isolated cumulus clouds (or in some cases cloud streets) was examined through flights above, through, and below clouds. The in-cloud penetrations were made primarily to obtain cloud droplet size distributions. Incident solar radiation was also measured in-cloud.

Data collected from these flights are being analyzed. Aerosol concentrations and size distributions are compared to aerosol light scattering and light absorption measurements. Vertical profiles of aerosol light scattering and shortwave radiation are derived to evaluate the redistribution of insolation. Radiation transfer through isolated cumulus clouds is studied. These results will be described in a subsequent report.

Table 1.4. Cessna-411 Flights During the June 1980 Eastern Washington Aerosol/Radiation Experiments

Date	Time (PDT)	Location	Comments
6-2	1435-1531	Tri-Cities, WA	Vertical profile to 11,000 ft; cloud base 7800 ft.
6-4	1246-1459	Tri-Cities, WA	Vertical profile to 10,000 ft; scattered Cu/haze/radiation
6-6	1257-1525	Tri-Cities, WA Pasco-Okanogan-Pasco	Vertical profile to 10,500 ft. Transects across ash deposition track at 4500 ft and 5500 ft, respectively.
6-10	1111-1455	Tri-Cities, WA Royal Slope-Moses Lake-Ephrata	Vertical profile to 12,500 ft. Box pattern at 2500 ft.
6-11	0901-1157	Yakima-Wenatchee Royal Slope-Moses Lake-Ephrata	Transect across ash deposition track. Box pattern at 2500 ft.
6-17	1134-1531	Tri-Cities, WA Hanford/Rattlesnake Mt. Hanford - Mt. Adams	Vertical profile to 10,500 ft. Cloud/haze/radiation at different levels. Along ash deposition track (south edge).
6-24	1058-1336	Tri-Cities, WA Hanford/Rattlesnake Mt.	Vertical profile to 10,000 ft. Cloud/haze/radiation at different levels.
6-27	0839-1205	Hanford	Vertical profile to 12,000 ft. Cloud/haze/radiation.

Ash Loading and Insolation at Hanford, Washington, During and After the Eruption of Mt. St. Helens

N. S. Laulainen

Abstract

The effects of volcanic ash suspended in the atmosphere on the incident solar radiation was monitored at the Hanford Meteorological Station (HMS) subsequent to the major eruption of Mt. St. Helens on May 18, 1980. Passage of the ash plume over Hanford caused a very dramatic decrease of solar radiation intensity to zero. Visibility was reduced to less than 1 km, as great quantities of ash fell out of the plume onto the ground. Ash loading in the atmosphere remained quite high for several days following the eruption, primarily as a result of resuspension from the surface. Visibilities remained low (2 to 8 km) during this period. Estimates of atmospheric turbidity were made from the ratio of diffuse-to-direct solar radiation; these turbidities were further used to estimate extinction along a horizontal path, a quantity that can be related to visibility. Comparison of observed and estimated visibilities was quite good, in spite of the rather coarse approximations used in the estimates. Atmospheric clarity and visibility improved to near pre-eruption conditions following a period of rain showers. The diffuse-to-direct ratio of solar radiation provided a useful index for estimating volcanic ash loading of the atmosphere.

Introduction

Major volcanic eruptions, although infrequent, have injected considerable quantities of dust and ash into the atmosphere. Volcanic ash penetrating into the stratosphere may remain suspended for several years. Such dust layers have the potential to alter climate by redistribution of solar radiation reaching the earth's surface. The eruption of Mt. St. Helens on May 18, 1980, with its associated massive ash plume spread across the United States, was of sufficient magnitude to be seriously studied for possible climate and weather modification. The eruption has been documented better than any other in historical times by means of satellite images, atmospheric and surface dust collections for analysis of chemical and optical properties, and, in certain locations, solar radiation measurements.

Pacific Northwest Laboratory (PNL) has a continuing program of monitoring insolation and atmospheric turbidity in addition to other meteorological parameters at the Hanford Meteorological Station (HMS). Insolation and turbidity measurements are carried out routinely at the Rattlesnake Mountain Observatory (RMO). These measurement programs have been used for insolation assessment for solar energy applications and for research into the optical properties of atmospheric hazes and clouds and their effects on the redistribution of solar radiation received at the earth's surface.

This paper describes observations of insolation before and after the May 18, 1980, eruption of Mt. St. Helens. The results inferred from the insolation records during the time period May 16-31, 1980, are based on an empirical relationship between the ratio of diffuse-to-direct solar radiation and atmospheric turbidity (aerosol optical depth) at 550 nm wavelength. This relationship was derived from insolation and turbidity measurements obtained from an intensive experiment conducted during September and October 1979 (Michalsky et al. 1979). Turbidities derived from the diffuse-to-direct ratio are used to estimate visibilities, which are then compared to observed visibilities.

Observational

King (1979) and King and Herman (1979) have defined the ratio of diffuse-to-direct solar radiation flux as

$$\Phi = \frac{\mu_0 F^-}{(G - F^-)} \qquad (1)$$

where G = measured global solar radiation flux,
F^- = measured downward component of diffuse solar radiation flux
$\mu_0 = \cos Z$
Z = solar zenith angle

They have further shown that Φ is sensitive to turbidity (aerosol optical depth), ground albedo and the light absorption index of atmospheric particles.

An empirical relationship between the diffuse-to-direct ratio, Φ, as defined by Equation 1 and atmospheric turbidity (aerosol optical depth), τ, at a wavelength of 550 nm, was derived from insolation and turbidity measurements made during September/October 1979 at HMS and RMO (Michalsky et al. 1979). Instrumentation consisted of Eppley precision spectral pyranometers (used for calibration) and Lambda silicon cell pyranometers, each equipped with a motorized shadow band that occluded the direct solar beam every 5 minutes (Wesley 1975). Operating in this manner, the silicon cell pyranometers provided direct values for the global solar radiation, G, and the downward component of diffuse solar radiation, F^-. Since both G and F^- were measured with the same instrument and since G and F^- also occur only in a ratio, no absolute values of solar radiation were required. Multi-wavelengths sunphotometers were used to determine atmospheric turbidities. The results of the 1979 study are shown in Figure 1.17 for a variety of solar zenith angles and turbidities.

Two curves are shown in Figure 1.17. The dashed curve represents a least squares fit to a limited set of data points ($\tau < 0.22$) while the solid curve is a least squares fit to all data, including a dust storm event on October 8, 1979 (not shown). The correlation coefficients of the fits are better than 0.97, indicating an excellent correlation between Φ and τ. For the purposes of this study, the relationship derived from all the data is used:

$$\Phi = 0.52\,\tau + 0.014 \qquad (2)$$

From measurements of Φ during cloud-free sky conditions, estimates of τ may be obtained from Equation 2.

Use of Equation 2 as a turbidity estimator implicitly assumes that the aerosol size distributions during the present study period were similar to those from which Equation 2 was derived (King 1979). Following turbidity conditions (e.g., $\tau < 0.1$), turbidity measurements at HMS since 1974 indicate that size distributions of atmospheric haze are indeed quite similar. High turbidity conditions (e.g., $\tau > 0.4$) have occurred usually during dust storm events, where aerosol-size distributions are dominated by coarse particles typically larger than 1 μm. Comparison of particle size distributions measured at Hanford during dust storms and suspended volcanic ash after the May 18 eruption indicated that the latter distributions had a larger fraction of mass in the 0.5 to 1 μm size range. The influence of this size difference on the relationship between Φ and τ given by Equation 2 is not known at this time, but other evidence indicates that the slope would not change by more than 20 to 30%.

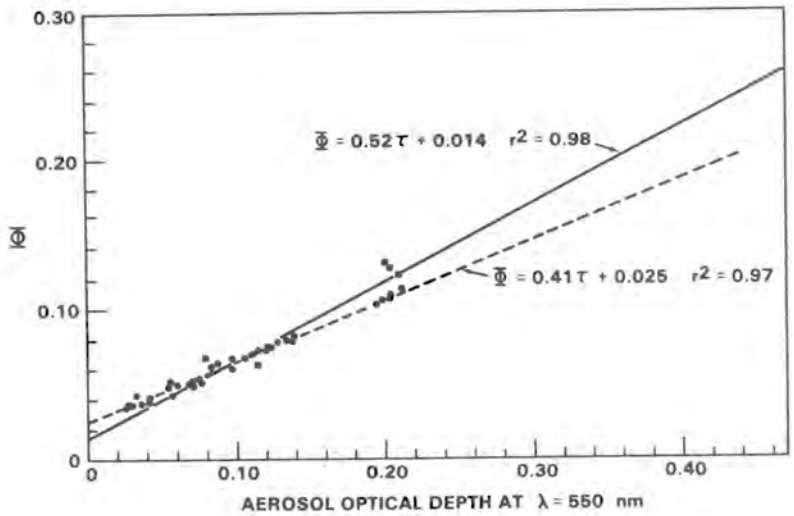

Figure 1.17. Least Squares Fit of the Diffuse-to-Direct Ratio, Φ, Against Measured Aerosol Optical Depth, τ, at λ = 550 nm. Solid curve represents the fit for all data, while the dashed curve excludes data points ($\tau > 0.6$) from a dust storm event.

Examples of the insolation records during the time period of May 16-31, 1980, are shown in Figures 1.18-1.22 for May 16, 18, 19, 20, and 31, respectively. Excepting May 16 and 31, which were clear, cloud interference (e.g., cirrus, altocumulus or fair weather cumulus) presented a severe problem in evaluating the diffuse-to-direct ratios. Only those portions of the charts where cloud effects were thought to be minimized were used in obtaining Φ. In some cases, the National Oceanographic and

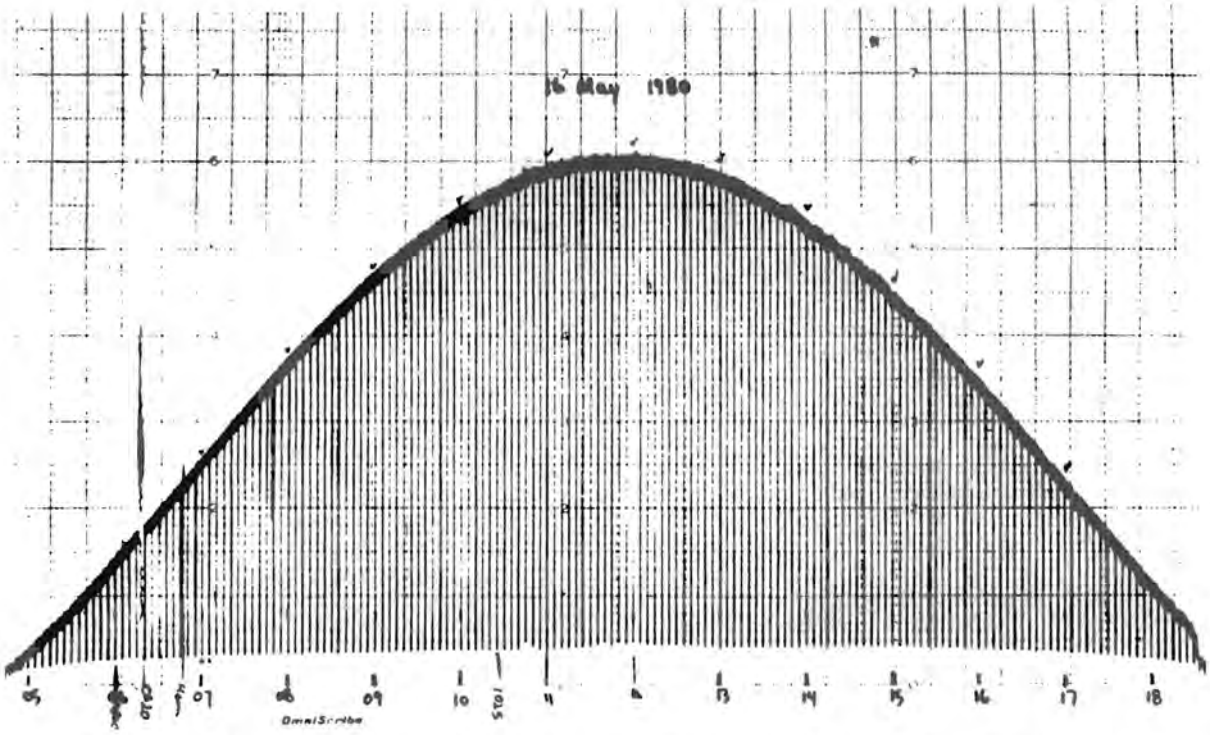

Figure 1.18. Global and Diffuse Solar Radiation Records for Friday, May 16, 1980, for Clear, Cloud Free Skies

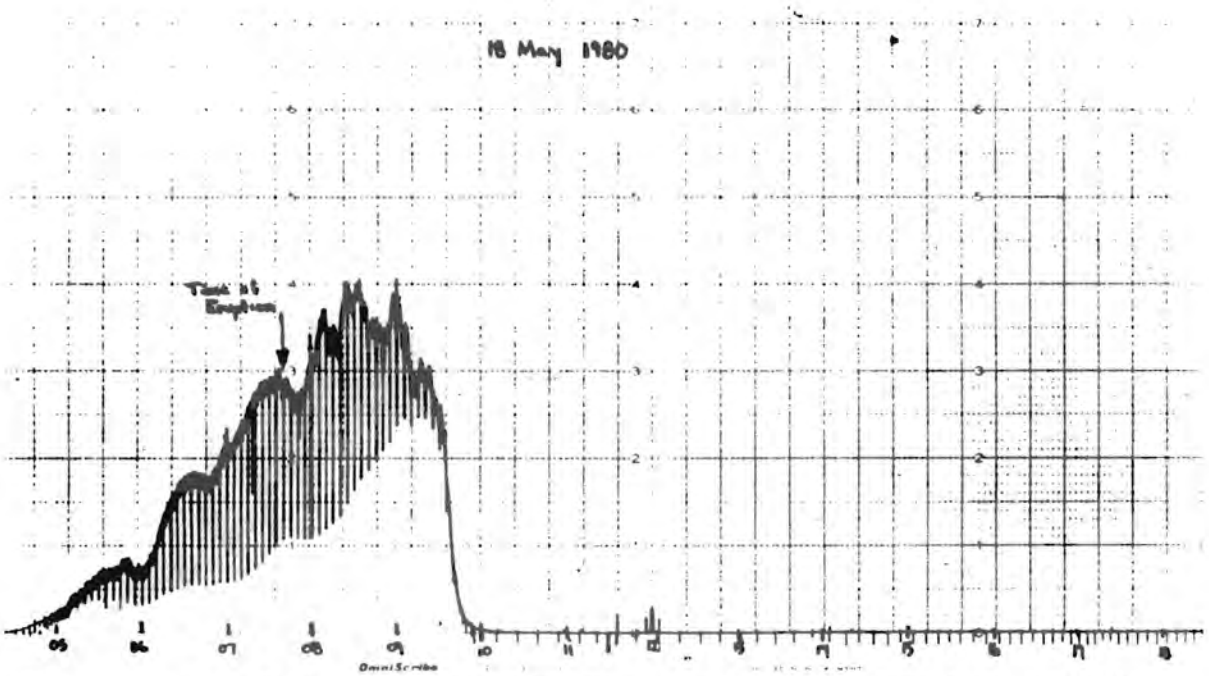

Figure 1.19. Insolation Record for Sunday, May 18, 1980, Showing Early Morning Cirro-Stratus Clouds and the Abrupt Decrease of Insolation to Zero after 0930 PST

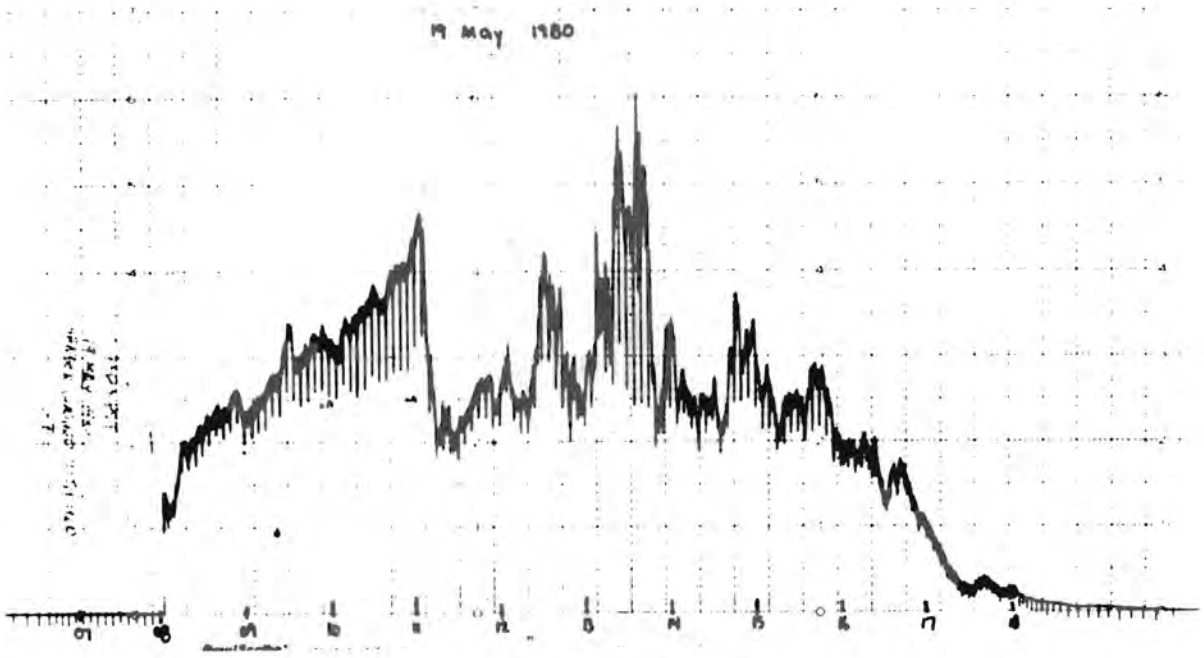

Figure 1.20. Insolation Record for Monday, May 19, 1980, Showing Not Only Cloudiness But Also Highly Turbid Air Resulting in a Large Diffuse Component

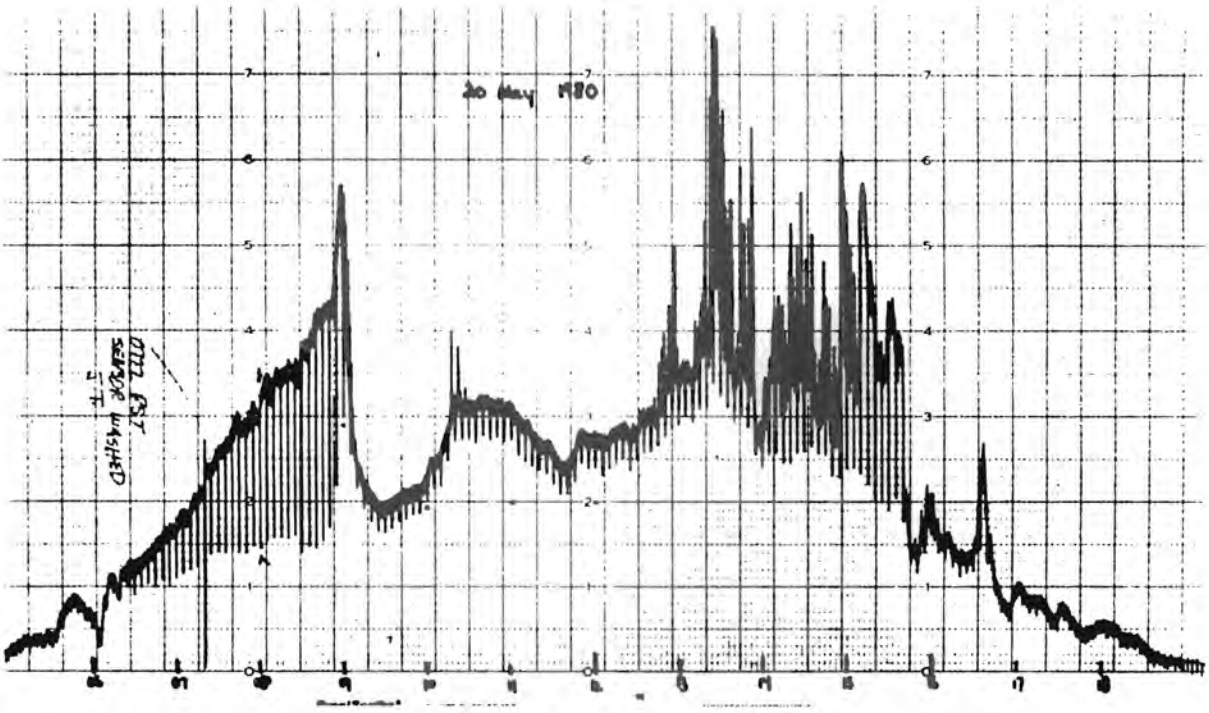

Figure 1.21. Insolation Record for Tuesday, May 20, 1980, Showing a Continued Large Diffuse Component

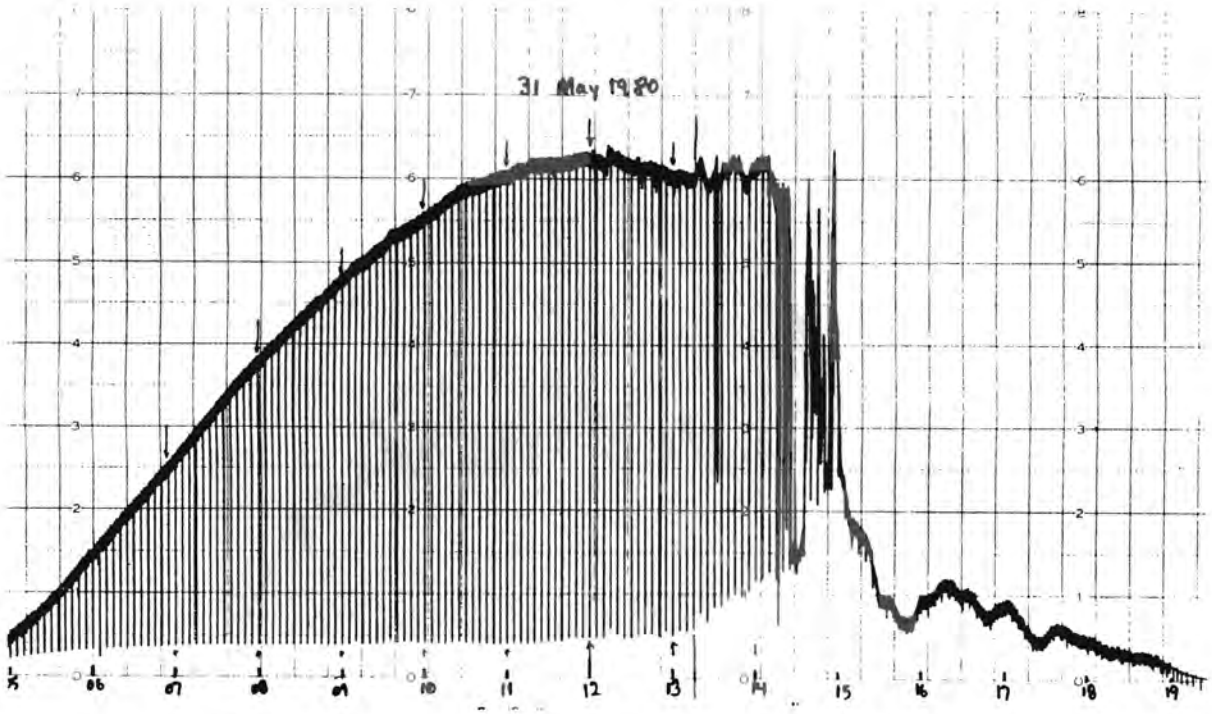

Figure 1.22. Insolation Record for Saturday, May 31, 1980, Showing Diffuse Component at Nearly Normal Values

Atmospheric Administration (NOAA) weather satellite images were useful in selecting appropriate portions. Cloud effects would tend to increase ϕ and hence to overestimate the turbidity.

The record for May 16 (Figure 1.18), two days prior to the eruption, is typical of clear, low haze conditions. Figure 1.19 shows the progression of solar radiation on May 18. Scattered to broken cirrus clouds were reported over HMS prior to the arrival of the ash plume. A dramatic increase in diffuse radiation is seen after ~0830 PST, approximately 1 hour after the eruption. Shortly after 0900 PST, total insolation began to decrease and then sharply decreased around 0930 PST. By 1000 PST insolation was essentially zero and remained zero for the rest of the day. Ash fall began around 1100 PST. Prior to ash fallout, visibilities were in excess of 24 km but rapidly deteriorated to ~2 km after 1100 PST. A surface accumulation of 2.5 mm of ash was recorded at HMS. Satellite (GOES-West) images of the volcanic plume approximately 2 hours and 7.5 hours after eruption are shown in Figures 1.23 and 1.24, respectively. In these images, the eastward motion and lateral spread of the plume is clearly evident.

On May 19, visibility continued to be very low (~2 km) for most of the day because of the fine volcanic ash still suspended in the atmosphere. Although surface observations of cloud cover were difficult to make during this period, a satellite image 24 hours after eruption clearly showed cirrus bands over most of Eastern Washington (Figure 1.25). Diffuse-to-direct ratios were quite large (Figure 1.20), very probably as a result of the cirrus. Mass loadings of suspended ash on

Figure 1.23. GOES-West Satellite Image Showing that the Volcanic Plume, Approximately 2 Hours after the Eruption of Mt. St. Helens, has Spread out over Central and Eastern Washington

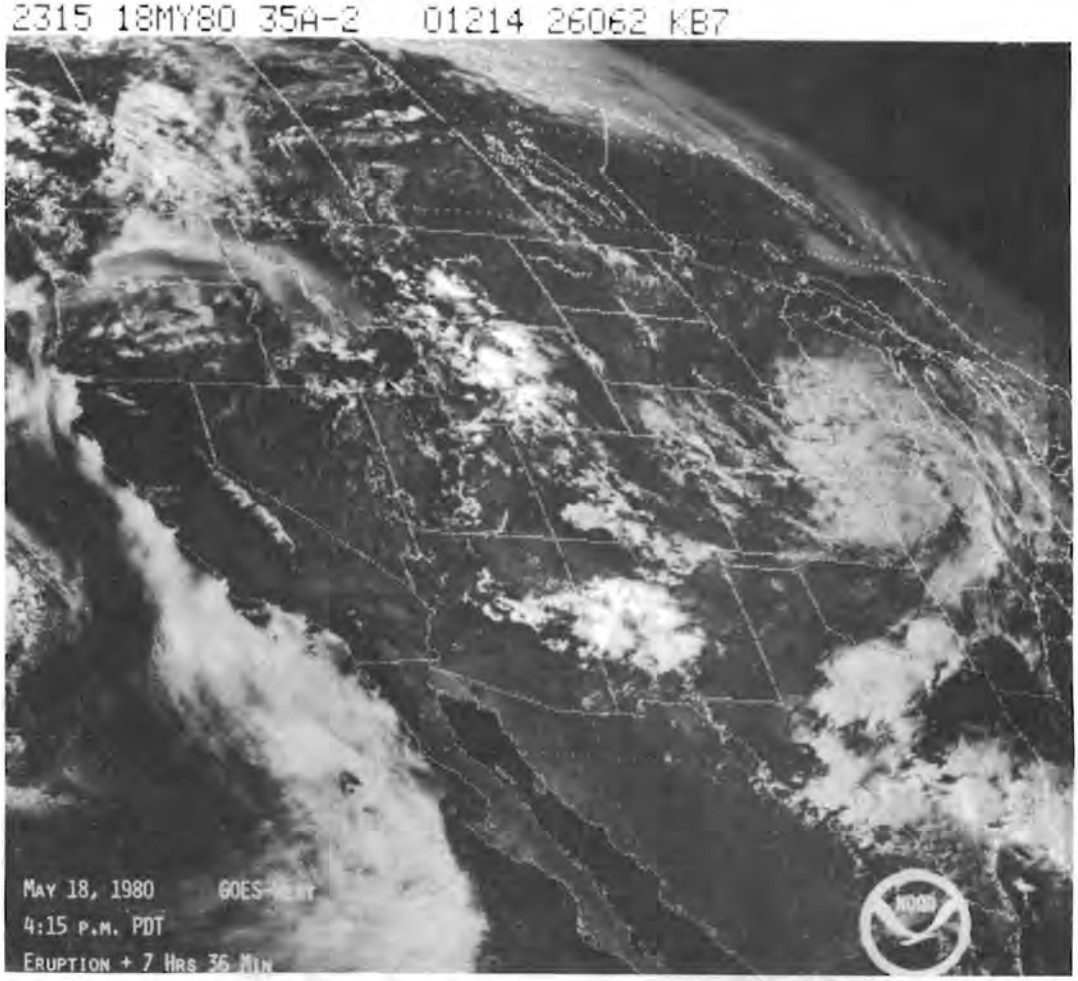

Figure 1.24. GOES-West Satellite Image Showing the Volcanic Plume Spreading into Western Montana Approximately 7.5 Hours after Eruption

the southern boundary of the Hanford Site ranged between 150 to 600 $\mu g/m^3$.

Visibilities improved only very slowly during the next 4 or 5 days. After May 27, conditions dramatically improved as a result of a substantial precipitation (~2 cm). Mass loading decreased by a factor of 100 to near normal values of 1 to 6 $\mu g/m^3$. By May 31, visibilities and diffuse-to-direct insolation values also had returned to near normal values (Figure 1.22).

Results

The results of the diffuse-to-direct ratio determinations and turbidities at 550 nm estimated from these ratios (assuming that Equation 2 is valid for suspended volcanic ash) are shown in Table 1.5. In many cases, as pointed out earlier, the values are probably overestimated because of cirrus or other cloud contamination. Table 1.5 also shows a comparison of visibilities derived from the diffuse-to-direct ratio through the turbidity.

The chain of reasoning leading to an estimate of visibility from Φ proceeds in the following manner. Visibility depends upon extinction along a horizontal path while turbidity depends upon extinction integrated along a vertical path. If it is assumed that the aerosol particles are well mixed up to some height, H, with a negligible amount above H, then the mean extinction coefficient in the mixed layer is

$$b_{ext} = \frac{\tau}{H} \qquad (3)$$

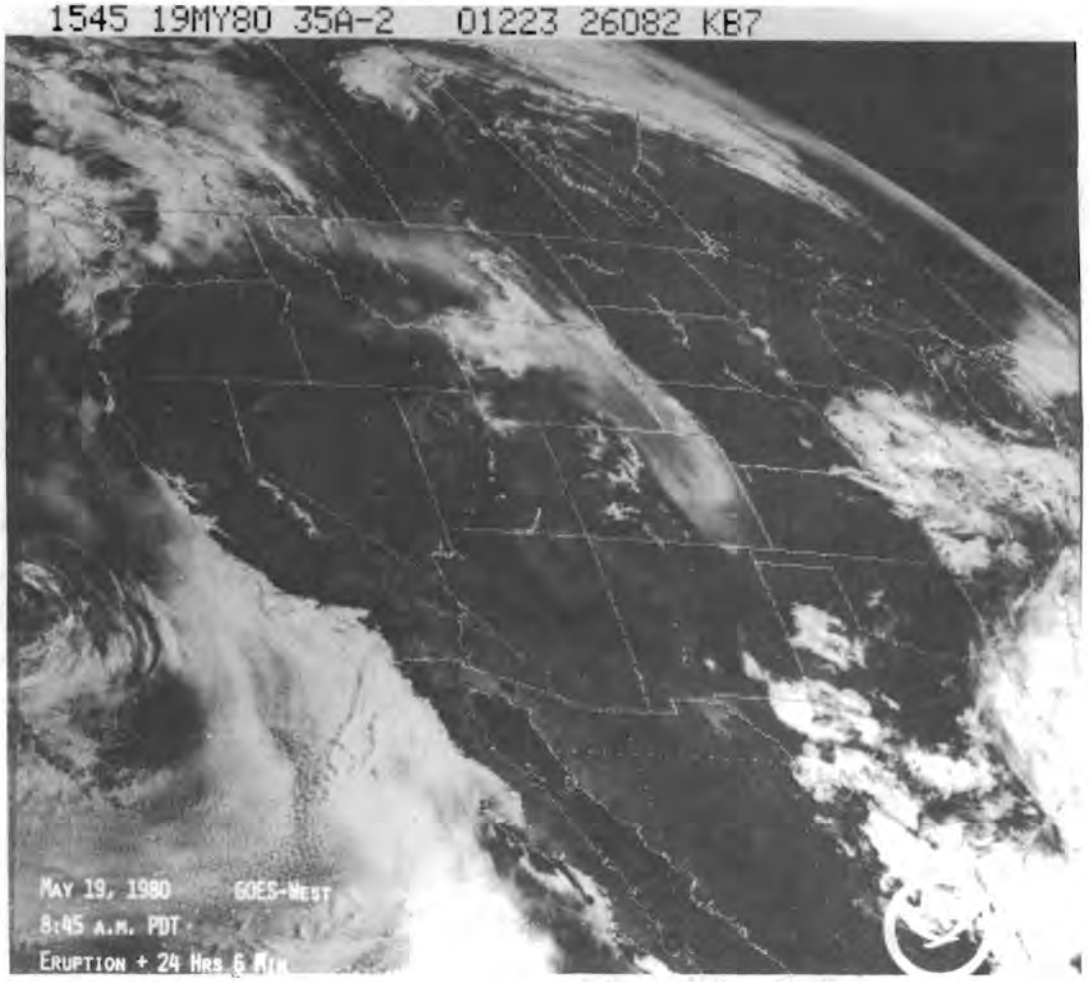

Figure 1.25. GOES-West Satellite Image Showing the Volcanic Plume Approximately 24 Hours after Eruption over Montana, Wyoming and Eastern Colorado

where Φ is derived from Equation 1. The Koschmeider formula (Middleton 1963) relates the visual range to the effective atmospheric extinction coefficient along the line of sight by

$$V = \frac{K}{b_{ext}} \qquad (4)$$

The constant K, which is related to the threshold contrast, has been frequently set at a value of 3.9 although other values between 1.7 and 4 have been suggested (see Griffing 1980 for a discussion). For this study, a value of 3 is arbitrarily used. Combining Equations 3 and 4, the expression

$$V = \frac{3H}{\tau} \qquad (5)$$

is easily found. From aircraft soundings conducted during June 1980, a value of H between 1 and 2 km was frequently observed in this work, and H = 1 km was adopted to a first approximation.

Table 1.5 shows that the comparison between the visual range (visibility) derived from Equation 5 is generally much better than might be expected considering the number of approximations used in proceeding from the measurement of Φ to the estimate of V. Only on May 18 and 19 were the estimated visibilities poor in comparison to the observations. On May 18 the plume was overhead with very little ash between it and the surface. Therefore, vertical extinction could not be easily related to horizontal extinction. When the ash was falling, the insolation was zero and conse-

Table 1.5. Measured Diffuse-to-Direct Solar Radiation Ratio, Turbidity at 550 nm and Estimated/Observed Visibilities at Hanford Meteorological Station for Various Days Before and After the Mt. St. Helens Eruption of 18 May 1980

Date	Φ	τ' (550)	V*(km)	Vo(km)	Comment
16 May 80 a	0.063	0.10	30	24+	Clear sky, light haze
p	0.071	0.11	27	24+	
17 May 80 a	0.11	0.19	16	24+	CS (1.0)
p	.095	.16	19	24+	Scattered Ci (0.1)
18 May 80 8	0.24	0.44	6.9		Scattered Ci (0.3)
9	0.59	1.11	2.7		Broken Ci (0.6)
10	3.2	6.1	0.5		CS, Volcanic plume (1.0)
19 May 80 a	3.2	6.2	0.5	2.7	Ci (1.0?), very dusty, hazy
20 May 80 a	0.49	0.92	3.3	3.6	Ci, (0.8) Continued hazy
21 May 80 a	0.28	0.51	5.9	7.5	Scattered AC (0.4)
22 May 80 9	0.46	0.88	3.4	2.7	Broken Cu (0.6)
10	0.29	0.53	5.6	6.4	Scattered Cu (0.2)
11/12	0.23	0.42	7.2	16	Scattered Cu (0.4)
23 May 80 a	0.14	0.24	12.4	24+	Ci, AC (0.8)
28 May 80 a	0.185	0.33	9.1	24+	Scattered Ci, AC, Cu (0.4)
30 May 80 p	0.15	0.26	11.5	24+	Scattered Ci, AC, Cu (0.5)
31 May 80 a	0.067	0.10	29	24+	Clear sky, light haze
p	0.082	0.13	23	24+	Scattered Ci (0.5)

$\tau' = 1.92\ \Phi - 0.027$
$V^* = 3\ H/\tau$, $H \simeq 1$ km

quently no estimate for Φ could be made. On both May 18 and 19, cirrus clouds were probably present in sufficient quantity to invalidate the use of Equation 2.

A number of problems with the ash fallout continue to occur. Ash from subsequent eruptions (e.g., the July 22 eruption) and ash resuspended from the surface will continue to produce significant atmospheric ash loadings, especially in those areas where ash fall was the greatest. Continued observations of insolation and turbidity will be required to document any significant changes in atmospheric transparency as a result of the Mount St. Helens eruption.

Conclusions

The insolation and turbidity monitoring program at HMS has provided a method of

estimating ash loading in the atmosphere after the May 18 eruption of Mt. St. Helens. Comparisons of visibilities derived from the diffuse-to-direct insolation ratio with those observed at HMS were generally good, in spite of the rather coarse approximations and assumptions made.

Additional work relating insolation and turbidity at Hanford over more varied conditions than those encountered during the 1979 study, from which Equation 2 was derived, are required. Documentation of subsequent eruptions of Mount St. Helens resulting in ash fallout over Hanford and/or resuspension of ash already present will continue. Hopefully, these studies may provide insights into understanding radiative effects of volcanic aerosol and therefore the effects of volcanic aerosol on climate modification.

References

King, M. D. 1979. "Determination of Ground Albedo and the Index of Absorption of Atmospheric Particulates by Remote Sensing, Part 2, Application." J. Atmos. Sci. 36:1072-83.

King, M. D. and B. M. Herman. 1979. "Determination of Ground Albedo and the Index of Absorption of Atmospheric Particles by Remote Sensing, Part 1, Theory." J. Atmos. Sci. 36:163-173.

Michalsky, J. J., N. S. Laulainen, G. M. Stokes and E. W. Kleckner. 1979. "Differential Turbidity in an Arid Environment. Abstract Digest of Workshop on Atmospheric Aerosols--Their Formation, Optical Properties and Effects." Paper presented November 6-8, 1979, at the Institute for Atmospheric Optics and Remote Sensing, Baltimore, Maryland.

Wesley, M. L. 1975. "Measurement of Atmospheric Turbidity in an Arc Downwind of St. Louis." Radiological and Environmental Research Division Annual Report--Atmospheric Physics, ANL-75-60, Part IV, pp. 28-30, Argonne National Laboratory, Argonne, Illinois.

Middleton, W. E. K. 1952. Vision Through the Atmosphere, University of Toronto Press.

Griffing, G. W. 1980. "Relationships Between the Prevailing Visibility, Nephelometer Scattering Coefficient and Sunphotometer Turbidity Coefficient." Atmos. Environ. 14:577-584.

• Pollutant Transformation in the Atmosphere

Objectives of this study are:

- Measuring chemical transformation rates of polycyclic aromatic hydrocarbons and other organic compounds emitted by fossil-fueled power plants.
- Correlating transformation rates with distance from the source, ambient temperature, light intensity and concentrations of sulfur dioxide, nitrogen oxides, and ozone.
- Evaluating the results of laboratory studies on discrete reaction steps in the overall transformation processes.

Transformation of Energy-Related Pollutants

D. R. Kalkwarf and K. B. Olsen

Chemical transformations of polycyclic aromatic hydrocarbons (PAHs) in power plant plumes were evaluated under both simulated and field conditions. Laboratory experiments showed that several PAHs, adsorbed on fly ash or pure-silica surfaces, reacted with sunlight-irradiated SO_2 gas to form a variety of products, and methods for their characterization were developed. Preliminary tests did not indicate significant differences between the mutagenicities of these products and those of the parent PAHs. Continued evaluation of PAH transformation in stack plumes from the power plants at Colstrip, Montana, showed that PAH concentrations under plant start-up conditions were substantially higher than those found under steady-state conditions, and were poorly correlated with distance from the stacks.

The purpose of this study is to measure the chemical transformation rates of polycyclic aromatic hydrocarbons (PAHs) and other undesirable organic compounds emitted by fuel-fired power plants as these compounds are transported through the atmosphere. This information is needed to more accurately assess the potential environmental impact of such plants. There is less concern for compounds shown to degrade rapidly into relatively innocuous products. Conversely, however, any compounds that are transformed into more toxic and/or carcinogenic products should be identified so that procedures for limiting their emissions can be instituted.

Laboratory experiments performed this year showed that fluoranthene, pyrene, chrysene, and benzo[a]pyrene adsorbed on fly ash or pure-silica surfaces reacted with sunlight-irradiated SO_2 gas to form a variety of products. The mutagenicities of the product mixtures tested so far, however, did not differ significantly from those of the parent compounds. Air sampling by helicopter in the stack plume from the power plants at Colstrip, Montana, was continued this year to test for anticipated changes in the plume composition following plant start-up. Under these conditions PAH concentrations were substantially higher than those found under steady-state conditions and were poorly correlated with distance from the stacks.

Laboratory experiments were directed toward developing methods for the chemical analysis of stack-plume samples and identifying possible mechanisms for chemical transformations in a plume. Since only small amounts of PAH-transformation products can be expected in the Colstrip plumes, the larger amounts required for methods development were generated by chemically transforming PAHs. This was done in the laboratory under conditions that are qualitatively similar to, but more intensive than, those that occur in a plume.

As an example, several PAHs adsorbed on pure-silica surfaces were found to be transformed in sunlight-irradiated SO_2 gas; the extent of these transformations are shown in Figure 1.26. Irradiation of PAH-coated fly ash in atmospheres of pure SO_2 produced almost identical results. The products were separable by high-performance, thin-layer chromatography (HPTLC) on silica gel using 2:1 n-propanol: concentrated NH_4OH solution as the mobile phase. The variety of products that can be visualized by fluorescent light is illustrated in Figure 1.27. Blackened zones indicate products found to contain substantial amounts of sulfur by X-ray fluorescence measurements. The average degree of sulfurization was calculated to be four moles of sulfur per mole of PAH-transformation product. Preliminary tests of these product mixtures on the Ames TA-100 strain of Salmonella typhimurium indicated that their mutagenicities were not significantly different from those of the parent PAHs. We found that fluoranthene, pyrene, and their photosulfurization products were nonmutagenic, whereas chrysene and its photosulfurization products were equally mutagenic. Similar tests on benzo[a]pyrene and its products have not been completed. Although the chemical structures of the products are currently unknown, their presence in plume samples can now be identified by their R_f values and their characteristic fluorescence emission spectra on HPTLC plates.

Experimental evidence indicates that the mechanism of these photosulfurization reactions involves formation of triplet state SO_2, which then abstracts a hydrogen atom from the PAH. No reaction was observed either between the PAHs and SO_2 in the dark or between then PAHs and pre-illuminated SO_2. Illumination of only the SO_2 component in a reaction vessel loaded with SO_2 and PAH produced the same yield as did illumination of both the SO_2 and PAH components simultaneously. In addition, the hypothesized hydrogen-abstraction product, a PAH-free radical, was observed by electron spin resonance spectrometry of the reaction products in atmospheres of pure SO_2 gas. A spectrum, typical of that for any of the four PAHs cited above, is shown in Figure 1.28. Unfortunately, any hyperfine structure indicative of the radical's structure was lost, presumably because of exchange narrowing. Immediately upon contracting the radical with oxygen, the spectrum disappeared.

In view of the probable mechanism outlined above and the large rate constants reported for quenching of $^3SO_2$ by O_2 and N_2 ($k = 9 \times 10^7$ ℓ mol^{-1} s^{-1}, Sidebottom et al. 1972), it is likely that the rate of PAH photosulfurization will decrease rapidly with distance from the stacks. An exception might arise, however, if SO_2 was adsorbed tenaciously on the PAH-coated fly ash and then illuminated. That possibility is currently being explored at PNL.

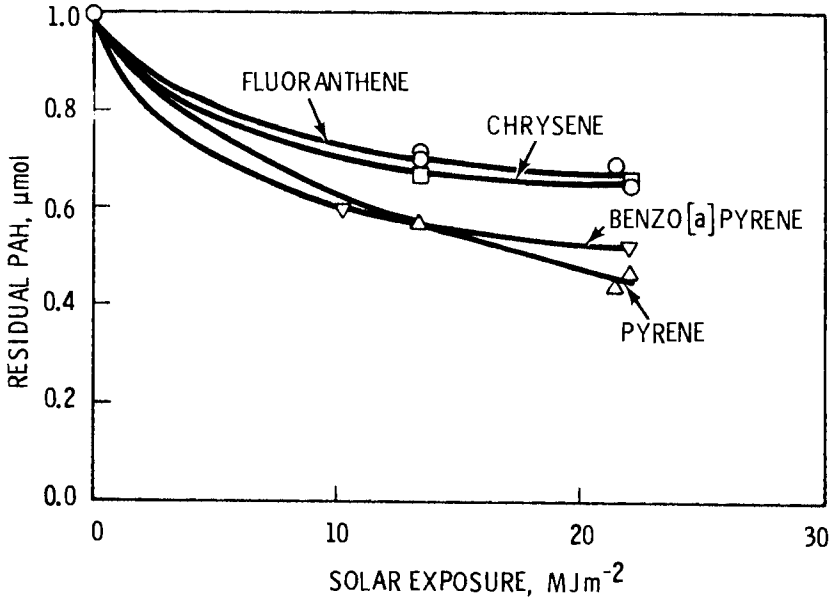

Figure 1.26. Chemical Degradation of Polycyclic Aromatic Hydrocarbons on Quartz Surfaces Exposed to a Solar-Irradiated Atmosphere of Pure SO_2 Gas

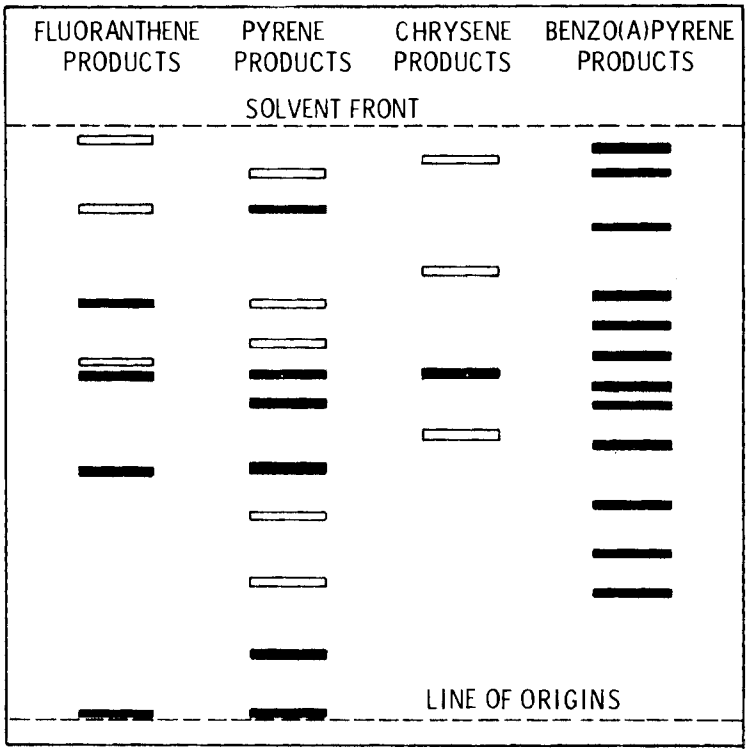

Figure 1.27. Thin-Layer Chromatographic Separations on Silica Gel of Products from Reactions of Various Polycyclic Aromatic Hydrocarbons with Solar-Irradiated SO_2 Gas. Chromatograms were developed with 2:1 n-Propanol: NH_4OH, and sulfur-containing products are indicated by blackened zones.

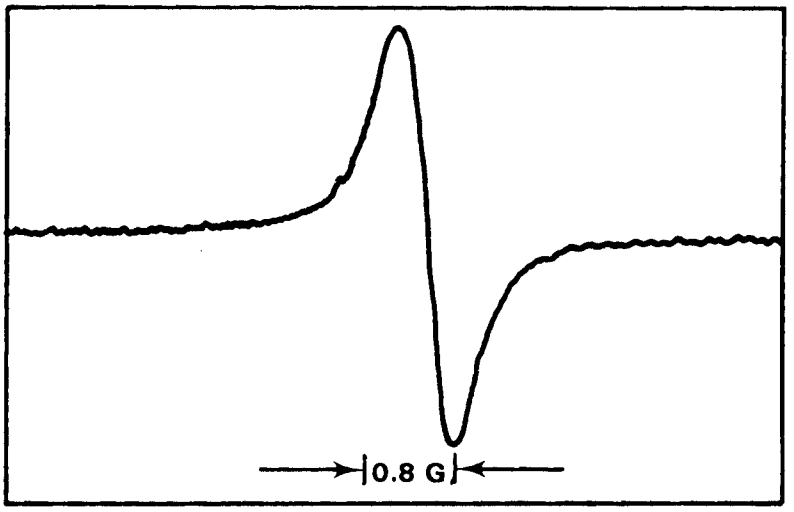

Figure 1.28. ESR Spectrum of Pyrene-Coated Quartz after Photolysis in SO_2 with 8.0×10^4 Jm^{-2} of 254-mm Light

Stack-plume sampling focused on testing for anticipated differences in composition of the Colstrip power-plant plume between start-up and steady-state conditions. Recent examinations of fly ash from a bench-scale coal burner have indicated that more mutagenic combustion products were formed during start-ups or at other times when combustion was incomplete (Kubitschek and Williams 1980). Concentrations of PAHs found at various distances from the Colstrip stacks during a plant start-up this year are listed in Table 1.6. The sampling methods, analytical techniques and comparative data obtained under steady-state conditions have been described previously (Kalkwarf and Garcia 1979 and 1980). Concentrations of fluoranthene, benzo[a]anthracene, perylene and benzo[a]pyrene were found to be 10- to 20-fold greater than those observed under steady-state conditions, although these concentrations were poorly correlated with distance from the stacks. Identification of the polar PAH-derivatives in the sample is being pursued to test their mutagenicities.

Table 1.6. Concentrations of Fly Ash-Bound Polycyclic Aromatic Hydrocarbons in the Atmosphere at Various Distances Downwind from the Colstrip Stacks During Start-up Operations

		Compound, ng/m³								
Date	Distance km	Fluoranthene	Pyrene	Triphenylene	Benzo[a]-anthracene	Chrysene	Benzo[e]-pyrene	Perylene	Benzo[a]-pyrene	Calcium
June 8	-3[a]	<1	<1	<1	<1	<1	<1	<1	<1	90
	1	334	<1	<1	123	<1	<1	<1	<1	2010
	3	278	<1	<1	376	<1	<1	<1	<1	260
	5	<1	<1	<1	162	<1	<1	<1	<1	90
June 9	1	348	<1	<1	386	<1	<1	392	247	4730
	5	32	<1	<1	<1	<1	<1	8	<1	4300
June 10	1	24	<1	<1	524	<1	<1	<1	<1	4040
	2	526	<1	<1	110	<1	<1	803	601	870
	3	2817	<1	<1	1692	<1	<1	404	180	10,860
	5	949	<1	<1	354	<1	<1	659	65	3060

[a]Sample taken upwind from stacks.

References

Kalkwarf, D. R. and S. R. Garcia. 1979. "Pollutant Transformation in the Atmosphere." In Pacific Northwest Laboratory Annual Report for 1978 to the DOE Assistant Secretary for Environment, Part 4, Physical Sciences. PNL-2850, PT4, pp. 1.3-1.5, Pacific Northwest Laboratory, Richland, Washington.

Kalkwarf, D. R. and S. R. Garcia. 1980. "Pollutant Transformation in the Atmosphere." In Pacific Northwest Laboratory Annual Report for 1979 to the DOE Assistant Secretary for Environment, Part 3, Atmospheric Sciences. PNL-3300, PT3, pp. 22-25, Pacific Northwest Laboratory, Richland, Washington.

Kubitschek, H. E. and D. M. Williams. 1980. "Mutagenicity of F17 Ash from a Fluidized-Bed Combustor During Start-Up and Steady Operating Conditions." Mutation Res. 77:287-291.

Sidebottom, H. W., C. C. Badcock, G. E. Jackson, J. G. Calvert, G. W. Reinhardt, and E. K. Damon. 1972. "Photooxidation of Sulfur Dioxide." Environ. Sci. Tech. 6:72-79.

• Atmospheric Carbon Dioxide Abundance - An Archival Study of Spectroscopic Data

Objectives of this study are:

- Determining the current and past abundance of the carbon dioxide in the earth's atmosphere by spectroscopic means.
- Providing independent corroboration of the CO_2 increase that has been observed by other in-situ techniques.
- Extending the knowledge of the total atmospheric CO_2 burden back to a time for which no information now exists.

Atmospheric CO_2 Abundance--An Archival Study of Spectroscopic Data

G. M. Stokes

This article describes progress in a program to determine the atmospheric abundance of carbon dioxide (CO_2). Efforts are directed toward measuring the abundance of CO_2 dating back to the 1890s, using absorption spectra of the sun as the source of data.

Discussion

The relationship between the atmospheric abundance of CO_2 and various anthropogenic factors, most notably fossil fuel burning, has become a matter of great concern. CO_2 has a significant effect on the average temperature of the earth's surface and lower atmospheric layers, largely a result of the gas's large infrared opacity producing a "greenhouse effect." Because of the importance of CO_2 to the energy budget of the atmosphere, it is possible that changes in its abundance could have a major effect on the earth's climate.

In order to understand how man's consumption of fossil fuels could affect climate through changes in the atmospheric CO_2 abundance, it is necessary to understand all the factors that control its atmospheric abundance. Unfortunately, the atmosphere represents a relatively small reservoir of carbon when compared to other reservoirs such as the deep oceans or sedimentary deposits. Therefore, relatively modest changes in these much larger reservoirs can have an overwhelming effect on the atmospheric CO_2 abundance. It is thus not surprising that intense debates continue as to which processes affecting which sources and sinks of carbon control the atmospheric CO_2 abundances.

This interest in changes in atmospheric carbon dioxide (CO_2) abundance has led to a critical evaluation of the existing data that may relate to the history of that abundance. As a result, an attempt is being made to extract the abundance of CO_2 from spectra of the sun that have been accumulated since the 1890s.

As sunlight passes through the earth's atmosphere, the molecules in the atmosphere absorb and scatter the radiation. A substantial fraction of this absorption is caused by the excitation of various energy levels in atmospheric molecules. Absorption of this kind occurs at specific wavelengths and results in what are called absorption lines. The strength of these lines is primarily a function of the properties of the molecule and the amount of the molecule between the observer and the sun. It should therefore be possible to determine the amount of CO_2 in the atmosphere from solar spectra. Such spectroscopic data exist for a period extending back to at least the mid-1890s when Samuel P. Langley began observing and recording the spectrum of the sun with a prism spectrobolograph.

There are several important phases to a project of this kind. First, the existence of old spectral data needs to be established and the actual data then must be recovered from its storage location. This process may be as simple as a review of published literature or may entail searching the archives of major observatories. One collection of data that will be analyzed in the current program was recovered from a cellar at a remote observing site where it had been stored and forgotten for more than 50 years. Once a data set has been located, its potential value to the program needs to be assessed. While the utility of a particular data set may not actually be known until a final carbon dioxide abundance is determined from the data, there are preliminary analyses which can be used to determine if further analysis is warranted.

In the current program our approach has been to develop a plausible reduction technique for each collection of spectral data as a basis for assessing utility of the data. The development of this preliminary reduction plan has the important advantage of forcing an evaluation of the complete process of data reduction of a particular data set as early as possible in the program. For example, much of the data cannot be analyzed without other supplementary data such as molecular constants or special information relating to the circumstances of the observations. The preliminary analysis plan identifies the needs for supplementary data and either the existence of the required data or the possibility of obtaining new data suitable for program requirements.

The final phase of the program is the actual analysis of the individual data sets and their intercomparison to determine the changes in atmospheric carbon dioxide. We will now describe the current status of the program in terms of these three phases: archival investigation, preliminary reduction plan, and analysis.

The emphasis of the archive studies of the past year has been to locate data in the critical 1895-1920 period. Dr. Robert Stokes of Pacific Northwest Laboratory has been trying to locate spectrobolograms that were taken during expeditions to Mt. Wilson by staff members of the Smithsonian Astrophysical Observatory. It now appears that if any of these plates still exist they are most likely to be found in the plate archives of the Mt. Wilson Observatory. This possibility will be pursued in the coming year.

In the course of this search, reports were received of the existence of copies of the plates taken at Mt. Montezuma, Chile, during the Smithsonian Solar Constant program. The originals of these plates were destroyed at the end of the Smithsonian Program, but if copies do exist they may well double the existing data base for the 1920-1950 period. Next year our searches for the 1895-1920 data will continue. We will also attempt to locate further corroborative data for the period 1920-1957. Of particular interest in this regard is Arthur Adel's data, accumulated in Flagstaff, Arizona, in the 1930s. His data represent observations of the sun in a different wavelength region than was covered by the Smithsonian spectrobolograms and thus offer an independent test of the results that will be based on the Smithsonian data set.

The development of reduction methods for the individual data sets has occupied most of the program resources, with particular emphasis being placed on the Smithsonian spectrobolograms. This data set consists of approximately 2000 8- x 24-in. glass plates on which spectra have been recorded in a fashion similar to a chart recorder. Each plate contains two to six solar spectra covering the 0.3 to 2.5 μm wavelength region. Figure 1.29 shows an example of plates. Each of the spectra on the plates was taken through a different amount of the atmosphere. This amount generally varies between two and five times the amount of atmosphere that would be encountered if the sun were observed while directly overhead.

The reduction plan for this data, developed in conjunction with Drs. R. Roosen and R. Angione of San Diego State University, is shown schematically in Figure 1.30. The plan addresses four problems: 1) extraction of the data in a computer-readable form from the plates; 2) characterization of each day's observations on the basis of the spectral and other data; 3) identification of the source of absorption at each wavelength in the spectra; and 4) determination of abundances from the spectra that can be compared with other data. The entire process of turning the Smithsonian spectrobolograms into useful data has involved or will involve the efforts and cooperation of innumerable institutions and government agencies, including NASA's Goddard Space Flight Center, the

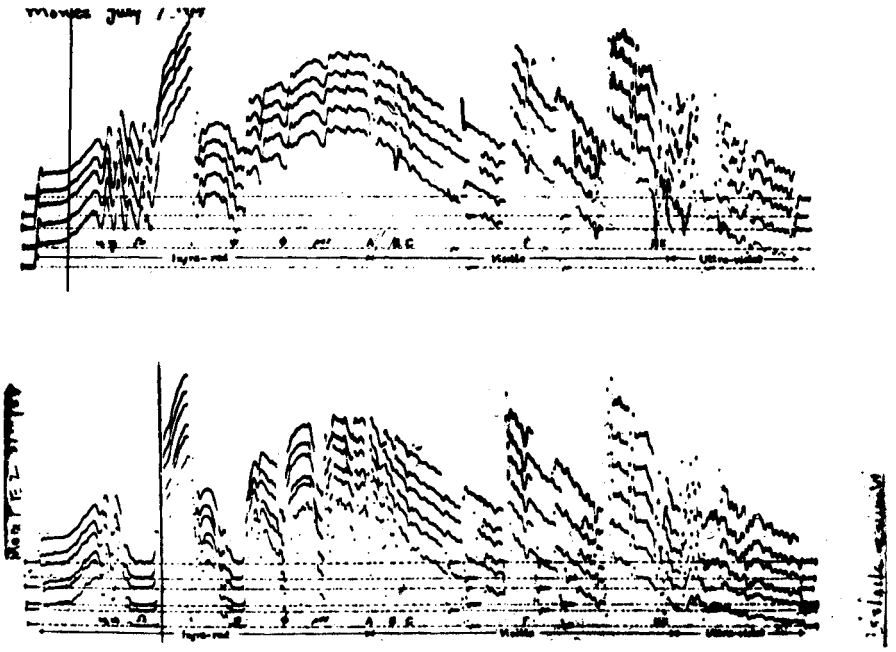

Figure 1.29. Solar Spectra Recorded on Glass Plates, Similar to a Chart Recorder, Containing Two to Six Solar Spectra Covering the 0.3 to 2.5 m Wavelength Region. The original plates measured 8 x 24 inches.

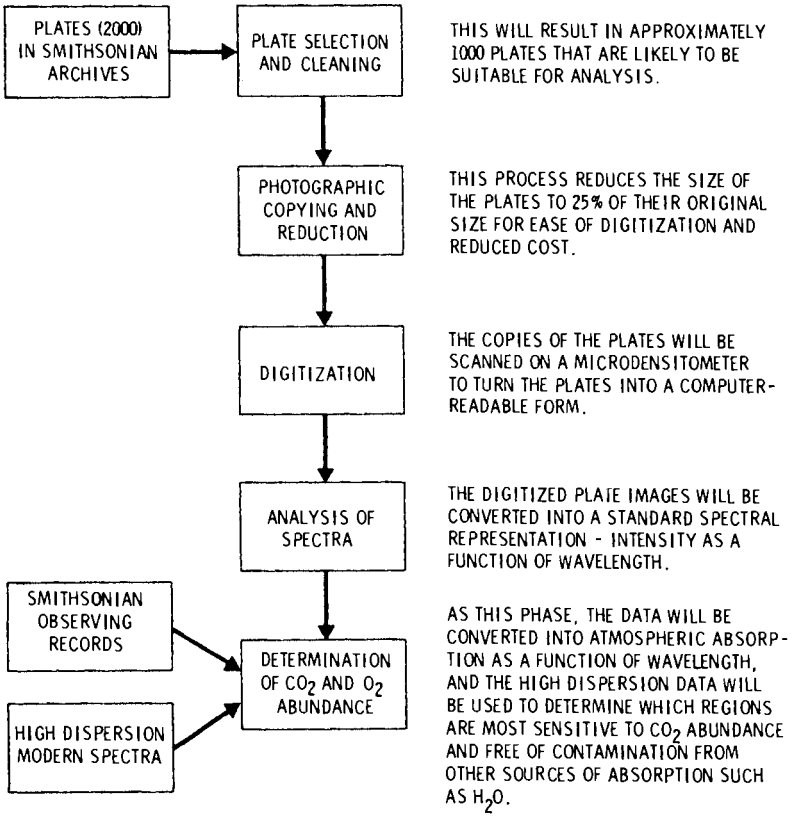

Figure 1.30. Reduction Plan for the Smithsonian Spectrobolograms

Smithsonian Archives, the United States Naval Observatory, and the National Oceanic and Atmospheric Administration.

Several precautions are being taken to guarantee the quality of the analysis of all data sets, including the Smithsonian spectrobolograms. The abundance of molecular oxygen, O_2, is being determined from the same spectral data that are used to analyze the CO_2 abundance. Since the atmospheric abundance of O_2 is not expected to have changed over the period of the study, its abundance can be considered a control. Because most of the data being analyzed have been taken at low spectral resolution, weak lines of other gases such as water may contaminate the lines of CO_2 and O_2 by an unknown amount. Using very high spectral resolution, new data have been accumulated at Kitt Peak National Observatory (KNPO) for the identification of these weak interfering lines.

The data being taken at Kitt Peak National Observatory are central to the final phase of the program, the actual analysis of the data to extract carbon dioxide abundances. At present the Kitt Peak facilities are being used in three important ways.

First, high dispersion solar spectra of the 1.0 to 2.5 micron region are being accumulated on a monthly basis with the Fourier Transform Spectrometer (FTS) at the McMath Solar Telescope. These data are being used to search for seasonal or other systematic effects that might affect a carbon dioxide abundance determination based on an isolated observation such as might be found in many of the various solar atlases. Next, the data are being analyzed to identify sources of atmospheric absorption that may contaminate regions of CO_2 and O_2 absorption. This line identification procedure is based on a nonlinear, least-squares analysis procedure developed by Dr. J. Brault at KPNO. The procedure is being applied to individual lines in the atmospheric (telluric) spectra from which the solar lines have been removed. An example of the success of the procedure is illustrated in Figure 1.31 where the residuals are the difference between the telluric spectrum and the results of the deconvolution. The result of this procedure is a line list which can then be used to identify the extent of contamination of O_2 and CO_2 absorption. Finally, the KPNO FTS can and will be used in conjunction with a long path absorption cell to obtain spectra of CO_2 and O_2 lines under controlled laboratory conditions. This data will allow us to tie the data to a reference scale and provide some absolute calibration for any observed changes in atmospheric CO_2 abundance.

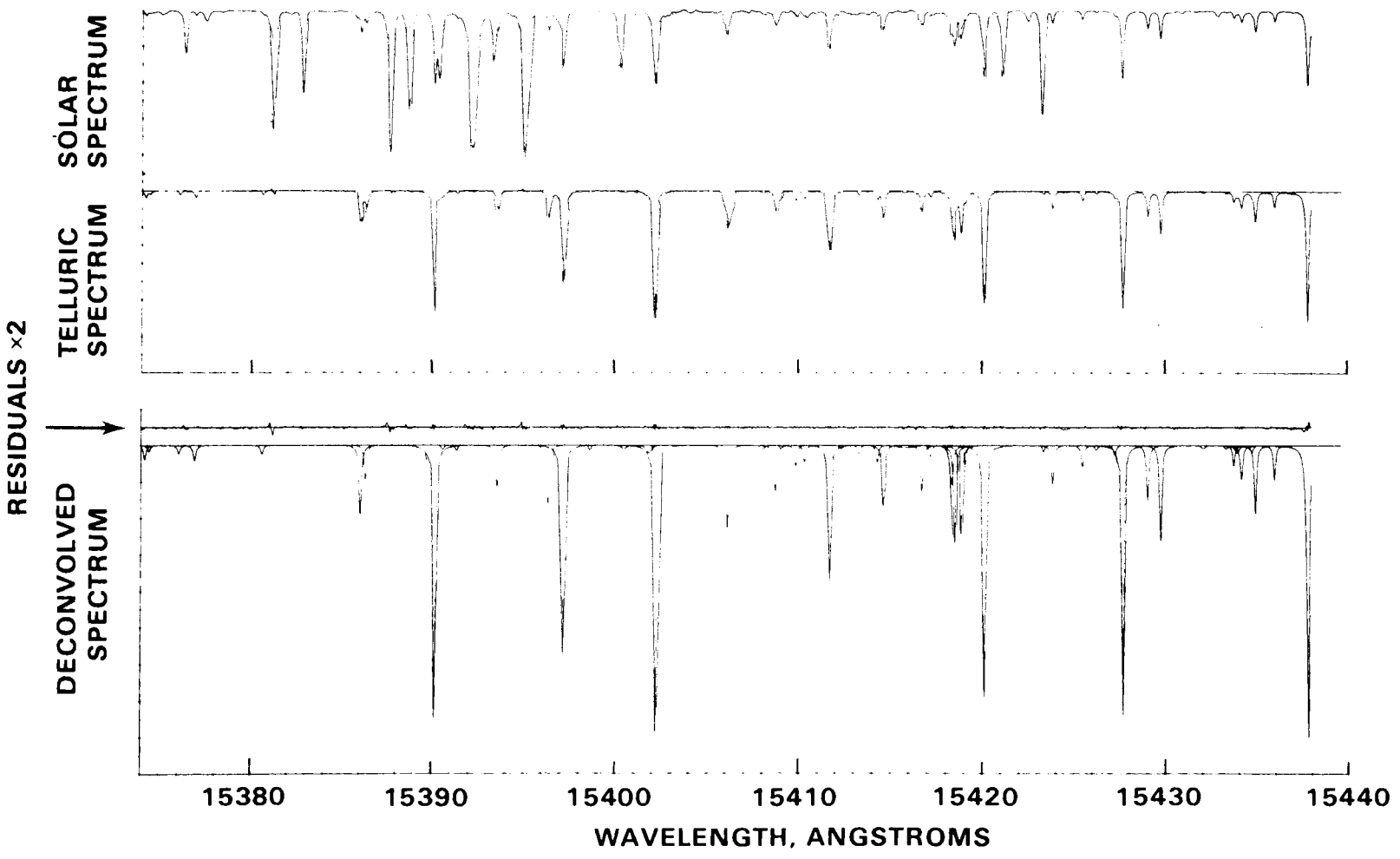

Figure 1.31. The Deconvolution of Lines in the Telluric Spectrum. This figure illustrates the use of a non-linear least squares line fitting procedure in the analysis of the Telluric Spectrum.

Mt. St. Helens Related Aerosol Properties from Solar Extinction Measurements

J. J. Michalsky, E. W. Kleckner, and
G. M. Stokes

The long range goal of this research is to quantify, as a function of time, the optical extinction due to introduction of aerosols and aerosol-precursors into the troposphere and stratosphere during the major eruptive phase of Mount St. Helens, Washington. In this report we concentrate on the 2-week period centered on the major eruption of July 22, 1980.

Investigation Technique

Direct solar radiation was measured with the Mobile Automatic Scanning Photometer. Two 45° altazimuth-mounted mirrors transferred radiation from any direction in a hemisphere to a 6-inch refracting telescope. Interference filters defined 12 passbands through which direct and circumsolar radiation are measured within a 1.5° field of view. Sampling was done from sunrise to sunset every 5 minutes in 7 filters and every 15 minutes in 5 additional filters.

By plotting the natural logarithm of the measured flux versus airmass (approximately the secant of the zenith angle), one obtains a straight line whose slope is equal to the total optical depth. This follows from the equation in Figure 1.32, namely

$$\ln F(\lambda) + \ln F_0(\lambda) - \tau(\lambda)m \quad .$$

The total optical depth is due to Rayleigh scattering, ozone absorption, and aerosol extinction (absorption and scattering). Molecular absorption bands are avoided because of their nonlinear dependence on airmass. Subtracting Rayleigh and ozone attenuation and plotting the optical depth due to aerosols versus wavelength for each filter yields a plot similar to that in Figure 1.33.

Junge noted that optically important (>0.1μm) aerosols often have a size distribution of the form

$$\frac{dN(r)}{dr} = Cr^{-\nu-1} \quad ,$$

where N(r) is the number of particles with radii between r and r + dr and C and ν are constants. Further, he showed that under certain assumptions about the upper and lower limits of the size distribution, namely that these limits can be neglected, that the attenuation due to Mie aerosols depended on wavelength λ according to

$$\tau = \beta\lambda^{-\nu+2} = \beta\,\lambda^{-\alpha} \quad .$$

β characterizes the total loading and α is a function of the mean particle size. If the particles are very small then α ≈ 4, i.e., Rayleigh scattering occurs. If the particles are large compared with the wavelength, then α ≈ 0, i.e., netural attenuation occurs. For hazes that normally occur over land masses, α ≈ 1.3. Taking the natural logarithm of both sides of the above equation yields

DIRECT BEAM MEASUREMENTS

- BOUGUER-LANGLEY METHOD

$F(\lambda) = F_0(\lambda) \exp -\tau(\lambda)m$

$F(\lambda)$	NARROWBAND TERRESTRIAL SOLAR FLUX
$F_0(\lambda)$	NARROWBAND EXTRATERRESTRIAL SOLAR FLUX
$\tau(\lambda)$	OPTICAL DEPTH
m	AIR MASS

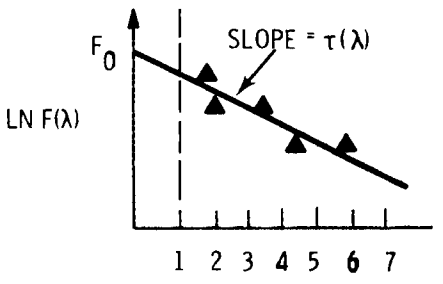

$\tau(\lambda) = \tau_R(\lambda)$ RAYLEIGH
$+\tau_A(\lambda)$ AEROSOL
$+\tau O_3(\lambda)$ OZONE
$+\tau_{MOL}(\lambda)$ MOLECULAR

Figure 1.32. The Boguer-Langley Method of Extracting Aerosol Optical Depth

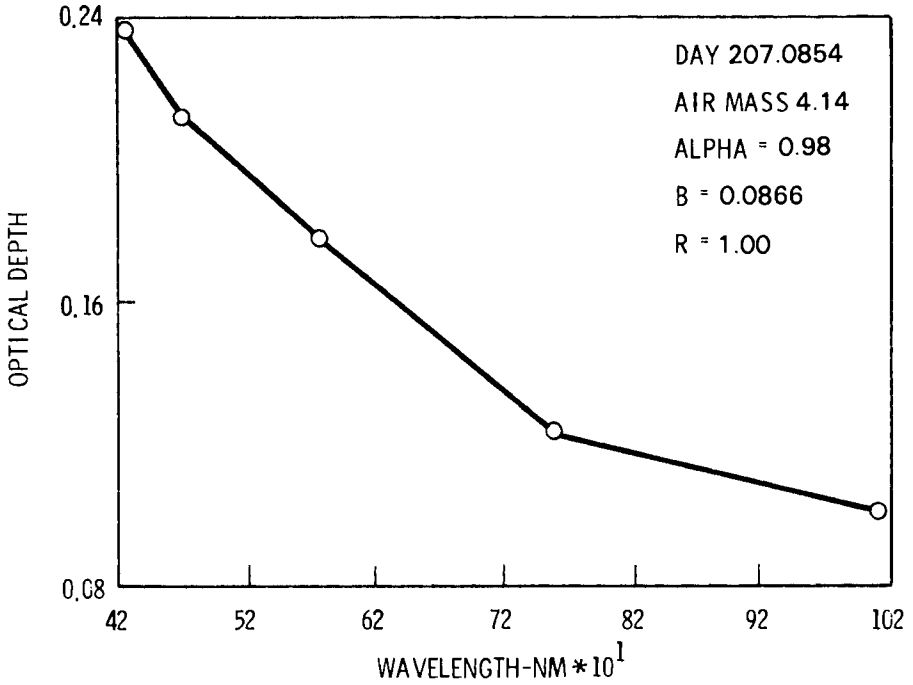

Figure 1.33. Typical Plot of Aerosol Optical Depth Versus Wavelength

$$\ln \tau = \ln \beta - \alpha \ln \lambda \quad .$$

By plotting $\ln \tau$ versus $\ln \lambda$, the numerical value of α can be obtained from the slope of the resulting straight line. Traditionally, the optical depth is evaluated at some standard wavelength (0.5 μm) and in terms of the decadic turbidity, i.e.,

$$B = \log_{10} e\tau \ (0.5\mu m) \quad .$$

Observations/Conclusions

The event around July 22, 1980, was chosen because of the preponderance of clear and partially clear days before and after this event. Figure 1.34a is a plot of the decadic turbidity coefficient, B, versus the day number. Figure 1.34b is a plot of the wavelength exponent, α, versus the day number (day 204 is 22 July). Referring to Figure 1.33, we have derived for each such plot the correlation coefficient, R. This coefficient is a measure of the linearity of the relationship, in other words, an evaluation of the appropriateness of the Junge distribution. We have included in Figure 1.34 only turbidity and wavelength coefficients from Junge-distributed aerosols. Because of diurnal variations associated with various uses of the land surrounding the Battelle Observatory site, the data plotted are from the same time period each day.

Figure 1.34a indicates rather low, but not unreasonable, turbidity before the eruption, followed by a sharp increase immediately following the eruption. The turbidity rose even higher 2 and 3 days after the eruption before dropping to more normal background values. In Figure 1.34b the exponent α was slightly below normal, indicating rather large particles on the low turbidity days preceding the eruption. This is, perhaps, indicative of large, resident stratospheric aerosols from the three previous stratospheric injections due to eruptions. On the day following the eruption, α assumed a very low value indicating a preponderance of large particles. Then on days 2, 3 and 4 following the eruption α climbed to values larger than normal for hazes over land masses, i.e., the particles were quite small. The tentative interpretation of this change is that the dust from the volcano clearly dominated on the day following the eruption, but after that, small sulfate aerosols formed from the precursor gases SO_2 and H_2S assumed a dominant role in the extinction. This latter interpretation is consistent with the large release of these gases by Mount St. Helens, but may not be consistent with their conversion to optically important aerosols in the time it takes the winds to carry these gases over the observatory site.

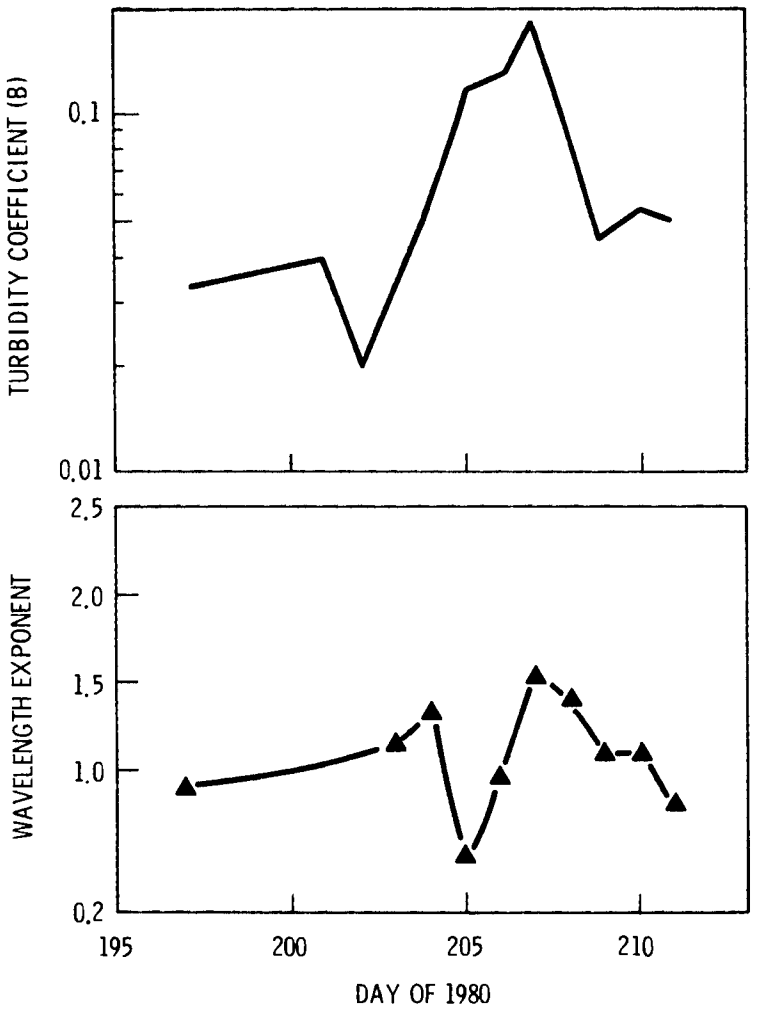

Figure 1.34. (a) Decadic Turbidity Coefficient as a Function of Day of 1980 (b) Wavelength Exponent as a Function of Day of 1980

Summary

We have reported on the optical extinction due to aerosols above Battelle Observatory around the time of the July 22 eruption of Mt. St. Helens. We have also identified, albeit somewhat crudely, the mean size of these aerosols.

While the present results are of considerable interest in their own right, we would most like to address the more significant question of climatological consequences of extinction resulting from aerosols introduced into the stratosphere.

Figure 1.35 is a map of the Mobile Automatic Scanning Photometer (MASP) sites on the North American continent. On the average, two years of data preceding the eruption of Mt. St. Helens were obtained at each site giving us some notion of seasonal changes in turbidity. We would now like

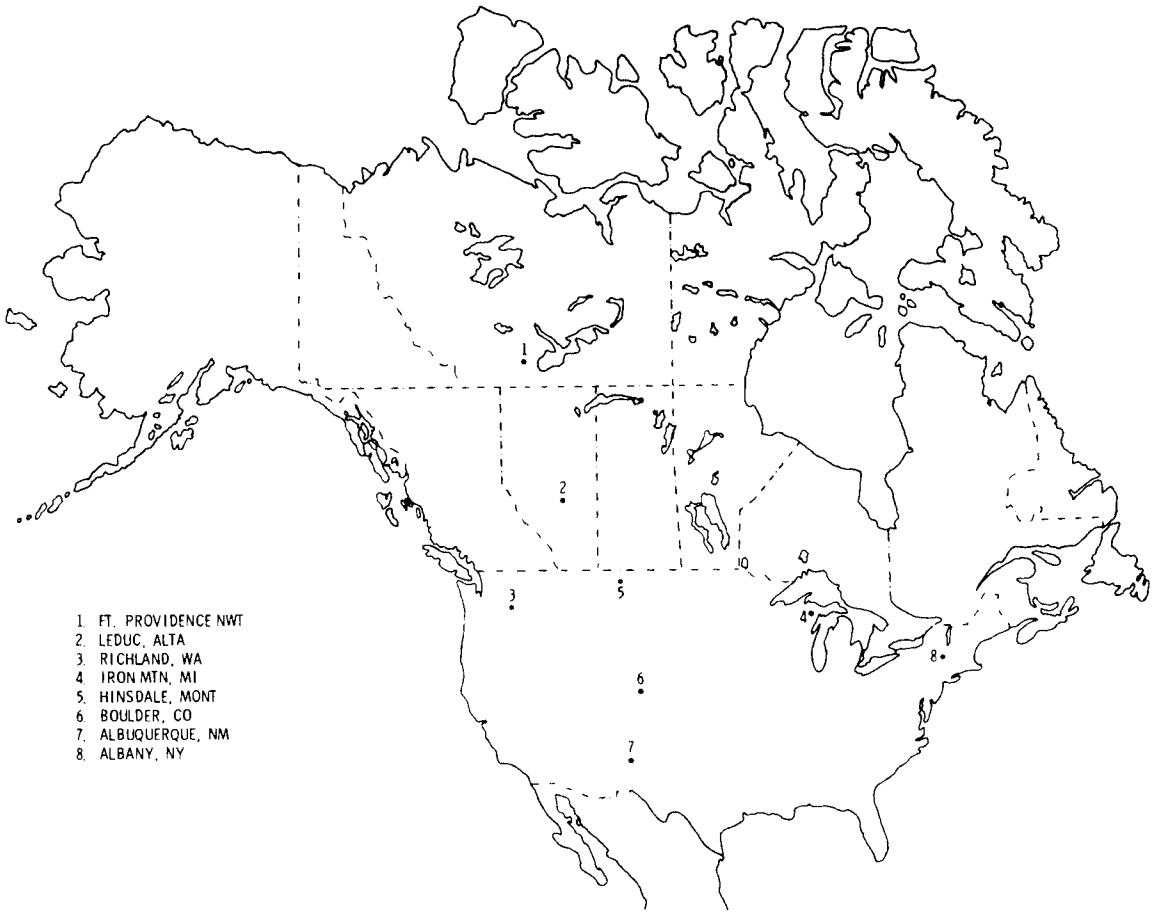

Figure 1.35. Nine Photometer Site Locations Throughout the United States and Canada

to assess the differences in the mean turbidity on a continental scale following the eruptive phase of this volcano and, perhaps, track it until the stratosphere returns to pre-18 May 1980, conditions.

Reference

Junge, Christian E. 1963. Air Chemistry and Radioactivity. Academic Press, New York, New York.

• Meteorological Effects of Thermal Energy Releases (METER)

Objectives of this study are:

- Developing technical data bases for assessing the potential effects of waste heat sources on weather, climate and ecosystems.
- Determining the importance of waste heat releases on the spacing and location of groups of thermal power plants.
- Conducting field studies on surface shadowing by cooling tower plumes, surface deposition of chemical drift from towers, augmented precipitation as the result of plume scavenging, and increased incidence of fogging and icing from plumes.

PNL Participation in Winter Study of Power Plant Effects

P. W. Nickola, N. S. Laulainen, and
M. T. Dana

In December 1979 a joint field project was carried out under the Meteorological Effects of Thermal Energy Resources (METER) program by personnel from The Pennsylvania State University (PSU), Oak Ridge National Laboratory (ORNL), and Pacific Northwest Laboratory (PNL). This two-week field study, sited near the Bowen coal-fired power plant in northwest Georgia, was entitled Winter Study of Power Plant Effects (WISPE).

The 3200-megawatt Bowen plant, one of the largest coal-fired plants in the world, has four 120-m natural draft cooling towers and two 300-m stacks for combustion products. The objective of the study was to investigate the effects of the addition of chemical, thermal and humidity plumes to the atmosphere relatively near the plant.

The Oak Ridge laboratory was charged with project direction and precipitation chemistry studies. PSU was charged with air chemistry measurements--primarily collected via air sampling. PNL made local meteorological measurements; assembled, reduced and analyzed local and regional meteorological data; provided supplemental air chemistry measurements to PSU; investigated plume condensate scavenging by rainfall; and investigated the near source effect of the cooling tower temperature/humidity plumes.

At a site about 4 km west-southwest of the Bowen plant, PNL continuously recorded temperature and wind speed and direction during daylight hours. Four (sometimes five) pilot balloon ascents also were made daily from this site. These measurements (as well as wind measurements made by ORNL at three sites, and temperature, wind, humidity, and solar radiation data collected on a 35-m Georgia Power Company tower) were assembled, reduced and analyzed for periods of interest to any of the experimental groups.

Additional meteorological data, collected at six regional National Weather Service stations also were obtained and summarized. These regional summaries, as well as the local meteorological summaries, are included in tabular and narrative form in the final WISPE report (Patrinos 1980).

PNL provided samplers to monitor total ammonia and SO_2 at selected ground locations during WISPE. The samplers were deployed by PNL and ORNL personnel. Quantitative analysis of the resulting 57 SO_2 and 14 NH_4/NH_3 samples was carried out at PNL, and results were forwarded to PSU.

A network of 140 rain gauges was deployed within 1.2 km to the east of the Bowen plant. The purpose of this network

was to investigate the possible enhancement of rainfall in the zone embraced by the cooling tower condensate plumes. During the WISPE experimental period, only one significant rainfall occurred. During this rainfall the plumes lay over one edge of the rain gauge network. Although the depth pattern suggested rainfall enhancement under the tower plumes, the modest rate of rainfall (4 mm in roughly 45 minutes) and uncertainty as to the duration of the plume traversal over the edge of the network led to statistically inconclusive results.

The cooling tower temperature/humidity plumes were investigated by means of a sensor package suspended from a tethered balloon. Figures 1.36 and 1.37 plot vertical profiles of potential temperature from flights presumably in and out, respectively, of the cooling tower plumes. During in-plume Flight 10 (Figure 1.36), the ground tether position was approximately 1 km downwind of the nearest cooling tower. Flight 11 (Figure 1.37) was made as soon as practical after Flight 10, and in a location well outside the cooling tower plume. The in-plume temperature profiles showed markedly more variation than the ambient profiles. However, note that the potential temperature has warmed during the interval between flights. Thus, attempts to quantify the effects of the cooling tower plume are on shaky ground. Although no humidity data are presented here, similar uncertainties associated with temporal changes existed in the humidity profiles.

The conclusion concerning the temperature/humidity plume measurements was that more than one tethered-balloon package should have been flown so that simultaneous in-plume and ambient conditions could have been monitored. Without these simultaneous measurements, temporal changes in atmospheric conditions precluded meaningful quantitative assessment of the effects of the temperature/humidity plume.

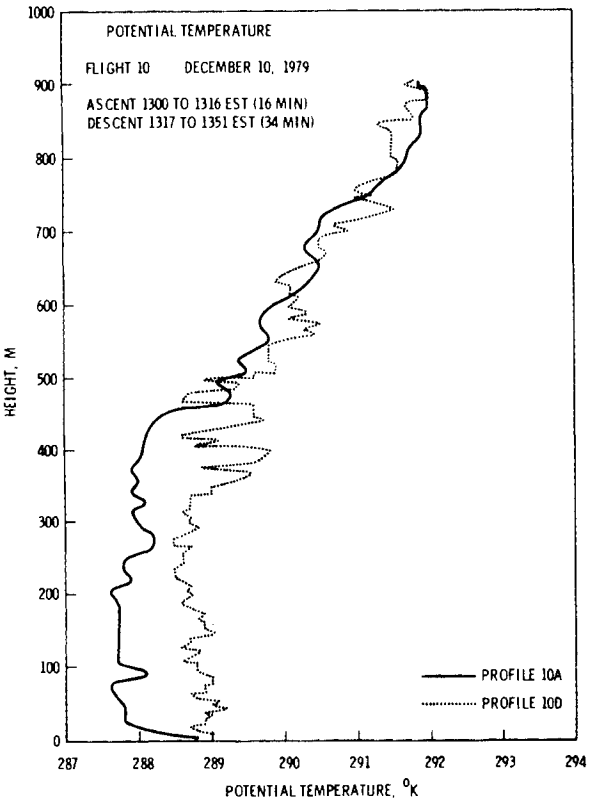

Figure 1.36. Vertical Profiles of Potential Temperature During Tethered Balloon Flight 10 Show Great Variation

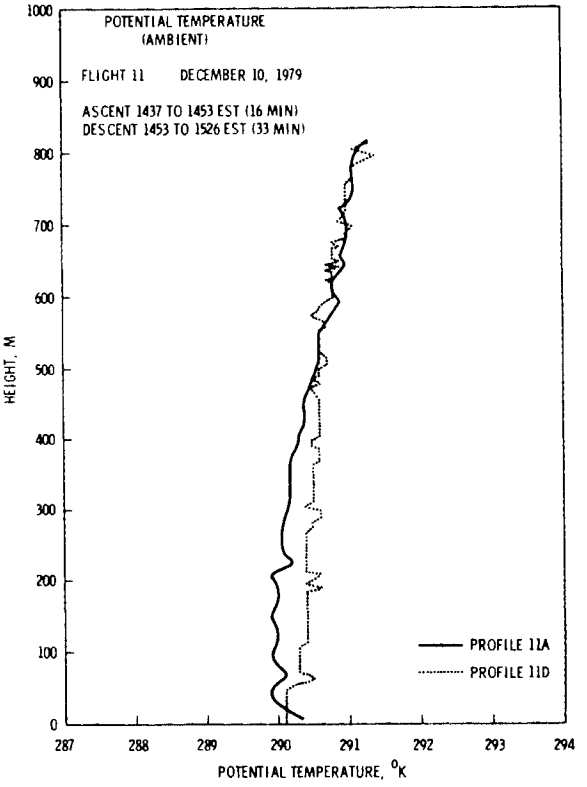

Figure 1.37. Vertical Profiles of Potential Temperature During Tethered Balloon Flight 11 Show Markedly Less Variation than Flight 10 (Fig. 1.36)

References

Patrinos, A. A. N. 1980. Winter Study of Power Plant Effects. ORNL/TM-7402, Oak Ridge National Laboratory, Oak Ridge, Tennessee.

Variations in Precipitation Statistics Caused by Raingage Type

J. M. Thorp

Introduction

Hourly precipitation data for many sites in the United States is currently made available on magnetic tapes. The data tape for January 1978 indicates that information is available for 883 stations in the 19 northeastern states. The information is from two kinds of precipitation recorders. The most common type seems to be the one which records precipitation to 1/10 in. At about 80 sites, which are mostly or all National Weather Service stations, precipitation is recorded to 1/100 in. Precipitation statistics such as average precipitation rates, precipitation event length, and storm length, can be quite unrealistic if hourly data from the 1/10-in. gages are used. (The metric system notwithstanding, precipitation is recorded in inches in this nation.)

Discussion

Regional or local studies and research in climatology may require the calculation of average precipitation rates, average precipitation event duration and other similar statistics. Because some precipitation recording stations use a gage that records in increments of 1/10 in. of water, the data from these stations produce quite different statistics from those calculated from data supplied by National Weather Service stations which record hourly precipitation in 1/100-in. increments. A monthly total precipitation amount as recorded by the two gages will agree within 0.1 in. In a very wet climate this discrepancy may not be significant but in arid regions even this difference will need to be considered when compiling precipitation statistics.

The 1/100-in. increment gage is a tipping bucket-type gage that marks a chart or activates a counter each time one of the chambers of the tipping bucket fills with an amount of water equivalent to 1/100 in. of precipitation. The filled chamber causes the pivoted "bucket" to tip. This action causes 1) the filled chamber to empty, 2) the previously emptied chamber to come into position beneath the collecting funnel, and 3) sends a simultaneous electrical impulse to the recorder. The tipping of the bucket takes about 0.2 sec., thus in regions with heavy rainfall (on the order of 2 in. h^{-1} or more) an error correction may be required (Middleton 1947).

The 1/10-in. increment gage makes a determination every 15 minutes. It is a weighing type gage and only registers an amount when 1/10 in. of precipitation has fallen. The disadvantage of this gage in regions of light to medium rainfall is that a number of hours of precipitation may elapse before an accumulation of 1/10 in. is reached. When 1/10 in. has accumulated, the recorder will show that amount has fallen during the past hour.

Table 1.7 illustrates the problem in calculating average precipitation event duration and average precipitation event rate when using data from a 1/10-in. sensitivity gage. Data for January 1978 at Wallops Island, Virginia, (U.S. Dept. of Commerce 1978) were chosen to illustrate the variation in statistical results

Table 1.7. Precipitation Statistics at Wallops Island, VA - January 1978
Comparison of Results from 1/100-in. and 1/10-in. Recording Gages

Statistic	1/100-in. Gage	1/10-in. Gage
Total Monthly Precipitation, inches	6.14	6.10
Number of Days with Precipitation	10	9
Total Hours with Precipitation	85	45
Total Number of Precipitation Events	17	21
Average Precipitation Event Duration, hours	5.0	2.14
Average Monthly Precipitation Event Rate,[a] hr^{-1}	.04	.14

[a] Σ Event Rates/No. of Events

depending on which type gage was employed. In reality, Wallops Island uses a 1/100-in. recording gage; the statistics for the 1/10-in. gage are calculated to illustrate what would have been recorded had a 1/10-in. gage been in use.

Table 1.7 shows that the total monthly precipitation as recorded by the two gages agrees within about 1%. However, the 1/10-in. gage greatly under-measures the monthly number of hours with precipitation and the average precipitation event duration, but overestimates the average event rate. Only with the unlikely situation of storms occurring that produce 0.10-in. h^{-1}, or multiples thereof, can the statistics from the two types of gages be the same.

Unfortunately most of the hourly precipitation recording stations in the U.S. seem to use the 1/10-in. gage. Research in regional precipitation studies or models which incorporate the above or similar statistics must take account of the consequences of using precipitation data from 1/10-in. gages.

References

Middleton, W. E. K. 1947. Meteorological Instruments, University of Toronto Press, p. 116.

U.S. Department of Commerce. 1978. National Oceanic and Atmospheric Administration, Environmental Data Service, hourly precipitation data.

• Long Range Transport Modeling

Objectives of this study are:

- Developing national interregional transport matrices for sulfur dioxide and other pollutants.
- Using the derived matrices in models for assessing the air pollution impacts of future energy scenarios.
- Improving the air pollution models in order to produce more efficient and cost-effective assessments.

The Use of Time-Averaged Precipitation for Wet Removal in a Regional Air Pollution Assessment Model: an Update

W. E. Davis and W. J. Eadie

Introduction

One of the problems that confronts regional scale computer modelers is how to incorporate precipitation into a model with precipitation removal. In particular, one problem is what kind of average precipitation data should be used. A number of different approaches to this problem in the regional scale assessments have been used in the past. In Johnson et al. (1978), six-hour precipitation was used for an assessment. In Eliassen (1978) six-and twelve-hour precipitation was used in an assessment for 1974. In Slinn (1978), a recommendation was made that researchers use a constant wet deposition velocity based on the average annual precipitation. At Pacific Northwest Laboratory, hourly precipitation is used for most assessments (Powell et al. 1979; McNaughton 1980). However, the production of hourly precipitation tapes is long and costly; and an alternative approach is desired.

A study by Wendell, Powell, and McNaughton (1977) demonstrated that the use of average precipitation would cause an overestimate of the amount of SO_4 deposited in a regional study when compared to results using hourly precipitation. This prompted two papers, one by Davis (1979), and a second by Davis and Eadie (1979). These papers showed that increasing the averaging times increased the amount of deposition generally. It was also shown in the first paper that when the average precipitation, corrected to the average intensity during wet periods, was turned on and off with the average frequency and for the average duration of naturally occurring precipitation, that the mass balance was approximately the same as when hourly precipitation was used. The second paper extended the test to SO_2 and SO_4 but only for a monthly assessment. Comparison of results obtained with the different precipitation modes showed that problems exist in the SO_4 air concentration and deposition patterns. It is the purpose of this paper to test whether extending the assessment to a four-month period will result in comparable patterns of SO_4 air concentration and deposition using average precipitation turned on and off with its average natural frequency to those obtained using the hourly precipitation.

The model used in this study is described in Eadie and Davis (1979).

Precipitation Frequency

Two techniques were used to treat precipitation frequency. One method was to examine hourly precipitation data and compute a mean dry period and a mean duration of precipitation. The other method was based on a paper by Henmi and Reiter (1978). These authors produced an analysis of United States precipitation frequency east of 105°W longitude based on records for 61 stations for 1974.

Case Studies

Two sites were selected for analysis for January, April, July and October, 1974. They were Anaconda, Montana, and central Arkansas.

For the site in the west, a 3-hour duration of precipitation was selected for every 120 hours. These values were chosen based on a rough average of values presented by Henmi and Reiter (1978). A different set of averages was used for central Arkansas based on the observed frequencies.

The PNL model was run in two precipitation modes for each of these sites for hourly and average precipitation turned "on" and "off" (on/off). The coefficients used in this study for SO_2 and SO_4 are shown in Table 1.8. These were obtained from Sandusky, Eadie and Drewer (1979).

Results

The results of the mass balance comparison for the four months are shown in Table 1.9. These demonstrate that good agreement occurs between the hourly and average (on/off) precipitation.

Comparison of the SO_2 air concentrations, SO_2 deposition, and SO_4 air concentration patterns predicted for the four months for both the Anaconda source and the Eastern source using average precipitation (on/off) and hourly precipitation show excellent agreement.

The comparison of the SO_4 deposition patterns gave mixed results. It was found that in the SO_4 deposition pattern for Anaconda using the average (on/off) precipitation differences of factors of 2 and 3 were found near the source when compared to patterns produced using the hourly precipitation. The SO_4 deposition pattern for the Eastern source using average (on/off) precipitation (Figure 1.38) shows a good comparison to the pattern obtained using the hourly precipitation (Figure 1.39). The reason for the improved comparison in the east is that the precipitation frequency was computed for the Eastern source for each month. For Anaconda a constant frequency of 3 hours of precipitation every 120 hours was used for each of four months. This points out the importance of using computed monthly precipitation frequencies in running the assessment.

Basically, the results confirm the results earlier found by Davis and Eadie. That is, when the average precipitation is turned on and off at approximately the same frequency that occurs and for the same intensity in the area of interest, the mass balance is approximately the same as that obtained using hourly precipitation. Also, the same result was found that the monthly SO_4 deposition patterns calculated using average precipitation (on/off) were quite different from the SO_4 deposition calculated using hourly precipitation. This points out the importance of using hourly precipitation when considering episodal cases. The reason for the difference is

Table 1.8. Model Input Data

Time period for meteorological data	January, April, July and October
Advection grid spacing (35°N latitude)	321 km
Grid spacing for precipitation data and sampling of results (35°N latitude)	32 km
Effective stack height	200 m
Mixing height	Variable
Stability	Variable
Dry deposition velocities:	
• SO_2	1.4 cm/sec
• Sulfates	0.23 cm/sec
Wet removal coefficients[a]:	
• SO_2	0.058 P/hr
• Sulfates	0.38 $P^{.73}$/hr
Transformation rate of SO_2 to sulfates	0.005/hr
Percentage of emissions as primary sulfates	0.02 (2% of emission)

[a] P = rainfall rates mm/hr

Table 1.9. Total Mass Balance for January, April, July and October 1974
Mass Balance (% of Release)

Station	TYP Precipitation	SO_2 Air	SO_4 Air	SO_2 Deposit	SO_4 Deposit	SO_2 Off	SO_4 Off	SO_2 Drop	SO_4 Drop
Anaconda Montana	Hourly	3.09	1.58	84.24 (3.50)	8.55 (5.12)	0.20	0.96	0.14	1.25
	Average (On/Off)	3.20	1.93	84.10 (3.20)	8.66 (5.30)	0.21	0.92	0.13	0.86
Central Arkansas (East)	Hourly	2.82	0.86	84.73 (8.86)	9.03 (6.66)	1.15	1.17	0.04	0.22
	Average (On/Off)	2.91	1.04	84.86 (10.42)	8.77 (6.87)	1.17	1.17	0.03	0.06

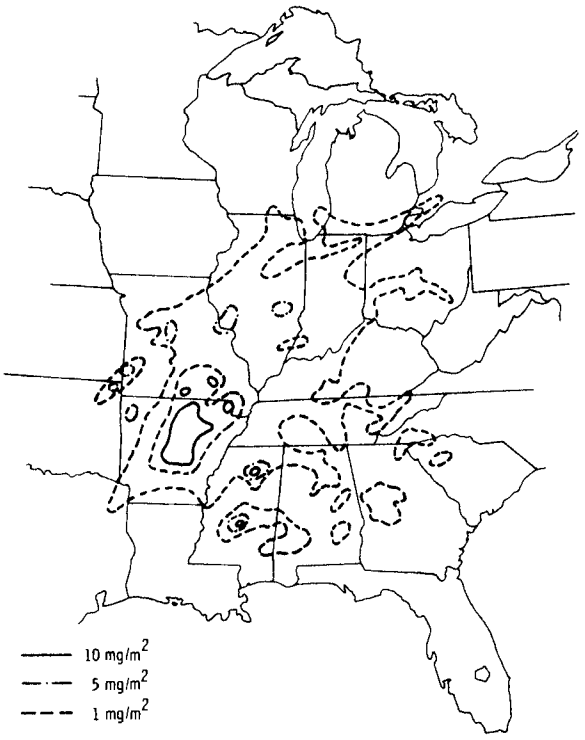

Figure 1.38. Average Monthly Deposition of SO_4 Using Average (On/Off) Precipitation

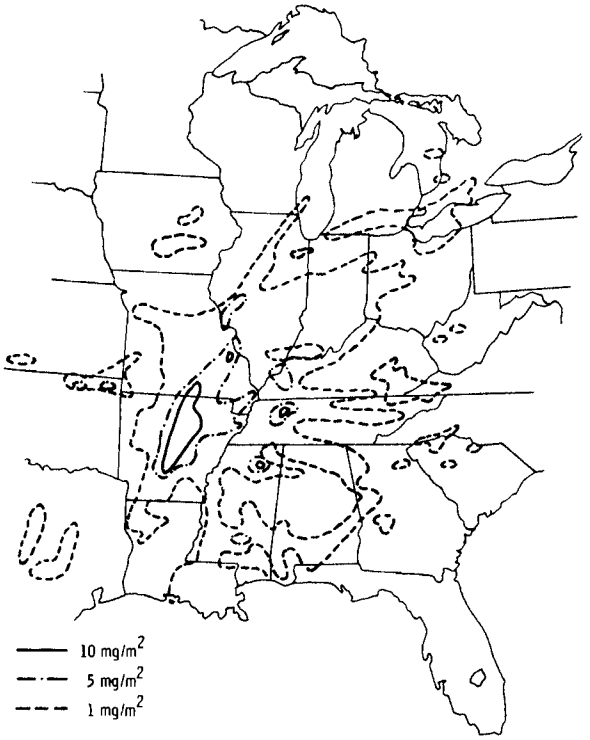

Figure 1.39. Average Monthly Deposition of SO_4 Using Hourly Precipitation

that precipitation events are relatively infrequent and using the time averaged precipitation, turning it off and on from 7 to 12 times a month will cause the deposition pattern to be heavily influenced as to when the precipitation is turned off and on. However, for the four-month long-term assessments, these differences averaged out and the patterns became more similar.

Conclusions and Recommendations

PNL regional scale model results for SO_2 and SO_4, using average precipitation turned off and on at approximately the same frequency of naturally occurring rain in the region, has yielded mass balances and SO_4 deposition patterns that compare favorably with model results using hourly precipitation for two sites in the United States for four months in 1974. This confirms earlier results by Davis and Eadie. It was found that average frequencies of wet and dry periods computed on a monthly basis yielded better results than a simple average for all four months.

The technique of turning on and off the precipitation is recommended for use in annual assessments. For shorter term studies, i.e. a month or less, hourly precipitation should be used.

References

Johnson, W. B., D. E. Wolf, and R. L. Mancuso. 1978. "Long-Term Regional Patterns and Transfrontier Exchanges of Airborne Sulfur Pollution in Europe." Atmospheric Environment, 12 (1-3).

Eliassen, A. 1978. "The OCED Study of Long-Range Transport of Air Pollutants: Long-Range Transport Modelling." Atmospheric Environment, 12 (1-3).

Slinn, W. G. N. 1978. "Parameterization for Resuspension and for Wet and Dry Deposition of Particles and Cases for Use in Radiation Dose Calculations." Nuclear Safety, 19(2):205-219.

Powell, D. C., D. J. McNaughton, L. L. Wendell, and R. L. Drake. 1979. A Variable Trajectory Model for Regional Assessments of Air Pollution from Sulfur Compounds. PNL-2734. Pacific Northwest Laboratory, Richland, Washington.

McNaughton, D. J. 1980. "Initial Comparisons of SURE/MAP3 Sulfur Oxide Observations with Long-Term Regional Model Predictions." Atmos. Envir., 64:55-63.

Wendell, L. L., D. C. Powell, and D. J. McNaughton. 1977. "A Multi-Source Comparison of Real Time Versus Time Averaged Precipitation Data on SO_2 and Sulfate Particulate Removal in a Regional Assessment Mode." Joint Conference on Applications of Air Pollution Meteorology. November 29-December 2, Salt Lake City, Utah.

Davis, W. E. 1979. "The Effect of Using Time Averaged Precipitation for the Estimation of Wet Deposition in a Regional Scale Model." Presented at the 10th International Technical Meeting on Air Pollution Modeling and Its Application. Sponsored by NATO Committee on Challenges of Modern Society, October 23-26, Rome, Italy.

Eadie, W. J. and W. E. Davis. 1979. "The Development of a National Interregional Transport Matrix for Respirable Particulates." PNL-RAP-37. Pacific Northwest Laboratory, Richland, Washington.

Henmi, T. and E. R. Reiter. 1978. "Regional Residence Time of Sulfur Dioxide over the Eastern United States." Atmos. Envir., 12:1489-1495.

Sandusky, W. F., W. J. Eadie, and D. R. Drewes. 1979. Long-Range Transport of Pollutants in the Pacific Northwest. Preprint from the 25th Annual Meeting of the Institute of Environmental Sciences, April 20-May 3, Seattle, Washington.

Another Look at the Use of Average Precipitation for Use in Wet Deposition

W. E. Davis

The problem with using different averaged precipitation in regional assessment models is not new. Papers by Wendell et al. (1977), Davis (1979), and Davis and Eadie (1980), all have addressed the differences in deposition that can occur using different average precipitation in regional assessment models.

Because of the complexities in the flow, as well as the sporadic nature of precipitation events, calculation of average rates of deposition becomes rather complex (see Roche and Grandell 1972). Arguments are still raised to reduce these complexities by incorporating the use of annual average precipitation (Slinn 1978). Slinn suggests that wet deposition velocity calculated through use of the annual average precipitation can be used to calculate wet removal. This would avoid the problem of incorporating the duration and frequency of precipitation.

This paper presents a very simplistic model that demonstrates the difficulties inherent in any approach that fails to take into account the natural frequency and duration of rain.

Model

Assume that we have a transport model with constant wind (1 box/1 time step), with constant release rate (1Qo/time step), with a constant removal coefficient when rain falls λ (sec^{-1}), with rain occurring 6 hours at the end of a 72-hour period.

It is assumed that $\frac{dQ}{dt}$ is given by

$$\frac{dQ}{dt} = 0 \quad \text{no rain}$$

$$\frac{dQ}{dt} = Q\lambda \text{ rain or } Q_i = Q_{i-1}e^{-\lambda t}$$

where t is the constant time step.

Starting with an initial Qo which is released undisturbed for 66 hours; at 67 hours, a uniform rain turns on for 6 hours and promptly turns off at 72 hours.

With such a simple model the resulting deposition in each box is given by:

$$\text{Box 1} \quad D1 = 6\,Qo\left(1-e^{-\lambda t}\right)$$

$$\text{Box 2} \quad D2 = Oo\left(1-e^{-\lambda t}\right)\left(1 + 5e^{-\lambda t}\right)$$

$$\text{Box 3} \quad D3 = Qo\left(1-e^{-\lambda t}\right)\left(1 + e^{-\lambda t} + 4e^{-2\lambda t}\right)$$

$$\vdots$$

$$\text{Box 6} \quad D6 = Qo\left(\sum_{i=1}^{6} e^{-(i-1)\,\lambda t}\right)$$

$$\vdots$$

$$\text{Box 72} \quad D72 = D6$$

If, however, an average rain is used the deposition takes the form of:

$$DA1 = 72\,Qo\left(1-e^{-\lambda dt}\right)$$

$$DA2 = Qo\left(1-e^{-\lambda dt}\right)\left(1 + 71e^{-\lambda dt}\right)$$

$$DA3 = Qo\left(1-e^{-\lambda dt}\right)\left(1 + e^{-\lambda dt} + 70e^{-2\lambda dt}\right)$$

$$\vdots$$

$$DA72 = Qo\left(1-e^{-\lambda dt}\right)\left(1 + \sum_{i=1}^{71} e^{-i\lambda dt}\right)$$

where λd is the average rain removal coefficient (sec^{-1}).

Obviously the two forms are not equal and should give considerably different results depending on the value given to λd and λ.

To compare values, the depositions in the first box are set equal. A comparison of the deposition further from the source then can be made.

a) For $\lambda = 10^{-3}$ sec^{-1}, Qo = 1, t = 3600 seconds at 72 days the deposition will be D1 = 5.8. Then setting DA1 = D1 results in

$$\lambda d = 2.4 \times 10^{-5} \text{ sec}^{-1}.$$

For the 6th box after 72 hours the amount deposited will be

$$D6 \cong 1.0$$

and using the average precipitation

$$DA6 \cong 3.9$$

or the average precipitation yield ~4X larger deposition.

b) For $\lambda = 10^{-4}$ sec^{-1}, Qo = 1, t = 3600 seconds at 72 days the deposition will be D1 = 1.8. Then setting DA1 = D1 results in

$$\lambda d = 7 \times 10^{-6} \text{ sec}^{-1}.$$

For the sixth box after 72 hours the amount deposited will be D6 = 0.89 and using λd, DA6 = 1.6 or approximately 2X larger deposition.

c) for $\lambda = 10^{-5}$ sec^{-1}, Qo = 1, t = 3600 seconds at 72 days the deposition will be D1 = 0.212. Then setting DA1 = D1 and solving the λd results in

$$\lambda d = 8.2 \times 10^{-7} \text{ sec}^{-1}.$$

For the sixth box after 72 hours the amount deposited will be D6 = 0.193 and using λd DA6 = 0.21 or approximately the same results.

Conclusion

Using a very simple model, two techniques are compared where the amount deposited in the first box is used to control the removal coefficient for the average rain case. The use of average precipitation removal coefficient calculated in this way can lead to serious errors for $\lambda > 10^{-5}$ sec^{-1}. However for $\lambda \leq 10^{-5}$ sec^{-1}

essentially the same deposition result was found using the two techniques.

References

Davis, W. E. 1979. "The Effect of Using Time Averaged Precipitation for the Estimation of Wet Deposition in a Regional Scale Model." Fourth Symposium on Turbulence, Diffusion, and Air Pollution, Jan. 15-18, Reno, Nevada.

Davis, W. E. and W. J. Eadie. 1980. "The Effect of Using Time Averaged Precipitation in a Lagrangian Assessment Model." 89th National Meeting of the American Institute of Chemical Engineers. Aug. 17-20, Portland, Oregon.

Roche, H. and J. Grandell. 1972. "On the Removal Time of Aerosol Particles from the Atmosphere by Precipitation Scavenging." Tellus, 24(5):442-454.

Slinn, W. G. N. 1978. "Parameterization for Resuspension and for Wet and Dry Deposition of Particles and Gases for Use in Radiation Dose Calculations." Nuclear Safety, 19(2):205-219.

Wendell, L. L, D. C. Powell and D. J. McNaughton. 1977. "A Multi-Source Comparison of Real Time Versus Time Averaged Precipitation Data on SO_2 and Sulfate Particulate Removal in a Regional Assessment Model." Joint Conference on Applications of Air Pollution Meteorology. Nov. 29-Dec. 2, Salt Lake City, Utah.

• Theoretical Studies and Applications

Objectives of this study are:

- Developing theoretical models for describing the fate of energy-related air pollutants.
- Translation of theory and data into forms useful for evaluating the consequences of airborne pollutant releases.

Precipitation Efficiency and Scavenging

W. G. N. Slinn

The tropospheric residence (or turnover) time for atmospheric particles can be written as

$$\frac{1}{\bar{\tau}} = \frac{1}{\bar{\tau}_w} + \frac{1}{\bar{\tau}_d} + \frac{1}{\bar{\tau}_o} \qquad (1)$$

where separate contributions, which add like resistances in parallel, are from wet (w) and dry (d) removal, and from other processes such as coagulation. Elsewhere, (Slinn 1980), it is suggested that wet removal dominates for "accumulation mode" aerosol particles (i.e., for particles of radii, a, in the range $0.1 \lesssim a \lesssim 1$ μm). In this report, some data useful for estimating τ_w are examined.

There are a number of ways to estimate τ_w for particles.

1. If an average scavenging rate, $\bar{\psi}$, is known, then $\tau_w = \bar{\psi}^{-1}$. For example, using $\bar{\psi} = \bar{E}\bar{p}/D_m$ (Slinn 1977) with an average collection efficiency $\bar{E} = 0.1$, an average rainfall rate $\bar{p} = 100$ cm yr^{-1}, and a mean drop diameter $D_m = 1$ mm, then for particles with this $\bar{E}$, $\bar{\tau}_w \simeq 4$ d; if $\bar{p} = 35$ cm yr^{-1}, $\bar{\tau}_w \simeq 10$ d. In this method, however, $\bar{E}$ is uncertain at least by a factor of 3.
2. Using a wet deposition velocity, $v_w = ps_o$ (Slinn 1978), where s_o is the surface-level scavenging ratio, then the wet flux $W = v_w X_o$ where X_o is the surface-level air concentration. Therefore, following Junge's development that the mean residence time is the average amount of pollutant present divided by its rate of removal (Junge 1963),

$$\tau_w = \frac{\int X dz}{W} = \frac{\int X dz}{v_w X_o} = \frac{h_w}{v_w} = \frac{h_w}{ps_o} \qquad (2)$$

which defines the scale height h_w. For example, if $\bar{h}_w = 1$ km, $\bar{p} = 100$ cm yr^{-1}, and $\bar{s}_o = 10^5$, then $\bar{\tau}_w = 4$d; if $p = 35$ cm yr^{-1}, $\bar{\tau}_w = 10$ d. When using this method to estimate $\bar{\tau}_w$, there are substantial uncertainties in both h_w and s_o.
3. Using the average efficiency with which storms remove particles, $\bar{\varepsilon}$, and the average frequency with which storms are encountered, $\bar{\nu}$, then $\bar{\tau}_w = (\bar{\varepsilon}\bar{\nu})^{-1}$ (Slinn et al. 1978). For example, if $\bar{\varepsilon} = 1/2$ and $\bar{\nu}^{-1} = 2$ d, then $\tau_w = 4$ d; if $\bar{\nu}^{-1} = 5$ d, then $\tau_w = 10$ d. In this report, the focus is on examining available data from which ε can be estimated.

It is assumed that the efficiency with which a storm removes particles, ε, is comparable to the storm's efficiency for removing its condensed cloud water, ε_{cw}. This assumption is consistent with Junge's suggestion that, in clouds, a large fraction of atmospheric particulate mass becomes associated with the condensed cloud water. It is conceivable (e.g., for especially large and soluble particles) that $\varepsilon > \varepsilon_{cw}$, and it is conceivable (e.g., if there are many particles--say above an urban area--active as cloud condensation nuclei) that $\varepsilon < \varepsilon_{cw}$. However, as a first estimate, we take $\varepsilon \simeq \varepsilon_{cw}$, and now examine available data for ε_{cw}.

Unfortunately, there is a proliferation of different "precipitation efficiencies" reported in the scientific literature. We define ϵ_{CW} as the outflow of precipitation from the storm, divided by the flow of precipitable water through the storm. Thus, for an orographic cloud or storm,

$$\epsilon_{cw}^{OR} = \frac{\text{Precipitation Out (e.g., in kg/s)}}{\text{Inflow Moisture-Vapor Flow Above Barrier Crest}} \quad (3)$$

in which "precipitation out" could be replaced by the difference in moisture flows: upwind minus downwind of the topographical barrier. Comparable to what other authors call a "precipitation efficiency" is

$$\epsilon_{p}^{OR} = \frac{\text{Precipitation Out}}{\text{Moisture Inflow}} \quad (4)$$

From a comparison of (3) and (4), note that $\epsilon_{p}^{OR} < \epsilon_{cw}^{OR}$, because usually some of the inflow moisture does not condense.

Elliott and Hovind (1964) reported increases in precipitation, from frontal storms, caused by airflow over two mountain barriers in California. Thus, they reported what we will call "reduced," orographic, cloud-water-removal efficiencies:

$$(\epsilon_{cw}^{OR})' = \frac{\text{Outflow of Orographic-Induced Precipitation}}{\text{Moisture Inflow - Vapor Flow Above Crest}} \quad (5)$$

Their results for $(\epsilon_{cw}^{OR})'$ are shown in Table 1.10. They found that, generally, the higher the barrier and the more unstable the air, then the greater was $(\epsilon_{cw}^{OR})'$.

Dirks (1972) improved on Elliott and Hovind's technique by deducing the precipitation from differences in moisture, sampled by aircraft, upwind and downwind of the Medicine Bow Mountains in Wyoming. Dirks reported ϵ_{cw}^{OR}, not reduced values:

Table 1.10. Topographic Enhancement of Cloud Water Removal Efficiency as Deduced by Elliott and Hovind (1964)

Mountain Range	Approximate Height	Storm Stability	No. of Cases	$(\epsilon_{cw}^{OR})'$
San Gabriel	8000′	Stable	31	0.26
San Gabriel	8000′	Unstable	8	0.27
Santa Ynez	4000′	Stable	21	0.17
Santa Ynez	4000′	Unstable	22	0.26

the orographic storms he sampled were not imbedded in larger, precipitating storms. As shown in Table 1.11, Dirks found the lowest ϵ_{cw}^{OR} for the case with lowest cloud-top temperature. Also included in Table 1.11 is the case studied by Marwitz (1974) who made still another improvement to the measurement technique: he measured the vapor flow above the crest, via aircraft soundings, whereas early researchers had deduced this vapor flow from numerical models of flows over barriers. From the results shown in Tables 1.10 and 1.11, it appears reasonable to expect that somewhere between 1/5 and 2/3 of the condensed cloud water, and therefore of the ingested particles, are scavenged by precipitating orographic storms.

For cumulonimbus clouds (Cb's), the data illustrated in Figure 1.40 can be used to illustrate different efficiencies:

$$(\epsilon_{p}^{Cb})_{net} = \frac{\text{Precipitation Out}}{\text{Net Vapor in Cloud Base}} =$$

$$\frac{4.0}{(8.8-4.3)} \approx 0.9, \quad (6)$$

$$\epsilon_{cw}^{CB} = \frac{\text{Precipitation Out}}{\text{Precipitable Water Flow}} =$$

$$\frac{4.0}{(8.8+0.7-0.6)} \approx 0.4, \quad (7)$$

$$\epsilon_{p}^{Cb} = \frac{\text{Precipitation Out}}{\text{Vapor Into Cloud Base}} = \frac{4.0}{8.8} \approx 0.5. \quad (8)$$

That is, efficiencies for Cb's are complicated both by the moisture entrained especially with mid-level air feeding the downdraft, and by evaporation in the downdraft. In general, though, since moisture inflow in the updraft is dominant in a mature Cb, it can be expected that $\epsilon_{cw}^{Cb} \approx \epsilon_{p}^{Cb}$.

Marwitz (1972) has brought some order to available data for ϵ_{p}^{Cb} by plotting the data as a function of wind speed (see Figure 1.41). This shear is the wind speed at cloud top (say 25 m s^{-1}), less the wind speed at cloud base (say 5 m s^{-1}), divided by the cloud height (say 10 km, and then for this case the wind-speed shear would be 2×10^{-3} s^{-1}). Presumably, ϵ_{p}^{Cb} would return to a value near zero for no wind shear, since without shear a Cb's downdraft will suppress its updraft. On the other hand, for large wind shear Marwitz suggests the strong winds aloft will blow the ice off the Cb's anvil (leading to "orphaned anvils "), and/or cause the precipitation to fall outside the saturated cloud

Table 1.11. Cloud Water Removal Efficiencies for Isolated Orographic Storms

Location	Cloud Top Height, ft.	Cloud Top Temp., °C	Mean Wind Speed, ms^{-1}	ϵ_{cw}^{OR}
Medicine Bow Mts. Wy[a]	13,400	-23	12	65%
Ht. ~ 3500' Wd. ~ 40-50 km (Dirks 1972)	13,400	-19	22	55%
San Juan Mts., Colo. Ht. ~ 4-5000' Wd. Contin. Divide (Marwitz 1974)	~18,000	-35	20	25%
		-28	30	62%

[a]Heavily Rimed Ice; unstable

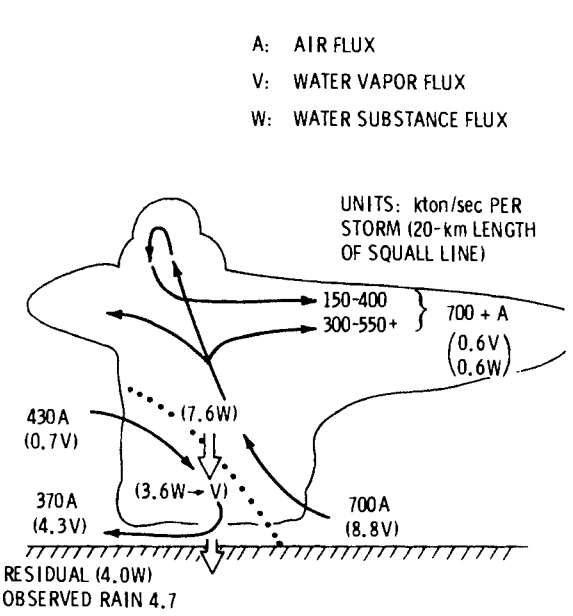

Figure 1.40. Principal Branches of the Circulation with Fluxes of Air (A), Water Vapor (V), and Water (W), Corresponding to a Single Thunderstorm in a Squall Line Studied by Newton (1966). Figure from Palmen and Newton (1969).

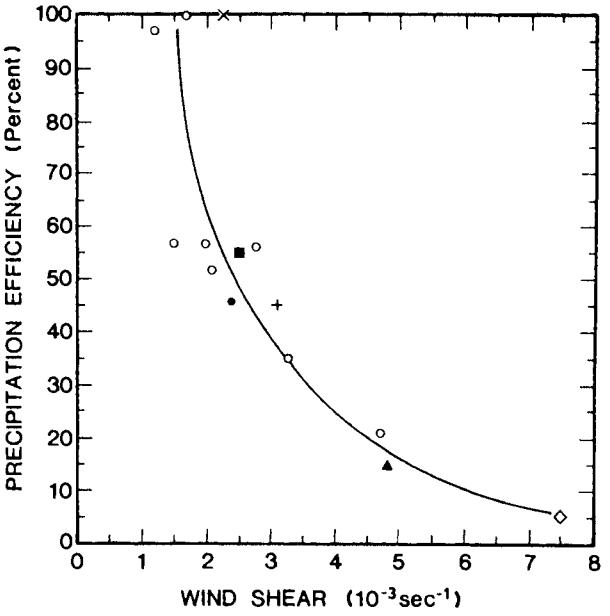

Figure 1.41. Precipitation Efficiencies, ϵ_p^{Cb} for Cumulonimbus Storms as a Function of Wind Shear. Figure after Foote and Fankhauser (1973); in turn adapted from Marwitz (1972); original data (referenced in Foote and Fankhauser) are as follows: ■ - Newton (1966); o - Auer and Marwitz (1968); X - Chisholm (1970); + -Hartsell (1970), ● - Fankhauser (1971), ◆ - Marwitz (1972), ▲ - Foote and Fankhauser (1973).

environment. For convective storms, therefore, ϵ_p^{Cb} appears to be in the range from 20% (as suggested by Braham (1952) to be typical for thunderstorms), to 50% (as deduced by Newton (1966) for a squall line), to even greater than 100% if the wind shear is optimum (~2 x 10^{-3} s^{-1}). The possibility that, at any instant, ϵ_p^{Cb} > 100% is not unrealistic, because account for actual time lags between precipitation outflow and vapor inflow is not normally included in the data reduction.

Data for precipitation or cloud-water-removal efficiencies for entire frontal storms have not yet been found in our literature search. However, University of Washington researchers recently conducted an impressive series of field studies of ϵ_{cw} for individual rainbands within frontal storms. These rainband efficiencies are defined by

$$\epsilon_{cw}^{RB} = \frac{\text{Ground-Level Precipitation Rate}}{\text{Total Condensation Rate}} \quad (9)$$

Table 1.12 shows deductions by Hobbs, et al. (1980) of these ϵ_{cw}s for rainbands associated with a western Washington cold front. For a particular band associated with a warm front, it it is assumed that none of the 400 gs^{-1} of water entering the convective column leaves the column as vapor (see Houze et al. 1980), then for this case $(\epsilon_{cw}^{RB})_{wf} \geq 80\%$. Presumably, these rainband efficiencies are near their maximum value in western Washington and would decrease substantially as the storm moves inland.

In conclusion, the following points are made:

- Estimates for τ_w based on $\tau_w = (\bar{\epsilon}\bar{v})^{-1}$ are as reliable as other methods.
- As a first approximation, it is reasonable to take $\epsilon = \epsilon_{cw}$.
- Some data for ϵ_{cw} are available, but more are needed before average value for different storm types can be estimated with confidence.
- In the meantime, it appears reasonable to use $\bar{\epsilon}_{cw} = 1/2 \pm 1/4$.
- Data for average times between storms, $\bar{v}^{-1}$, as encountered by pollution (i.e., in a Lagrangian sense) are needed.
- If for the winter months (October through March), $\bar{v}^{-1} = (3 \pm 1.5)$ d, and for the summer $\bar{v}^{-1} = (6 \pm 3)$ d, then the average tropospheric residence time of accumulation mode aerosol particles would be

$$\tau \approx \tau_w \approx \begin{cases} (6 \pm 3) \text{ d, winter} \\ (12 \pm 6) \text{ d, summer} \end{cases} . \quad (10)$$

These estimates are consistent with suggestions made by Junge (1963), but they are inconsistent with essentially all long-range transport models in current use. The latter are expected to be wrong, as will be described in detail in a forthcoming publication (Slinn 1981).

Table 1.12. Cloud-Water-Removal Efficiencies for Rainbands Associated with a Cold Front Striking Western Washington (Hobbs et al. 1980)

Rainband	Total Precipitation Rate, kg s^{-1}[a]	Total Condensation Rate, kg s^{-1}[a]	ϵ_{cw}^{RB}, %
Warm-sector rainband[b]	100 - 123	244	40 - 50
Wide cold-frontal band #1	40 - 50	52	80 - 100
Wide cold-frontal band #3	6	27	20
Narrow cold band #5	11 - 18	33[c]	30 - 50
		PrecipitationWeighted Average:	55

[a] In a strip 1 m wide, perpendicular to the rainband.
[b] Includes leading; developing sub-band; and light, trailing precipitation associated with the warm-sector rainband.
[c] Updraft assumed to extend to 3.5 km.

Preliminary Identification of Some Natural Sources and Sinks for Gaseous Sulfur Compounds

E. H. Haas[a] and W. G. N. Slinn[b]

The atmospheric sulfur cycle continues to contain many uncertainties, especially about natural sources and sinks. In turn, these uncertainties arise from measurement difficulties when concentrations are in the parts per billion (ppb) range, and from the many potential causes of natural variations in these concentrations. In addition, substantial complications result from the great variety of interacting forms of sulfur in the atmosphere: "particulate" sulfur in the form of $(NH_4)_2SO_4$, NH_4HSO_4, and H_2SO_4, for example, and gaseous sulfur in oxidation states from -2 (CS_2, COS, H_2S) to +4 (SO_2). A decade ago, it was thought that natural sources of gaseous sulfur primarily released H_2S, but subsequently it has been suggested that the primary natural forms are organic sulfides such as dimethyl sulfide (DMS or $(CH_3)_2S$), carbon disulfide (CS_2), and carbonyl sulfide (COS). In the brief study reported here, we performed a number of measurements of gaseous sulfur concentrations, generally remote from anthropogenic sources, to gain familiarity both with the measurement system and with the expected range of concentration variability.

Measurements were made with a commercially-available, flame-photometric sulfur detector.[a] Figure 1.42 schematically illustrates the measurement system onboard a light aircraft; ground-level measurements were taken with the instruments mounted in

(a) Present address: Institut für Mechanishe Verfahrenstechnik, Univ. Stuttgart, Böblingerst. 72, 7000 Stuttgart-1, W. Germany.

(b) The authors wish to thank P. C. Katen, Oregon State University, for his substantial contribution to these studies.

(a) Melloy Industries SA 260, SS 60 and FSC 195; trade names are mentioned only to convey additional information.

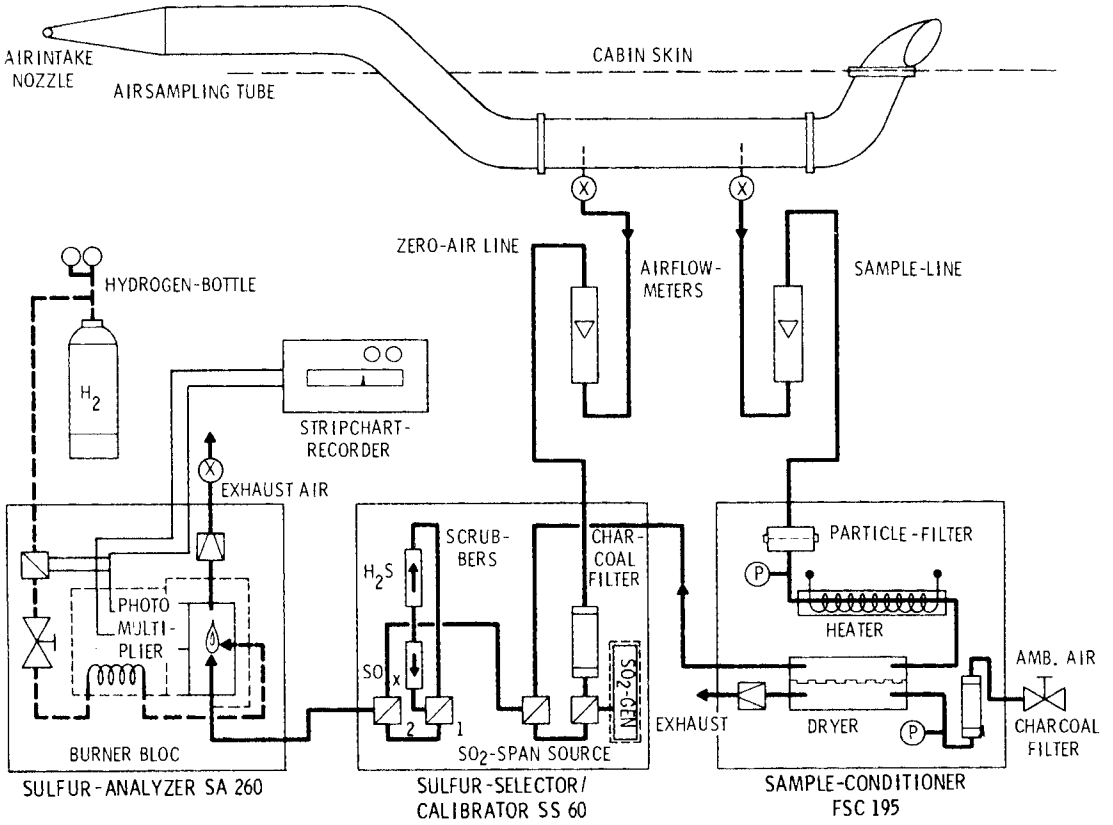

Figure 1.42. Airborne Measurement System

a light van. Frequent overhauls of the particle filter and scrubber systems (see Figure 1.42) were required to maintain instrument stability; a major source of instrument unreliability was moisture accumulation in the zero-air-line charcoal filter and in the scrubbers. Reliability was improved by using the sample-conditioner permanently, and by regenerating the zero-air filter and scrubbers by drawing dried air slowly through these parts over a period of several days before each measurement period. Without such precautions, the zero-air mode requires 4 to 12 hours to stabilize after system inactivity. Also, flame-intensity variations with altitude required the re-establishment of the zero baseline at every level for the airborne measurements.

Although the system was expected to provide concentrations of total gaseous sulfur, SO_x, and H_2S, the actual species measured is not clear. Presumably, some aerosol particles could pass the 5 μm-membrane filter, and sulfur could be vaporized from these particles in the heater. Also, as the results demonstrate, there was relatively little difference in the behavior of the H_2S and SO_x scrubbers, though generally the H_2S-mode scrubbed most sulfur. However, it appears the H_2S-mode does not pass just H_2S--it may also pass some organic sulfur--otherwise, our measurements would suggest the presence of much more H_2S than has been found by other researchers. Therefore, although we report the measurements of total sulfur, "TS," and of "SO_x" and "H_2S," we put these identifications in quotation marks to remind the reader that these are the instrument's measurement modes, and not necessarily the concentrations of these species. Clearly, additional work is required defining the instrument's response.

Results are shown in the accompanying figures. Figure 1.43 shows increases in airborne sulfur at the estuary at Newport, Oregon, as the ocean tide fell. The measurements were taken near the tidal flats, at the Newport Marine Science Center on 5 October, 1979; the wind was from the west at 4 knots (≈7.4 km hr^{-1}). A crude estimate of the gaseous sulfur production rate from these tidal flats, corresponding to the observed increase in S, is ~10 gS m^{-2} yr^{-1}. Figure 1.44 shows rapid decrease of airborne sulfur near sunset, measured at Oregon State University; winds

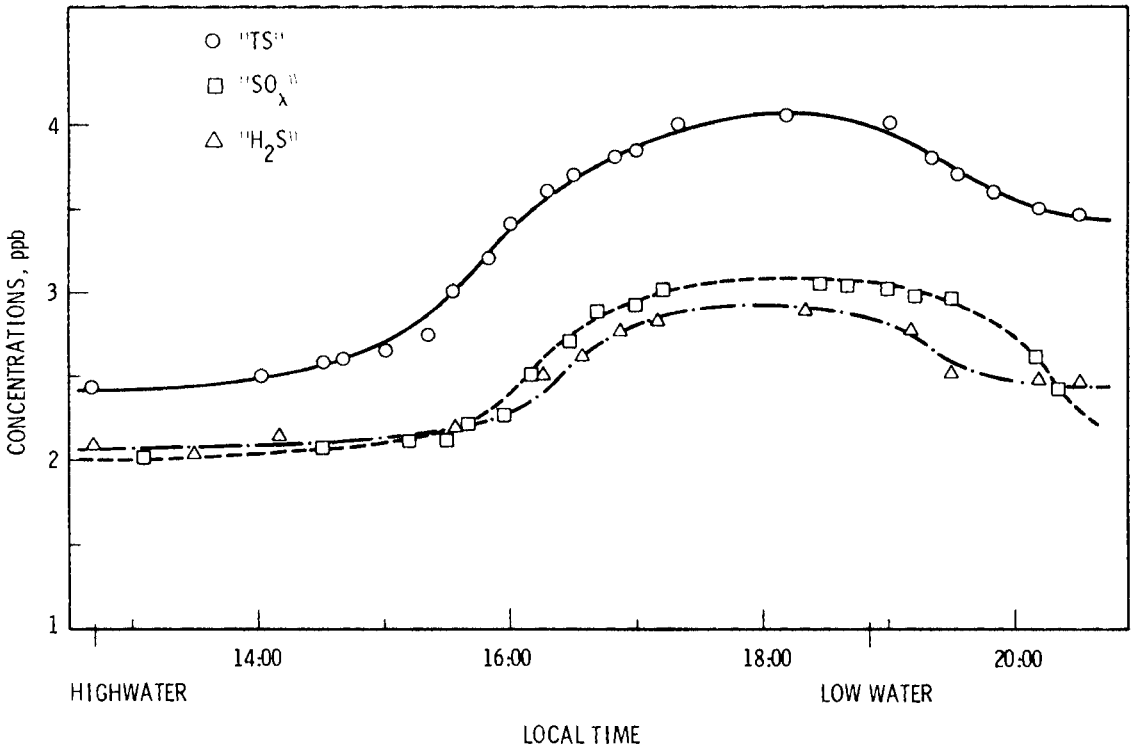

Figure 1.43. Increase in Airborne Gaseous Sulfur as Tide Fell at the Estuary at Newport, Oregon. See text for comments about uncertainties in the species identifications.

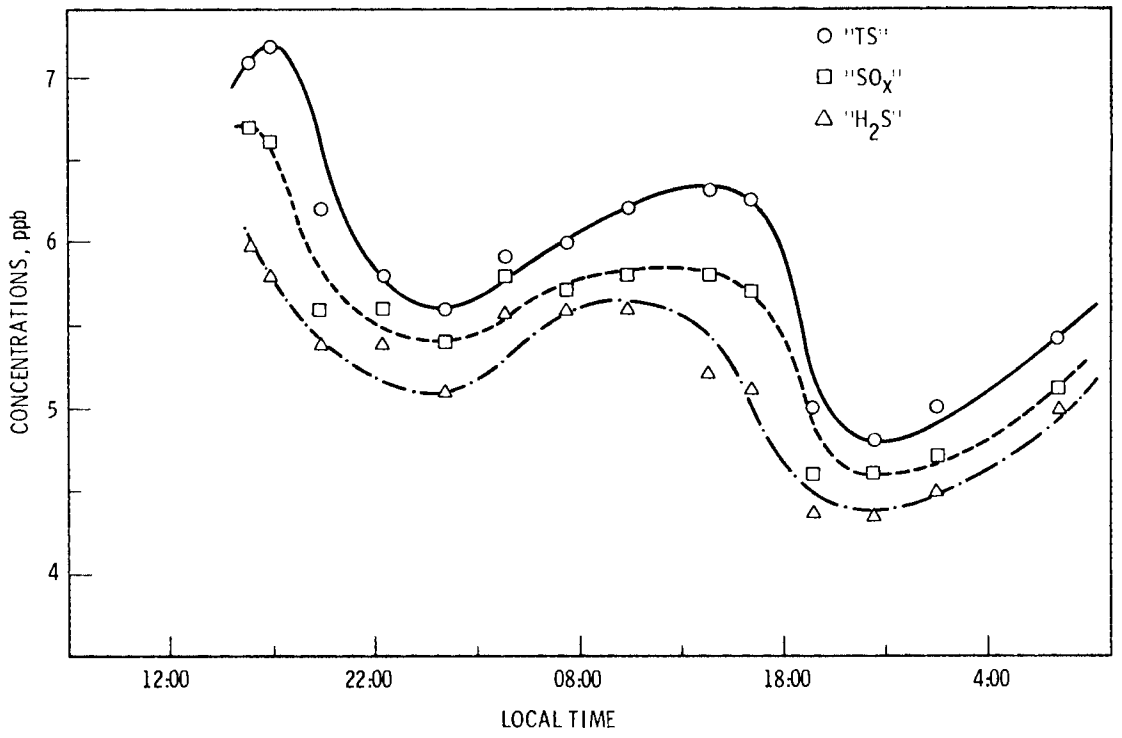

Figure 1.44. March of Concentrations of Gaseous Sulfur Compounds Measured at Corvallis, Oregon. Decreases after sunset can be attributed to either dry deposition or decreased emission, or both.

were almost calm during the 2-day period; the sky was clear; daytime humidity was 35% to 40%; temperatures ranged between 73°F at night to about 85°F during the day. The possibility of anthropogenic contributions to the observed variability cannot be dismissed. Figure 1.45 shows that at the altitude of scattered clouds (cumulus fractus) there is a sink of both condensation nuclei and total gaseous sulfur. Figure 1.46 also suggests a sulfur sink in clouds. At the start of these measurements at the top of the highest mountain in Oregon's coast range (Mary's Peak; measurements at 4097 ft ASL), the site was above an inversion layer with dense haze and mixed stratocumulus clouds. At this time, the site temperature was 61°F and the humidity was 64%. At the end of the 1-hr measurement period, the "undercast" had risen above the measurement site, the temperature had fallen to 49%, and the humidity was 100%.

From these measurements, the following conclusions were drawn:

- Increases in airborne sulfur during low tides at coastal estuaries are readily detectable.
- Clouds are a sink for gaseous sulfur.
- Background gaseous sulfur concentrations in Western Oregon are in the range of 1 to 10 ppb.
- Substantially greater effort will be needed, both in instrument development and in sampling, before natural sources and sinks of sulfur are quantified.

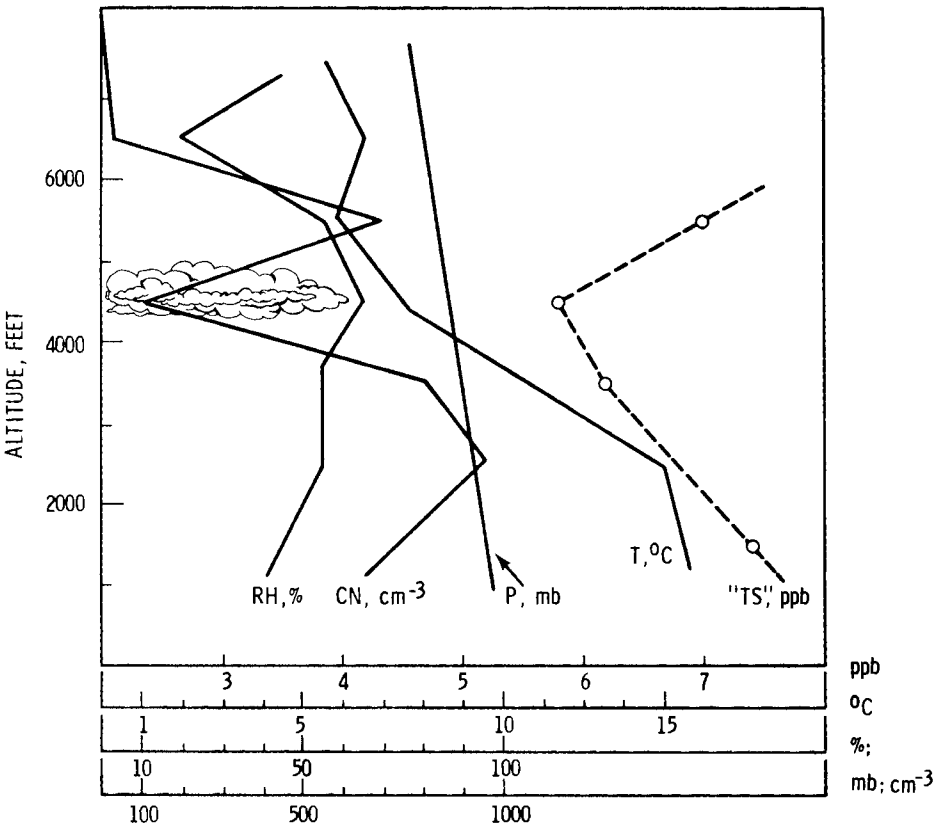

Figure 1.45. Vertical Profiles of Condensation Nuclei (CN) and Total Gaseous Sulfur (TS), Suggesting that Clouds are a Sink for both CN and TS

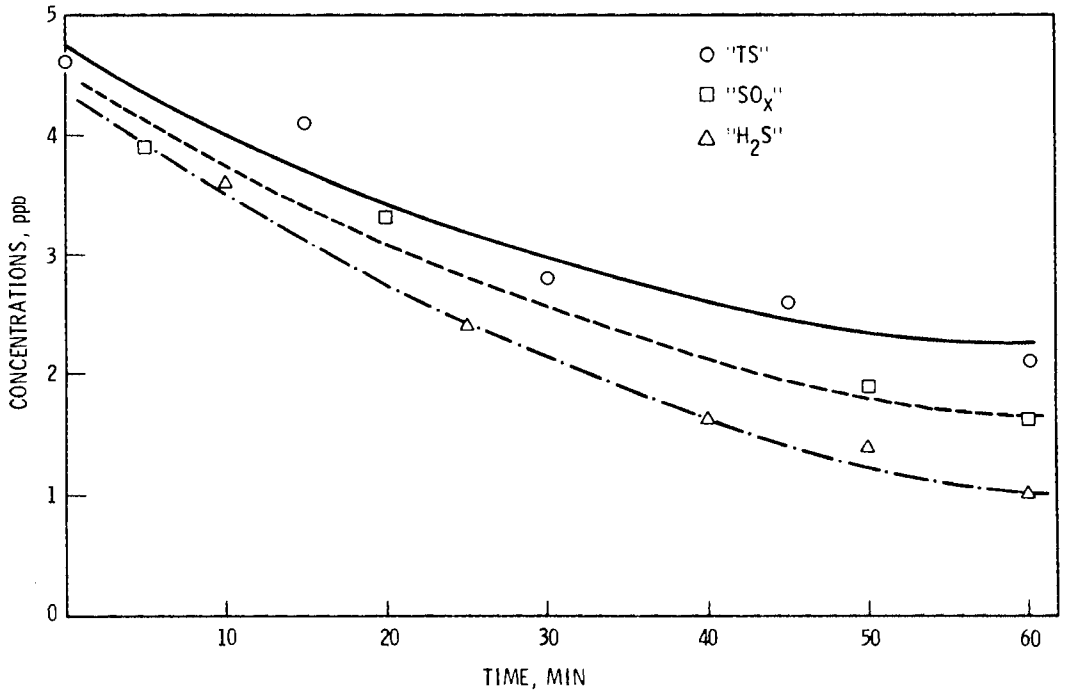

Figure 1.46. Decreases in Gaseous Sulfur Compounds as an "Undercast" Climbed to the Mountain-Top Measurement Site, and Enveloped the Site in Fog

Predictions for Particle Deposition on Natural Waters[a]

S. A. Slinn and W. G. N. Slinn

A simple two-layer model, shown schematically in Figure 1.47, has been used to develop predictions for aerosol particle deposition to lakes and oceans. The essence of the model is to account for possible particle-growth by water-vapor condensation in the humid region next to the water's surface.

The dry flux (positive, down) at the reference height $z = h$ is taken to be

$$D_{z=h} = k_C'(\chi_h - \chi_\delta) + v_g(a_d)\chi_h \qquad (1)$$

where $v_g(a_d)$ is the gravitational settling speed of a particle of (dry) radius a_d, and where the turbulent transfer velocity through the constant flux layer is taken to be

$$k_C' = \frac{1}{(1-\kappa)} C_D \bar{u}_h \qquad (2)$$

in which κ is von Karman's constant, $C_D = u_*^2/u^2$ is the drag coefficient based on reference height h, u_* is the friction velocity, and $\bar{u}$ is the mean wind speed. The factor $(1-\kappa)^{-1}$ in (2) was chosen to force the "deposition velocity for momentum" to have its correct value of $C_D \bar{u}$. For open waters, steady wind, near-neutral stability, and a 10-m reference height, Krauss (1972) gives $C_D = (1.3 \pm 0.3) \times 10^{-3}$; corrections for other than neutral stability are available.

For transport across the lower layer (approximately, the viscous sublayer), we used

$$D_{z=\delta} = k_D'(\chi_\delta - \chi_i) + v_g(a_w)\chi_\delta \qquad (3)$$

where $v_g(a_w)$ is the gravitational settling speed for a particle of (wet) radius a_w, and [based on earlier studies (Slinn 1977)], the "deposition layer's transfer velocity" was taken to be

$$k_D' = -\alpha m'' + \frac{1}{\kappa} C_D \bar{u} \left[Sc^{-1/2} + 10^{-3/St}\right] \qquad (4)$$

where the first term represents the contribution from diffusiophoresis [m" is the rate of water evaporation and $\alpha = 10^3$ cm $s^{-1}/(1$ g cm^{-2} $s^{-1})$ is a constant]; $Sc = \nu/D$ is the particle's Schmidt number (in which ν is air's kinematic viscosity and $D(a_w)$ is the particle's diffusivity); and $St = \tau u_*^2/\nu$ is the Stokes number or impaction parameter based on the height of the viscous sublayer ν/u_* (in which $\tau = v_g(a_w)/g$ is the particle's relaxation time). The change from a $Sc^{-2/3}$ to a $Sc^{-1/2}$ dependence of k_D' was suggested by attempts to account for slip of the water surface; typically, this slip is in the direction of the mean wind and with a speed equal to a few percent of the 10-m wind speed (i.e., comparable to u_*).

To obtain an expression for the deposition velocity, v_d, defined via

$$D_{z=h} = v_d (\chi_h - \chi_i) \qquad (5)$$

the following steps were taken: First, let $\chi_i = 0$ (i.e., ignore resuspension); secondly, assume steady-state conditions (i.e., take $D_h = D_\delta$); thirdly, use (1) and

(a) Atmospheric Environment, 14:1013-1016 (1980).

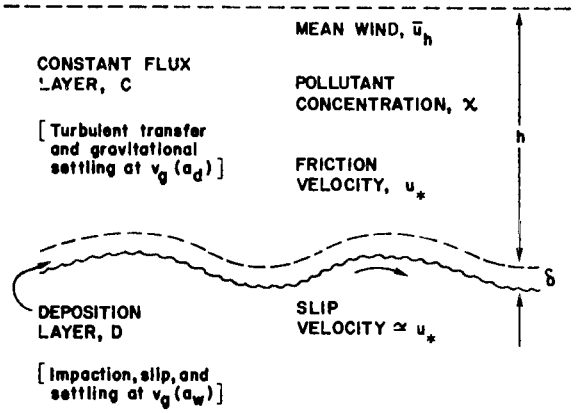

Figure 1.47. Schematic of the Two-Layer Model and Definition of Symbols

(3) to eliminate χ_δ in (1) and then set the resulting expression for D_h equal to (5). The result is

$$\frac{1}{v_d} = \frac{1}{k_c} + \frac{1}{k_D} - \frac{v_g(a_d)}{k_c\, k_d} \qquad (6)$$

where

$$k_c = k_c' + v_g(a_d) \qquad (7)$$

and

$$k_D = k_D' + v_g(a_w) \quad . \qquad (8)$$

Three features of this result are:

- Equation (6) is similar to the familiar result that the "overall transfer resistance," v_d^{-1}, is like a sum of transfer resistances in series, but the overall resistance is reduced by gravitational settling.
- If the only transfer process is gravitational settling, then $k_C = v_g(a_d)$, $k_D = v_g(a_w)$, and therefore $v_d = v_g(a_d)$, as desired.
- For momentum transfer, with $v_g = 0$ and $D = \nu$, the $v_d = C_D\, \bar{u}_h$, as desired.

Figure 1.48 shows plots of (6) for three wind speeds, m" = 0, and for three cases of particle growth: a) hydrophobic particles (i.e., $a_w = a_d$); b) particles that grow to the equilibrium size of ammonium sulfate particles for a relative humidity of 99% in the deposition layer; and c) the expected behavior of $(NH_4)_2SO_4$ particles depositing on lakes (i.e., using the equilibrium particle size as given by Fitzgerald (1975), for a relative humidity in the deposition layer of 100%). The assumption of equilibrium size for particles smaller than about 10 μm is consistent with the analysis by Toba (1965).

These results suggest to the authors that for most aged, atmospheric particles with mass-mean radii near 1 μm, it would be an acceptable approximation to assume their deposition on natural water is rate limited by turbulent transfer through the constant flux layer, and to use

$$(V_d)_h \approx C_D\, \bar{u}_h = 1.3 \times 10^{-3}\, \bar{u}_h \qquad (9)$$

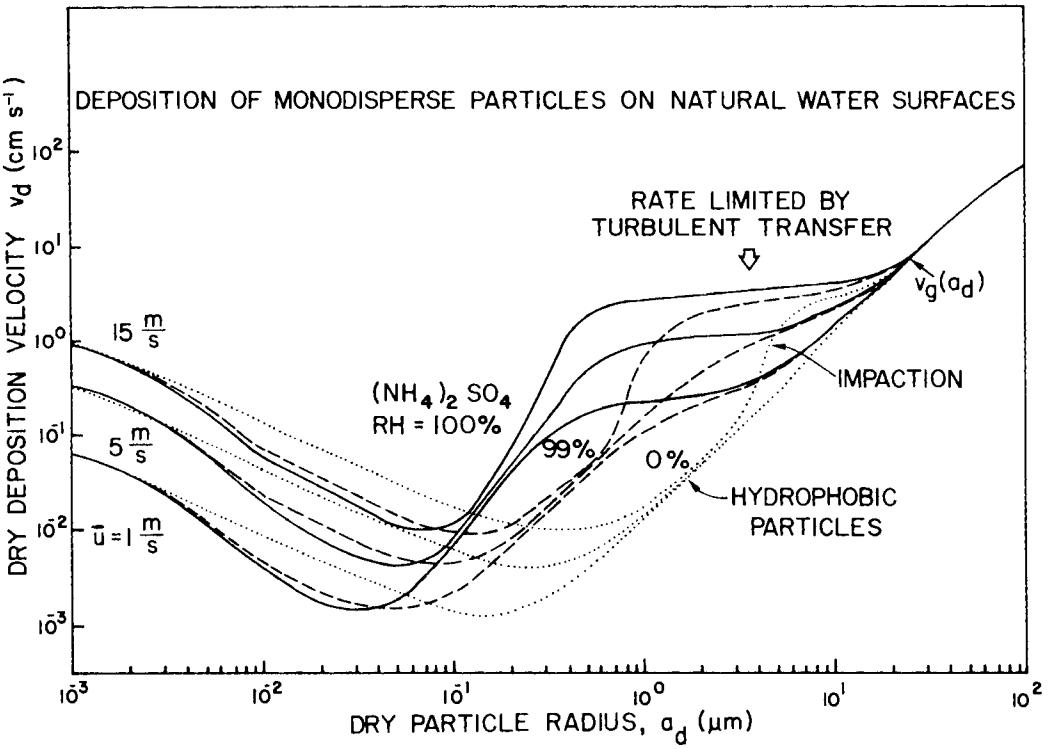

Figure 1.48. Plots of Equation (6) for Three Wind Speeds (1, 5 and 15 m s^{-1}), and for Three Types of Particles, as Described in the Text

This suggestion is consistent with recently reported data, although there are a number of factors that complicate interpretation of the data (see the published report).

References

Fitzgerald, J. W. 1975. "Approximate Formulas for the Equilibrium Size of an Aerosol Particle as a Function of its Dry Size and Composition and the Ambient Relative Humidity." J. Appl. Met. 14:1044-1049.

Krauss, E. B. 1972. Atmosphere-Ocean Interactions. Clarendon Press, Oxford.

Slinn, W. G. N. 1977. "Some Approximations for the Wet and Dry Removal of Particles and Gases from the Atmosphere." J. Water, Air, and Soil Poll., 7:513-543.

Toba, Y. 1965. "On the Giant Sea-Salt Particles in the Atmosphere II. Theory of the Vertical Distribution in the 10-m Layer over the Ocean." Tellus, 17:365-380.

Resuspension of Respirable Particles Deposited on Soil, Gravel, and Grass[a]

B. W. Reynolds[b] and W. G. N. Slinn[c]

Some of the many complexities of the resuspension of particles are indicated by Figure 1.49 (Slinn 1976). Most previous resuspension field studies have been of particle resuspension from sandy soils, and caused by natural wind (e.g., Anspaugh et al. 1975; Proch and Gillette 1977; Sehmel 1979). In this study, we seeded mown fescue grass, barren silt-loam soil, and medium-coarse gravel with known quantities of respirable-size, zinc-cadium sulfide particles (Leighton et al. 1965), and used a portable "wind-stress" generator to resuspend the particles. Details of the seeding method, the generator, and the sampling methods can be found in the full report (Reynolds and Slinn 1979). Here, results are emphasized, and can be summarized as follows:

- Resuspension rates are highest for gravel followed by soil and mown grass. Average rates during the period of observations were 1.3×10^{-8}, 2.3×10^{-8}, and 5.6×10^{-8} sec^{-1} for grass, soil, and gravel, respectively.

- The rates exhibited a strong dependence on the friction velocity exerted over these surfaces, with dependencies ranging from u_* raised to the 0.86 to 3.08 power, 0.49 to 3.18 power and 0.35 to 3.08 power for grass, soil, and gravel, respectively. Regression correlation coefficients varied from about 0.7 to nearly 1.0 for these data. Figure 1.50 illustrates the case of silt loam soil and is a representative set of results for this experiment.

- The different power-dependencies of the resuspension rates, Λ, on u_* are attributed mostly to varying surface moisture content of each surface during the measurement period. Gravel exhibited the most variability, very closely followed by soil and then mown grass. During the driest conditions, each surface's Λ showed a power dependence on u_* closely approximating u_*^3, agreeing with published results of other authors who conducted experiments in dry conditions.

- Consecutive, short bursts of wind stress were applied to the surfaces to determine how the resuspension rate changed in short periods of time during the moist, early part of the study. For grass and soil, Λ's were seen to decrease with increasing time steps, possibly indicating a depletion of readily available tracer with time. The trend was reversed in the case of gravel, for which it is postulated the drying effect of the passing airstream liberated orginally moisture-bonded particles on this less moisture-retentive surface.

- Some of each of the surfaces were exposed to selected wind and precipitation events and their impacts were measured by matching a sample from a weathered surface with a protected surface of the same type. With the exception of one nonrepresentative wind speed, soil followed by mown grass and then gravel appeared least-affected to most-affected by the defined weathering events (see Figure 1.50).

(a) Presented at the 73rd Annual Meeting of the Air Pollution Control Association, June 22-27, 1980, Montreal, Quebec. Reprint No. 80-68.4.

(b) Present address: Missouri Department of Natural Resources, Jefferson City, Missouri.

(c) The authors thank J. C. Correy, Savannah River Laboratory, for his initial guidance, and P. C. Katen and M. A. Wolf, Oregon State University, for their helpful suggestions.

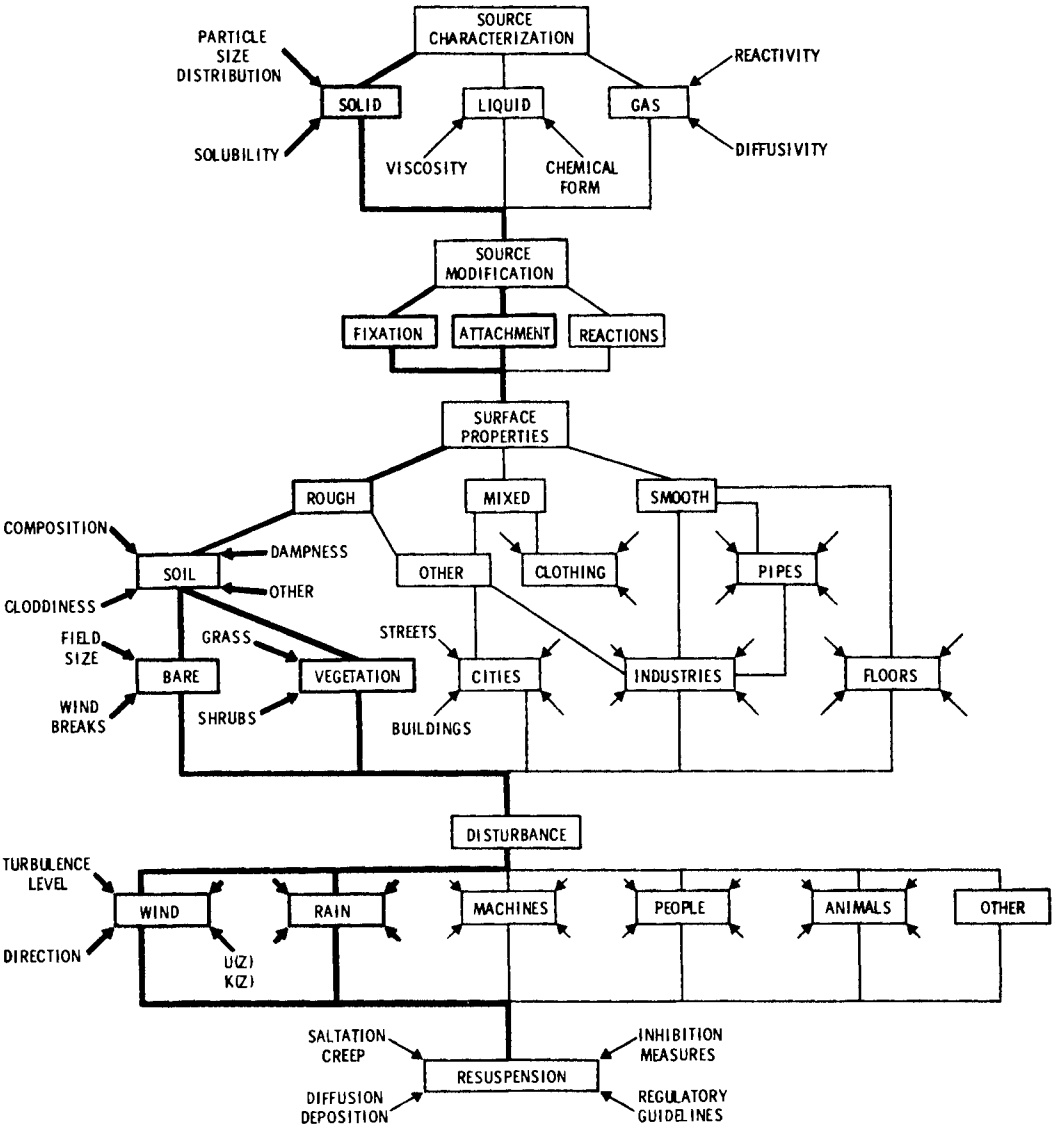

Figure 1.49. This Diagram Indicates Some of the Many Complicating Features of Resuspension

- Resuspension rates were plotted as functions of time since deposition in each friction velocity class for each surface to investigate the concept of a weathering rate. For soil and gravel, Λ's actually increased with increasing time. The decrease with time of resuspension from mown grass may be artificial in the sense that new growth and increased height of the grass blades increased filtering efficiency within the confines of the wind tunnel. The data suggest that the variation with time is more a seasonal characteristic than a depletion-by-fixation-to-nonresuspendibles as the weathering rate is normally defined. See Figure 1.51 for the case of silt-loam soil.

- In Figure 1.52, the characteristic roughness height, z_0, of each surface was matched with the corresponding average Λ obtained from the surface, and the results correlated with other authors' data. The results showed the average $\Lambda \propto z_0^{-1.4}$ with a regression correlation of about 0.8 for z_0s up to 0.10 m. It is postulated that for $z_0 > 0.1$ m, competitive processes arise such as enhancement caused by

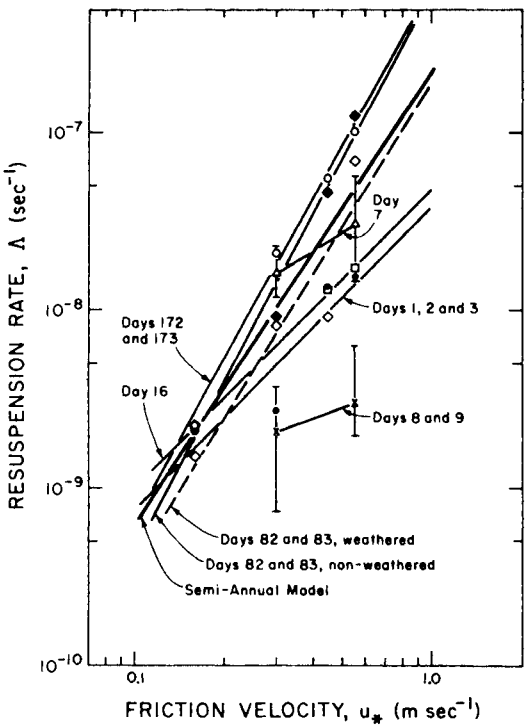

Figure 1.50. Resuspension Rates from Silt Loam Soil as a Function of Friction Velocity.

- ● = Days 1, 2 and 3; subjected to 1.5 hours intense drying.
- △ = Day 7; samples subjected to 4 hours intense drying
- X = Days 8 and 9; no surface drying and most moisture observed
- □ = Day 16; no surface drying but drier than all earlier samples
- ◇ ◆ = Days 82 and 83; no drying but driest samples to date for weathered and nonweathered samples, respectively
- 0 = Days 172 and 173; driest of all samples obtained
- ⊥ ‡ = Arithmetic means within a range of 4 data points

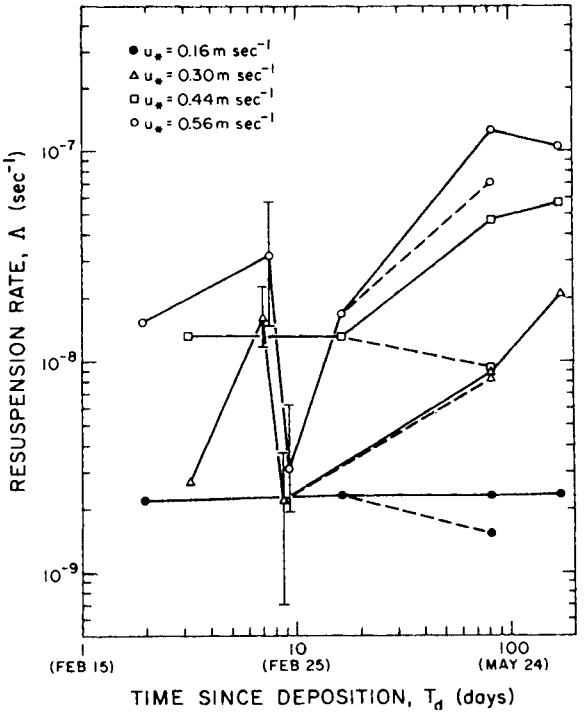

Figure 1.51. Resuspension Rates from Silt Loam Soil Displayed as a Function of Time Since Depositon for Weathered Samples (dashed lines) and Nonweathered Samples (solid lines) for Each of the Indicated Friction Velocities. ‡ Indicates the range for 4 data points; curves are drawn through the arithmetic mean of the range in each instance.

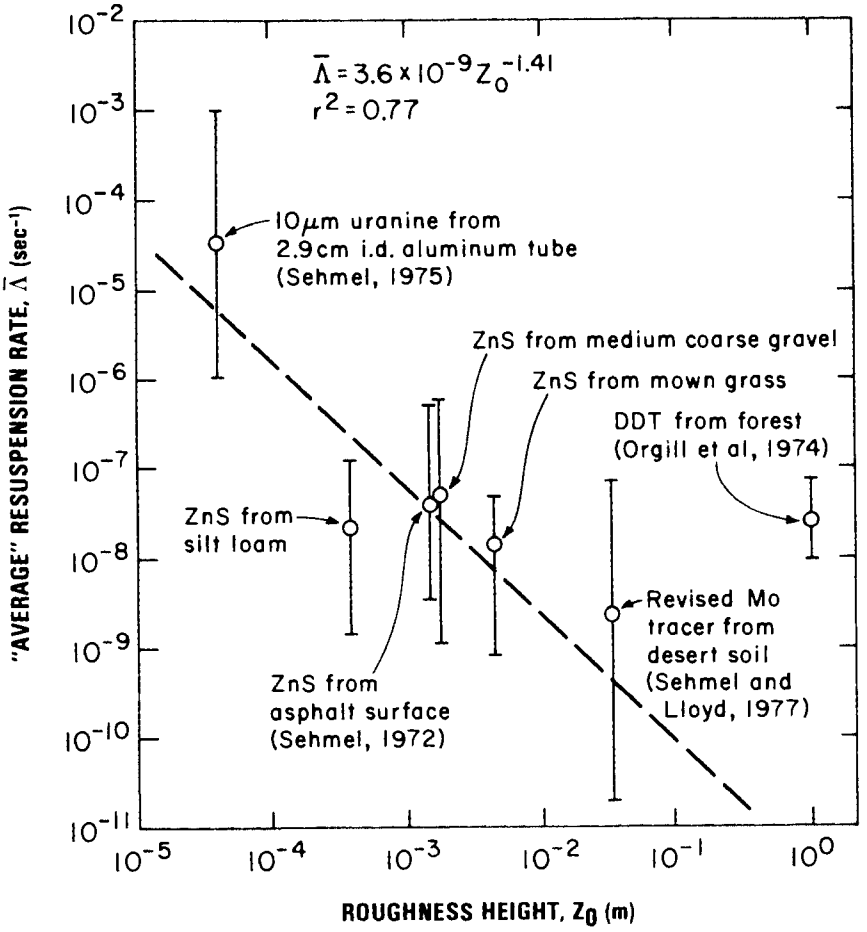

Figure 1.52. Average Resuspension Rates from Various Surfaces as a Function of Surface Roughness Height. The least-squares-fit model of the present data with the data of others (excluding the DDT data point) appears near the upper margin along with the regression correlation coefficient, r^2. Φ, represents the average resuspension rate and the range of values obtained in each instance.

swaying motions of individual roughness elements or inhibitions caused by increased filtration when the roughness elements are densely packed.

References

Anspaugh, L. R., J. H. Shinn, and P. L. Phelps. 1975. Resuspension and Redistribution of Plutonium in Soils, UCRL-76419, Lawrence Livermore Laboratory, Livermore, California. Available from NTIS, Springfield, Virginia.

Leighton, P. A., W. A. Perkins, S. W. Grinnel and F. X. Webster. 1965. "A Fluorescent Particle Atmospheric Tracer." J. Appl. Meteorology., 4:334-348.

Orgill, M. M., M. R. Peterson and G. A. Sehmel. 1974. "Some Initial Measurements of DDT Resuspension and Translocation from Pacific NW Forests." PNL Annual Report 1974 to the USAEC DBER, part 3, BNWL-1950, pp. 231-236, Pacific Northwest Laboratory, Richland, Washington. Available from NTIS, Springfield, Virginia.

Porch, W. A. and D. A. Gillette. 1977. "A Comparison of Aerosol and Momentum Mixing in Dust Storms Using Fast Response Instruments." J. Applied Meteorol., 16:1273-1281.

Reynolds, B. W. and W. G. N. Slinn. 1979. Experimental Studies of Resuspension and Weathering of Deposited Aerosol Particles, SR-0980-5, Air Resources Center, Oregon State University, Corvallis, Oregon. Available from NTIS.

Sehmel, G. A. 1972. "Particle Resuspension from an Asphalt Road Caused by Car and Truck Traffic." Atmos. Environment, 7:291-309.

Sehmel, G. A. 1975. "Initial Correlation of Particle Resuspension Rates as a Function of Surface Roughness Height." PNL Annual Report 1974 to the USAEC DBER, part 3, BNWL-1950, pp. 209-212, Pacific Northwest Laboratory, Richland, Washington. Available from NTIS.

Sehmel, G. A. 1979. "Deposition and Resuspension." Chapter 12 of Atmospheric Sciences and Power Production, ed. D. Randerson. PNL-SA-6746, Pacific Northwest Laboratory, Richland, Washington.

Sehmel, G.A. and Lloyd. 1977. "Wind-Caused Particle Resuspension Rates." PNL Annual Report for 1976 to USERDA DBER, BNWL 21000, Part 3, pp. 74-78, Pacific Northwest Laboratory, Richland, Washington. Available from NTIS.

Slinn, W. G. N. 1976. "Dry Deposition and Resuspension of Aerosol Particles." Atmosphere-Surface Exchange of Particulate and Gaseous Pollutants--1974, coords. R. J. Englemann and G. A. Sehmel, pp. 1-40. Available as CONF-740921 from NTIS, Springfield, Virginia.

Analytical Investigations of Inertial Deposition of Small Aerosol Particles from Laminar Flows onto Large Obstacles. Part E--Particle Motion Along the Upstream Axis of Symmetry[a]

S. C. Yoon[b] and W. G. N. Slinn[c]

Introduction

One of the fundamental problems in aerosol mechanics is to describe particle collection by various obstacles, such as raindrops, filter fibers, and elements of vegetation. A number of numerical calculations of particle trajectories are available.[a] In contrast, in the present series of reports, analytical solutions to the governing equations have been sought. These solutions have been in the form of perturbation series, and have been found by the method of matched asymptotic expansions and other methods developed for singular perturbation problems. In this report, perturbation solutions are compared with a new, exact solution we have found that is valid only for particle motion in potential flow about a sphere, along the upstream axis of symmetry near the stagnation point. In spite of these limitations, the exact solution will be extremely useful as the search continues for perturbation solutions valid for all values of the relevant perturbation parameter, for example, the Stokes number.

Along the upstream axis of symmetry, for potential flow about a spherical obstacle, the equation for a point particle's velocity, u, simplifies to

$$su\frac{du}{dx} + u = 1 + \frac{1}{x^3} \qquad (1)$$

where s is the particle's Stokes number and x is the distance from the center of the obstacle ($x \leq -1$, upstream). Near the stagnation point ($x = -1$), we use $x' = 1 + x$. A perturbation solution of (1) in the neighborhood of the stagnation point can be easily found:

$$u(x'; s) = -x'\,(A_1 + A_2\, s + \cdots + A_n\, s^{n-1} + \cdots) \qquad (2)$$

where $A_1 = 3$, and

$$A_n = \sum_{k=1}^{n-1} A_k\, A_{n-k},\quad n \geq 2 \qquad (3)$$

A Domb-Sykes plot (Van Dyke 1974; 1975) for A_{n+1}/A_n (see Figure 1.53) shows that the radius of convergence of (2) (i.e., the critical Stokes number s_*) is $s = s_* = 1/12$. This result is in agreement with Taylor's critical Stokes number, found in a different manner (see Fuchs 1964 or Parts C and D of the 1974 Annual Report).

In Parts C and D, some of limitations of these perturbation solutions were described. In particular, it was suggested that for $s > s_*$ the solution in the (u,x) plane could be a multi-valued spiral around $x = -1$. A significant advance in this reporting period was to find an exact

---

(a) Earlier reports in this series, by W. G. N. Slinn, are Parts A and B, contained in the 1973 Annual Report, and Parts C and D, contained in the 1974 Annual Report.

(b) Department of Atmospheric Sciences, Oregon State University, Corvallis, OR.

(c) The authors thank Professor Milton Van Dyke, Stanford University, for his valuable advice.

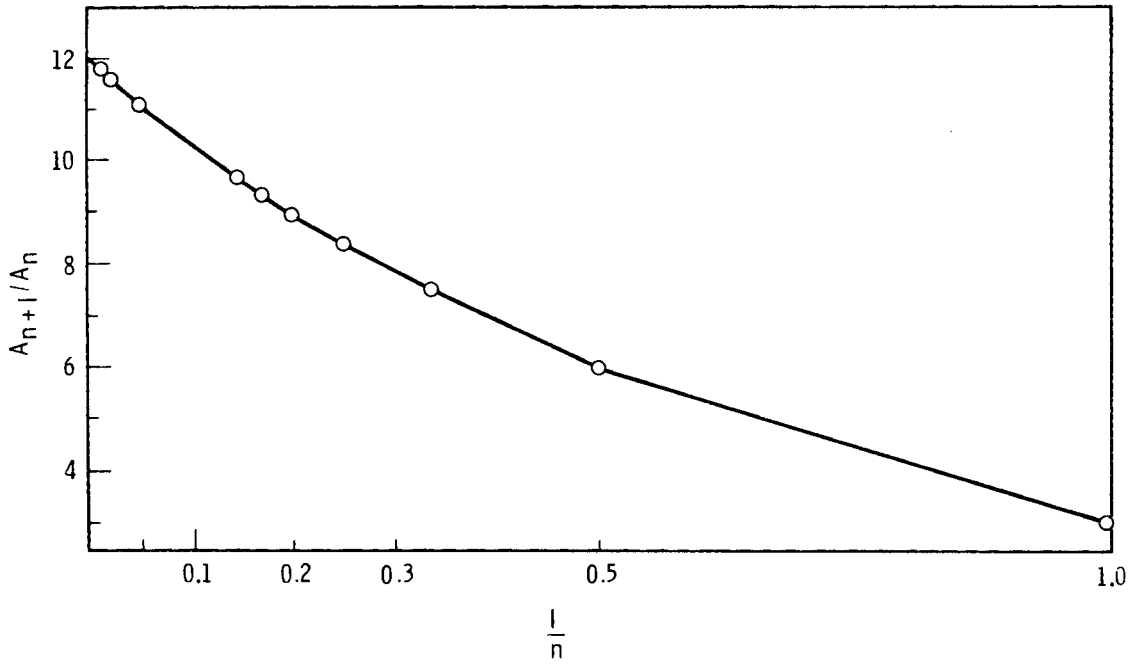

Figure 1.53. Domb-Sykes Plot Showing that the Radius of Convergence of Equation (2) is $s = s_4 = 1/12$

solution for this spiral form. To obtain the result, variables were transformed according to

$$u = r\cos\phi$$

$$x' = -\sqrt{\frac{s}{3}}\, r \sin\phi \qquad (4)$$

Near the stagnation point, (1) then becomes

$$\frac{dr}{r} = \frac{\cos^2\phi\, d\phi}{\sqrt{3s} - \cos\phi \sin\phi} \qquad (5)$$

whose solution for $s < 1/12$ is

$$r\left|\sqrt{12s} - \sin 2\phi\right|^{1/2} = r_0$$

$$\left|\frac{\sqrt{12s}\tan\phi - 1 - \sqrt{1 - 12s}}{\sqrt{12s}\tan\phi - 1 + \sqrt{1 - 12s}}\right|^{1/2\sqrt{1-12s}} \qquad (6)$$

and, for $s > 1/12$,

$$r\left|\sqrt{12s} - \sin 2\phi\right|^{1/2} = r_0 \exp$$

$$\left[\frac{1}{\sqrt{12s - 1}}\ \tan^{-1}\left\{\frac{\sqrt{12s}\tan\phi - 1}{\sqrt{12s - 1}}\right\}\right] \qquad (7)$$

where r_0 is a constant determined by boundary conditions.

As an example of this new, exact solution given by (6) and (7), consider the case with the boundary condition $u = 3$ at $x' = -1$ (i.e., $x = -2$). Exact solutions are plotted in Figure 1.54 for several Stokes numbers and compared with the perturbation solutions. For large s, the perturbation solution is obtained as in Part A by solving

$$u\frac{du}{dx'} + \sigma(u + 3x') = 0,\ \sigma = 1/s << 1 \qquad (8)$$

The solution with $u = 3$ at $x' = -1$ is

$$u(x';\sigma) = 3 - \frac{1}{2}(x' + 1)^2\,\sigma - \frac{(x' + 1)^3}{72}$$

$$[3(x' + 1) - 4]\,\sigma^2 - \frac{(x' + 1)^4}{2160}$$

$$[15(x' + 1)^2 - 26(x' + 1) + 10]$$

$$\sigma^3 + 0(\sigma^4) \qquad (9)$$

The exact solution clearly shows that all particles with $s < 1/12$ stop at the sphere's surface, and those with $s > 1/12$ impinge on the sphere's surface with increasing spead as s increases. Obviously, the perturbation solutions are quite accurate compared with the exact solution.

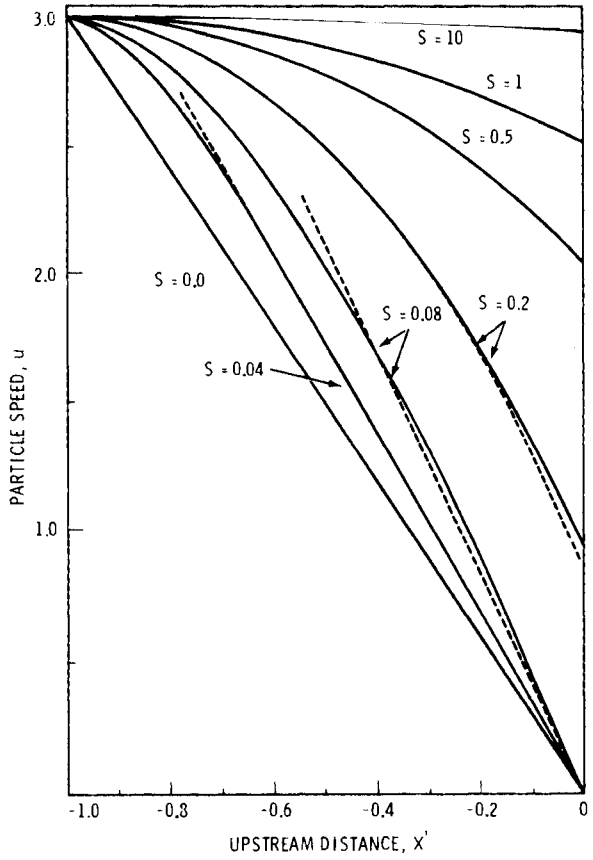

Figure 1.54. Comparison of the Exact Solution (solid lines) with the Perturbation Solutions (dotted lines); Only the First Three Terms in the Perturbation Solutions were Used; the Upstream Boundary Condition was Forced

The main significance in having an exact solution available, even if it is valid only near the stagnation point and along the axis of symmetry, is that we can now study the nature of the critical-Stokes-number singularity. From (6) and (7), it is clear that the singularity is complicated. Additional investigations are planned.

References

Fuchs, N. A. 1964. The Mechanics of Aerosols, Pergamon Press, New York.

Van Dyke, M. 1974. "Analysis and Improvements of Perturbation Series." Quart. J. Mech. Appl. Math., 27:423-450.

Van Dyke, M. 1975. "Computer Extension of Perturbation Series in Fluid Mechanics." SIAM J. Appl. Math., 28:720-734.

2 Fission and Fusion

FISSION AND FUSION

- **Air Pollution Dry Deposition: Radioisotopes as Particles and Volatiles**
- **Fallout Rates and Mechanisms**
- **Particle Resuspension and Translocation**
- **ALE Climatology**
- **Reactor Safety Study**

The major pollutants of concern from the nuclear energy industry are long-lived particles (i.e., plutonium and other radionuclides) and waste heat and water vapor from power plant cooling systems. Since these pollutants may affect living species and local and regional climate in an adverse manner, field, laboratory and theoretical investigations of their fate are important to human welfare.

Research activities at PNL include studies of atmospheric diffusion and deposition of material on the earth's surface, resuspension of particulate matter, and regional and global transport of material. Transport studies include the modeling of vertical diffusion and deposition, the determination of the effect of wind speed on resuspension rates and the study of the vertical temperature structure.

• Air Pollution Dry Deposition: Radioisotopes as Particles and Volatiles

Objectives of this study are:

- Developing an experimental basis for models predicting removal of airborne particles and gases by dry deposition onto outdoor surfaces.
- Developing predictive models accounting for the influence of particle size, gas characteristics, wind velocity, deposition surface, and other variables on deposition rates.
- Determining deposition rates using dual tracer techniques in the field and in a wind tunnel in the laboratory.

Volcanic Ash and Ambient Airborne Solids Concentrations at Hanford, Washington, Sampling Sites Subsequent to the Mt. St. Helens' Eruption

G. A. Sehmel

Introduction

A major eruption of Mt. St. Helens, Washington, occurred on May 18, 1980, resulting in an airborne plume of volcanic ash (pulverized rock) transported by easterly winds. Particle dry deposition from this plume resulted in downwind ash fallout of varying depths. The Hanford area, northwest of Richland, Washington, was within the edge of the fallout plume. Located within this area are airborne particulate sampling sites used in prior wind resuspension experiments. These sampling sites were reactivated to collect airborne volcanic ash. The Horn Rapids sampling site is near the southwestern boundary of the Hanford area, and the meteorological station sampling site is 24 km northwest of the Horn Rapids Dam site. Both sites received relatively low ash deposits which were about 1- to 2-mm and 3- to 4-mm in depth, respectively.

This investigation set out to determine a time history of airborne volcanic ash concentrations (Sehmel 1980) immediately after the eruption (starting the following day, May 19). In addition to recording airborne solid concentrations, any changes in airborne volcanic ash concentrations with time were of potential use to wind-resuspension investigations of surface-contaminated areas. Volcanic fallout ash was a tracer of opportunity for investigating wind resuspension from a near "infinite" surface source area of freshly deposited solids.

Sampling Equipment

Airborne solids concentration was measured using filters for solids collection on an average daily basis (or several days) by 1) sampling continuously for all wind directions and speeds at the Horn Rapids and meteorological station sampling sites, and 2) sampling only during 220° to 290° wind directions at the meteorological station sampling site. Winds from the south are from 180° while winds from the west are from 270°.

Airborne particulates were classified (while airborne) into two or more size fractions with three different types of sampling equipment:

- A cyclone preseparator[a] with a 5.5-μm 50% cut-off diameter, followed by a 20- x 25-cm^2 glass-fiber filter. During sampling, the cyclone-preseparator cylindrical sampler inlet was continuously oriented into

(a) Model 230CP cyclone preseparator, Sierra Instrument Co., Carmel Valley, CA 93924.

the wind with a tail fin. Except during rain, sampling was continuous for 24 hours.

- A 20- x 25-cm^2 filter sampler. In this sampler (Sehmel 1978), airborne particles either settled in the sampler inlet (1.9- x 25-cm^2 cross section) or were collected on the backup filter. Airborne solids concentration was calculated from only the filter collection.

- A laser optical particle counter.(a) This optical counter sizes airborne particles electronically and accumulates number counts in diameter increments as small as 0.07 μm. Measurements were taken during 30-min increments at a site near the Hanford meteorological station. Results are reported as the volume distribution:

$$\frac{\Delta V}{\Delta \ln D} = \frac{\pi D^4}{6} \frac{\Delta N}{\Delta D}$$

which has units of μm^3/cm^3. The particle volume is V, the diameter is D, and the number of particles per unit volume is N.

(a) Active Scattering Aerosol Spectrometer, Particle Measuring Systems, Inc., Boulder, CO 80301.

Airborne Solids Concentration

Airborne solids concentration, μg/m^3, is shown in Figure 2.1 along with selected meteorological data (shown below the figure) recorded at the Hanford meteorological station.

Horn Rapids Site Results

Two cyclone filter samplers were used at the Horn Rapids sampling site to investigate airborne solids concentration and sampling reproducibility. The two samplers were 2 m apart. Average concentrations for these two samplers are shown by both open- and solid-data symbols in Figure 2.1. Each datum point is plotted at the average concentration calculated from these two samplers. The limits of the vertical bar through each datum point are solid concentrations determined from each sampler. If limits are not shown, the limits are within the datum symbol.

During the day after the eruption, the daily average concentration for respirable particles (i.e., <5.5-μm dia. was 1430 μg/m^3), the total, including the cyclone-preseparator collection, was 2610 μg/m^3. The respirable content of the airborne solids was 55%. Subsequently, the daily average airborne solids concentration decreased. From May 20 to 27, concentrations of 150 to 600 μg/m^3 were measured and

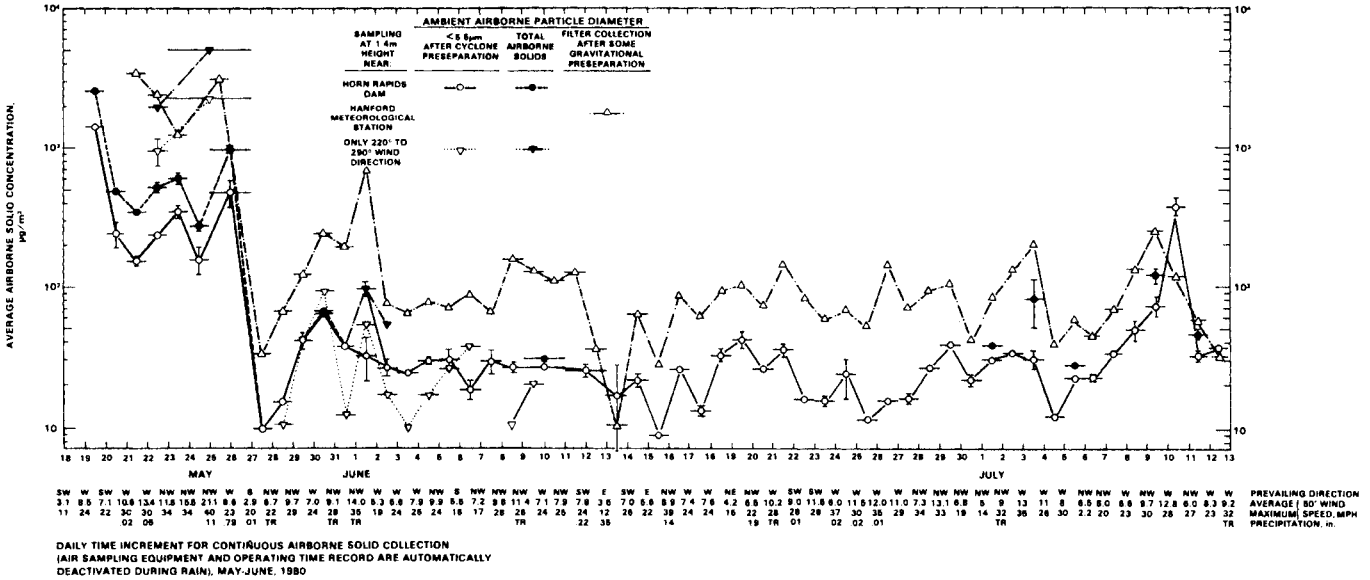

Figure 2.1. Airborne Solid Concentrations Measured at Two Hanford Area Sampling Sites after the Mt. St. Helens Eruption on May 18, 1980.

were still high compared to normal (prior to eruption) concentrations.

There were three rain periods, including four successive days from May 25 to 28, which could have affected the wind resuspendability of volcanic ash, 0.11 in., 0.79 in., 0.01 in. From a comparison of rain accumulated each day and airborne solids concentration, an estimate can be made of the rain accumulation that can remove airborne particulates and prevent wind resuspension of surface solids by wetting ground surfaces. Decreased airborne solids concentration was evident on May 27 to 28 when the concentrations decreased two orders of magnitude at both sampling sites, and on June 12 to 13 when the concentrations decreased one order of magnitude at the meteorological station sampling site. Subsequently, airborne solids concentration increased as ground surfaces dried and resuspension occurred.

Although resuspension and, hence, airborne solids concentration are a function of both surface and meteorological parameters, an estimate is made for the amount of rain required to significantly reduce resuspension. There were only three significant rain periods recorded:

- 0.79 in. on May 26
- 0.22 and 0.35 in. (0.57 in. total) on June 12 and 13
- 0.19 in. on June 20.

Significant (i.e., an order of magnitude) reductions in airborne solids concentration occurred only during the first two rain periods (0.79 and 0.57 in.) and not during the last period (0.19 in.). Thus, a tentative conclusion is that from 0.2 to 0.6 in. of rain may be required to significantly reduce airborne solids concentration arising from wide-area resuspension sources. However, the duration of reductions may be as short as a day.

Airborne-Volume Distribution Ranges

Airborne-volume distributions calculated from the optical counter operated near the Hanford Meteorolgical Station are shown in Figure 2.2 as a function of particle diameter. The ranges of optical counter results from May 22 to 30, 1980, are shown by the cross-hatched area. Also shown are ranges determined at Hanford in 1975 (Sehmel 1976) during dust storms and on clear days. The ranges for the volcanic ash overlay the 1975 data, showing that during measurement

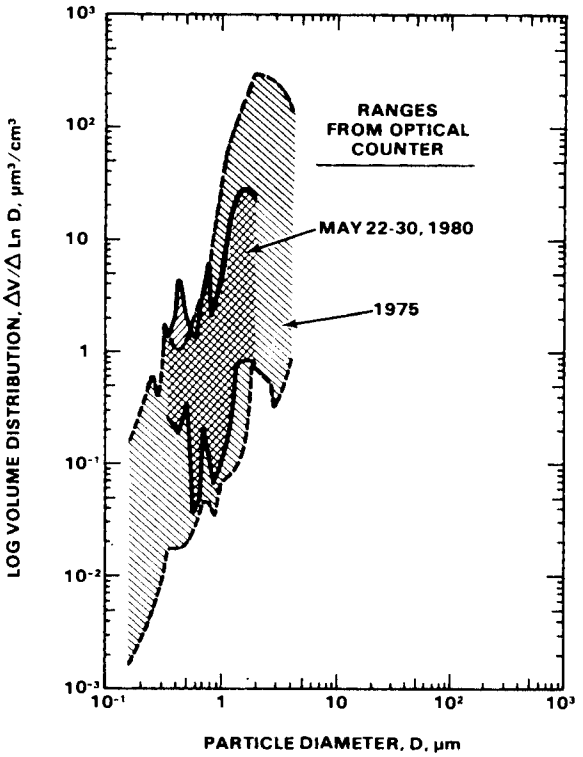

Figure 2.2. Airborne-Volume Distributions

times the maximum airborne volcanic ash concentrations for the particle diameters investigated were similar to dust concentrations during the most severe dust storms measured in 1975 by Sehmel (1976). However, a significant difference between volcanic ash and dust storm data occurs for particle diameters between 0.3 and 0.5 μm. For this diameter range, the maximum ash concentration was about four times greater than reported for dust storms.

Conclusions

Airborne solids concentrations of volcanic ash increased from a sampling site in the Hanford area to another site 24 km northwest. This second site was closer to the maximum ash fallout area. At both sampling sites, a rain of 0.79 in. on May 26 decreased airborne solids concentration by two orders of magnitude. Subsequently, airborne solids concentration increased as surfaces dried and resuspension occurred. Changes in airborne solids concentration after subsequent rains were interpreted to indicate that 0.2 to 0.6 in. of rain may be required to significantly reduce, at least for a day, airborne solids concentration from area-wide resuspension sources. Even after the initial rain, airborne solids concentration remained relatively

high at the meteorological station sampling site. Airborne solids concentration data are still being obtained at both sampling sites so the longer-term airborne effects of this surface resuspension source can be investigated.

References

Sehmel, G. A. 1980. "Ambient Airborne Solids Concentrations Including Volcanic Ash at Hanford, Washington, Sampling Sites Subsequent to the Mount St. Helens Eruption." PNL-SA-8772, Pacific Northwest Laboratory, Richland, Washington.

Sehmel, G. A. 1978. "Isokinetic Air Sampler." In: Pacific Northwest Laboratory Annual Report for 1977 to the DOE Assistant Secretary for the Environment, Atmospheric Sciences, PNL-2500-3, pp. 1.32-1.34. Pacific Northwest Laboratory, Richland, Washington.

Sehmel, G. A. 1976. "The Influence of Soil Insertion on Atmospheric Particle Size Distributions." In: Pacific Northwest Laboratory Annual Report for 1975, Atmospheric Sciences, BNWL-2000-3, pp. 99-102. Pacific Northwest Laboratory, Richland, Washington.

Plutonium Dry Deposition Experiments Using Ambient Airborne Plutonium Near Horn Rapids, Washington

G. A. Sehmel

Airborne concentrations of solids and plutonium were measured (Sehmel 1979a) at two sampling sites separated by a distance of 305 m near the Horn Rapids Dam, Washington. The purpose of these measurements was to determine the deposition or resuspension of ambient soil and plutonium between two sampling towers. In the experimental design, a uniform, crosswind airborne plume of resuspended soil was anticipated to be approaching the upwind tower. Subsequently, plume depletion between towers would occur as a result of dry deposition. The decreased concentration near the surface would be measured at the downwind tower. The deposition rate would be estimated from the differences between towers in the integrated concentrations as a function of height.

Air samplers were located on each tower at six sampling heights from 0.3 m to 20 m above ground. Three sets of isokinetic air samplers (Sehmel 1978 and 1979b) were attached on each tower. When the wind speed and wind direction were identical at each tower (i.e., a wind direction of 233° ± 45° and wind speed increments of 3 to 5, 5 to 7, and 7 to 11 m/sec measured at an elevation of 30 m), the three sets of isokinetic air samplers were automatically turned on at both upwind and downwind towers.

An inlet closure on the isokinetic air samplers was opened when the wind direction and speed criteria were satisfied. "Larger" particles collected by gravity settling in the isokinetic sampler inlet, whereas "small" particles remaining airborne within the sampler were collected on a 20- x 25-cm filter. The sampling rate was 1.1 m^3/min (40 cfm).

All collected samples were weighed for total collected solids and, in some cases, analyzed for plutonium content. Calculated results are shown here for the airborne solids concentration, $\mu g/m^3$, and for material collected on the filter as well as for the total including the sampler inlet collection. For plutonium analysis, only filter samples for the 5- to 7-m/sec wind speed increment were analyzed.

Airborne Solids

Airborne solids concentration for both upwind and downwind sampling towers are shown as a function of height in Figure 2.3. Upwind and downwind concentrations are shown by solid and dashed lines, respectively. Airborne solid concentrations determined from only filter collection are shown in three sections on the left side of the figure. On the right side of the figure, total airborne solids collected on both the filter and the isokinetic sampler inlet are shown. For the 3- to 5-m/sec wind speed increment, airborne concentrations determined from filter collection were less at the downwind tower for sampling heights below about 5 m. This decrease indicated deposition between towers. Unexpectedly, however, for heights above about 5 m, airborne solids concentrations were greater downwind.

For the 5- to 7-m/sec wind speed increment, airborne concentrations decreased with downwind distance for both solids collected on the filter as well as total solids collected on the filter plus sampler inlet. Similarly, for the 7- to 11-m/sec wind speed increment, airborne solid con- centrations decreased with downwind distance.

Changes in the total airborne solids between towers were calculated. For the calculations, concentrations at each tower were integrated with respect to height. A

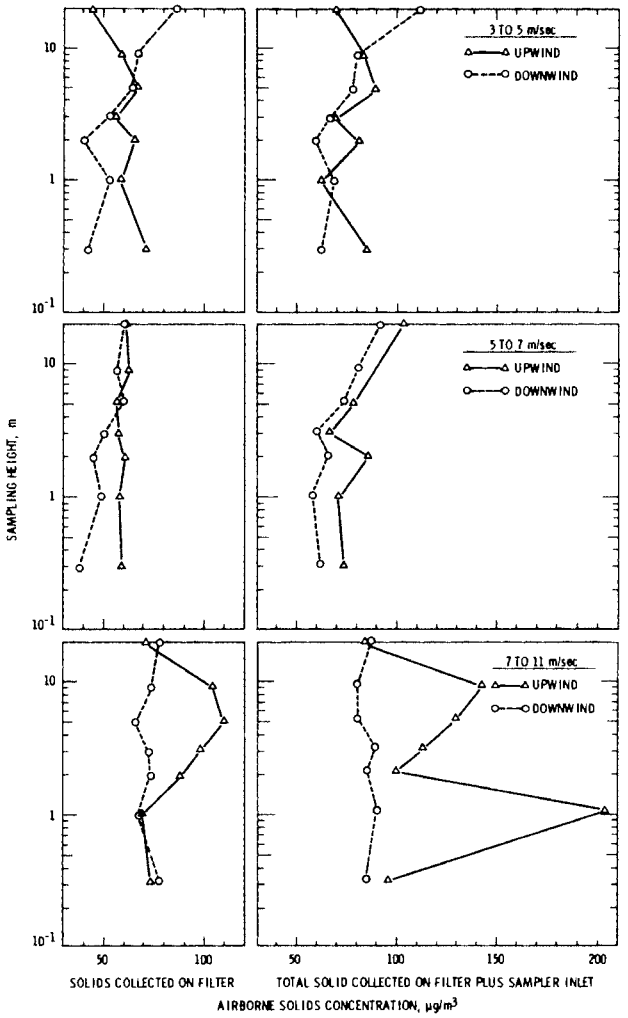

Figure. 2.3. Average Airborne Solids Concentration During Identical Wind Speed Increments and Direction 233° ± 45° at an Upwind Site and a Sampling Site 305 m Downwind Along 233° Collected from July 21 to November 20, 1978.

constant air speed with height was assumed. Then, the ratio of the downwind to upwind integrated concentrations were calculated. These ratios are shown in Table 2.1. Although ratios do change as a function of sampling height, the ratios do decrease with downwind distance. At a sampling height of 20 m, the ratio ranges from 0.60 up to 0.84 with one exception at a ratio of 1.05. One interpretation of these data is that approximately 16% to 40% of the total solids was lost either by dry deposition or was transported above the downwind sampling sampler.

Airborne Plutonium

Airborne plutonium concentrations are compared for the 5- to 7-m/sec wind speed increment in Figure 2.4. Shown in this figure are plutonium solids concentrations, µCi/g, airborne plutonium concentrations, $\mu Ci/cm^3$, and airborne solids concentrations, $\mu g/m^3$, for comparison purposes. It is surprising that at the 2- and 3-m heights of the upwind sampling tower the µCi/g are approximately three times greater than for any other sample at the upwind tower.

Table 2.1. Downwind to Upwind Ratio of Airborne Solids: Integrated Total From Ground Level to Indicated Heights

	Ratio: Downwind/Upwind					
	Wind Speed 3 to 5 m/sec		Wind Speed 5 to 7 m/sec		Wind Speed 7 to 11 m/sec	
Sampling Height, m	Filter Collection	Filter + Inlet	Filter Collection	Filter + Inlet	Filter Collection	Filter + Inlet
20	0.60	0.73	0.65	0.84	1.05	0.84
9	0.72	0.87	0.73	0.83	1.02	0.83
5	0.73	0.88	0.76	0.82	0.96	0.82
3	0.75	0.87	0.78	0.82	0.89	0.82
2	0.83	0.88	0.86	0.87	0.79	0.87
1	0.93	0.90	0.91	0.91	0.72	0.91
0.3	1.23	1.11	0.94	0.92	0.82	0.92

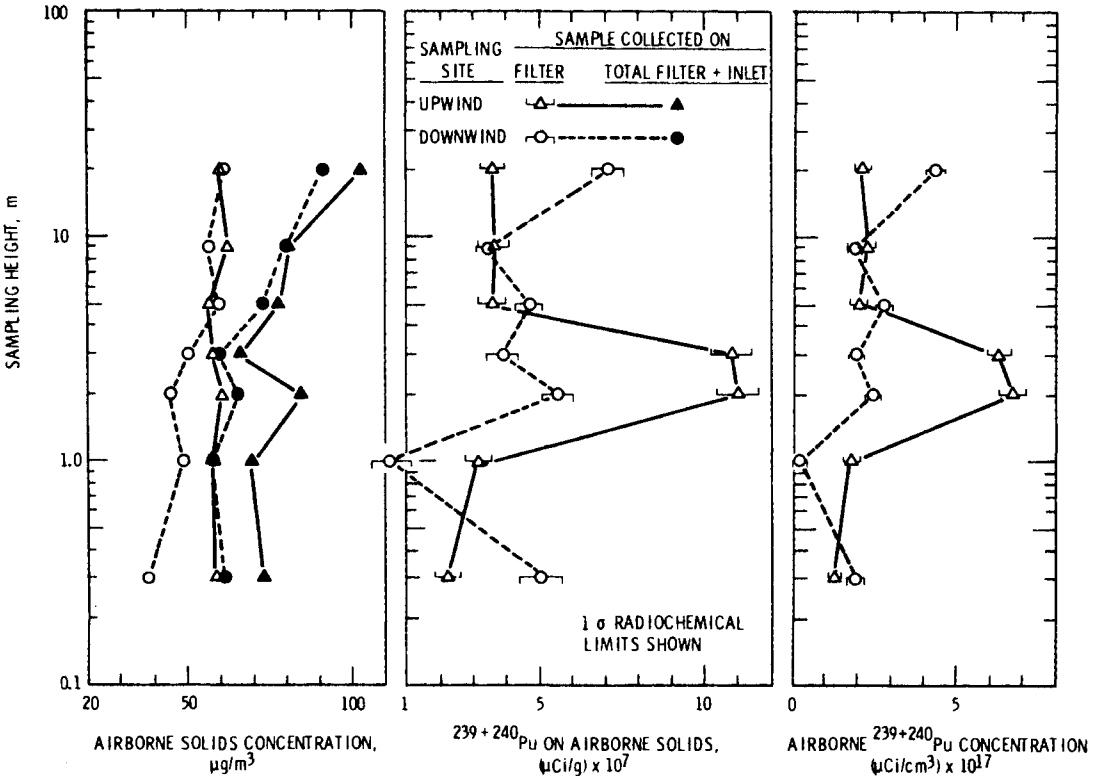

Figure 2.4. Average Airborne Solids and $^{239-240}Pu$ Concentrations as a Function of Height Near Horn Rapids at Hanford from July 21 to November 20, 1978, When Sampling an Identical Wind Speed Increment of 5 to 7 m/sec and Direction 233° ± 45° (Measured at a Height of 30 m) at Both an Upwind Site and a Sampling Site 305 m Downwind Along 233°

Airborne plutonium concentrations, $\mu Ci/cm^3$, are shown on the right side of Figure 2.4. Again, airborne concentrations at the upwind tower sampling heights of 2 and 3 m are approximately three times greater than for any other sample at the upwind tower.

An estimate of the total airborne plutonium changes between upwind and downwind sampling towers was made after integrating the airborne plutonium concentrations with respect to height. We assumed the air speed to be 5 to 7 m/sec at all sampling heights. The ratios of upwind to downwind integrated airborne plutonium concentrations are shown in Table 2.2. Although the total airborne plutonium below 20 m is nearly constant between sampling towers, there are unresolved questions concerning these airborne plutonium concentrations.

Table 2.2. Downwind to Upwind Ratio of Airborne Plutonium: Integrated Total From Ground Level to Indicated Height for a 5 to 7 m/sec Wind Speed Increment

Sampling Height, m	Ratio: Upwind/Down for Filter-Collected Plutonium
20	1.02
9	0.67
5	0.48
3	0.36
2	0.38
1	0.64
0.3	1.46

Plutonium-240/239 Atom Ratios

Plutonium isotopic analyses were made on filter samples because further explanations about the measured atom ratios might be found. The results are shown in Figure 2.5. The $^{240/239}Pu$ atom ratios reflect the presence of both fallout and locally-produced plutonium.

Fallout is indicated by the ratios above about 0.15; at the 2- and 3-m height of the upwind tower the lower ratios from 0.0829 to 0.1142 reflect the presence of locally-produced plutonium. These results are a further confirmation that Hanford process-grade plutonium is transported from off-site near the Hanford southwestern boundary.

Conclusions

At the upwind sampling tower the airborne plutonium concentrations are greatest for sampling heights of 2 and 3 m. For all other sampling heights at both the upwind as well as all sampling heights at the downwind tower, the airborne plutonium concentrations appear to be reasonably uniform as a function of height. Surprisingly, the total airborne plutonium appears to be constant with downwind distance. Additional data are needed to interpret these plume depletion differences between airborne

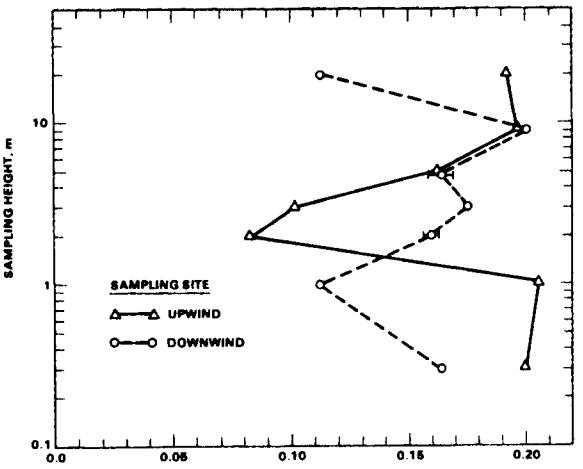

Figure 2.5. $^{240}Pu/^{239}Pu$ Atom Ratios for Airborne Solids Collected on Filters as a Function of Height Near Horn Rapids at Hanford from July 21 to November 20, 1978, When Sampling an Identical Wind Speed Increment of 5 to 7 m/sec and Direction 233° ± 45° (Measured at a Height of 30 m) at Both an Upwind Site and a Sampling Site 305 m Downwind Along 233°

solids concentrations and airborne plutonium concentrations with downwind distance.

References

Sehmel, G. A. 1978. "Isokinetic Air Sampler." In Pacific Northwest Laboratory Annual Report for 1977 to the DOE Assistant Secretary for the Environment, Part 3, Atmospheric Sciences. PNL-2500-3, PT 3, pp. 1.32-1.34, Pacific Northwest Laboratory, Richland, Washington.

Sehmel, G. A. 1979a. "Particle Dry-Deposition Experiment Using Ambient Airborne Soil." In Pacific Northwest Laboratory Annual Report for 1978 to the DOE Assistant Secretary for the Environment, Part 3, Atmospheric Sciences. PNL-2850-3, PT 3, pp. 3.12-3.15, Pacific Northwest Laboratory, Richland, Washington.

Sehmel, G. A. 1979b. Isokinetic Air Sampler, U.S. Patent 4,159,635, July 3, 1979.

• Fallout Rates and Mechanisms

Objectives of this study are:

- Measuring radionuclide concentrations at Barrow, Alaska, and Richland, Washington, for the assessment of the hazard to the environment presented by future radionuclide releases.
- Determining the physical and chemical forms of airborne radionuclides and their deposition rates.
- Calculating the rates of atmospheric mixing of radionuclides.

Fallout Rates And Mechanisms

J. A. Young and C. W. Thomas

Atmospheric concentrations of a wide spectrum of radionuclides produced by nuclear weapons, nuclear reactors, cosmic rays and radium and thorium decay have been measured bimonthly at Richland, Washington, (46°N, 119°W) since 1961 and monthly at Barrow, Alaska, (71°N, 159°W) since 1964. These measurements provide the continuous record of radionuclide concentrations necessary for assessment of the environmental hazard presented by future radionuclide releases. The average yearly atmospheric radionuclide concentrations at Richland from 1961 through 1980 and at Barrow from 1964 through 1980 (extrapolated to the end of 1980 using past seasonal variations and ignoring possible contributions from the October 16, 1980, Chinese test) are reported in Tables 2.3 and 2.4. Concentrations of a few of the radionuclides at Richland are plotted versus time in Figure 2.6.

Radionuclides Produced By Nuclear Weapons

For the past several years virtually all atmospheric radionuclides produced by nuclear weapons have come from nuclear tests by the People's Republic of China. On October 16, 1980, the Chinese conducted an atmospheric test that reportedly had a yield between 0.2 and 1 megatons. Because of the relatively large yield of this test, much of the debris should have risen into the stratosphere. As a result, only very small concentrations of short-lived radionuclides have been observed through October 27, 1980, in surface air at Richland, Washington. Molybdenum-99, ^{103}Ru, ^{131}I, ^{141}Ce, and ^{237}U concentrations of 0.75, 0.56, 0.46, 1.2, and 4.6 dpm/10^3m^3, respectively, were measured on October 25-26. It is expected that debris from the October 16 test would first be seen in large quantities in the spring of 1980, when the rate of transfer from the lower stratosphere into the lower atmosphere reaches a maximum.

The last Chinese nuclear test prior to the October 16 test was the <20 kiloton test conducted on December 14, 1978. As a result, in 1980 the atmospheric concentrations of nuclear weapons radionuclides (ignoring possible contributions from the October 16 test) fell to the lowest levels observed since the 1961-62 test series by the USA and the USSR. The ^{137}Cs concentrations at Richland in 1980, for example, averaged only 0.5% of the maximum average annual concentrations observed in 1963. Prior to the October 16 test the concentrations of all radionuclides having half-lives shorter than ^{144}Ce (285d) had fallen below detection limits. The October 16, 1980, test should cause the nuclear weapons radionuclide concentrations to rise sharply again in 1981.

Radionuclides Produced By Cosmic Rays

Spallation reactions of cosmic rays with atmospheric gases produce ^{7}Be (53d) and many other radionuclides. The production rates of these radionuclides vary with the cosmic ray flux in the earth's atmosphere, and therefore should vary inversely with the sunspot number since the magnetic fields associated with sunspots inhibit the penetration of cosmic rays into the solar system. The ^{7}Be concentrations at Barrow

Table 2.3. Average Annual Radionuclide Concentrations in Surface Air at Richland, Washington (46°21'N, 119°17'W)

Disintegrations Per Minute Per 10^3 M^3

Year	^{7}Be	^{22}Na	^{46}Sc	^{54}Mn	^{55}Fe	^{57}Co	^{58}Co	^{60}Co	^{65}Zn	^{88}Y	^{90}Sr	$^{95}ZrNb$	^{95}Zr	^{95}Nb	^{103}Ru	^{106}Ru
1961												10,900			6,820	
1962		.388		64.9				1.19		.96		4,380			2,300	766
1963		.642		238				1.82	16.2	1.35	95.7	3,970				899
1964	170	.329	.201	49.9	107			.741	26.0	.608	35.5	81.1				284
1965	158	.118	.289	9.70	75.0			.945	6.66	.041	16.7	38.0				60.9
1966	170	.051	.263	2.13	25.6			1.21	7.97	.005	9.50	9.50			20.2	30.2
1967	179	.034	.489	.770	19.5	.048	.146	.750	5.81	.064	4.25	42.4			19.4	14.5
1968	202	.042	1.14	1.01	13.6	.106	.300	.968	2.87	.006	5.41		24.1	47.5	11.3	47.3
1969	199	.032	1.35	.767	4.65	.166	.105	.200	1.11	.013	6.22		60.1	117	40.1	54.8
1970	210	.024	.544	.940	3.46	.280	.129	.182	.309	.154	6.93		55.5	120	21.4	128
1971	208	.036	ND	1.34		.211	.105	.058	.102	.442			84.4	159	28.6	75.3
1972	237	.029	ND	.220		.073	.038	.056	.084	.030			27.4	37.2	19.5	14.9
1973	242	.030	ND	.067		.022	.009	.077	.019	ND			2.05	2.81	3.46	2.65
1974	234	.025	ND	.489		.024	.018	.034	.035	.054			25.8	50.8	6.37	25.6
1975	241	.024	ND	.293		.016	.013	.054	.035	.148			10.4	21.2	2.62	11.4
1976	238	.022	ND	.092		.027	.293	.119	.015	ND			9.53	8.41	10.1	1.60
1977	253	.030	ND	.499	3.29	.054	.155	.029	.06	.251	4.99		45.2	83.1	23.1	26.3
1978	212	.021	.011	.349	6.28	.026	.026	.203	.08	.049	4.96		3.15	5.87	6.88	18.7
1979	208	.017	.013	.084	1.55	.005	.048	.052	.016	.014	10.1		.034	.053	.085	3.10
1980	160	.013	<.013	.029		<.005	<.007	.021	<.016	<.014			<.019	<.017	<.012	.653

Disintegrations Per Minute Per 10^3 M^3

Year	^{110m}Ag	^{124}Sb	^{125}Sb	^{134}Cs	^{137}Cs	^{140}Ba	^{141}Ce	^{144}Ce	^{155}Eu	^{210}Pb	^{238}Pu	^{239}Pu	^{241}Am
1961						7,720	9,820						
1962			87.5	.38	98.1	3,420	1,850	1,480			.023	.858	
1963	.174	4.89	149	.511	152			1,800	84.8			.603	.253
1964		1.70	71.1	.425	78.2			471	64.1		.007	.470	.120
1965	.060	.099	27.8	.185	34.4	14.5		88.4	14.1		.006	.395	.153
1966	.050	.059	18.7	.182	18.9	11.2	43.4	27.9	6.19		.009	.143	.078
1967	.055	.142	6.60	.050	11.7	9.72	17.7	19.7	.820		.032	.123	.045
1968	.084	.034	6.54	.162	11.9	6.79	10.1	118	1.60		.028	.114	.035
1969	.040	.017	7.77	.178	14.0	2.36	35.4	139	1.71		.041	.116	.0046
1970	.029	ND	7.19	.188	18.4	1.38	16.7	156	2.34		.019	.131	.0037
1971	.026	ND	6.06	.092	16.3	1.50	17.2	151	1.17		.007	.121	.0059
1972	ND	ND	1.60	.243	14.5	5.85	20.2	30.0	.42		.007	.076	.0025
1973	ND	ND	.595	.021	3.02	1.89	1.94	4.64	.152		.0025	.0232	
1974	ND	ND	2.55	.012	6.19	.789	3.97	59.2	.608		.0019	.0533	
1975	.032	.029	1.34	.010	3.68	.088	1.30	26.6	3.03	18.1	.0019	.0366	
1976	ND	.028	.269	.007	1.75	10.7	11.6	4.16	.085	23.9	.0006	.0168	
1977	ND	.045	2.57	.011	5.23	5.44	15.2	56.8	.558	23.4	.0024	.0397	.0010
1978	.062	.19	2.73	.020	5.68	10.9	4.07	37.3	.569	19.8	.0018	.0581	.0027
1979	.058	.027	.681	.017	1.98	.306	.174	4.97	.166	25.4	.0008	.0220	.0034
1980	<.030	<.030	.225	<.009	.814	.160	<.016	.887	.058	16.9			

Table 2.4. Average Annual Radionuclide Concentrations in Surface Air at Barrow, Alaska (71°10'N, 156°30'W)

Disintegrations Per Minute Per 10^3 M^3

Year	^{7}Be	^{22}Na	^{54}Mn	^{55}Fe	^{57}Co	^{58}Co	^{60}Co	^{65}Zn	^{88}Y	$^{95}ZrNb$	^{95}Zr	^{95}Nb
1965		.066	5.35	11.6			.078	.035	.026	3.96		
1966	117	.028	1.21	6.63			.032	.155	.003	7.95		
1967	85.0	.014	.175	3.22	.025	.022	.013	.062	.026	13.9		
1968	81.0	.014	.334	2.44	.036	.108	.026	.267	.002		9.12	17.2
1969	95.9	.011	.210	.821	.054	.082	.016	.105	.003		9.19	19.2
1970	68.7	.012	.183	.874	.054	.066	.006	.12	.021		7.34	16.2
1971	84.7	.014	.296		.063	.060	.008	.012	.075		12.6	25.8
1972-3	101	ND	.066		.023	ND	ND	ND	ND		6.78	10.3
1974	115	.011	.138		ND	ND	ND	ND	.013		8.47	16.9
1975	120	.011	.156		.009	.012	.008	.023	.091		9.11	16.5
1976	123	.010	.026		.009	.081	.002	.007	ND		2.56	3.75
1977	129	.011	.133		.015	.078	.006	.015	.049		9.45	17.8
1978	108	.011	.190		.013	.018	.008	.009	.036		1.98	4.37
1979	91.0	.008	.022		.002	.003	.001	.001	.002		.017	.032
1980	123	.009	.005		<.002	<.003	<.002	<.004	<.004		<.006	<.004

Disintegrations Per Minute Per 10^3 M^3

Year	^{103}Ru	^{106}Ru	^{110m}Ag	^{124}Sb	^{125}Sb	^{134}Cs	^{137}Cs	^{140}Ba	^{141}Ce	^{144}Ce	^{155}Eu	^{210}Pb
1965		27.3			11.5	.020	14.8	2.84		49.2		
1966	3.77	6.45	.008	.014	3.73	.006	7.87	8.38		8.83		
1967	6.66	2.26	.003	ND	.90	ND	2.76	7.57	3.08	3.93		
1968	4.01	12.8	.013	.045	1.76	ND	3.64	2.74	4.25	26.2		
1969	6.42	11.8	.009	.007	1.71	ND	2.58	.761	5.30	30.8		
1970	2.74	14.4	.004	.009	1.60	.008	2.34	.48	2.07	26.9		
1971	4.58	15.2	.003	.005	1.42	.011	2.84	.42	2.93	32.3		
1972-3	2.75	3.55	ND	.012	.456	ND	1.08	.68	3.80	7.54	.146	
1974	1.98	7.81	ND	ND	.751	ND	1.92	.19	.98	19.6	.211	15.9
1975	2.66	7.25	ND	ND	.719	.006	1.80	ND	1.23	16.6	.191	19.7
1976	3.51	.764	ND	ND	.105	.003	.391	1.50	3.15	1.61	.029	20.1
1977	5.40	6.99	.013	.016	.728	.005	1.33	3.74	4.13	13.4	.142	15.5
1978	1.72	11.4	.012	.055	1.47	.004	2.68	.93	.725	17.4	.293	13.5
1979	.056	1.45	.007	.011	.303	.002	.688	.08	.081	2.14	.067	12.2
1980	<.008	.388	<.007	<.013	.127	<.002	.390	<.43	<.024	.475	.033	15.1

and Richland (Figure 2.7) have shown the expected correlation with cosmic ray (neutron) flux and anticorrelation with sunspot number (except at Richland prior to 1968, when the measured concentrations were probably less reliable because they were measured with NaI(Tl) detectors in the presence of large amounts of ^{103}Ru). From 1968 through 1980 the minimum annual average ^{7}Be concentration at Richland was 35% lower than the maximum concentration, while the minimum concentration at Barrow was 47% lower than the maximum concentration. The larger variation at Barrow might be expected, because magnetic fields associated with solar activity have the greatest effect on low rigidity cosmic rays, which are deflected toward high latitudes by the earth's magnetic field.

Radionuclides Produced By Nuclear Reactors

Concentration ratios of the various nuclear weapons radionuclides have been about the same at Richland and at Barrow. However, the concentrations of ^{46}Sc, ^{55}Fe, ^{60}Co, ^{65}Zn and ^{134}Cs at Richland in the past have been considerably higher than would be predicted from their concentrations at Barrow if they were produced entirely by nuclear weapons, especially prior to 1971. The elevated concentrations of these radionuclides at Richland resulted from the operation of eight plutonium-producing reactors on the Hanford Reservation 20 to 30 miles north of the Richland air sampling site. During the passage of Columbia River cooling water through the reactors, the neutron activation of

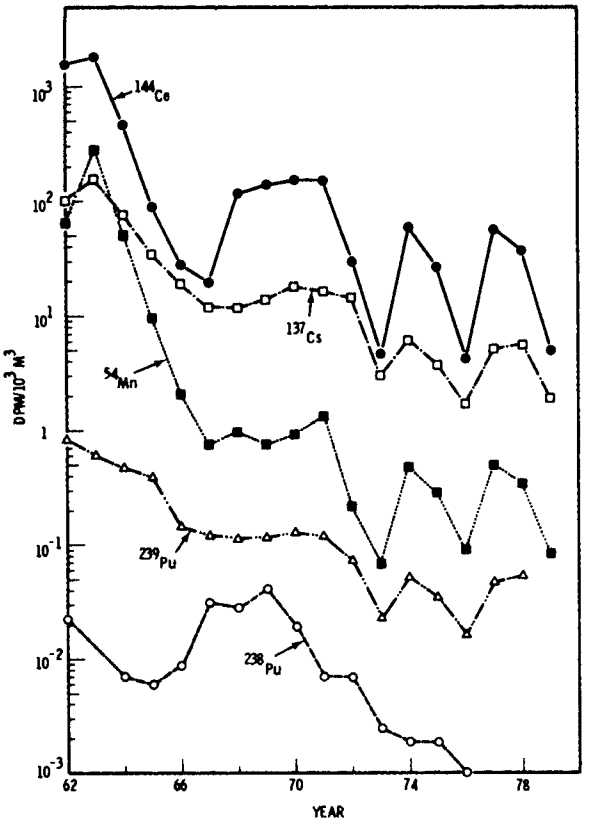

Figure 2.6. Average Yearly Radionuclide Concentrations at Richland, Washington.

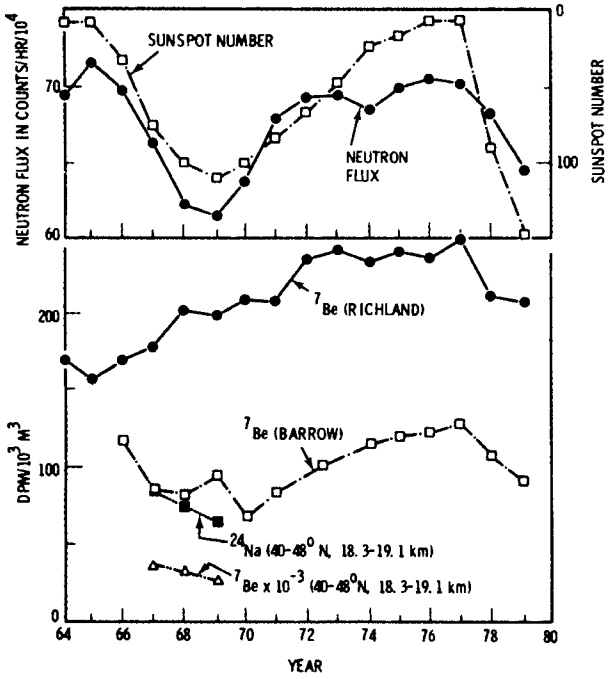

Figure 2.7. ^{7}BE Concentrations, Sunspot Number, and Neutron Flux (Green River, Canada) as Functions of Time

impurities in the water, the leaching of corrosion products and occasional fuel element failure added radionuclides to the cooling water. These radionuclides became deposited in Columbia River sediments, where they could later be resuspended into the atmosphere. The Hanford plutonium-producing reactors began to be shut down in the late 1960s, and since 1971 the only reactor in operation has been N-reactor, which produces both electricity and plutonium. Therefore, the atmospheric concentrations of ^{46}Sc, ^{55}Fe, ^{60}Co, ^{65}Zn and ^{134}Cs at Richland decreased in the late 1960s and 1970s, with the radionuclides having the shortest half-lives showing the fastest decrease (Figure 2.8). The half-times for the decreases of ^{65}Zn and ^{134}Cs were about equal to their half-lives. By 1980, atmospheric concentrations of ^{46}Sc, ^{65}Zn and ^{134}Cs had fallen below detection limits, and only ^{60}Co showed measurable concentrations. The ratios of ^{60}Co to the nuclear weapons radionuclides at Richland and Barrow indicated that the ^{60}Co was still of nuclear reactor origin. Iron-55 has not been measured in 1980 so it is not possible to determine whether nuclear reactor ^{55}Fe is still present in the atmosphere at Richland. Measurements from previous years, however, indicate that it probably still is.

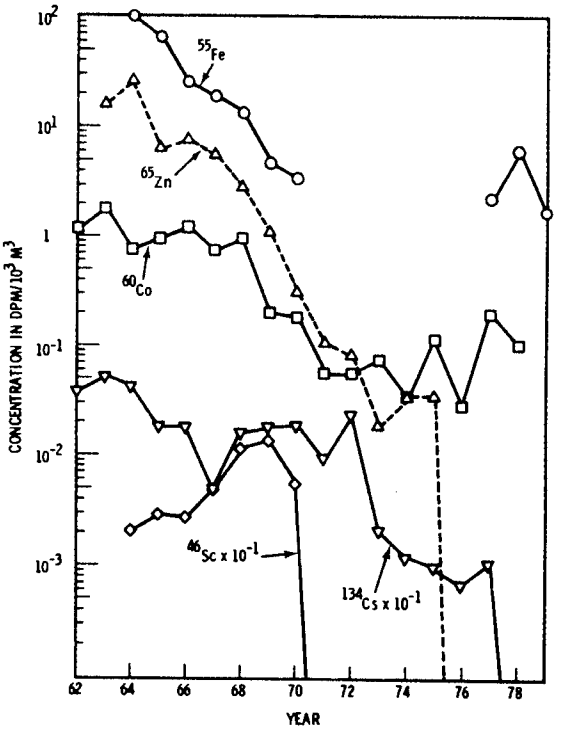

Figure 2.8. Average Yearly Concentrations at Richland, Washington of Radionuclides Released by Hanford Nuclear Reactors

• Particle Resuspension and Translocation

Objectives of this study are:

- Investigating particle resuspension rates and air concentrations as functions of atmospheric stresses, local soil-working stresses, particle variables and surface variables.
- Developing an experimental resuspension data base to aid in establishing surface contamination limits to assure adequate public protection from hazardous materials.
- Factoring time-varying resuspension rates into models describing delivery of surface contaminants to man.

Airborne Plutonium-240 Isotopic Composition Near Hanford

G. A. Sehmel

Introduction

Airborne plutonium was sampled during southwesterly winds in both resuspension and dry deposition investigations near the southwestern Hanford area boundary from 1976 to 1979. For these samples, the maximum calculated airborne plutonium-239, -240 concentration was 2×10^{-16} $\mu Ci/cm^3$, which is only 0.3% of the 6×10^{-14} $\mu Ci/cm^3$ 168-hr maximum permissible concentration guide (ERDA 1977a).

In these samples, stratospheric fallout plutonium can be identified by the ratio of ^{240}Pu to other plutonium isotopes. For samples collected in 1970-71 with atom ratios corrected to January 1971, worldwide fallout $^{240}Pu/^{239}Pu$ atom ratios in surface soils average 0.18 ± 0.01 (Krey et al. 1976). These results are given with one standard deviation precision. In comparison to fallout, Hanford process-grade plutonium (ERDA 1977a) as reflected in high-level waste decayed to 1990 (from reactor production--1944 to 1971) has an average ^{240}Pu composition of 6.3 atom percent and an average $^{240}Pu/^{239}Pu$ atom ratio of 0.067.

In the resuspension studies, airborne solids were sampled as a function of wind speed, anticipating that airborne plutonium concentrations would reflect the wind speed dependency of resuspension from a uniform area source consisting of stratospheric fallout plutonium. Similarly, for the particle dry deposition studies, airborne fallout plutonium was expected to be evenly distributed in the atmosphere. In this case, particle dry deposition was to be measured during airborne plutonium transport from an upwind to a downwind air sampling tower.

Unexpectedly, however, plutonium isotopic results from selected filter resuspension samples were different than expected since these samples were mainly process-grade plutonium rather than fallout plutonium. Now, the source locations of the process-grade plutonium source are unknown.

For samples collected during the dry deposition experiment, additional quality assurance measures were taken to confirm sample integrity throughout the analytical procedure. These deposition sample results, as well as results from earlier resuspension and deposition experiments, are summarized in this report.

Data Review

In these resuspension and deposition investigations, ^{240}Pu and ^{239}Pu isotopic compositions were determined at five sites: 1) near the Prosser Barricade; 2) near the top of Rattlesnake Mountain (Sehmel 1979a); 3) at a site near the downwind tower used in a particle dry deposition experiment near Horn Rapids; 4) at both the upwind and downwind towers of a second particle dry

deposition experiment conducted near Horn Rapids (Sehmel 1979b); and 5) west of the Hanford central stores.

Airborne plutonium similar to process-grade, i.e., 6% ^{240}Pu, was first identified in samples collected near the Prosser Barricade from April 12 to June 29, 1976, and also from August 12, 1976, to January 11, 1977. In these two experiments airborne samples were collected in cowl particle cascade impactor systems (Sehmel 1978) at heights of 0.3, 2.0, and 5.8 m. Samples were collected only if the wind direction was from off-site toward[a] the Hanford area, i.e., from 225° ± 35°. "Small" particles were collected in particle cascade impactors, and "large" particles were collected by gravity settling within the cowl inlet.

For the first sampling period, plutonium isotopic ratios were determined for only the "large" particles: the ^{240}Pu atom percent ranged from 6.1 to 6.3; the $^{240}Pu/^{239}Pu$ atom ratios ranged from 0.065 to 0.068. For the second collection period, isotopic analyses were made for both "small" and "large" particles. For "small" particles, the ^{240}Pu atom percent ranged from 5.6 to 8.1, and the $^{240}Pu/^{239}Pu$ atom ratio ranged from 0.060 to 0.089. For "large" particles the ^{240}Pu atom percent ranged from 6.6 to 6.8, and the $^{240}Pu/^{239}Pu$ atom ratio ranged from 0.071 to 0.074.

Expecting to measure only fallout plutonium resuspension, airborne plutonium also was collected near the top of Rattlesnake Mountain from June 30 to November 17, 1978. Samples were collected to a height of 2.1 m during southwesterly winds, i.e., 240° ± 45° for seven wind speed increments within the range of 4.5 to 31 m/sec. For seven samples collected from June 30 to November 17, 1978, $^{240}Pu/^{239}Pu$ atom ratios ranged from 0.152 ± 0.010 to 0.229 ± 0.024. For wind speeds below 15 m/sec, the $^{240}Pu/^{239}Pu$ atom ratio was between 0.20 and 0.23. For the highest wind speed increments from 15 to 31 m/sec, the $^{240}Pu/^{239}Pu$ atom ratio decreased to 0.15. For the combined sample "large" particles collected in the seven cyclone preseparators, the $^{240}Pu/^{239}Pu$ atom ratio was 0.102 ± 0.008.

The consistent identification during southwesterly winds of airborne process-grade plutonium near the Prosser Barricade was confounded in a subsequent resuspension experiment from May 11 to July 2, 1979. This experiment was performed at an air sampling site near the Horn Rapids downwind deposition tower. At this downwind site, airborne solids were collected continuously for all wind directions 1.4 km south (176°) of the Prosser Barricade. The ^{240}Pu and ^{239}Pu isotopic compositions were 17.3 ± 0.1 and 81.3 ± 0.1 atom percent, respectively. The $^{240}Pu/^{239}Pu$ atom ratio was 0.213 ± 0.002. Simultaneously, a continuous air sample was collected near the top of Rattlesnake Mountain. At Rattlesnake Mountain, the ^{240}Pu and ^{239}Pu isotopic compositions were 14.43 ± 0.08 and 83.35 ± 0.09 atom percent, respectively. The $^{240}Pu/^{239}Pu$ atom ratio was 0.173 ± 0.001. These compositions reflect only fallout plutonium at both sites.

An apparent inconsistency in the isotopic composition was evident between this Horn Rapids sample and the earlier Prosser Barricade samples: the isotopic composition in the Horn Rapids sample is similar to fallout rather than process-grade plutonium as measured in the Prosser Barricade samples. This inconsistency was surprising since these two sites are separated by only 1.4 km.

Results from a dry deposition experiment at Horn Rapids shed further light on this inconsistency (Sehmel 1980). Indeed, now there may no longer be an inconsistency between the data sets. The particle dry deposition experiment measured ambient airborne plutonium using two sampling towers 305 m apart located near the Horn Rapids Dam. When wind speed and direction were identical at each tower (i.e., a wind direction of 233° ± 45° and a wind speed increment of 5 to 7 m/sec measured at an elevation of 30 m), isokinetic particulate samplers were automatically turned on at both upwind and downwind towers. "Large" particles were collected by gravity settling in the inlets of isokinetic samplers, whereas "small" particles remained airborne within the samplers and collected on filters. The filter samples were analyzed for plutonium.

At the upwind towers at 2- and 3-m heights, airborne plutonium concentrations were approximately three times greater than for any other sample collected from the upwind tower. See Figure 2.4 of "Plutonium Dry Deposition Experiment Using Ambient Airborne Plutonium Near Horn Rapids" in this Annual Report. These elevated

(a) North is 0°; angles are measured clockwise from 0°.

concentrations were caused by process-grade plutonium rather than from stratospheric fallout.

One would expect airborne fallout plutonium concentrations to be reasonably uniform with respect to sampling height since the fallout atmospheric source is worldwide. If airborne plutonium concentrations showed significant changes with height, the source of that change might be resuspension from a local, i.e., process-grade versus fallout plutonium, source. Non-uniform airborne plutonium concentrations were measured during the dry deposition experiment.

Increased plutonium concentrations measured at the 2- and 3-m heights at the upwind tower site indicate process-grade plutonium was transported across the upwind tower. Thus, at both the upwind Horn Rapids site and the Prosser Barricade site, airborne plutonium is partially the result of process-grade plutonium. Process-grade plutonium was absent at the downwind 0.3-m site, partly because of complex airflow patterns in this region, but process-grade was present at sampling heights of 1 and 20 m.

Results: Plutonium Atom Ratios

Data symbol identifications are shown in Table 2.5 for plutonium atom ratios shown in Figure 2.9, $^{240}Pu/^{239}Pu$ as a function of $^{241}Pu/^{239}Pu$. The $^{240}Pu/^{239}Pu$ atom ratio range is from 0.0376 to 0.227, while the $^{241}Pu/^{239}Pu$ atom ratio range is from 0.00188 to 0.013. Although the relationship is not completely defined, the $^{240}Pu/^{239}Pu$ atom ratio tends to increase as the $^{241}Pu/^{239}Pu$ atom ratio increases. A line,

$$^{240}Pu/^{239}Pu = 15.00\ (^{241}Pu/^{239}Pu) + 0.0285 \quad (1)$$

represents the general increase.

Conclusions

Although airborne plutonium transport occurs near the Hanford area U pond,[a] the BC crib area[b] (Sehmel 1978) and even up to 125-m heights as measured from the Hanford Meteorological Station tower, the body of data summarized here for ^{240}Pu isotopic analysis is nearly the entire data base for isotopic analysis of airborne plutonium near the Hanford boundary. Isotopic analysis of airborne material in monitoring studies has probably not been deemed necessary because airborne plutonium concentrations were significantly below airborne maximum concentration guide levels, even though process-grade plutonium was transported by southwesterly winds near the Prosser Barricade and at the upwind tower near Horn Rapids. The maximum calculated airborne $^{239-240}Pu$ concentration of 2×10^{-16} $\mu Ci/cm^3$ is 0.3% of the 6×10^{-14} $\mu Ci/cm^3$ 168-hr maximum permissible concentration guide (ERDA 1977b).

The possibility of some process-grade plutonium transport during southwesterly winds also may be concluded for the Rattlesnake Mountain site experiment. Near the top of Rattlesnake Mountain there was a decrease in the airborne $^{240}Pu/^{239}Pu$ atom ratio from the 0.20 to 0.23 range to 0.15 during southwesterly winds above 15 m/sec. This decrease during high wind speeds might be interpreted as resuspension occurring from unknown sources. For "large" particles, an even lower $^{240}Pu/^{239}Pu$ atom ratio of 0.10 tends to further confirm some resuspension source(s) with lower atom ratios than current fallout airborne atom ratios. It is unknown now whether samples collected for wind speeds above 15 m/sec reflect only a change in isotopic composition as a result of airflow patterns introducing stratospheric fallout or whether at higher wind speeds there may be airflow patterns reflecting resuspension from sources previously released from Hanford.

(a) Southwest of 200-West area.
(b) South of 200-East area.

Table 2.5. Data Symbol Identifications

LOCATION (WIND DIRECTION)	DATE	SYMBOL KEY	WIND SPEED u INCREMENT, m/sec OR CONDITIONS	HOST PARTICLE SIZE
MT. ST. HELENS	6-6-75	X	SMOKE	SMALL
PROSSER BARRICADE	4-12 TO 6-29-76	● 1	ALL u	LARGE
(225° ± 35°)	8-12-76 TO 1-11-77	● 2	ALL u	LARGE
		○ 3	3-5	SMALL
		○ 7	7-11	SMALL
HORN RAPIDS	7-21 TO 11-20-78		5-7	SMALL
(233° ± 45°)	UPWIND HEIGHT	□ U0.3	0.3m	SMALL
		□ U1	1m	SMALL
		□ U2	2m	SMALL
		□ U3	3m	SMALL
		□ U9	9m	SMALL
		□ U20	20m	SMALL
	DOWNWIND HEIGHT	□ D0.3	0.3m	SMALL
		□ D1	1m	SMALL
		□ D2	2m	SMALL
		□ D3	3m	SMALL
		□ D9	9m	SMALL
		□ D20	20m	SMALL
RATTLESNAKE MOUNTAIN	6-30 TO 11-17-78	△ 0.5	0.5-3	SMALL
(240° ± 35°)		△ 3	3-5	SMALL
		△ 5	5-7	SMALL
		△ 7	7-11	SMALL
		△ 11	11-15	SMALL
		△ 15	15-17.5	SMALL
		△ 17.5	17.5-31	SMALL
		▲	0.5-31	LARGE
RATTLESNAKE MOUNTAIN (ALL)	5-11 TO 7-2-79	▽	ALL u	SMALL
HORN RAPIDS (ALL)	5-11 TO 7-2-79	◇	ALL u	SMALL
RATTLESNAKE MOUNTAIN (ALL)	7-5 TO 11-8-79	▼	ALL u	1.7um STAGE SMALLER
STORES - 1100 AREA (ALL)		▶	ALL u	1.7um STAGE SMALLER
PROSSER BARRICADE	9-17 TO 11-8-79	◐	ALL u	6μm PRESEPARATOR SMALLER
(240° ± 15°)		◑		
(240° ± 30°)		◒		6μm PRESEPARATOR SMALLER
		◓		
(240° ± 45°)		◕		6μm PRESEPARATOR SMALLER
		◔		
HORN RAPIDS (240° ± 15°)		◐	ALL u	6μm PRESEPARATOR SMALLER
		◑		

1σ MASS SPECTROMETER LIMITS: 

LESS THAN $^{241}Pu/^{239}Pu$ LIMIT: 

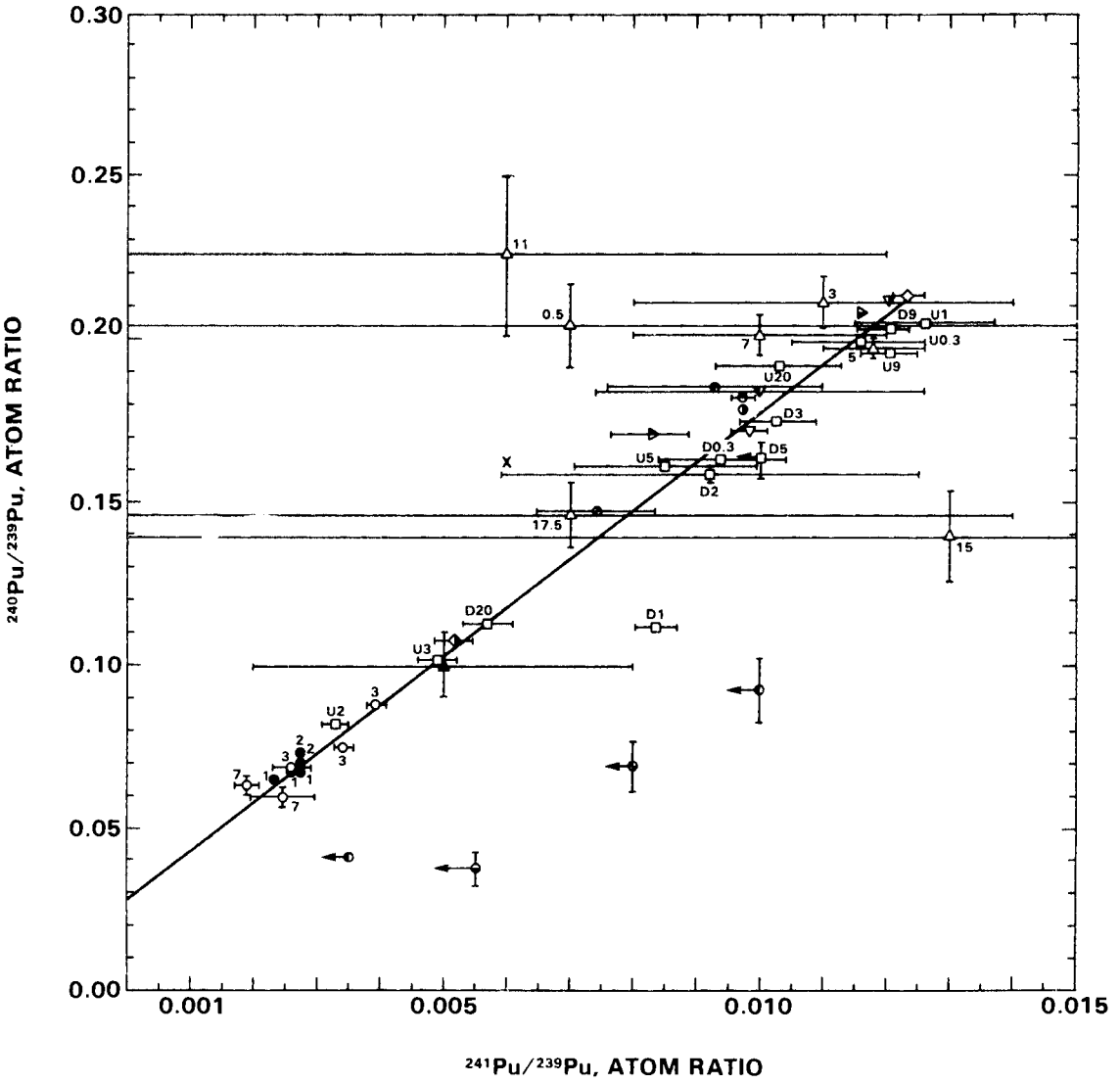

Figure 2.9. Comparison of $^{240}Pu/^{239}Pu$ with $^{241}Pu/^{239}Pu$ Atom Ratios for Airborne Collected Particulates

References

Code of Federal Regulations. 10 CFR Part 20, Appendix B, Table II.

ERDA. 1977a. Alternatives for Long-Term Management of Defense High-Level Radioactive Waste, Hanford Reservations. ERDA 77-44, p. 3.8, Energy Research and Development Administration, Washington, DC.

ERDA. 1977b. ERDA, Manual of Operation. Chapter 0524, March 1977, "Standards for Radiation Protection," Appendix A, Table II. U.S. Energy Research and Development Administration, Washington, DC.

Krey, P. W., E. Hardy, P. Pachucki, C. Rourke, J. Coluzza, and W. K. Benson. 1976. "Mass Isotopic Composition of Global Fallout Plutonium in Soil." In Transuranic Nuclides in the Environment, pp. 671-678, International Atomic Energy Agency, Vienna, Austria.

Sehmel, G. A. 1978. "Plutonium Concentrations in Airborne Soil at Rocky Flats and Hanford Determined During Resuspension Experiments." In Airborne Radioactivity, ed. D. Shaw, pp. 81-102 (selected papers from the 1977 American Nuclear Society Winter Meeting).

Sehmel, G. A. 1979a. "Airborne Plutonium and Americium Concentrations and Plutonium Isotopic Ratios Measured Near the Top of Rattlesnake Mountain." (This Annual Report.)

Sehmel, G. A. 1979b. "Plutonium Dry Deposition Experiments Using Ambient Airborne Plutonium Near Horn Rapids." (This Annual Report.)

Airborne Plutonium Transported During Southwesterly Winds Near the Hanford Prosser Barricade

G. A. Sehmel

Introduction

Stratospheric fallout from resuspension of deposited nuclear weapons testing could result in airborne plutonium. To determine this possible resuspension at the Hanford site, two field experiments were conducted near the Prosser Barricade in the Hanford area. The primary objective of these experiments was to determine if stratospheric fallout resuspension was reflected by airborne plutonium concentrations increasing with increasing wind speed. A secondary objective was to "fingerprint" the source of the airborne plutonium by determining the plutonium-240 isotopic content.

Experiment

Airborne solids were collected as a function of wind speed increments within cowl particle cascade impactor systems (Sehmel 1978) located at heights of 0.3, 2.0, and 5.8 m above ground. The air was sampled only if the wind was blowing from off-site towards[a] the Hanford area from 190° to 260°. "Small" particles were samples within particle cascade impactors and "large" particles were collected within the particle inertial-collection sampling-cowl.

Results

In the first experiment, airborne plutonium-239 concentrations were measured near the Prosser Barricade from April 12 to June 29, 1976. The sampling experiment was repeated from August 12, 1976, to January 11, 1977, to confirm results from this initial experiment. For the second experiment $^{239-240}Pu$ isotopic analysis were made for both small and large particle samples.

Airborne plutonium concentrations, $\mu Ci/cm^3$, were calculated. From August 12, 1976, to January 11, 1977, airborne concentrations ranged from 4×10^{-18} up to a maximum of 2×10^{-16} $\mu Ci/cm^3$.

At the lowest sampling height of 0.3 m, the airborne $^{239-240}Pu$ concentration was nearly constant at about 5×10^{-17} $\mu Ci/cm^3$ for all wind speeds. In contrast to concentrations at the 0.3-m height, plutonium concentrations at the 2-m and 5.8-m heights increased with increasing wind speed. For the highest point sampled (5.8 m), both the airborne plutonium and airborne solids concentrations increased with the wind speed to the 2.7 to 2.8 power. The ^{240}Pu isotopic content in atom percent ranged from 5.6 to 8.1 for "small" particles; for "large" particles the percentage was similar, 6.6 to 6.8.

Analysis

Plutonium-239, -240 was transported during southwesterly winds on both "small" and "large" particles. Although maximum airborne concentrations were far below the 168-hr maximum permissible concentrations guidance levels (0.3%), possible sources of this airborne plutonium are of interest. In considering possible sources, ^{240}Pu isotopic ratios are investigated.

Plutonium-240 isotopic content can be used to "fingerprint" the plutonium source as being similar to nuclear weapons-testing stratospheric fallout or Hanford process-grade plutonium. An average Hanford-process ^{240}Pu content of 6.3 atom percent (ERDA 1977a) is much less than 18.8 atom percent for an airborne (fallout) sample collected near Mt. St. Helens, Washington. For the Prosser Barricade samples, the maximum observed ^{240}Pu concentration is 8.1 atom percent (see Table 2.6 for a summary of ^{240}Pu atom percent). Thus, the maximum observed ^{240}Pu concentration at 8.1 atom percent for the Prosser Barricade samples is a fraction (0.59) of the atom percent for the Mt. St. Helens' sample.

These percentages were used to estimate the fraction of fallout in the Prosser Barricade sample. The estimated fraction of fallout in the 8.1 atom percent ^{240}Pu sample is 0.24. For the other Prosser Barricade samples with ^{240}Pu atom percentage less than 8.1, the estimated fallout contribution is even less than 0.24.

(a) North is 0°; angles are measured clockwise from 0°.

Table 2.6. Prosser Barricade Plutonium-240 Isotopic Content Summary

Sampling Height, m	Wind Speed Sampling Increment, m/sec	Atom Percent: Large Particles Collected in Cowls, 12 April to 29 June, 1976	Atom Percent: Large Particles Collected in Cowls, 12 August, 1976 to 11 January, 1977	Atom Percent: Small Particles Collected Cascade Impactor, 12 August, 1976 to 11 January, 1977
0.3	All	6.10 ± 0.02	NA	NA
	3 to 5	NA	NA	6.4 ± 0.2
	7 to 11	NA	NA	5.6 ± 0.2
2.0	All	6.31 ± 0.02	6.85 ± 0.09	NA
	3 to 5	NA	NA	8.1 ± 0.1
	7 to 11	NA	NA	6.0 ± 0.2
5.8	All	6.28 ± 0.03	6.6 ± 0.1	NA
	3 to 5	NA	NA	7.0 ± 0.01

(NA) Not Analyzed

Conclusions

Plutonium was transported onsite during southwesterly winds during the two study periods at the Prosser Barricade. Airborne $^{239-240}Pu$ concentrations varied as powers of wind speed (U): $U^{-0.2}$ to $U^{7.8}$. As wind speed increases, airborne concentrations increase, indicating a surface resuspension source. More research is planned to determine relationships between airborne and any surface concentrations. The airborne solids content ranged from 6×10^{-8} to 1.7×10^{-6} μCi/g. The ^{240}Pu isotopic content ranged fom 5.6 to 8.1 atom percent. The estimated fraction of stratospheric fallout plutonium in these samples was 0.24 or less. The remaining airborne plutonium was probably of Hanford origin. This airborne plutonium probably represents resuspension of plutonium from undetermined sites by mechanisms and events not clear at this time. The maximum calculated airborne $^{239-240}Pu$ concentration of 2×10^{-16} μCi/cm^3 is 0.3% of the 6×10^{-14} μCi/cm^3 168-hr maximum permissible concentration guide (ERDA 1977b; Code of Federal Regulations).

References

Code of Federal Regulations. 10 CFR Part 20, Appendix B, Table II.

ERDA. 1977a. Alternatives for Long-Term Management of Defense High-Level Radioactive Waste, Hanford Reservations. ERDA 77-44, pp. 3-8, Energy Research and Development Administration, Washington, DC.

ERDA. 1977b. ERDA, Manual of Operation. Chapter 0524, "Standards for Radiation Protection," Appendix A, Table II. U.S. Energy Research and Development Administration, Washington, DC.

Sehmel, G. A. 1978. "Offsite Plutonium Resuspension Near Hanford." In Pacific Northwest Laboratory Annual Report for 1977 to the DOE Assistant Secretary for the Environment, Part 3, Atmospheric Sciences. PNL-2500-3 PT 3, pp. 2.4-2.5, Pacific Northwest Laboratory, Richland, Washington.

Airborne Plutonium and Americium Concentrations and Plutonium Isotopic Ratios Measured Near the Top of Rattlesnake Mountain

G. A. Sehmel

Introduction

Radionuclide fallout from stratospheric and tropospheric debris is deposited throughout the world. It is possible that this fallout could be used to determine the resuspension rate dependency upon wind speed for a large, uniform resuspension source. In order to investigate the potential resuspension rate of this deposited fallout, airborne concentrations of plutonium and americium were measured at a remote Hanford site near the top of Rattlesnake Mountain.

The experiment was conducted from June 30 to November 17, 1978. (A previous

experiment took place from May 27 to June 2, 1978.) Airborne solids were sampled with a modified cyclone preseparator followed by a cascade particle impactor.[a] The cyclone preseparator was modified by attaching an inlet closure on the preseparator. The closure was opened with a solenoid when the cascade impactor was activated by a signal from a controller. When wind speed and direction criteria were satisfied, the controller automatically activated a designated cascade particle impactor. Airborne solids were sampled during southwesterly winds, i.e., 220° ± 45° for seven wind speed increments within the range of 0.5 to 31 m/sec.

At the end of the experiment, collected solids were removed for radiochemical analysis. The non-respirable particles collected in all seven cyclone preseparators were combined to form one sample. In contrast, the identity of the total sample collected within each cascade impactor was retained. After sampling and radionuclide analysis,[b] samples were analyzed at the Pacific Northwest Laboratory (PNL) for plutonium isotopic ratios.

Results

The following results are shown in Figures 2.10 and 2.11: 1) airborne radionuclide concentration, $\mu Ci/cm^3$ of sampled air; 2) the activity density, $\mu Ci/g$ airborne solids; 3) airborne solid concentrations, $\mu g/m^3$ of sampled air; 4) the $^{241}Am/^{239}Pu$ activity ratio, $\mu Ci\ ^{241}Am/\mu Ci\ ^{239}Pu$; and 5) the $^{240}Pu/^{239}Pu$ atom ratio.

Airborne Concentrations

Airborne ^{239}Pu and ^{241}Am radionuclide concentrations are illustrated in Figure 2.10. Shown in the upper and lower portions of the figure are airborne concentrations in $\mu Ci/cm^3$ of sampled air and $\mu Ci/g$ of airborne solids, respectively. The vertical line through each data point shows the radiochemical counting statistic limits, 1 σ. The range of each wind speed increment is shown by a horizontal line through each data point.

Airborne plutonium concentrations were a function of wind speed. For five wind speed sampling increments between 0.5 and 15 m/sec, airborne plutonium concentrations decreased with increasing wind speed. Above a wind speed of 15 m/sec, airborne plutonium concentrations increased rapidly with increasing wind speed. In contrast, airborne americium concentrations tended to remain constant for all wind speeds except for a rapid increase at the highest wind speed increment of 17.5 to 31 m/sec.

Microcuries per Gram on Airborne Solids

The radionuclide content on airborne solids was calculated from the combined weights of solids collected on impactor stages and from the backup filter. The plutonium concentration on airborne solids ranged within one order of magnitude and were inconsistent as a function of wind speed. Americium concentrations on the airborne solids also varied. However, the absolute values are even less certain because of the large radiochemical counting limits around each data point. For the nonrespirable particles, the plutonium and americium concentrations were $9.4 \times 10^{-7} \pm 1.9 \times 10^{-9}$ $\mu Ci/g$ and $0.0 \pm 1.6 \times 10^{-8}$ $\mu Ci/g$, respectively.

Airborne Solids Concentrations

Airborne solids concentration, $\mu g/m^3$, was also determined as a function of wind speed and is shown in the upper portion of Figure 2.11. Concentrations ranged from 8 to 25 $\mu g/m^3$ for wind speeds below 17.5 m/sec. This low concentration might reflect concentrations expected in a pristine region. However, for the highest wind speed increment investigated, airborne concentrations dramatically increased to 200 $\mu g/m^3$. For nonrespirable particles the average concentration was 5.6 $\mu g/m^3$.

Americium-241/Plutonium-239 Activity Ratio

The $^{241}Am/^{239}Pu$ activity ratios are shown in the lower portion of Figure 2.11. Although the radiochemical counting limits are large for the activity ratio, that ratio is about 10^{-1} for most conditions. Only for the highest wind speed increment is there a significant increase in the activity ratio.

Plutonium-240/239 Atom Ratio

Plutonium atom ratios, $^{240}Pu/^{239}Pu$, were determined for each sample. Ratios are shown in Table 2.7. For wind speeds below

---

(a) Model 230CP cyclone preseparator, Sierra Instrument Co., Carmel Valley, CA 93924.

(b) LFE Environmental Analysis Laboratory, 230 Wright Ave., Richmond, CA 94804.

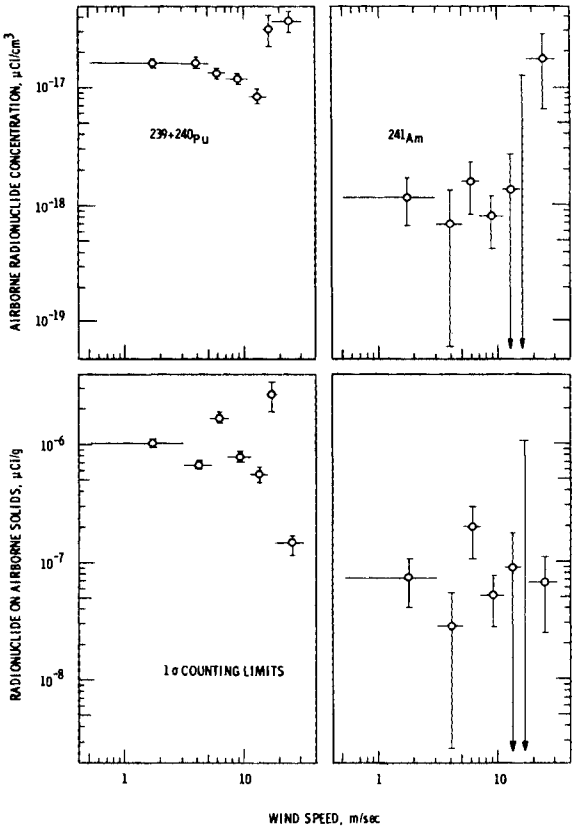

Figure 2.10. Airborne $^{239+240}Pu$ and ^{241}Am Concentrations in Air and on Airborne Solids Collected at the Top of Rattlesnake Mountain from June 30, 1978, to November 17, 1978, When Sampling 205° to 275° Winds Coming from Offsite

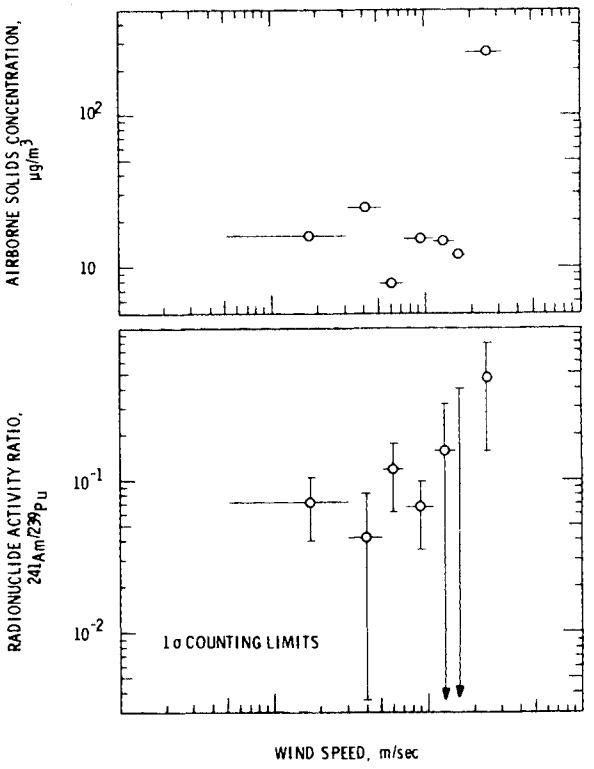

Figure 2.11. Airborne Solids Concentration and $^{241}Am/^{239}Pu$ Radionuclide Ratio for Airborne Solids Collected at the Top of Rattlesnake Mountain from June 30 to November 17, 1978, When Sampling 205° to 275° Winds Coming from Offsite

Table 2.7. Plutonium Atom Ratios for Airborne Solids Collected at the Top of Rattlesnake Mountain From June 30 to November 17, 1978, When Sampling Winds Coming From Offsite

Particle Diameter	Wind Speed Increment Sampled, m/sec	$^{240}Pu/^{239}Pu$ Atom Ratio, ± Standard Error
"Respirable," Total Impactor Collection	0.5 to 3	0.21 ± 0.01
	3 to 5	0.22 ± 0.01
	3 to 7	0.20 ± 0.00
	7 to 11	0.20 ± 0.01
	7 to 15	0.23 ± 0.02
	15 to 17.5	0.15 ± 0.01
	17.5 to 31	0.15 ± 0.01
"Non-Respirable," Total Collection in Cyclone Preseparator	0.5 to 31	0.10 ± 0.01

15 m/sec the atom ratio tended to remain constant between 0.20 and 0.23. For the two highest wind speed increments, from 15 to 31 m/sec, the plutonium atom ratio decreased to 0.15. The reason for this decrease is unknown. Similarly, the reason for the low 0.10 atom ratio for the nonrespirable particles is unknown.

Conclusions

Plutonium and americium concentrations were measured from the top of Rattlesnake Mountain during two periods. Concentrations were previously measured (Sehmel 1979) from May 27 to June 2, 1978. In comparing data from these two experiments, the results are shown to be significantly different. In the first experiment, airborne plutonium concentrations $\mu Ci/m^3$, were independent of wind speed. In contrast, during this second experiment, airborne plutonium concentrations were a function of wind speed. Similarly, airborne americium concentrations show significant differences in both experiments. During the first experiment, airborne americium concentrations were lowest at a wind speed of about 7 m/sec. However, during the second experiment, these concentrations were nearly constant and only increased at the highest wind speed increment, 17.5 to 31 m/sec.

Possibly of more significance in the results for both experiments is the americium to plutonium activity ratio. For both time periods the ratio was a function of wind speed. During the first experiment, the ratio was near unity for only the lowest and highest wind speed increment. In contrast, during the second experiment the ratio was not unity. The ratio tended to increase with increasing wind speed.

Reference

Sehmel, G. A. 1979. "Airborne Plutonium and Americium Concentrations Measured from the Top of Rattlesnake Mountain." In Pacific Northwest Laboratory Annual Report for 1978 to the DOE Assistant Secretary for the Environment, Atmospheric Sciences. PNL-2850-3, pp. 2.4-2.7, Pacific Northwest Laboratory, Richland, Washington.

Airborne Plutonium as a Function of Southwesterly Wind Direction Sectors Near the Southwestern Hanford Boundary

G. A. Sehmel

Introduction

Airborne plutonium collected during southwesterly winds near the Prosser Barricade had $^{240}Pu/^{239}Pu$ atom ratios similar to Hanford process-grade plutonium (Sehmel 1979). The $^{240}Pu/^{239}Pu$ atom ratios ranged from 0.065 to 0.089 and the ^{240}Pu isotopic contents range from 5.6 to 8.1 atom percent. In comparison, average Hanford process-grade ^{240}Pu content as reflected in high-level waste decayed to 1990 (from reactor production--1944 to 1971) is 6.3 atom percent (ERDA 1977a), which is much less than in stratospheric fallout plutonium. Worldwide fallout $^{240}Pu/^{239}Pu$ mass ratios in surface soils average 0.18 ± 0.01 (Krey et al. 1976). These results are given with one standard deviation precision. The estimated fraction of stratospheric fallout plutonium in these Prosser Barricade samples was less than 0.24. The remaining airborne plutonium was probably of Hanford process-grade origin. The maximum calculated airborne $^{239,240}Pu$ concentration of 2×10^{-16} $\mu Ci/cm^3$ was only 0.3 percent of the 6×10^{-14} $\mu Ci/cm^3$ 168-hr maximum permissible concentration guide (ERDA 1977b; Code of Federal Regulations).

The collection of airborne process-grade plutonium probably reflects resuspension of plutonium from undetermined sites by mechanisms and events that are not clear now. If identified, the source might be used as a site for investigating plutonium resuspension. The source direction, as reflected in increased airborne plutonium concentrations and in decreased $^{240}Pu/^{239}Pu$ atom ratios, is known (Sehmel 1979) to be southwesterly, 205° to 275°, at the Prosser Barricade. However, how far the southwest winds transported the plutonium is unknown. The airborne areal extent is at least to a Horn Rapids sampling site 1.4 km south (176°) of the Prosser Barricade.

Consequently, experiments were conducted to expand our information about the downwind airborne concentrations attributable to process-grade plutonium sources. Sampling site locations are shown on the map, Figure 2.12.

Airborne plutonium concentrations and $^{240}Pu/^{239}Pu$ atom ratios were investigated at the Prosser Barricade and Horn Rapids sampling sites by simultaneously collecting airborne solids only during southwesterly winds. The wind direction at each site was used to automatically activate the air sampling pumps. The sampling time period was September 17 to November 8, 1979. To further investigate the areal extent of airborne plutonium similar to Hanford process-grade, airborne solid samples also were collected by continuous sampling from July 25 to November 8, 1979, near Central Stores and from the top of Rattlesnake Mountain.

Reported here are plutonium results from subsequent analyses of those airborne solid sampling experiments: 1) $^{240}Pu/^{239}Pu$ and $^{241}Pu/^{239}Pu$ atom ratios for collected airborne plutonium; 2) airborne concentrations, $\mu Ci/cm^3$ of sampled air; and 3) plutonium activity densities on airborne respirable and nonrespirable solids, $\mu Ci/g$ on collected airborne solids.

Experiments

Airborne solids were collected as a function of wind direction at the Prosser Barricade and Horn Rapids sampling sites. At the Prosser Barricade site, selected

Figure 2.12. Map Showing Airborne Particulate Sampling Sites Located at the Prosser Barricade, the Horn Rapids Dam, the Top of Rattlesnake Mountain and at the Hanford Central Stores

airborne solid samplers were automatically activated (an air flow sampling rate of 1.1 m^3/min at a sampling height of 1.4 m) for three wind directions centered around 240°: 240° ± 15°, 240° ± 30°, and 240° ± 45°. During these wind directions, airborne solids were continuously collected during all wind speeds. Only a wind direction of 240° ± 15° was investigated at the Horn Rapids sampling site.

Plutonium transport on both respirable and nonrespirable airborne solids was investigated at both sampling sites. Airborne solids were collected in samplers consisting of a cyclone-preseparator and a backup filter. Manufacturer's specifications(a) are 5.5-μm 50 percent cutoff diameter for the cyclone-preseparator.

Sampling reproducibility was investigated at the Prosser Barricade sampling site. For the 90° wind direction sector, 195° to 285°, the solids collected in two cyclone-preseparator systems were analyzed for plutonium. Multiple cyclone-preseparator systems also were used at the 15° and 60° wind direction increments in order to collect sufficient airborne plutonium for radiochemical analysis. There were four systems used for the 15° wind direction sector and two each for the 60° and 90° wind direction sectors. Samples in each of the 15° and 60° wind direction sectors were combined for plutonium analysis.

In comparison to sampling as a function of wind direction, airborne solids were also collected for all wind directions using massive-volume air samplers located near Central Stores and the top of Rattlesnake Mountain. This impactor (Mitchell et al. 1978) consists of a two-stage particle cascade impactor followed by an electrostatic precipitator for collection of smaller particles. The 50% cutoff diameter for the first impactor stage is 3.5 μm while the 50% cutoff diameter for the second impactor stage is 1.7 μm.

After weighing, samples were analyzed for $^{239+240}Pu$ by a commercial laboratory.(b) For analysis, samples were dissolved and the plutonium electroplated on platinum discs. After analysis, the plutonium on these platinum discs was analyzed at Pacific Northwest Laboratory (PNL) with a mass spectrometer for plutonium atom ratios.

(a) Model 230 CP Cyclone Preseparator, Sierra Instrument Co., Carmel Valley, CA 93924.

(b) LFE Environmental Analysis Laboratory, 230 Wright Avenue, Richmond, CA 94804.

Results

Calculated results are shown in Figures 2.13 through 2.15. Each figure is composed of a left and a right subfigure. The left subfigure corresponds to samples collected as a function of wind direction with cyclone-preseparators at the Prosser Barricade and Horn Rapids. The right subfigure corresponds to samples collected for all wind directions, using massive-volume air samplers near Central Stores and the top of Rattlesnake Mountain.

Airborne plutonium data are shown as a function of size, the host airborne particle size as reflected in the solid collection sites within each sampler. For the cyclone-preseparator systems, data are shown for solids collected in the cyclone (a 5.5-μm 50% cutoff diameter), on the backup filter, and the total of cyclone plus backup filter collections. For the massive-volume air-samplers, data are shown for 1.7-μm diameter particles (the 50% cutoff diameter for the second impactor stage), for solids collected on the backup electrostatic precipitator plates, and the total of the 1.7 μm diameter stage plus backup electrostatic precipitator collections. In either system, the total-collection data-symbol, when accurately plotted, often would be almost superimposed on the smallest particle symbols. Consequently, data symbol offsets are used in Figures 2.14 and 2.15 to decrease the visual superposition of data symbols. In these cases, data symbols for total sampler collection are offset to the right with arrows pointing to locations where data points are located.

Plutonium-240/239 Atom Ratios

The $^{240}Pu/^{239}Pu$ atom ratios are shown in Figure 2.13, ranging from about 0.04 to 0.21. This indicates that both fallout and process-grade plutonium were collected within these samples. The atom ratios are a function of both particle size and the type of sampler used. For particles collected within cyclone-preseparator systems at the Prosser Barricade, the $^{240}Pu/^{239}Pu$ atom ratio range is about 0.15 to 0.19 for "small" particles collected on the backup filter, a range expected for a fallout plutonium source.

In contrast, the $^{240}Pu/^{239}Pu$ atom ratio range, 0.04 to 0.07 for "large" particles

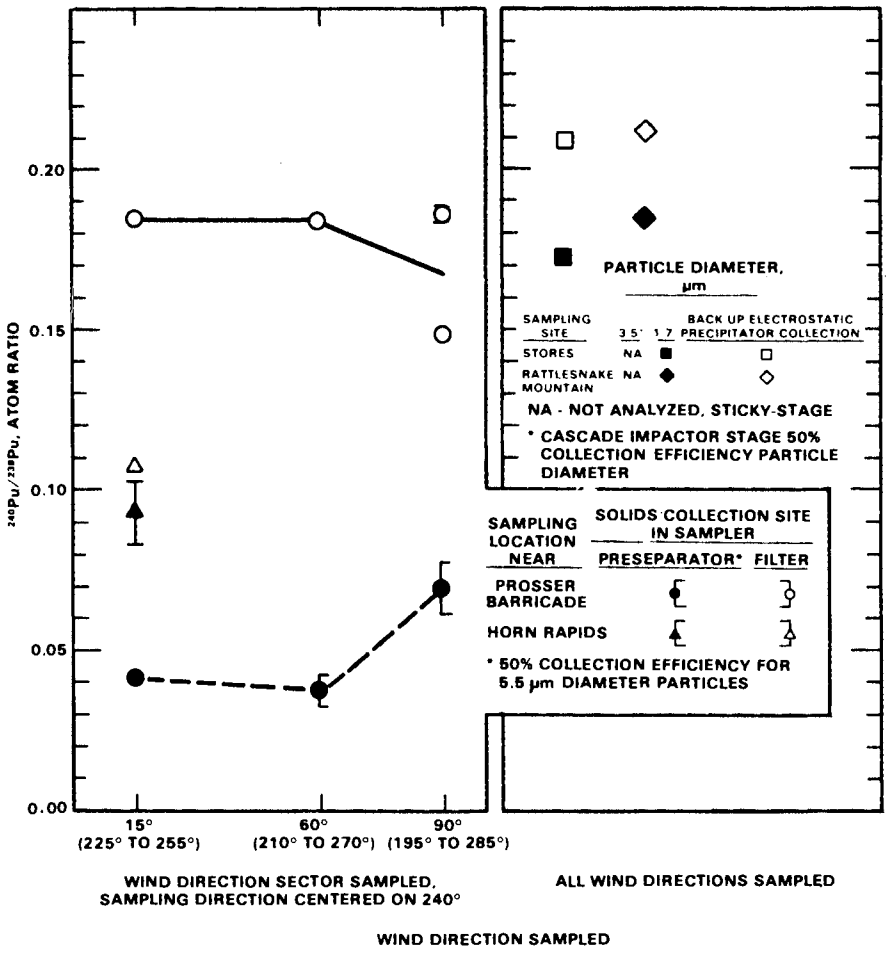

Figure 2.13. $^{240}Pu/^{239}Pu$ Atom Ratios for Airborne Solids Collected in 1979 near the Prosser Barricade, Horn Rapids, Central Stores, and from the Top of Rattlesnake Mountain

"greater" than 5.5 µm diameter, is smaller for solids collected within the cyclone-preseparator. This range on large particles reflects significant collections of Hanford process-grade plutonium in the cyclone-preseparator. Less source distinction as a function of particle size is indicated by the $^{240}Pu/^{239}Pu$ results at the Horn Rapids site. At the Horn Rapids site, the $^{240}Pu/^{239}Pu$ atom ratios are between about 0.09 to 0.11 for both particle size fractions. This range indicates a mixture of fallout and process-grade plutonium.

Although the experiment was designed to investigate the wind direction and hence the source from which process-grade plutonium was transported in the air, identifying wind direction is complicated by the effects of particle size. As shown in Figure 2.13, the $^{240}Pu/^{239}Pu$ atom ratios were not strongly affected by sampling direction. The greatest effect on atom ratios is the separation within the samplers of airborne solids as a function of particle size. This separation effect occurs even for $^{240}Pu/^{239}Pu$ atom ratios which are typical of fallout, i.e., the data for Central Stores and Rattlesnake Mountain. At these two locations the $^{240}Pu/^{239}Pu$ atom ratios for the larger particles (1.7-µm 50% stage cutoff diameter) had lower ratios than smaller size particles collected on the backup electrostatic precipitator collections. This is, however, not surprising. The larger particles include some plutonium resuspended from prior fallout deposition, while smaller particles mainly indicate fresh stratospheric fallout.

Airborne Plutonium Concentrations

Airborne $^{239+240}Pu$ concentrations, $\mu Ci/cm^3$, are shown in Figure 2.14.

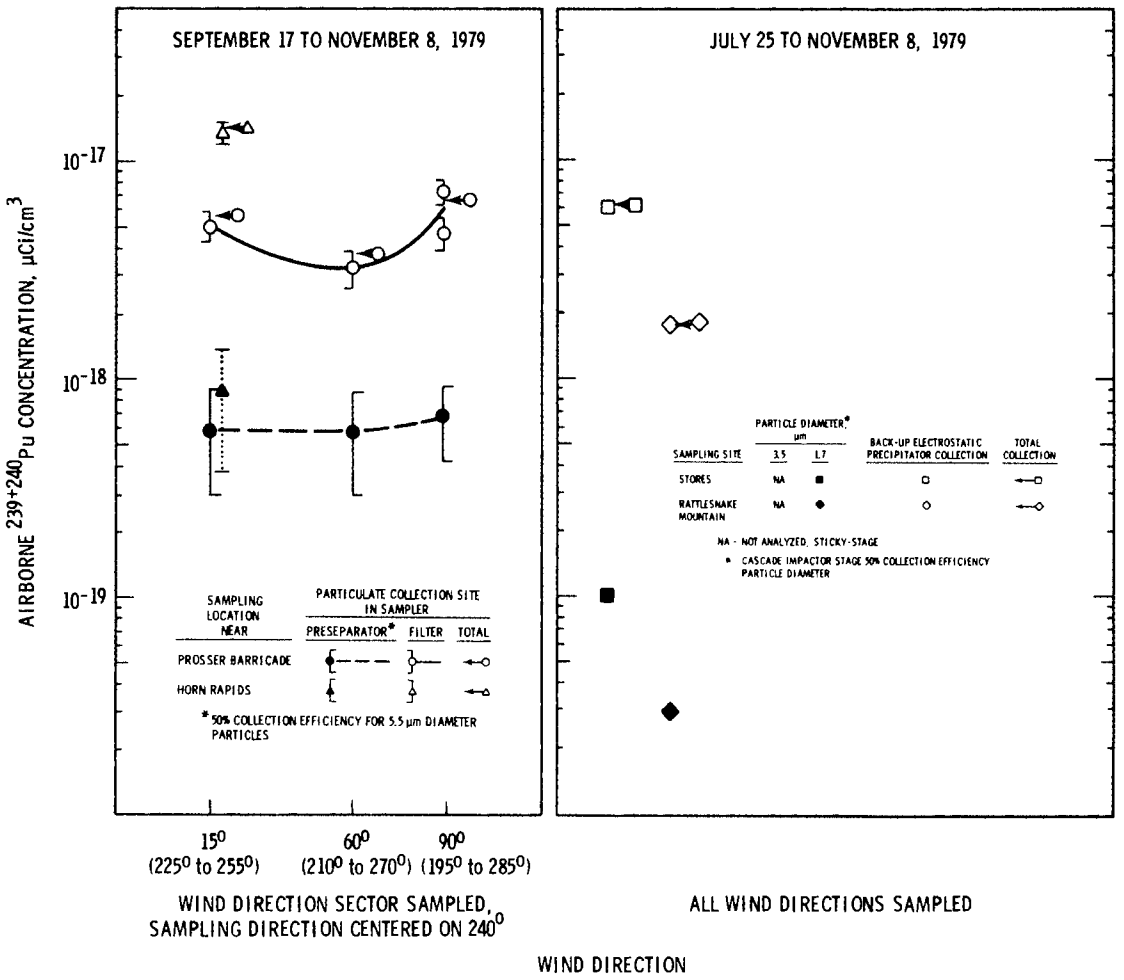

Figure 2.14. Airborne $^{239+240}Pu$ Concentrations for Samples Collected in 1979 near the Prosser Barricade, Horn Rapids, Central Stores, and from the Top of Rattlesnake Mountain

Airborne concentrations are low, the maximum is only 1 x 10^{-17} µCi/cm^3. This maximum concentration is only 0.02% of the 6 x 10^{-14} µCi/cm^3 168-hr maximum permissible concentration guide (ERDA 1977b). Since these concentrations reflect plutonium collected on solids, the activity density per gram of airborne solids is also of interest.

Activity Density on Airborne Solids

The $^{239+240}Pu$ activity density on airborne solids, µCi/g, is shown for collected solids in Figure 2.15. All the activity densities range from about 1 x 10^{-7} to 3 x 10^{-7} µCi/g, except for two data points. The two exceptions are for the large particles collected near Central Stores and the top of Rattlesnake Mountain. For these exceptions, the activity densities range from about 2 x 10^{-8} to 6 x 10^{-8} µCi/g, which is about a factor of three less than the average activity densities in the other samples.

Conclusions

Airborne plutonium similar to both fallout and process-grade plutonium was measured at the Prosser Barricade and Horn Rapids sampling sites. At the Prosser Barricade, the process-grade plutonium was associated with larger than 5.5-µm diameter particles. For smaller particles, passing through a cyclone-preseparator, the plutonium source was principally stratospheric fallout. Even though plutonium for both sources was airborne, the maximum airborne concentration was only 0.02% of the 6 x 10^{-14} µCi/cm^3, 168-hr maximum permissible guide (ERDA 1977b). The directional source of process-grade material on the larger particles was at least from 195° to

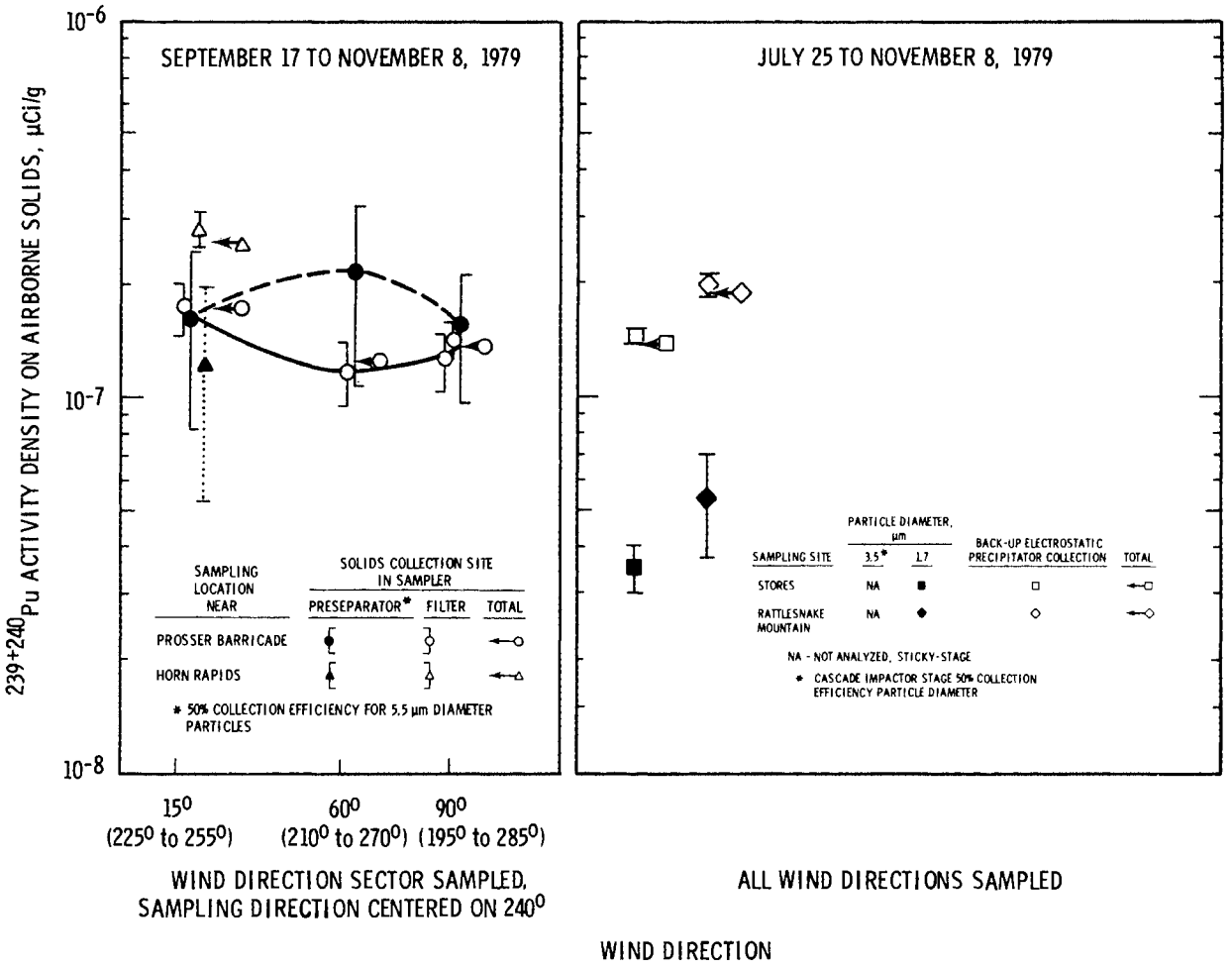

Figure 2.15. $^{239+240}$Pu Activity Density on Airborne Solids Collected in 1979 near the Prosser Barricade, Horn Rapids, Central Stores, and from the Top of Rattlesnake Mountain

285°, that is, the entire wind sector investigated for turning on the air sampling pumps. Process-grade plutonium, however, was not measurable in samples collected from the top of Rattlesnake Mountain. Although process-grade plutonium was transported across the Prosser Barricade sampling site, and some across the Horn Rapids sampling site, the source is yet to be identified. These results further confirm evidence that process-grade plutonium is airborne. Although airborne, the maximum concentration is a small percentage of permissible concentration guidance level.

References

Code of Federal Regulations. 10 CFR Part 20, Appendix B, Table II.

ERDA. 1977a. Alternatives for Long-Term Management of Defense High-Level Radioactive Waste, Hanford Reservations. ERDA 77-44, pp. 3-8, Energy Research and Development Administration, Washington, DC.

ERDA. 1977b. ERDA, Manual of Operation. Chapter 0524, "Standards for Radiation Protection," Appendix A, Table II. U.S. Energy Research and Development Administration, Washington, DC.

Krey, P. W., E. Hardy, P. Pachucki, C. Rourke, J. Coluzza, and W. K. Benson. 1976. "Mass Isotopic Composition of Global Fallout Plutonium in Soil." In Transuranic Nuclides in the Environment, pp. 671-678, International Atomic Energy Agency, Vienna, Austria.

Mitchell, R. I., W. M. Henry, and N. C. Henderson. 1978. Fabrication, Optimization, and Evaluation of a Massive Volume Air Sampler of Sized Respirable Particulate Matter, EPA-600/4-78-031, available National Technical Information Service, Springfield, Virginia.

Sehmel, G. A. 1979. "Airborne Plutonium Transported During Southwesterly Winds Near the Hanford Prosser Barricade," PNL-SA-7839 presented November 11-16, 1979, at the American Nuclear Society National Meeting in San Francisco, California.

• Arid Lands Ecology (ALE) Climatology

Objectives of this study are:

- Operating the temperature and precipitation network on the Arid Lands Ecology (ALE) reserve at Hanford.
- Issuing daily and monthly summaries of data from the network.
- Analyzing climatological data from the network, such as cross-correlations between daily and monthly temperature stations.

Ten-Year Precipitation Averages at the ALE Reserve Microclimatological Sites

J. M. Thorp

There are five microclimatological transects crossing the Arid Lands Ecology Reserve. The central three extend from Cold Creek Valley at 200 m and less to the crest of Rattlesnake Mountain at about 1000 m. The western- and eastern-most transects end at 540 m and 750 m, respectively (Thorp and Hinds 1977). Monthly precipitation measurements have been made for more than 10 years now at 26 sites placed along these five transects.

The National Weather Service of the National Oceanic and Atmospheric Administration defines "normal" precipitation as the 30-year running average updated every 10 years. However, instead of waiting 20 more years to calculate normal precipitation amounts for the ALE Reserve stations, it seemed appropriate that use be made of the data in hand to calculate the 10-year annual average precipitation at each site.

In Figure 2.16, average annual precipitation (1969-1978) is plotted versus station elevation. The average annual precipitation increases with elevation to about 700 m. Above that height precipitation amounts on each of the four transects that go to the crest of Rattlesnake Mountain remain about the same or decrease. The

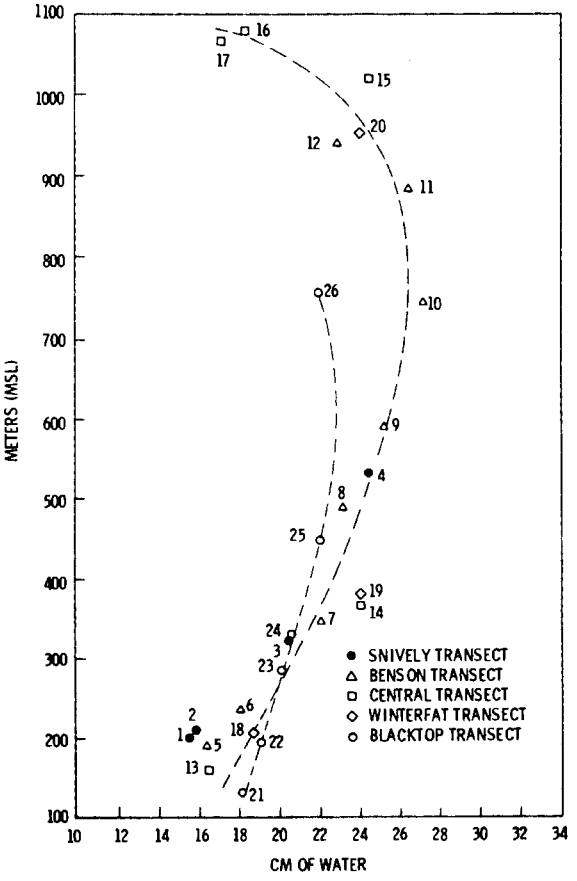

Figure 2.16. Average Annual Precipitation Versus Elevation for the ALE Reserve

Snively transect, which terminates at 533 m, well below the crest of the Rattlesnake Hills, would likely exhibit the same characteristics if extended to the top of the hills.

The increase of precipitation with elevation is nearly linear to about 700 m, with the Snively, Benson, Central, and Winterfat transects showing about the same slope. The Blacktop transect, which has its stations near or on the southeast edge of the mountain, shows less change with elevation. Wind effects across this edge of Rattlesnake Mountain probably are important in explaining this difference.

The majority of winter storms in the Columbia Basin have airflow from the southwest. This flow is perpendicular to the Rattlesnake Mountain crest, and because these southwest winds are frequently strong across the crest it is likely that significant amounts of precipitation are blown across the mouth of a raingage rather than falling into it. This helps account for the large reduction in catch measurement at stations 16 and 17 compared to Station 15 less than 1000 horizontal feet away, but which is on the northeast (lee) slope.

Reference

Thorp, J. M. and W. T. Hinds. 1977. Microclimates of the Arid Lands Ecology Reserve, 1968-1975, BNWL-SA-6231, Pacific Northwest Laboratory, Richland, Washington.

• Reactor Safety Study

Objectives of this study are:

- Review the meteorological aspects of the Reactor Safety Study, WASH-1400.
- Identify areas requiring improved descriptions for more realistic assessments of reactor-accident consequences.

Meteorological Aspects of the Reactor Safety Study Requiring Further Study[a]

W. G. N. Slinn[b]

The goal of this short study was to review meteorological aspects of the Reactor Safety Study, WASH-1400 (U.S. NRC 1975), to identify topics whose improved descriptions might lead to more realistic assessments of reactor-accident consequences. The method used was to perform a few, simple, "back-of-the-envelope" calculations to identify what can be called "stochastic dominating" features (Slinn 1975). In this extended abstract, results will be emphasized; developments leading to these results can be found in the report, with the same title, now being prepared for distribution.

There are a number of inadequacies in this simple analysis. One is derived from assumptions, generally, of negligible correlations among the relevant random variables. These assumptions fail in some cases, but even when they do, informative results are obtained. A second inadequacy is derived from the emphasis on radionuclide concentrations, rather than doses, and therefore the important influence of threshold dose values (e.g., to differentiate between acute fatalities and latent cancers) is not revealed. In spite of these inadequacies, however, the simple analysis does provide revealing results that, as a minimum, can guide future, more accurate studies.

Features dominating the average of the consequences are considered first. Of these features, the influence of the source term can be seen by writing the exposure from radionuclide i released during accident j, E_{ij}, as proportional to the amount of i released, Q_{ij}. Thus,

$$E_{ij} = A_{ij} Q_{ij} \qquad (1)$$

where A_{ij} symbolizes a host of atmospheric factors. If it were acceptable to ignore correlations between release type and atmospheric behavior of radionuclide i (see later comments about plume rise), then the average exposure from radionuclide i, where the average is over all accident types, is

$$\langle E_i \rangle_j = A_i \sum_j P_j Q_{ij} \qquad (2)$$

where P_j is the probability of occurrence of accident j. Through use of the probabilities and source strengths listed in WASH-1400, the following conclusions were reached:

- If credit cannot be taken for substantial additional plume rise, then to improve estimates of average consequences of reactor accidents, it is most important to improve descriptions for cases of overpressurization and failure of reactor-containment vessels (e.g., PWR-2 accidents). Put

---

(a) Proceedings Symposium on Intermediate Range Atmospheric Transport Processes and Technology Assessment, 1-3 October 1980, Gatlinburg, TN, Oak Ridge National Laboratory, 1980; work sponsored by the U.S. Nuclear Regulatory Commission via a sub contract with Sandia Laboratories and a Related Services Agreement under U.S. Department of Energy Contract No. DE-AC06-76RLO-1830.
(b) Substantial help with this paper was given by D. C. Aldrich and L. T. Ritchie of Sandia Laboratories.

more forcefully, until the consequences of a PWR-2 accident can be estimated to within about 10 percent accuracy, then for average estimates there is little point in considering the other 8 PWR accidents listed in WASH-1400.

- Improvements needed in describing containment-failure accidents include: estimates for the probabilities for failures to occur at different locations on the vessel, the size of the fracture, gas temperature and pressure, amounts of ablated material, chemical speciation of the radionuclides, etc.

- The actual plume rise of a (presumably) near-sonic jet, exiting horizontally and transferring heat to the earth's surface, is probably substantially different from available descriptions (Russo 1976). Field studies should be conducted, especially during stable atmospheric conditions, to develop descriptions of sonic jets (e.g., from a jet-engine exhaust) out to distances of 1 to 10 km.

- It may be possible to reduce reactor-accident risks by incorporating pressure-relief valves at the top of containment vessels (Russo 1976).

The influence of transport and diffusion on average consequences can be seen by writing the exposure averaged over all possible meteorological conditions k in the form

$$\langle E_{ij} \rangle_k = Q_{ij} \sum_k p_k A_{ijk} \qquad (3)$$

where p_k is the probability of meteorological condition k. From an examination of this average, the following conclusions were reached:

- Radionuclide concentrations in air, and therefore prompt human fatalities, are substantially higher for cases of low mixed-layer height or stable atmospheric conditions (common during clear nights). Therefore, it is most important that these cases be described accurately. If a modified Gaussian plume model is used, then modifications to describe plume lofting and fumigation should be incorporated. Also, Holzworth's single-value, mixed-layer heights should be abandoned in favor of a model that describes time-dependent behavior of the mixed layer.

- Improvements to the statistical sampling protocol should be sought; with an emphasis on accurately identifying worst-case conditions, describing plume behavior for these conditions, and defining their frequency of occurrence. Single-tower meteorological data as used in WASH-1400 should be supplemented with National Weather Service data. Progress toward these objectives will soon be reported by Sandia Laboratories.

- Alternatives to Gaussian plume models, e.g., K-theory, should be vigorously pursued, if not for use in the consequence calculations then for readily-available knowledge toward future applications.

Wet removal's influence on average concentrations of radionuclides in air, $\bar{\chi}$ (and on associated consequences), can probably be ignored within about 100 km from a reactor accident because with worst-case air concentrations (cases of poor ventilation), precipitation does not normally occur. However, even for cases of deep atmospheric mixing, precipitation scavenging can result in significant surface deposition of radionuclides, because precipitation "integrates" over a plume's vertical distribution. In other words, average consequences can probably be adequately estimated using expressions that describe average wet removal. Thus, for the average reduction in $\bar{\chi}$ by wet removal, use the following formula (and for average wet deposition use its complement):

$$\bar{\chi} = \bar{\chi}_0 \exp\{-t/\bar{\tau}_w\} \qquad (4)$$

where $\bar{\chi}_0$ is the air concentration in the absence of wet removal, and where the annual-average, e-fold residence time, $\bar{\tau}_w$, is approximately 1 week for all released radionuclides, except $\bar{\tau}_w \to \infty$ for noble gases. $\bar{\tau}_w$ can be rationally varied by season in direct proportion to seasonal precipitation.

On the other hand, dry deposition's influence on χ can be significant because maximum deposition normally occurs for worst-case surface χ values. A number of aspects of dry deposition treated in WASH-1400 should be improved. Some suggestions follow:

- Use of a single value for the dry deposition velocity, v_d, and the associated exponential decrease in χ, should be abandoned; there is as little justification for using a single v_d as there is, for example, for using a single wind speed or a single stability class.

- Specifying realistic distributions of deposition velocities is extremely difficult and will require substantial further study. Temporary improvements suggested for present methods include:

(a) Distribute to released particles a range of deposition velocities between 0.1 and 10 cm s^{-1}.

(b) Assign to inorganic iodine the following temporary values and ranges:

(i) Assume 10 to 50 percent of the released iodine is associated with the released particles, and has their v_d values.

(ii) With increasing distance from the reactor, associate a continuously increasing fraction of the gaseous iodine with ambient aerosol particles, with their v_d values, in the range from about 0.01 to 1 cm s^{-1}.

(iii) Estimate the number of I_2 molecules remaining in the gaseous state, e.g., via

$$N = N_0 - [S/(10^{-3}\ \mu m)^2]\ \sigma_y \sigma_z r \qquad (5)$$

where N_0 is the number of released I_2 molecules, S is the total surface area of ambient aerosol particles per unit volume (S is in the range of about $10^7\ \mu m^2\ m^{-3}$ for rural conditions to about $10^9\ \mu m^2\ m^{-3}$ for urban conditions), and σ_y and σ_z are diffusion parameters at downwind distance r.

(iv) Assign to gaseous I_2 the deposition velocity $v_d = C_D\ \bar{u}$, where C_D is the drag coefficient for appropriate surfaces and all quantities are related to the same reference height.

(v) Limit total deposition of the gaseous I_2 to other than natural water surfaces, to a value of about 100 Curies m^{-2}.

These estimates are not accurate and further study is needed even to estimate their accuracy. However, they are expected to be substantially more realistic than the single value for v_d used in WASH-1400.

Variance and Distributions

Table 2.8 summarizes estimates for the coefficients of deviation (standard deviations divided by mean values) resulting from variations in the indicated quantities. From this investigation, the following conclusions were reached:

- Overwhelmingly, the dominant stochastic process is the accident itself. Accident events can be modeled as Poisson processes; the variance is therefore approximately equal to the mean, and it is dominated by accidents involving containment-vessel failure.

- Conditional upon an accident occurring, the dominant variance of consequences appears to be caused by precipitation scavenging, which also can be approximately described as a Poisson process. Therefore, a first estimate for the probability distribution of consequences is that they have a Poisson distribution with variance equal to the mean value, which can be calculated as suggested in the previous section.

- At present, the major uncertainties in the consequence estimates probably arise from uncertainties in the description of major accidents, and in the stipulation of dry deposition velocities.

Table 2.8. Coefficients of Deviation (Standard Deviations Divided by Mean Values) Resulting from Variations in the Indicated Quantities and Processes

Variable	Coefficient of Deviation
Source Term	$(\lambda t)^{-1/2} \sim 10^3$ if t = 1 d
Wind Direction	< 1
Wind Speed	~ ½
Mixed-Layer Height	~ 1
Dry Deposition	~ 1
Precipitation Scavenging	~ 3

References

Russo, A. J. 1976. Reactor Accident Plume Rise Calculations. SAND76-0340, Sandia Laboratories. Available from NTIS, Springfield, Virginia.

Slinn, W. G. N. 1975. "An Analytical Search for the Stochastic-Dominating Process in the Drift-Deposition Problem," Cooling Tower Environment--1974. Coords. S. R. Hanna and J. Pell. TIC, ERDA, CONF-740302. Available from NTIS, Springfield, Virginia.

U.S. Nuclear Regulatory Commission. 1975. Reactor Safety Study. An Assessment of Accident Risks in U.S. Commercial Nuclear Power Plants. N. Rasmussen, convenor; WASH-1400 (NUREG-75/014). Available from the U.S. NRC or from NTIS, Springfield, Virginia.

3 Oil Shale

OIL SHALE

- **Oil Shale Fugitive Air Emissions**

- **DOE/RL Special Studies**

The primary oil shale regions of the country are in the Rocky Mountain West where any airborne pollutants will be emitted, transported, transformed and deposited over very complex terrain under meteorological conditions that are, at best, extremely complicated. This complexity dictates the development of a set of complex models and innovative field techniques.

PNL has assessed the future research needs in this area and has formulated an experimental design for atmospheric transport studies over the oil shale region. Other activities include:

- development of a tracer technique to measure dry deposition of pollutants over complex areas

- insolation and turbidity measurements over rough topography

- aerosol and visibility measurements

- deposition measurements of ambient airborne soil.

• Oil Shale Fugitive Air Emissions

Objectives of this study are:

- Evaluating fugitive airborne particulate and gaseous emissions from the present and future oil shale activities.
- Investigating emissions from mining, transportation, material handling, crushing, retorting, and spent shale disposal sites.
- Identifying and classifying pollutants such as carbon monoxide, hydrogen sulfide, oxides of nitrogen, ozone, sulfur dioxide, hydrocarbons, and suspended particles.

Lithium Detector Calibrations for Dual-Tracer Dry Deposition Experiments

G. A. Sehmel and W. H. Hodgson

Techniques for measuring airborne plume transport and plume depletion are being developed based on tracer techniques. At present, dual tracers of non-depositing SF_6 gas and lithium-traced particles are being used. Previously, the particle detectors were calibrated (Sehmel and Hodgson 1980) as a function of particle diameter. The lithium compound for particle generation was lithium stearate, selected because of minimal health concerns from the lithium content. In subsequent usage, lithium stearate was dissolved in methyl alcohol to generate particles from evaporated droplets from liquid sprays. However, because of the large volume of solutions required for field use, the resulting airborne concentrations of methyl alcohol gas presented a potential health concern. Consequently, further investigation of particle generation characteristics was required.

Originally, an organic compound of lithium was selected for particle generation because inorganic lithium compounds can be a health concern. Then during discussions of airborne methyl alcohol health concerns, it was suggested that one inorganic compound of lithium would be acceptable. This is lithium carbonate. Lithium carbonate is used medicinally in large quantities for improving mental health. Thus, lithium carbonate was selected for subsequent investigation of lithium tracer particles for several reasons:

- Lithium carbonate is water soluble and so the solvent is convenient for field use. Also, lithium carbonate solubility is greater than for lithium stearate.
- Airborne lithium tracer particle concentrations would be greater for lithium carbonate than for lithium stearate. Even though the particles are larger, there are no known health concerns using lithium carbonate.

Since particles for field use will be generated by spraying a solution of lithium carbonate, lithium particle detector responses are needed as a function of particle size. That is, we need to know what size range of polydispersed aerosol generated under field conditions is sensed by lithium detectors. The range was determined by using monodispersed particles generated in laboratory-controlled conditions. Reported here are calibration results of the lithium particle detectors using monodispersed lithium carbonate particles.

Lithium Detector Particle Calibration

Lithium particle detectors were calibrated with lithium carbonate particles generated with a vibrating-orifice particle-generator. During calibration the feed solution for particle generation contained lithium carbonate and uranine, a

tracer for determining the detector response efficiency. In addition to particles generated, there were also some ambient particles to which the detectors responded. However, the number of ambient particles is low since all air was filtered through high efficiency filters before being introduced within the sampling container.

The ratio of particles per unit volume sensed by the lithium detector divided by the true airborne concentration near the detector inlet is an efficiency ratio, i.e., instrument/true particle concentration. This ratio or efficiency is less than unity. Response efficiency is less than unity because of particle deposition losses within the detector sampling delivery system. Also there was possibly some inefficiency in particle detection during flame ionization depending on the location within the flame where each particle is burned. Sampled particles are detected by flame ionization within the lithium detectors. The "true" airborne particle concentration was calculated from a filter sample of particulates obtained near the detector inlet. This filter sample was analyzed for uranine fluorometrically to determine the number of tracer particles per unit volume of air.

Results

Lithium particle-detector calibrations are shown in Figure 3.1. In this figure are 3 subfigures: 1) the left subfigure corresponds to the true airborne particle concentrations as determined by the uranine tracers; 2) the mid-subfigure is the sampling efficiency uncertainty caused by ambient particles which respond/are detected as lithium particles; and 3) the right subfigure is the sampling efficiency for each lithium detector.

As shown in the left subfigure, airborne concentrations of monodispersed particles during calibration tended to decrease as particle diameter was increased. All concentrations are relatively low, from about 1 to 10 particles cm^3. During calibration these concentrations were sampled at an airflow rate of 50 cm^3/min.

The mid-subfigure shows errors associated with detector response to sampling ambient airborne particles rather than monodispersed particle concentrations. For particle diameters between about 0.5 to 1.5 μm in diameter, the uncertainty is less than 10%. The minimum uncertainty is for a particle diameter of about 0.7 μm. The uncertainties increase as either particle sizes decrease or increase. For particle diameters above approxmately 1.5 μm the uncertainty is greater than 50%, reflecting a low airborne true particle concentration and the presence of ambient airborne particles.

In the right subfigure lithium detector sampling efficiency responses for each monodispersed particle diameter are shown. Lithium carbonate particles have a maximum instrument efficiency of about 40% at a particle diameter of about 0.7 μm. For particle diameters below about 0.5 μm and above approximately 1.5 μm, lithium particle detector efficiencies decrease over one order of magnitude. Further decreases are shown for both smaller and larger particle diameters. Thus, these calibration curves show the greatest response for particle diameters in the range of about 0.5 to 1.5 μm in diameter. These efficiencies are somewhat similar to those previously reported for lithium stearate particles generated from methyl alcohol solutions.

Conclusions

Lithium-traced particles generated from lithium carbonate respond in a narrow size range, from about 0.5- to 1.5-μm diameter. In this size range, particle dry deposition velocities are nearly independent of particle diameter.

In field conditions, polydispersed particles are generated from water solutions sprayed through nozzles. The nozzles are used to generate large quantities of droplets, however, the droplets and resulting particles do extend beyond the size range sensed by the lithium particle detectors. Nevertheless, detector response efficiencies within a narrow range permit use of these lithium particle detectors for investigations of particle dry deposition under field conditions.

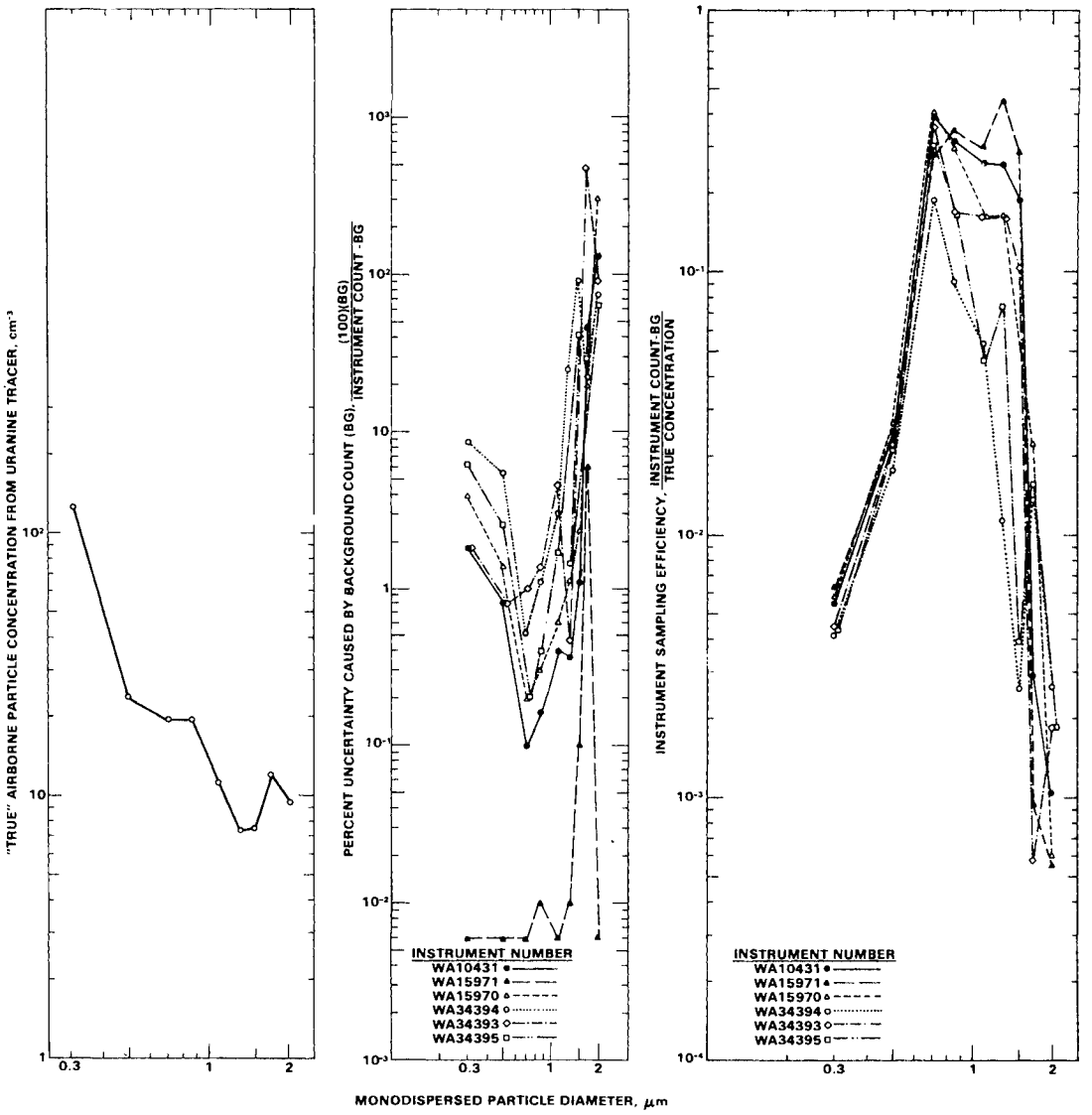

Figure 3.1. Lithium Detector Calibrations with Monodispersed Lithium Carbonate-Uranine Particles

Atmospheric Transport and Plume Depletion Investigations Using Dual Tracers in the Colorado Oil Shale Region

G. A. Sehmel

Atmospheric transport and plume depletion investigations were conducted in August 1980 with dual atmospheric tracers at the federal lease tract C-a, operated by Rio Blanco in Colorado. The tracers used were nondepositing SF_6 gas and depositing lithium-traced particles. Tracer concentrations were measured using three types of sampling instrumentation:

1. real-time measurements of both lithium-traced particles and SF_6 gas
2. bag samples of SF_6 gas collected by using radio transmissions to actuate sampling pumps
3. syringe-collected samples of SF_6 gas collected at the most remote sites investigated.

Tracers were released at surface level near the bottom of Corral Gulch at a site near the Rio Blanco process stacks. Downwind, there were four main sampling lines

for SF_6 operated by radio control. Along each line, seven or eight sampler stations were placed across the valley; two samplers were placed on each hillside, and either three or four stations were placed along the valley floor. The first sampling line was approximately 1.6 km downwind from the release point; the second line was 2.5 km; the third line was 4.6 km; and the fourth line was 5.6 km. Further downwind, at approximately 6.8 km, syringe samples of SF_6 were obtained along roads that crossed the valley.

Samples of airborne SF_6 were collected using air sampling pumps actuated by radio-control signals. Each pump discharge was collected in a bag. At each sampling station there were three sampling pumps. Although these pumps were placed near ground level, air sampler tubing inlets were located at several heights. Tubing inlets were located so either sequential or profile samples could be obtained along the sampling lines: sequential along lines 1 and 3, and profile along 2 and 4. The sequential inlets were located 1.7 m above ground, while the profile inlets were located at 0.3 m, 1.3 m, and 5 m above ground.

For a sequential sampling station, three tube inlets were located 1.7 m above ground. In this case, radio signals activated sequentially the three sampling pumps at that station. Thus, airborne SF_6 concentrations were investigated as a function of selected times. For profile stations, the three pumps were turned on simultaneously. Thus, the airborne SF_6 concentration profile was obtained during only one time interval.

There were five tracer releases. The first four were nighttime releases during drainage flow, while the fifth was a daytime release. Results will be reported at a later date. Included in the results will be meteorological data obtained by Pacific Northwest Laboratory (PNL), Los Alamos Scientific Laboratory (LASL), and Rio Blanco. It is anticipated that model validity will be tested, improved models developed, and a new concept for atmospheric transport in complex terrain developed. More importantly, however, results may indicate consideration should be given to relocating the present air quality sampling site to better serve as an index site for airborne concentrations of emissions.

Potential Contamination of SF_6 Bag Samples

G. A. Sehmel and W. H. Hodgson

Sulfur hexafluoride gas is used as a tracer for atmospheric diffusion, transport, and plume depletion investigations. Downwind tracer samples are often collected in sampling bags and then analyzed. Bag composition includes polyethylene and Tedlar.® In August 1980, polyethylene bags were used in plume depletion and transport studies in the oil shale region of Colorado, and some bag samples were analyzed for SF_6 content the day after samples were collected. The samples were reanalyzed two to three weeks later at Pacific Northwest Laboratory (PNL) to investigate 1) analysis reproducibility for field and laboratory conditions and 2) sample stability as a function of time. This article documents a potential contamination problem that arose.

A cross-comparison of the field data with subsequent laboratory data sets indicated significant differences. For field conditions, tracer gas concentrations differed significantly in each sampling bag. In contrast, when sample bags were analyzed in the laboratory, all sample bags tended to show nearly the same tracer gas concentrations. In addition, many bag samples showed a notable increase in SF_6 concentrations. Explanations for the SF_6 concentration changes were sought.

During the last tracer experiment in Colorado, a daytime release, the tracer release rate was markedly increased. Release rates were increased because little SF_6 was detected at the near-real-time detection stations. Nevertheless, it was possible that released tracer was transported and then stagnated around a truck in which the bag samples were stored in cardboard boxes. The polyethylene bags were stored within cardboard boxes, preventing exposure of the bags to sunlight. Decreasing or preventing light exposure is important since there is some information that sunlight can cause apparent increases in SF_6 concentrations in polyethylene containers caused by bag outgassing and reactions.

® Tedlar (PVF Film) is a registered trademark of DuPont.

There are several possibilities to explain the apparent SF_6 concentration changes in the bags. Increased ambient airborne SF_6 concentrations may have caused SF_6 to diffuse into the bag samples stored from prior days. Contamination during shipment from Colorado to PNL was another possibility. This contamination might be attributed to bag outgassing from elevated temperatures within the shipping truck. However, the potential contamination during transport was not caused by leaking SF_6 bottles in the truck, because the SF_6 bottles were always transported to and from Colorado on separate trucks. A third possibility was bag contamination while stored in the PNL laboratory. During storage, the possibility existed that some freon, a similar SF_6 detector response, was in ambient air and diffused in the bags.

Experiments

In an attempt to account for bag sample contamination, selected tests were carried out to determine mass transfer characteristics across sampling bags. An outer and inner test bag was used for the mass transfer tests. In the tests, oxygen-free nitrogen was inserted into the inner sampling bag. The sealed bag was then placed within a larger polyethylene bag. To investigate SF_6 transfer through the polyethylene bag, pure SF_6 was introduced into the volume between the inner and outer bags. In following tests, pure freon also was introduced into the outer bag. In still other tests, a Tedlar bag was used as the inner bag. After a day's diffusion time, a gas sample from the inner bag was analyzed with an SF_6 detector. In all cases, both SF_6 and freon diffused through the inner bag into the oxygen-free nitrogen.

Conclusions

Although SF_6 can diffuse through both polyethylene and Tedlar, mass transfer rates were not investigated. The outer bag was always filled with either pure SF_6 or freon, rather than the maximum SF_6 concentrations measured under field conditions. Concentrations in field conditions were obviously less than pure tracer gas. Thus, SF_6 mass transfer rates into sampling bags would be less than shown by current results. Although mass transfer occurs through the bag walls, the surprising results are that sampling bag SF_6 concentrations increased, rather than decreased as would be expected by diffusion out-of-the-bag. The decrease is expected since bags are always under a slight pressure, being partially full, and ambient SF_6 concentrations are less than the concentrations within the sampling bags. The causes for apparent increases in SF_6 concentrations within the stored sampling bags are still being investigated.

• DOE/RL Special Studies

Objectives of these studies are:

- Collecting data from an airborne platform on scattering extinction coefficients, relative humidity, sulfate and trace metals over mountainous terrain in the Northwest.
- Analyzing seasonal and monthly variations in spectral turbidity coefficients at Hanford.

Pollution Budgets Within a Regional Airshed

R. N. Lee and M. M. Orgill

This study was undertaken to explore the feasibility of using inventories of trace materials and gases within atmospheric airsheds to assess the transport, metamorphosis, and removal of airborne pollutants. If practical, the technique would make an important contribution to the understanding and prediction of long-range transport, chemical and physical transformation of aerosols, and the fate of energy-related pollutants that may affect human health, ecological systems and weather. This initial study was an attempt to describe atmospheric budgets for certain trace gases and aerosols generated in the metropolitan area of Puget Sound and to quantify the accumulation or removal of pollutants downwind in Central Washington.

The experimental plan for the study consisted of locating three hi-vol samplers at sites near the crest of the Cascade Mountains for securing near-surface aerosol samples. These sites were Paradise (5,400 ft), Stampede Pass (3,163 ft), and Stevens Pass (4,070 ft). The hi-vol sampling was done in conjunction with aircraft flights (Cessna 411 and DC-3) on two days, May 16 and June 18, 1980. These flights were made at different elevations along two areas downwind of metropolitan Seattle-Tacoma area (Figure 3.2) and provided air samples from within and above the mixing layer. Additional hi-vol sampling also occurred on May 18 and June 14. The sampling period on May 18 coincided with the major eruption of Mt. St. Helens. Duration of the hi-vol samples was approximately 8 hours while duration of aircraft-derived air samples varied from 1 hour to 3 hours.

Weather conditions for three experimental periods are summarized briefly in Table 3.1. The aircraft sampling days, May 16 and June 18, were both cloudy on the west side of the Cascades. On May 16 the cloud top heights were approximately 8,000 ft Mean Sea Level (MSL), while on June 18 they were around 4,500 ft MSL. Sky conditions improved during the sampling periods, and all sampling was conducted under visual flight rules. One sample was taken above the clouds and two samples were taken within the mixing layer below the cloud bases. On June 18, an elevated haze layer (dust) was observed at an elevation of about 10,000 ft MSL over the Cascade Mountains. This haze layer extended to the northeast and was apparently the result of emissions from Mt. St. Helens.

The aircraft and surface sample filters were analyzed by X-ray Fluorescence (XRF) and the resulting concentration data were used to calculate crustal enrichment factors for the respective elements (Duce et al. 1975). A crustal enrichment factor, $EF_{crustal}$, for any element X in the atmospheric aerosols relative to the crust is calculated as follows:

$$EF_{crustal} = \frac{(X/Al)\ air}{(X/Al)\ crust}$$

where (X/Al)air and (X/Al)crust refer, respectively, to the ratio of the concentration of X to that of Al in the atmosphere and in the average crustal material (Taylor 1964). Aluminum (Al), which comprises more than 8% of the average crustal material, is used as a reference element. $EF_{crustal}$ values near unity for any element X suggest that crustal material is the probable source for that element in the atmosphere in remote areas. This technique

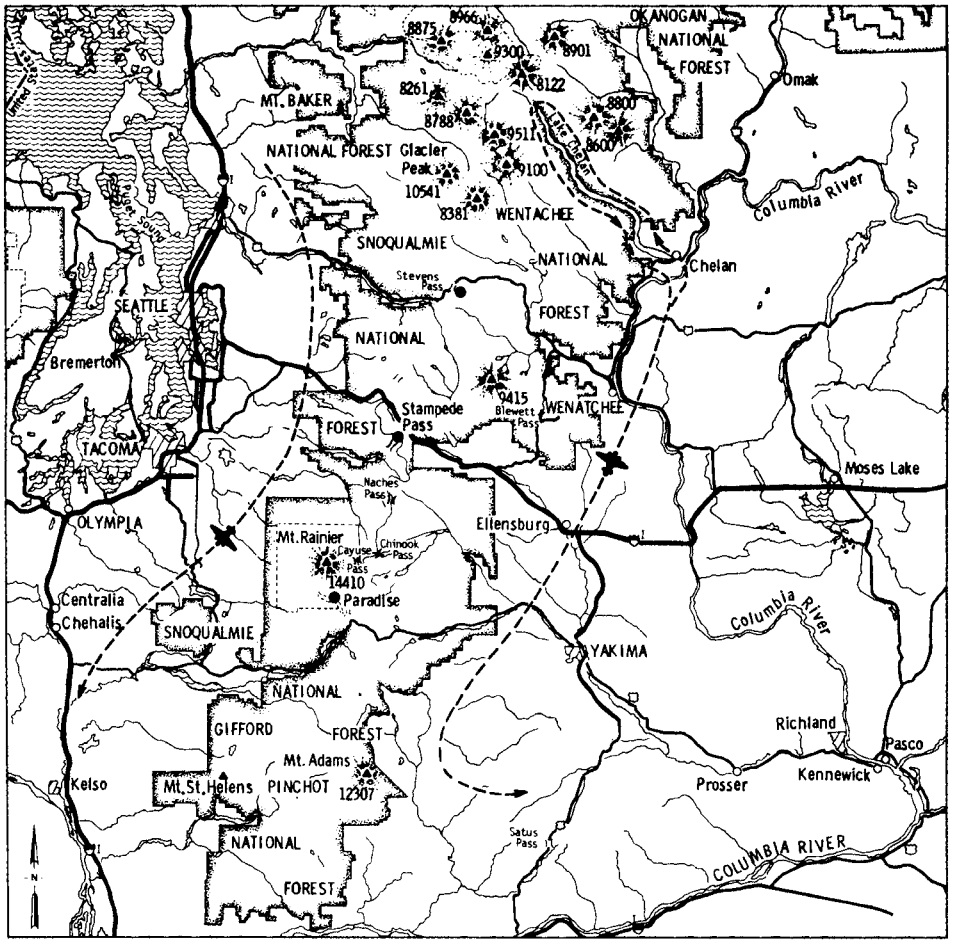

Figure 3.2. The Paths Taken by Two Aircraft Flights Performing Hi-Vol Sampling at Different Elevations Along Two Areas Downwind of the Metropolitan Seattle-Tacoma Area, May 16 and June 18, 1980

identified those elements present in the ambient atmosphere at levels exceeding that which could be attributed to suspension of crustal material.

All samples showed enrichment of lead, sulfur, chlorine, and bromine (Table 3.2). Lead concentrations may be attributed to the widespread distribution of vehicular sources while aerosol sulfur (sulfate) arises as a primary anthropogenic pollutant as well as the oxidation product of gaseous sulfur species. Chlorine and bromine enrichment may be accounted for, at least in part, by volcanic emissions from Mt. St. Helens during the experimental period. A PNL sampling flight that penetrated the Mt. St. Helens' plume on May 19 showed enrichment of these species as well as other volatile trace elements (Fruchter et al. 1980). One of these elements, arsenic, did not appear in most regional air-shed samples although an enrichment factor of 400 was calculated for the filter sample collected at Paradise on May 16, 1980.

Among the trace elements measured in the aircraft samples, lead, nickel, copper, and zinc appear to be associated with sources from the Seattle-Tacoma metropolitan area. Concentrations of these elements generally decreased in samples collected east of the Cascades. However, detection of significant zinc concentrations in several samples taken on the east side, notably those at Stevens Pass on May 16 and June 14 and 18 in which enrichment factors >10 were calculated, suggest an additional source. Elevated copper levels were found in all Cascade ridge surface samples that were attributed to contamination from the high volume samples motor brushes (Lynch, McQuaken, and Bram 1980).

Table 3.1. Daytime (8 a.m. - 17 p.m. PST) Weather Conditions for Experimental Periods

	Seattle-Tacoma	Cascades	Wenatchee-Yakima
May 16 1980	**Sky Condition:** Broken to overcast strato cumulus & cumulus.	**Sky Condition:** Fog to low overcast. Strato cumulus & cumulus	**Sky Condition:** Clear to sctd. cumulus & cirrus.
	Vsby: 15-20 mi.	**Vsby:** 5-25 mi.	**Vsby:** 50-60 mi.
	Wind: Calm to SW-NW	**Wind:** SW-NW	**Wind:** Calm, E-NW,SW
	Speed: 0-8 kts.	**Speed:** 9-15 kts.	**Speed:** 0-7 kts.
	Upper-Level Winds: Light and variable but with a weak general flow from West to Northwest.		
June 14 1980	**Sky Condition:** Low overcast.	**Sky Condition:** Fog.	**Sky Condition:** Sctd. low cloud, high broken-overcast clouds.
	Vsby: 12-25 mi.	**Vsby:** Zero	**Vsby:** 30-40 mi.
	Wind: S-SW	**Wind:** SW	**Wind:** SE-SW
	Speed: 03-08 kts.	**Speed:** 05-17 kts.	**Speed:** 04-11 kts.
	Upper-Level Winds: Generally, SW to NW 05-10 kts. changing to Easterly winds around 10,000 ft.		
June 18 1980	**Sky Condition:** Low overcast to sctd. cumulus.	**Sky Condition:** Fog to sctd. clouds. then clear to sctd.	**Sky Condition:** Clear to sctd. cumulus.
	Vsby: 20-45 mi.	**Vsby:** 3/4-40 mi.	**Vsby:** 40-60 mi.
	Wind: NE, NW, N	**Wind:** ESE, SW	**Wind:** NE, SE, SW, NW
	Speed: 04-11 kts.	**Speed:** 06-17 kts., 08-20 kits.	**Speed:** 03-07 kts.
	Upper-Level Winds: Light and variable up to 5,000 ft. Minor trough passage in the afternoon above 5,000 ft. N-NW winds 5 to 10 kts.		

Sulfate concentration was independently checked by aqueous extraction of the respective filters followed by ion chromatography (IC) analysis (Table 3.3). These results suggest that the lower mixing layer was not very turbulent on the west side during the sampling periods because sulfate concentration generally decreased with altitude. However, on the east side sulfate concentrations increased with height, suggesting greater mixing over the Cascades and the oxidation of gaseous sulfur species. Nitrate concentrations also derived from IC analysis showed a similar trend with nearly equivalent molar concentration. Ammonium aerosol concentration data reflected the surface origin of ammonia.

The trace gases, ozone and sulfur dioxide, also were investigated during the sampling flights. Ozone was measured in real-time using the chemiluminescent method. Typical background ozone concentrations were observed. The West-Gaeke method for sulfur dioxide determination was not sufficiently sensitive to quantify SO_2 levels. However, an upper limit to the sulfur dioxide concentrations can be assigned from these results.

In conclusion, the goal of estimating the pollutant budget over the Cascade Mountain airshed could not be completely satisfied because of insufficient meteorological data and the limited scope of the study. However, these tentative results suggest it may be feasible to assess atmospheric pollutant budgets over regional airsheds. Additional sampling and analysis of data over a smaller airshed with distinct pollutant sources could improve the approach to the problem. A feasible site would be the Geysers-Calistoga Geothermal Resource Area near Middletown, California. Such a study could provide an important contribution to the understanding and prediction of transport and fate of pollutants in that potentially energy-intensive area.

Table 3.2. Average Enrichment Factors for Selected Trace Elements Found in Surface and Airborne Samples

Trace Element	West Side (Airborne)	Ridge (Surface)	East Side (Airborne)
May 16, 1980			
Pb	331	136	88
Cl	136	62	189
S	169	347	339
Ni	16	<3	7
Cu	23	383[a]	8
Zn	7	8	18
Br	-	322	150
June 14, 1980			
Pb	-	1006	-
Cl	-	-	-
S	-	455	-
Ni	-	-	-
Cu	-	1664[a]	-
Zn	-	11	-
Br	-	2470	-
June 18, 1980			
Pb	146	132	58
Cl	385	58	133
S	287	165	91
Ni	7	-	2
Cu	8	396[a]	6
Zn	17	8	5
Br	125	323	146

[a]Cu enrichment due to contamination from hi-vol motor brushes.

Table 3.3. Sulfate, Nitrate and Ammonium Concentrations and Average Aerosol Scattering Coefficient for Aircraft Sampling Flights

May 16, 1980	West Side		
Elevation, Ft. msl	2000	4000	8500
b_{scat}	0.36	0.25	0.15
SO_4 (μgm^{-3})	1.8[a]	1.9	1.2
NO_3 (μgm^{-3})	[a]	0.84	0.13
NH_4 (μgm^{-3})	[a]	1.2	ND

	East Side				
Elevation, Ft. msl	2-3000	5000	5500	9000	9000
b_{scat}	0.31 DC-3	0.24 DC-3	0.27 Cessna	0.15 DC-3	- Cessna
SO_4	1.04	0.82	1.6[a]	0.73	2.4
NO_3	0.51	0.46	[a]	0.1	2.9
NH_4	0.44	0.29	[a]	0.2	<0.1

June 18, 1980	West Side		
Elevation, Ft. msl	1500-2000	2500-3000	5000
SO_4 (μgm^{-3})	6.6	4.3	2.2
NO_3 (μgm^{-3})	6.1	2.8	ND
NH_4 (μgm^{-3})	1.3	<0.1	ND

	East Side		
Elevation, Ft. msl	2000-3500	4000-5500	9000-9500
SO_4	1.2	1.0	1.9
NO_3	0.32	0.38	0.82
NH_4	0.23	0.3	<0.1

[a]Not analyzed by IC, XRF only
ND Not detected

References

Duce, R. A., G. L. Hoffman, and W. H. Zoller. 1975. "Atmospheric Trace Metals at Remote Northern and Southern Hemisphere Sites: Pollution or Natural?" Science 187(4171):59-61.

Fruchter, J. S., D. E. Robertson, J. C. Evans, K. B. Olsen, et al. 1980. "Mt. St. Helens Ash from the 18 May, 1980 Eruption: Chemical, Physical, Mineralogical, and Biological Properties." Science 209:1116-1125.

Lynch, A. J., N. R. McQuaker, and D. F. Brown. 1980. "ICP/AES Analysis and the Composition of Airborne Soil Materials in the Vicinity of a Lead/Zinc Smelter Complex." JAPCA 30(3):256-260.

Taylor, S. R. 1964. "Abundance of Chemical Elements in the Continental Crust: A New Table." Geochimica et Cosmochimica Acta 28:1273-1285.

Seasonal and Statistical Variability of Turbidity at Hanford

N. S. Laulainen

To evaluate potential visibility impairment caused by development of oil shale and coal areas in the west, it is essential to understand the variability of naturally-occurring hazes. While the Hanford site

cannot be classified as a remote, undisturbed site, it does provide a useful reference site for understanding natural variability. It appears, from an examination of turbidity observations made at the Hanford Meteorological Station (HMS) since 1974, that haze in the Lower Columbia Basin is modulated by synoptic meteorological patterns (Laulainen 1980). Consequently, atmospheric aerosols of local origin such as smoke, dust, vegetation, and automobile emissions only contribute significantly to the total particulate loading during periods of stagnation. The remaining turbidity variations then appear to be governed by sources distributed over larger than local scales.

In the Lower Columbia Basin several factors contribute to particulate loading in the atmosphere. These factors include wind blown dust, smoke from field burning and from more distant forest fires, vegetative volatile organic emissions, automobile exhaust and, more recently, volcanic ash. Of this list of factors, only volcanic ash, vegetative emissions, and some forest fires are independent of human activities. Dust storms, for example, are only partly natural because of human activities, particularly agricultural practices. Controlled burning of forested areas is increasingly replacing the natural process of uncontrolled wildfires.

It is difficult to estimate how often some of these practices or events occur or how greatly these factors contribute to particulate loading. Orgill and Sehmel (1976) have examined dust storm occurrences in the continental U.S. and have found that for the Rocky Mountain Region (which includes the Lower Columbia Basin) the highest frequency of occurrence is in March and April with a smaller maximum in October. The spring months also coincide with various agricultural activities that disturb natural soil surfaces, such as field burning in March through May and again in late August through October.

Forest fires occur most often during August and September, but they represent only a distant source of visibility-impairing haze. Unless the fires are of considerable magnitude, they contribute very little to the total particulate burden in the Lower Columbia Basin area.

Vegetative emissions may be transformed from the vapor state into particulate matter and are generally observed as blue haze, indicating very fine particles. Emissions tend to be greatest at higher temperatures, at lower elevations and in the spring. Desert sages and other desert shrubs can be expected to contribute to the haze in Eastern Washington, but the magnitude and timing of their emissions is largely unknown.

Other sources which could have contributed to the haze in the Lower Columbia Basin from 1974 through 1979 were the automobile and other processes relying on fossil fuel combustion. Data on how much these sources contribute is scanty. It is presumed, however, that these sources contribute a constant, moderate amount to the total burden during the year.

Prior to May 1980, the contribution to atmospheric particulate loading from volcanic ash was negligible.

On the basis of the above survey, limited as it was, one could expect to see a maximum haze effect in April and again in August through October as a result of the seasonal variability of dust, smoke and vegetative emissions. The turbidity data at HMS suggest possible seasonal variations (Laulainen 1980), but attempts to fit these data to annual and biannual harmonic terms were only of limited usefulness (Laulainen 1978). Further statistical analysis of these turbidity data was made to see if any obvious seasonal variations could be discerned and to examine the nature of the statistical variability of the data. The results of this analysis are shown in Figures 3.3 and 3.4.

The monthly average values of atmospheric turbidity from 388 days in four different wavelengths are shown in Figure 3.3. The values shown are the geometric means with their associated geometric standard deviations. Dust storm data have been omitted. The rationale for geometric rather than arithmetic means will be described later in this paper. There is evidence of a biannual variation with a pronounced maximum in April and a weaker maximum in August/September. The standard deviations or statistical variations, however, are quite large. This latter result accounts for the poor fit described earlier (Laulainen 1978).

Figure 3.4 shows the results of sorting the aerosol optical depth data according to magnitude to obtain a cumulative distribution of aerosol optical depth at each wavelength. The curves in Figure 3.4 represent the percentage of days at each wavelength for which the aerosol optical depths were below the magnitudes indicated.

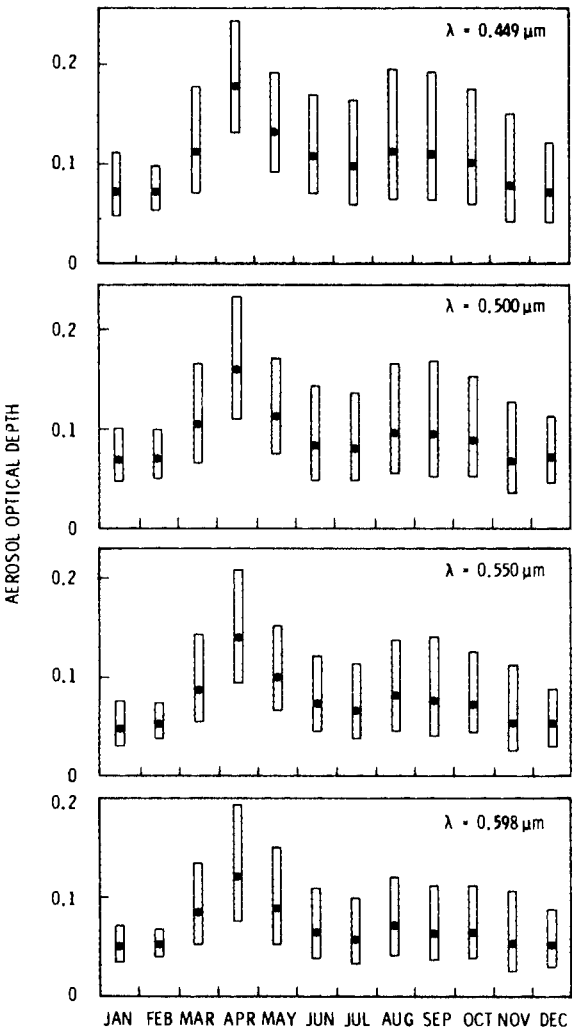

Figure 3.3. Geometric Mean Monthly Aerosol Optical Depth (Turbidity) at Hanford Meteorological Station from 1974 to 1979 for Wavelengths 0.449, 0.500, and 0.598μm, respectively

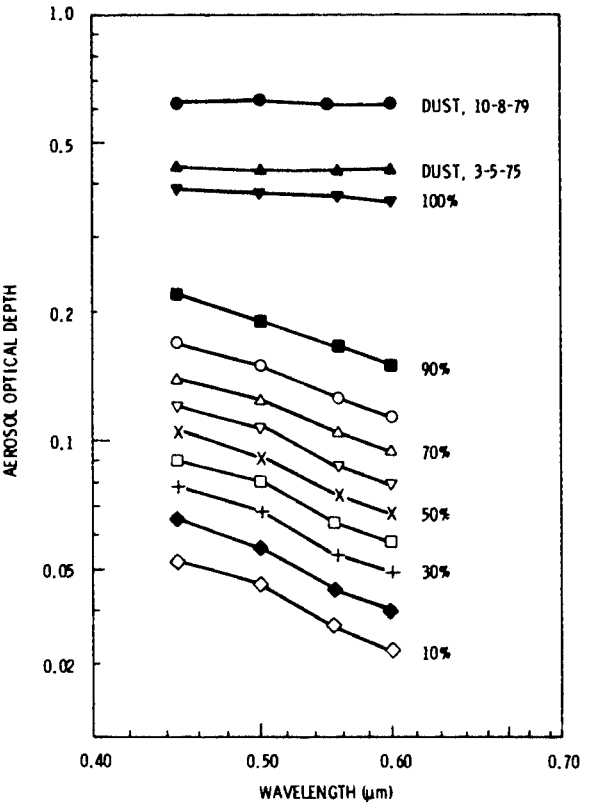

Figure 3.4. Percentage of Days at Each Wavelength for Which the Aerosol Optical Depths were Below the Magnitudes Indicated. The 50% Curve Represents the Median Values of Turbidity for the Entire 388 Observation-Day, 5.5-Year Record. Dust storm examples for 3-5-75 and 10-8-77 are given for comparison.

The 50% curve represents the median turbidity values and is very close to the geometric mean value at each wavelength. Also, inspection of Figure 3.4 shows that the probability distribution of turbidity values is nearly symmetric about the median level. Since the ordinate scale is logarithmic rather than linear, the implication is that aerosol optical depth is nearly log-normally distributed rather than normally distributed. This result has been observed by others (King et al. 1980; Malm et al. 1977).

With the exception of data taken during dust storms (of which two examples are given in Figure 3.4 for 3-5-75 and 10-8-79), the 100% curve represents the largest magnitude of turbidity over the observation period, 1974-1979. The minimum turbidity values, corresponding to the 0% value (not shown) in Figure 3.4, are smaller than 0.03.

The color dependence of the turbidity values gives a clue to the sizes of the particles responsible for extinction. A power law relationship of the form $\tau_p = \beta\lambda^{-\alpha}$ for the turbidity may be related to a similar power law relationship for the particle size distribution. Values of $\alpha = 4$ correspond to very small particles and molecules while values of $\alpha = 0$ correspond to large particles $\gtrsim 1$ μm (Middleton 1968). Most haze particles of secondary origin in the size range 0.1 to 1 μm are found with values of α in the range $0.5 \leq \alpha \leq 2.0$ with a most probable value near $\alpha = 1.3$.

Inspection of Figure 3.4 shows that dust particles produce neutral extinction, i.e., $a \approx 0$. The 100% curve of Figure 3.4 shows roughly the same behavior, indicating a

predominance of large particles (possibly dust). The 10%, 50%, and 90% curves have α values of 1.6, 1.5 and 1.3, respectively; this result implies that the fine particle mode is largely responsible for aerosol extinction over the Lower Columbia Basin.

The important conclusions from the statistical study of the 1974-1979 HMS turbidity data set are:

- Turbidity appears to be log-normally distributed.
- Weak seasonal turbidities are apparent with the strongest maximum in April and a weaker maximum in August/September. The variation, however, needs to be tempered with the large variability observed in any given month.
- Except for episodes relating to dust storms or other high dust-loading conditions, the fine particle mode (0.1 to 1.0 μm) appears to be largely responsible for aerosol extinction in the Lower Columbia Basin.

References

King, M. D., D. M. Byrne, J. A. Reagan, and B. M. Herman. 1980. "Spectral Variation of Optical Depth at Tucson, Arizona between August 1975 and December 1977." J. Appl. Meteor., 19:723-732.

Laulainen, N. S. 1978. "Turbidity Variations at Hanford Since July 1974." In Pacific Northwest Laboratory Annual Report for 1977 to the DOE Assistant Secretary for Environment, Part 3, Atmospheric Sciences. PNL-3300, pp. 143-145, Pacific Northwest Laboratory, Richland, Washington.

Malm, W. C., E. G. Walthers, and R. A. Cudney. 1977. "The Effects of Water Vapor, Ozone and Aerosol on Atmospheric Turbidity." J. Appl. Meteor., 16:268-274.

Middleton, W. E. 1968. Vision Through the Atmosphere. University of Toronto Press, Toronto, Canada.

Orgill, M. M. and G. A. Sehmel. 1976. "Frequency and Diurnal Variation of Dust Storms in the Contiguous U.S.A." Atmos. Environ., 10:813-125.

Publications and Presentations

PUBLICATIONS

Alkezweeny, A. J. and M. S, Laulainen. 1980. "Comparison Between Polluted and Clean Air Masses Over Lake Michigan." Accepted for publication in J. Applied Meteorology.

Davis, W. E., W. J. Eadie and D. C. Powell. 1979. A Users Guide to Regional-1: A Regional Assessment Model. PNL-3110, Pacific Northwest Laboratory, Richland, Washington.

Doran, J. and T. W. Horst. 1980. "Velocity and Temperature Oscillations in Drainage Winds." PNL-SA-8745. Presented at the ASCOT Review and Planning Meeting, April 15-18, Gettysburg, Pennsylvania. Accepted for publication in Journal of Applied Meteorology.

Drake, R. L. and M. M. Orgill. 1980. "Scale Analysis: Techniques and Review." Interim report for LNG Safety Studies Program (contributory).

Fruchter, J. S. and G. A. Sehmel et al. 1980. "Mt. St. Helens Ash from the 18 May, 1980 Eruption: Chemical, Physical, Mineralogical, and Biological Properties." Science, 209:1116-1128.

Horst, T. W. 1980. "Comments on 'A Numerical Study of the Vertical Dispersion of Passive Contaminants from a Continuous Source in the Atmospheric Surface Layer'." Atmos. Environ. 14:267-269.

Horst T. W. 1980. "A Review of Gaussian Diffusion--Deposition Models" in Atmospheric Sulfur Deposition--Environmental Impact and Health Effects, eds. D. C. Shriner, C. R. Richmond and S. E. Lindberg, Ann Arbor Science, Ann Arbor, Michigan.

McNaughton, D. J. and M. M. Orgill. 1980. "A Synoptic Case Study of Elevated Layers of High Airborne Sulfate Concentrations." Monthly Weather Review, 108(5):655-662.

Orgill, M. M. 1980. "Atmospheric Studies in Complex Terrain (ASCOT): A Planning Guide for Future Studies." PNL-3656 and ASCOT-80-4.

Orgill, M. M. et al. 1980. "Net Radiation, Vertical Profiles of Wind and Temperature, and Cross-Valley FP Tracer Sampling in the Anderson Creek Valley Area--July 1979." PNL-SA-8799 and ASCOT-80-7 (contributory).

Orgill, M. M. and D. J. McNaughton. 1980. "Trace Ecological Effects of Increased Ammonia Usage." PNL-3384. Report for LNG Safety Studies Program (primary).

Sehmel, G. A. and W. H. Hodgson. 1980. "A Model for Predicting Dry Deposition of Particles and Gases to Environmental Surfaces." In Implications of the Clean Air Act Amendments of 1977 and Energy Considerations for Air Pollution Control. American Institute of Chemical Engineers, Symposium Series No. 196, 76:218-230, New York, New York.

Sehmel, G. A. 1980. "Model Predictions and a Summary of Dry Deposition Velocity Data." PNL-SA-7944, Chapter 25 in Atmospheric Sulfur: Environmental Impact and Health Effects, eds. D. S. Shriner, C. R. Richmond, and S. E. Lindberg, Ann Arbor Science Publishers, Ann Arbor, Michigan.

Sehmel, G. A. 1980. "Particle and Gas Dry Deposition: A Review." Atmos. Environ. 14:983-1011.

Sehmel, G. A. 1980. "Particle Resuspension: A Review." Environment International, 4.

Sehmel, G. A. 1980. "Transuranic and Tracer Simulant Resuspension." BNWL-SA-6236--REV 1, Chapter B in Transuranic Elements in the Environment, TID-22800, pp. 236-287, ed. W. C. Hanson, National Technical Information Service, U.S. Department of Commerce, Springfield, Virginia.

Slinn, S. A. and W. G. N. Slinn. 1980. "Modeling of Atmospheric Particulate Deposition to Natural Waters." Chapter II of Atmospheric Input of Pollutants to Natural Waters, pp. 25-53, ed. S. J. Eisenreich, Ann Arbor Science, Inc.

Slinn, S. A. and W. G. N. Slinn. 1980. "Predictions for Particle Deposition on Natural Waters." Atmos. Environ. 14:1013-1016.

Slinn, W. G. N. 1980. "Releases of Radionuclides and Their Atmospheric Pathway." National Research Council, Assembly of Life Sciences, Proceedings of the Workshop on Federal Research on Biological and Health Effects of Ionizing Radiation, U.S. National Academy of Sciences, Washington, D.C.

Slinn, W. G. N. 1980. "Relationships Between Removal Processes and Residents Times for Atmospheric Pollutants." AICHE Symposium Series, 196, Vol. 76:185-203.

Webb, R. O.., E. D. Culver and N. S. Laulainen. 1980. "Calibration of Special Water Sensitive Paper Including Droplet Impaction at Oblique Angles." Atmos. Environ. 14:285-298.

Young, J. A. and W. B. Filker. 1980. "Aerosol Deposition Velocities on Pacific and Atlantic Ocean Waters Calculated from ^{7}Be Measurements." Earth and Planetary Science Letters, 50:92-104.

PRESENTATIONS

Alkezweeny, A. J., W. E. Davis and R. C. Easter. August 1980. "Comparison of Ozone in Polluted and Clean Air Masses Over Lake Michigan." PNL-SA-8424 A. Presented at the IAMAP Symposium on Atmospheric Ozone, Boulder, Colorado.

Davis, W. E. August 1980. "Preliminary Results of an Eight-Layer Regional Assessment Model Applied to the Problem of Acid Rain." PNL-SA-8835. Presented at the American Chemical Society Meeting, Las Vegas, Nevada.

Davis, W. E., and W. J. Eadie. 1980. "The Effect of Using Time-Averaged Precipitation for Wet Removal in Lagrangian Assessment Model." PNL-SA-8281. Presented at the 89th National Meeting of the American Institute of Chemical Engineers, Portland, Oregon.

Doran, J. C. 1980. "Gust Model for Design and Performance Analysis of Wind Turbines." Presented at the SERI/AIAA Meeting, April 9-11, Boulder, Colorado.

Doran, J. C. and T. W. Horst. 1980. "Velocity and Temperature Oscillations in Drainage Winds." PNL-SA-8745. Presented at the ASCOT Review and Planning Meeting, April 15-18, Gettysburg, Pennsylvania.

Drake, R. L. 1980. "Interfacing Air Pathway Models with Other Media Models for Impact Assessment." PNL-SA-8986. Presented at 20th Hanford Life Sciences Symposium, October 19-23, Richland, Washington.

Drake, R. L. 1980. "Mass-Consistent Modeling, Revisited." PNL-SA-8789. Presented at the ASCOT Review and Planning Meeting, April 15-18, Gettysburg, Pennsylvania.

Eadie, W. J., W. E. Davis, W. F. Sandusky, and R. H. Ball. 1980. "A New Application of the PNL Long-Range Transport Model to Assess the Air Quality Impacts of Fine Particles." PNL-SA-7999. Presented at the Second Conference on Industrial Air Pollution, March 28, New Orleans, Louisiana.

Horst, T. W. and J. C. Doran. 1980. "A Comparison of Observed and Predicted Slope Winds." PNL-SA-8785. Presented at the ASCOT Review and Planning Meeting, April 15-18, Gettysburg, Pennsylvania.

Kalkwarf, D. R. and S. R. Garcia. 1980. "A Search for PAH-Transformation Products in Coal-Fired Power Plant Plumes." Presented at the Conference on the Physics and Chemistry of Energy-Related Atmospheric Pollution, May 28-30, Harper's Ferry, West Virginia.

Kalkawarf, D. R. 1980. "High-Performance Thin-Layer Chromatography of Sulfonated Polycyclic Aromatic Compounds." Presented at the Second Symposium on Environmental Analytical Chemistry. June 18-20, Provo, Utah.

Kalkwarf, D. R. 1980. "Photochemical Reactions of Polycyclic Aromatic Hydrocarbons with SO_2 Gas." Presented at the 35th Regional Meeting of the American Chemical Society, June 12-14, Salt Lake City, Utah. Also presented at the Second Chemical Congress of the North American Continent, August 24-29, Las Vegas, Nevada.

Kalkwarf, D. R. and S. R. Garcia. 1980. "Sublimation of Polycyclic Aromatic Hydrocarbons from Coal Fly Ash." Presented at the 169th Annual Meeting of the American Chemical Society, March 23-28, Houston, Texas.

Orgill, M. M., R. I. Schreck, P. W. Nickola, T. W. Horst, J. C. Glover, J. C. Doran, and O. B. Abbey. 1980. "Net Radiation, Vertical Profiles of Wind and Temperature, and Cross-Valley FP Tracer Sampling in the Anderson Creek Valley Area--July 1979." PNL-SA-8799. Presented at the ASCOT Review and Planning Meeting, April 15-18, Gettysburg, Pennsylvania.

Reynolds, B. W. and W. G. N. Slinn. 1980. "Resuspension of Respirable Particles Deposited on Soil, Gravel and Grass." Presented at the 73rd Annual Meeting of the Air Pollution Control Association. Reprint No. 80-68.4, June 22-27, Montreal, Quebec.

Sehmel, G. A. 1980. "Ambient Airborne Solids Concentrations Including Volcanic Ash at Hanford, Washington. Sampling Sites Subsequent to the Mt. St. Helens Eruption." PNL-SA-8772. Presented at the 89th National Meeting of the American Institute of Chemical Engineers, August 17-20, Portland, Oregon.

Thorp, J. M. and B. C. Scott. August 1980. "Average Storm Duration and Seasonal Precipitation Rates for the Northeast Sector of the United States." PNL-SA-8793. Presented at the American Chemical Society, Division of Environmental Chemistry Meeting, San Francisco, California.

Author Index

AUTHOR INDEX

Organization Charts Distribution

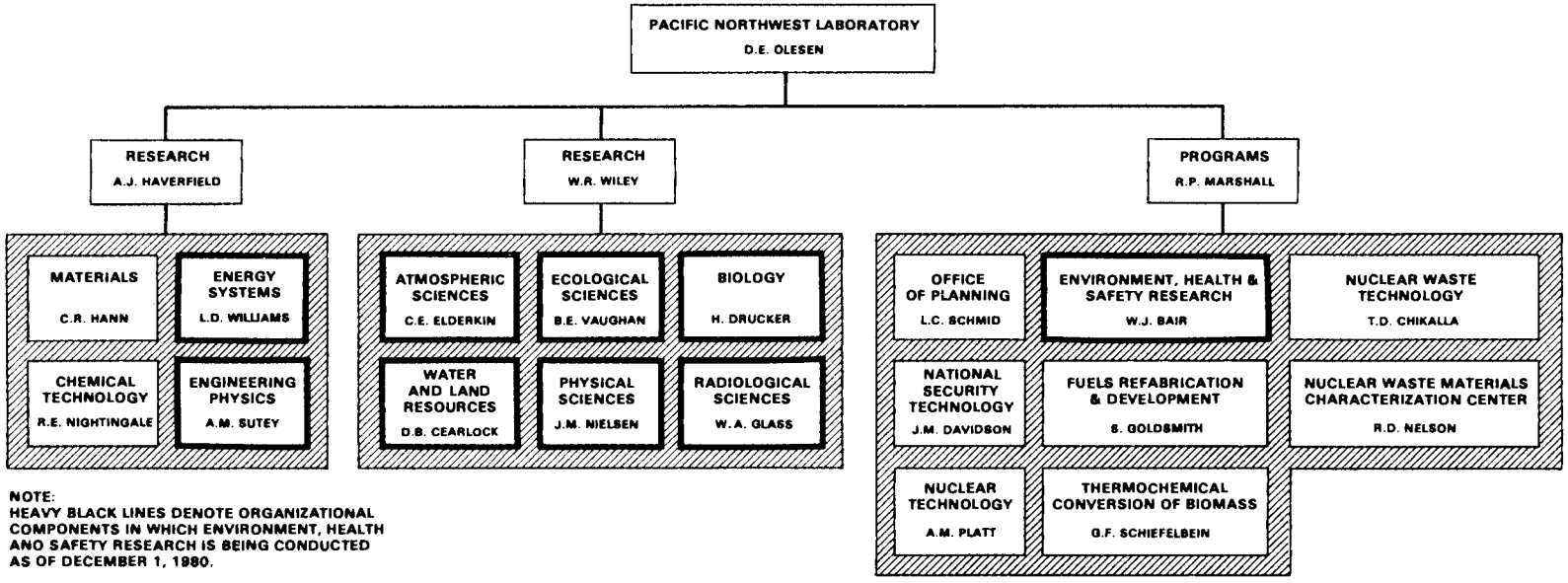

NOTE:
HEAVY BLACK LINES DENOTE ORGANIZATIONAL COMPONENTS IN WHICH ENVIRONMENT, HEALTH AND SAFETY RESEARCH IS BEING CONDUCTED AS OF DECEMBER 1, 1980.

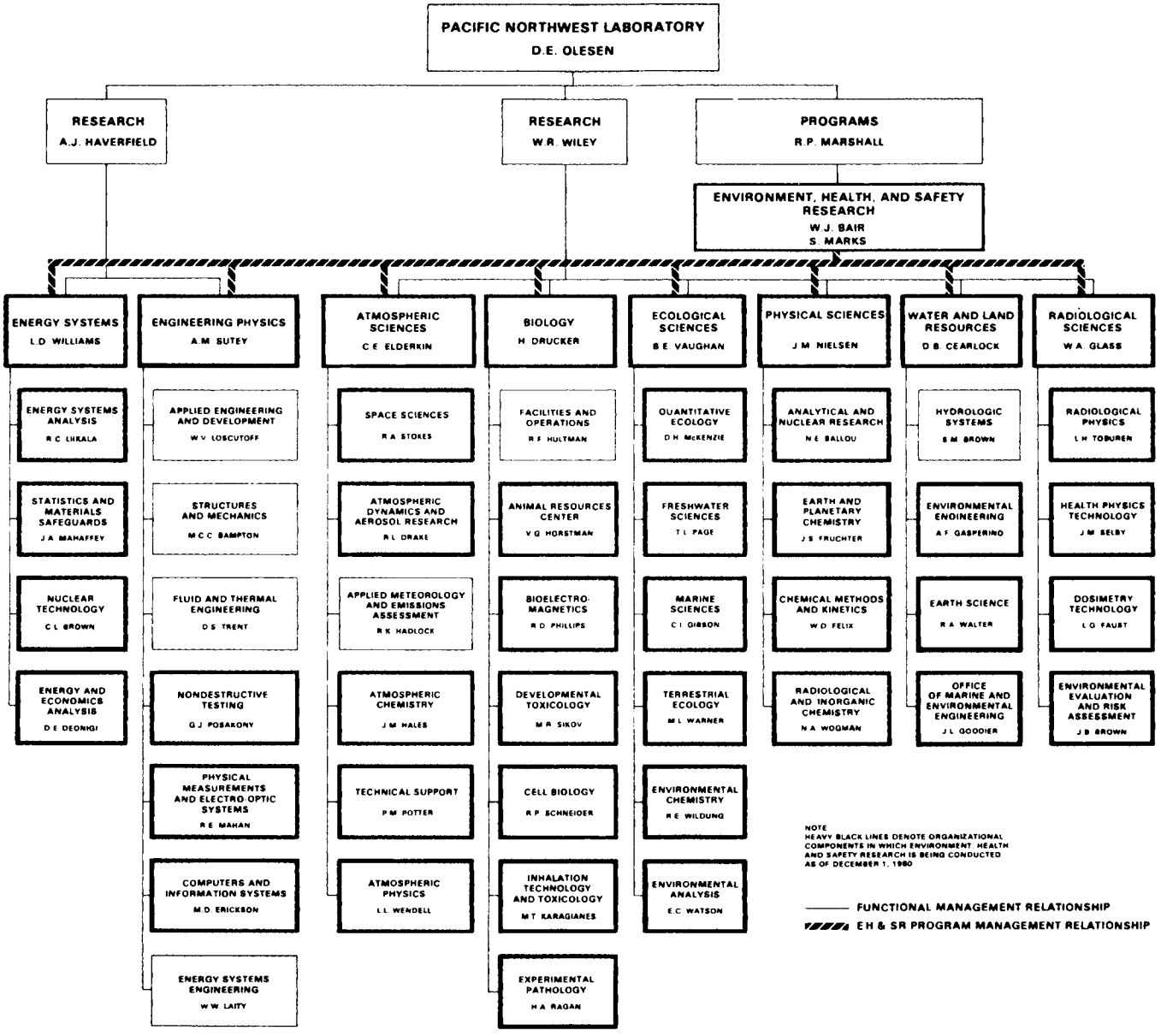
PACIFIC NORTHWEST LABORATORY
D.E. OLESEN
RESEARCH
A.J. HAVERFIELD
RESEARCH
W.R. WILEY
PROGRAMS
R.P. MARSHALL
ENVIRONMENT, HEALTH, AND SAFETY RESEARCH
W.J. BAIR
S. MARKS
ENERGY SYSTEMS
L.D. WILLIAMS
ENGINEERING PHYSICS
A.M. SUTEY
ATMOSPHERIC SCIENCES
C.E. ELDERKIN
BIOLOGY
H. DRUCKER
ECOLOGICAL SCIENCES
B.E. VAUGHAN
PHYSICAL SCIENCES
J.M. NIELSEN
WATER AND LAND RESOURCES
D.B. CEARLOCK
RADIOLOGICAL SCIENCES
W.A. GLASS
ENERGY SYSTEMS ANALYSIS
R.C. LIKALA
STATISTICS AND MATERIALS SAFEGUARDS
J.A. MAHAFFEY
NUCLEAR TECHNOLOGY
C.L. BROWN
ENERGY AND ECONOMICS ANALYSIS
D.E. DEONIGI
APPLIED ENGINEERING AND DEVELOPMENT
W.V. LOSCUTOFF
STRUCTURES AND MECHANICS
M.C.C. BAMPTON
FLUID AND THERMAL ENGINEERING
D.S. TRENT
NONDESTRUCTIVE TESTING
G.J. POSAKONY
PHYSICAL MEASUREMENTS AND ELECTRO-OPTIC SYSTEMS
R.E. MAHAN
COMPUTERS AND INFORMATION SYSTEMS
M.D. ERICKSON
ENERGY SYSTEMS ENGINEERING
W.W. LAITY
SPACE SCIENCES
R.A. STOKES
ATMOSPHERIC DYNAMICS AND AEROSOL RESEARCH
R.L. DRAKE
APPLIED METEOROLOGY AND EMISSIONS ASSESSMENT
R.K. HADLOCK
ATMOSPHERIC CHEMISTRY
J.M. HALES
TECHNICAL SUPPORT
P.M. POTTER
ATMOSPHERIC PHYSICS
L.L. WENDELL
FACILITIES AND OPERATIONS
R.F. HULTMAN
ANIMAL RESOURCES CENTER
V.Q. HORSTMAN
BIOELECTRO-MAGNETICS
R.D. PHILLIPS
DEVELOPMENTAL TOXICOLOGY
M.A. SIKOV
CELL BIOLOGY
R.P. SCHNEIDER
INHALATION TECHNOLOGY AND TOXICOLOGY
M.T. KARAGIANES
EXPERIMENTAL PATHOLOGY
H.A. RAGAN
QUANTITATIVE ECOLOGY
D.H. McKENZIE
FRESHWATER SCIENCES
T.L. PAGE
MARINE SCIENCES
C.I. GIBSON
TERRESTRIAL ECOLOGY
M.L. WARNER
ENVIRONMENTAL CHEMISTRY
R.E. WILDUNG
ENVIRONMENTAL ANALYSIS
E.C. WATSON
ANALYTICAL AND NUCLEAR RESEARCH
N.E. BALLOU
EARTH AND PLANETARY CHEMISTRY
J.S. FRUCHTER
CHEMICAL METHODS AND KINETICS
W.D. FELIX
RADIOLOGICAL AND INORGANIC CHEMISTRY
N.A. WOGMAN
HYDROLOGIC SYSTEMS
S.M. BROWN
ENVIRONMENTAL ENGINEERING
A.F. GASPERINO
EARTH SCIENCE
R.A. WALTER
OFFICE OF MARINE AND ENVIRONMENTAL ENGINEERING
J.L. GOODIER
RADIOLOGICAL PHYSICS
L.H. TOBUREN
HEALTH PHYSICS TECHNOLOGY
J.M. SELBY
DOSIMETRY TECHNOLOGY
L.G. FAUST
ENVIRONMENTAL EVALUATION AND RISK ASSESSMENT
J.B. BROWN
NOTE
HEAVY BLACK LINES DENOTE ORGANIZATIONAL COMPONENTS IN WHICH ENVIRONMENT, HEALTH AND SAFETY RESEARCH IS BEING CONDUCTED AS OF DECEMBER 1, 1980
FUNCTIONAL MANAGEMENT RELATIONSHIP
EH & SR PROGRAM MANAGEMENT RELATIONSHIP

DISTRIBUTION

No. of Copies

OFFSITE

A. A. Churm, Director
Patent Division
DOE--Chicago Operations Office
9800 S. Cass Avenue
Argonne, IL 60439

27 DOE Technical Information Center

W. R. Albers
Department of Energy
Office of the Asst. Sec. for Environment
Washington, DC

D. S. Ballantine
Department of energy
Office of the Asst. Sec. for Environment
Washington, DC

R. W. Barber
Department of Energy
Office of the Asst. Sec. for Environment
Washington, DC 20545

N. F. Barr
Department of Energy
Office of the Asst. Sec. for Environment
Washington, DC 20545

R. W. Beadle
Department of Energy
Office of the Asst. Sec. for Environment
Washington, DC 20545

R. P. Berube
Department of Energy
Office of the Asst. Sec. for Environment
Washington, DC 20545

No. of Copies

J. R. Blair
Department of Energy
Office of the Asst. Sec. for Environment
Washington, DC 20545

R. O. Blaunstein
Department of Energy
Office of the Asst. Sec. for Environment
Washington, DC 20545

C. M. Borgstrom
Department of Energy
Office of the Asst. Sec. for Environment
Washington, DC 20545

L. C. Brazely, Jr.
Department of Energy
Environmental Control Technology Division
Washington, DC 20545

L. Brothers
Department of Energy
Office of the Asst. Sec. for Environment
Washington, DC 20656

S. H. Bryan
Department of Energy
Office of the Asst. Sec. for Environment
Washington, DC 20545

P. Cho
Department of Energy
Office of the Asst. Sec. for Environment
Washington, DC 20545

R. C. Clusen
Department of Energy
Office of the Asst. Sec. for Environment
Washington, DC 20545

No. of Copies

J. A. Coleman
Department of Energy
Office of the Asst. Sec. for Environment
Washington, DC 20545

R. A. Conaway
Department of Energy
Office of the Asst. Sec. for Environment
Washingon, DC

D. K. Craig
Department of Energy
Office of the Asst. Sec. for Environment
Washington, DC 20545

R. C. Dahlman
Department of Energy
Office of the Asst. Sec. for Environment
Washington, DC 20545

L. J. Deal
Department of Energy
Office of the Asst. Sec. for Environment
Washington, DC 20545

J. M. Deutch
Department of Energy
Office of the Under Secretary
Washington, DC 20545

C. Dougherty
Department of Energy
Office of the Asst. Sec. for Environment
Washington, DC 20545

A. P. Duhamel
Department of Energy
Office of the Asst. Sec. for Environment
Washington, DC 20545

No. of Copies

C. W. Edington
Department of Energy
Office of the Asst. Sec.
for Environment
Washington, DC 20545

C. Eifert
Department of Energy
Office of the Asst. Sec.
for Environment
Washington, DC 20545

W. P. Elliot
Department of Energy
Office of the Asst. Sec.
for Environment
Washington, DC 20545

H. C. Field
Department of Energy
Office of the Asst. Sec.
for Environment
Washington, DC 20545

C. W. Fischer
Department of Energy
Office of the Asst. Sec.
for Environment
Washington, DC 20545

H. G. Fish
Department of Energy
Office of the Asst. Sec.
for Environment
Washington, DC 20545

T. G. Frangos
Department of Energy
Office of the Asst. Sec.
for Environment
Washington, DC 20545

R. E. Franklin
Department of Energy
Office of the Asst. Sec.
for Environment
Washington, DC 20545

P. M. Gerhardt
Department of Energy
Office of the Asst. Sec.
for Environment
Washington, DC 20545

G. Goldstein
Department of Energy
Office of the Asst. Sec.
for Environment
Washington, DC 20545

No. of Copies

T. J. Gross
Department of Energy
Office of the Asst. Sec.
for Environment
Washington, DC 20545

N. P. Hart
Department of Energy
Office of the Asst. Sec.
for Environment
Washington, DC 20545

E. B. Harvey
Department of Energy
Office of the Asst. Sec.
for Environment
Washington, DC 20545

J. C. Hock
Department of Energy
Office of the Asst. Sec.
for Environment
Washington, DC 20545

H. L. Hollister
Department of Energy
Office of the Asst. Sec.
for Environment
Washington, DC 20545

P. W. House
Department of Energy
Office of the Asst. Sec.
for Environment
Washington, DC 20545

F. P. Hudson
Department of Energy
Office of the Asst. Sec.
for Environment
Washington, DC 20545

C. A. Jolly
Department of Energy
Office of the Asst. Sec.
for Environment
Washington, DC 20545

F. A. Koomanoff
Department of Energy
Office of the Asst. Sec.
for Energy Technology
Washington, DC 20545

W. J. Little, Jr.
Department of Energy
Office of the Asst. Sec.
for Environment
Washington, DC 20545

No. of Copies

R. de Lorenzo
Department of Energy
Office of the Asst. Sec.
for Environment
Washington, DC 20545

H. M. McCammon
Department of Energy
Office of the Asst. Sec.
for Environment
Washington, DC 20545

T. McCraw
Department of Energy
Office of the Asst. Sec.
for Environment
Washington, DC 20545

B. F. McCully
Department of Energy
Office of the Asst. Sec.
for Environment
Washington, DC 20545

J. N. Maddox
Department of Energy
Office of the Asst. Sec.
for Environment
Washington, DC 20545

J. R. Maher
Department of Energy
Office of the Asst. Sec.
for Environment
Washington, DC 20545

D. D. Mayhew
Department of Energy
Office of the Asst. Sec.
for Environment
Washington, DC 20545

C. E. Miller, Jr.
Department of Energy
Office of the Asst. Sec.
for Environment
Washington, DC 20545

M. L. Minthorn, Jr.
Department of Energy
Office of the Asst. Sec.
for Environment
Washington, DC 20545

D. R. Monti
Department of Energy
Office of the Asst. Sec.
for Environment
Washington, DC 20545

No. of Copies

W. E. Mott
Department of Energy
Office of the Asst. Sec.
for Environment
Washington, DC 20545

W. A. Neustadt
Department of Energy
Office of the Asst. Sec.
for Environment
Washington, DC 20545

G. Ortel
Department of Energy
Office of the Asst. Sec.
for Energy Technology
Washington, DC 20545

D. E. Patterson
Department of Energy
Office of the Asst. Sec.
for Environment
Washington, DC 20545

R. P. Prichard
Department of Energy
Office of the Asst. Sec.
for Environment
Washington, DC 20545

R. E. Ramsburg
Department of Energy
Office of the Asst. Sec.
for Environment
Washington, DC 20545

S. L. Rose
Department of Energy
Office of the Asst. Sec.
for Environment
Washington, DC 20545

D. M. Ross
Department of Energy
Office of the Asst. Sec.
for Environment
Washington, DC 20545

M. Schulman
Department of Energy
Office of the Asst. Sec.
for Environment
Washington, DC 20545

G. R. Shepherd
Department of Energy
Office of the Asst. Sec.
for Environment
Washington, DC 20545

No. of Copies

R. J. Shull
Department of Energy
Office of the Asst. Sec.
for Environment
Washington, DC 20545

D. H. Slade
Department of Energy
Office of the Asst. Sec.
for Environment
Washington, DC 20545

D. A. Smith
Department of Energy
Office of the Asst. Sec.
for Environment
Washington, DC 20545

J. Snyder
Department of Energy
Office of the Asst. Sec.
for Environment
Washington, DC 20545

R. J. Stern
Department of Energy
Office of the Asst. Sec.
for Environment
Washington, DC 20545

J. Swinebroad
Department of Energy
Office of the Asst. Sec.
for Environment
Washington, DC 20545

J. W. Thiessen
Department of Energy
Office of the Asst. Sec.
for Environment
Washington, DC 20545

H. E. Thomas
Department of Energy
Office of the Asst. Sec.
for Oil and Gas
Technology
MS D-107-GTN
Washington, DC 20545

A. R. Vincent
Department of Energy
Office of the Asst. Sec.
for Environment
Washington, DC 20545

No. of Copies

R. Von Saunder
Department of Energy
Office of the Asst. Sec.
for Environment
Washington, DC 20545

B. W. Wachholz
Department of Energy
Office of the Asst. Sec.
for Environment
Washington, DC 20545

R. L. Watters
Department of Energy
Office of the Asst. Sec.
for Environment
Washington, DC 20545

S. Weinstein
Department of Energy
Office of the Asst. Sec.
for Environment
Washington, DC 20545

J. C. Whitnah
Department of Energy
Office of the Asst. Sec.
for Environment
Washington, DC 20545

E. R. Williams
Department of Energy
Office of the Asst. Sec.
for Environment
Washington, DC 20545

R. W. Wood
Department of Energy
Office of the Asst. Sec.
for Environment
Washington, DC 20545

M. Adams
Department of Energy
Office of the Asst. Sec.
for Fossil Energy
Washington, DC 20545

W. W. Burr, Jr.
Department of Energy
Office of the Asst. Sec.
for Research
Washington, DC 20545

G. W. Cunningham
Department of Energy
Office of the Asst. Sec.
for Nuclear Energy
Washington, DC 20545

No. of Copies

T. J. Dobry
Department of Energy
Office of the Dir. of Military Applications
Washington, DC 20545

F. Duncan
Department of Energy
Office of the Asst. Sec. for Nuclear Energy
Washington, DC 20545

G. C. Facer
Department of Energy
Office of the Asst. Sec. for Defense Programs
Washington, DC 20545

E. Frieman
Department of Energy
Office of the Dir. of Energy Research
Washington, DC 20545

G. Fumich
Department of Energy
Office of the Asst. Sec. for Fossil Energy
Washington, DC 20545

A. N. Heller
Department of Energy
Office of the Asst. Admin. for Conservation
Washington, DC 20545

A. H. Linden
Department of Energy
Office of the Admin., Energy Info. Admin.
Washington, DC 20461

A. Liccardi
Department of Energy
Office of the Asst. Sec. for Fossil Energy
Washington, DC 20545

G. B. Pleat
Department of Energy
Office of the Asst. Sec. for Defense Programs
Washington, DC 20545

R. Rabson
Department of Energy
Office of the Dir. of Energy Research
Washington, DC 20545

No. of Copies

R. G. Rader
Department of Energy
Office of the Dir. of Energy Research
Washington, DC 20545

T. E. Stelson
Department of Energy
Office of the Asst. Sec. for Conservation and Solar Energy
Washington, DC 20585

Tyler. E. Wiliams, Jr.
Industrial Reporting Program
Industrial Programs Office
CS-461, Mail Stop 2H-085
Department of Energy
Washington, DC 20585

J. S. Ball
Bartlesville Energy Research Center
Department of Energy
P.O. Box 1398
Bartlesville, OK 74003

Bartlesvile Energy Research Center
Attn: Library
Department of Energy
P.O. Box 1398
Bartlesville, OK 74003

E. W. Bean
Rocky Flats Area Office
DOE--Albuquerque Operations Office
P.O. Box 928
Golden, CO 80401

P. B. Dunnaway
DOE--Nevada Operations Office
P.O. Box 14100
Las Vegas, NV 89114

B. M. Erickson
DOE--Schenectady Naval Reactors Office
P.O. Box 1069
Schenectady, NY 12301

D. M. Gardiner
DOE--Chicago Operations Office
9800 S. Cass Avenue
Argonne, IL 60439

No. of Copies

M. E. Gates
DOE--Nevada Operations Office
P.O. Box 14100
Las Vegas, NV 89114

G. H. Gronhovd
Grand Forks Energy Research Center
Department of Energy
Box 8213, University Station
Grand Forks, ND 58202

C. Jackson
DOE--San Francisco Operations Office
1333 Broadway
Wells Fargo Building
Oakland, CA 94616

J. A. Lenhard
DOE--Oak Ridge Operations Office
P.O. Box E
Oak Ridge, TN 37830

B. Morgan
DOE--Savannah River Operations Office
P.O. Box A
Aiken, SC 29801

A. A. Pitrolo
Morgantown Energy Research Center
Department of Energy
P.O. Box 880
Morgantown, WV 26505

R. Ray
DOE--Nevada Operations Office
P.O. Box 14100
Las Vegas, NV 89114

W. Reese
DOE--Savannah River Operations Office
P.O. Box A
Aiken, SC 29801

J. R. Roeder
DOE--Albuquerque Operations Office
P.O. Box 5400
Albuquerque, NM 87115

No. of Copies

Librarian
Lawrence Radiation Laboratory
University of California
Technical Information Dept., L-3
P.O. Box 808
Livermore, CA 94550

Steven E. Lindberg
Environmental Sciences Division
Oak Ridge National Laboratory
P.O. Box X
Oak Ridge, TN 37830

L. Machta
Air Resources Laboratory
National Oceanic and Atmospheric Admin.
8060 13th Street
Silver Spring, MD 20910

C. B. Meinhold
Brookhaven National Laboratory
Upton, Long Island, NY 11973

M. L. Mendelsohn
University of California
Lawrence Livermore Laboratory
P.O. Box 808
Livermore, CA 94550

Paul Michael
Meteorology Group
Brookhaven National Laboratory
Upton, NY 11975

Charles Miller
Environment Sciences Building 7509
Oak Ridge National Laboratory
P.O. Box X
Oak Ridge, TN 37830

R. S. Paul
Battelle Memorial Institute
Columbus Laboratories
505 King Avenue
Columbus, OH 43201

No. of Copies

D. F. Petersen
University of California
Los Alamos Scientific Laboratory
P.O. Box 1663
Los Alamos, NM 87545

C. R. Richmond
Oak Ridge National Laboratory
P.O. Box X
Oak Ridge, TN 37830

W. K. Sinclair
Argonne National Laboratory
9700 S. Cass Avenue
Argonne, IL 60439

K. A. Smith
Sandia Laboratories
P.O. Box 5800
Albuquerque, NM 87187

I. Van der Hoven
Air Resources Laboratory
National Oceanic and Atmospheric Admin.
8060 13th Street
Silver Spring, MD 20910

G. L. Voelz
University of California
Los Alamos Scientific Laboratory
P.O Box 1663
Los Alamos, NM 87545

W. Woodley
Experimental Meteorology Laboratory
University of Miami Branch
NOAA P.O. Box 8044
Coral Gables, FL 33124

FOREIGN

M. Anderson
Library
Department of National Health and Welfare
Ottawa, Ontario
CANADA

No. of Copies

J. K. Basson
Vice-President
Read Op Atomaic
Atoomkrag Energy Board
Privaatsk X 256
Pretoria 0001
REPUBLIEK VAN SUID-AFRIKA

Z. M. Beekman
President of IRPA
Rooseveltlaan 197
1079 AP Amsterdam
THE NETHERLANDS

S. Beilke
Umveltbundesomt-Pilotstation, Frankfurt
6 Frankfurt/Main
Feldbergstrasse 45,
WEST GERMANY

A. Brink
Sasol-One Limited
P.O. Box 1
Sasolburg 9570
REPUBLIC OF SOUTH AFRICA

A. C. Chamberlain
Environmental and Medical Sciences Division
OXII ORA
AERA Harwell,
Oxfordshire, ENGLAND

G. H. Clark
Health Physics Research Section
A.A.E.C. Research Establishment
Private Mailbag, Sutherland
New South Wales 2232
AUSTRALIA

H. Daw
Director, Division of Health, Safety and Waste Management
International Atomic Energy Agency
Vienna 1, Kaerntnerring 11,
AUSTRIA

No. of Copies

Director
Commissiariat a l'Energie Atomique
Centre d'Etudes
Nucleaires de Fontenay-aux-Roses (Seine)
FRANCE

Director
Commonwealth Scientific and Industrial Research Organization
Aspendal, Victoria,
AUSTRALIA

G. W. Dolphin
National Radiological Protection Board
Harwell, Didcot
Oxfordshire OXII ORQ
ENGLAND

K. Edvarson
Forsvarets Forskingsanstalt
Research Institute of Nation Defense
Avdelning 4, Stockholm 80
SWEDEN

A. E. J. Eggleton
Atomic Energy Research Establishiment
Harwell, Oxfordshire
OXII ORB, ENGLAND

L. Feinendegen, Director
Institute of Medicine
Institut fur Medizin
Kernforschung sanlage Julich
Postfach 1913
517, Julich
FEDERAL REPUBLIC OF GERMANY

H. W. Georgii
Institut fur Meteorologie und Geophysik der Johann Wolfgang Geothe Universitat
600 Frankfurt am Main
Feldbergstrasse 47,
WEST GERMANY

A. R. Gopal-Ayengar
Institut fur Biophysik
Herrenhauser Str. 2
3000 Hannover, 21
FEDERAL REPUBLIC OF GERMANY

No. of Copies

S. Hartwig
Battelle-Institute e.V
Am Romerhof 35
6000 Frankfurt am Main 90
GERMANY

L. Jeanmaire
D.P.S.--S.C.S.
B.P. 6, Fontenay-aux-Roses (Seine) FRANCE

W. Jacobi
Institut fur Strahlenschutz
D-8042 Neuherberg
Ingolstaddter Landstrasse 1
FEDERAL REPUBLIC OF GERMANY

E. Komarov
HCS/EHE
World Health Organization
Geneva, SWITZERLAND

T. Kumatori, Director
National Institute of Radiological Science
4-9-1, Anagawa
Chiba-shi, JAPAN

D. Lal
Physical Research Laboratory
Nvrangpura
Ahmedabad-9, INDIA

K. E. Lennart Johansson
National Defense Research Institute
FOA 45 1
S-901-82
Umea, SWEDEN

Librarian, Building 465
Atomic Energy Research Establishment
Harwell, Didcot
OXION OXII ORD
ENGLAND

Librarian
Australian AEC
Post Office Coogee
New South Wales 2034
AUSTRALIA

No. of Copies

Librarian
Australian AEC
Riverina Laboratory
P.O. Box 226
Denliquin
New South Wales
AUSTRALIA 2710

Librarian
Centre d'Etudes
Nucleaires de Saclay
P.O. Box 2, Saclay
Fig-sur-Yvette (S&O)
FRANCE

Librarian
Commonwealth Scientific and Industrial Research Organization
314 Albert Street
P.O. Box 89
East Melbourne, Victoria
AUSTRALIA 3002

Librarian
National Radiological Protection Board
Harwell Didcot
Oxfordshire OXII ORQ
ENGLAND

Librarian
World Meteorological Organization
Geneva, 20
Case Postale No. 5, CH-1211
SWITZERLAND

T. Lyons
School of Environmental and Life Sciences
Murdock University
Murdock,
WESTERN AUSTRALIA 6153

Andrew McLean
National Radiological Protection Board
Harwell, Didcot
Oxfordshire OXII ORQ
ENGLAND

No. of Copies

A. M. Marko, Director
Atomic Energy of Canada Ltd.
Biology and Health Physics Division
Chalk River Nuclear Laboratories
Chalk River,
Ontario KOJ IJO
CANADA

M. O. Measures
Department of National Health and Welfare
Radiation Protection Division
Ottawa, CANADA

J. Z. Minczewski
International Atomic Energy Agency
Vienna 1,
Kaerntnerring 11,
AUSTRIA

U. C. Mishra
Head Air Monitoring Section
Bhabha Atomic Research Centre
Bombay-85 AS
INDIA

J. C. Nenot
Comite de Radioprotection
69, Rue de Micromesnil
75008 Paris
FRANCE

I. Ophel
Atomic Energy of Canada, Ltd.
Chalk River, Ontario,
CANADA

R. V. Osborne
Atomic Energy of Canada, Ltd.
Chalk River, Ontario,
CANADA

D. H. Pierson
Atomic Energy Research Establishment
Harwell, Oxfordshire
OXII ORB, ENGLAND

No. of Copies

M. Rzekiecki
Commissariat a l'Energie Atomique
Centre d'Etudes
Nucleaires de Cadarache
BP n 13-St. Paul
Les Durance
FRANCE

R. N. Sachdev
Air Monitoring Section
Bhabha Atomic Research Centre
Trombay, Bombay 400-085,
INDIA

V. V. Shirvaikar
Meteorology Group
Environmental Studies Section
Bhabha Atomic Research Centre
Bombay-85 AS, INDIA

C. Shorrock
Battelle-Geneva
Geneva Research Centre
7, Route de Drize
1227 Carogue-Geneva
SWITZERLAND

F. D. Sowby
International Commission on Radiological Protection
Clifton Avenue
Sutton, Surry
ENGLAND

M. J. Suess
Regional Officer for Environmental Hazards
World Health Organization
8, Scherfigsvej
DK-2100
Copenhagen, DENMARK

E. Wallauschek
ENEA (OECD) Health and Safety Office
38, Blvd. Suchet
Paris IV, FRANCE

No. of Copies

B. C. Winkler, Director
Licensing (Standards)
RAAD OP ATOOMKRAG/ATOMIC ENERGY BOARD
Privaatsak X 256/
Private Bag X 256
Pretoria 001
REPUBLIC OF SOUTH AFRICA

ALL OTHERS

F. I. Badgley
University of Washington
Department of Atmospheric Sciences
Seattle, WA 98195

B. Baskin
Wayne County Department of Health
Air Pollution Control Division
1311 E. Jefferson
Detroit, MI 48207

D. Beirman, Chief
Document Service Branch
Central Intelligence Agency
Attn: CRS/DPSD/DSB/IAS/409779/DB
Washington, DC 20505

Prof. P. E. Boynton
Associate Professor
Department of Astronomy
University of Washington
Seattle, WA 98195

Dr. Richard D. Brown
The MITRE Corporation (W-53)
1820 Dolley Madison Blvd.
McLean, VA 22102

Leo Bustand, Dean
College of Veterinary Medicine
Washington State University
Pullman, WA 99163

W. Cotton
Department of Atmospheric Sciences
Colorado State University
Fort Collins, CO 80521

No. of Copies

Council on Environmental Quality
72 Jackson Place, N.W.
Washington, DC 20006

A. N. Dingle
Department of Atmospheric and Oceanic Science
University of Michigan
Ann Arbor, MI 48104

Director
Joint Center for Graduate Study
100 Sprout Road
Richland, WA 99352

J. T. Goll
Conservation Division
U.S. Geological Survey
630 National Center
Reston, VA 22092

J. F. Johnson
Kenworth Trucking
P.O. Box 1000
Kirkland, WA 99033

Librarian
Joint Center for Graduate Study
100 Sprout Road
Richland, WA 99352

Mei-Kao Liu
Systems Applications, Inc.
950 Northgate Drive
San Rafael, CA 94003

W. E. Lotz
EPRI
1800 Massachusetts Ave. N.W.
Suite 7000
Washington, DC 20036

J. W. McCaslin
INEL, Aerojet Nuclear
550 Second Street
Idaho Falls, ID 83401

Dr. Roger O. McClellan
Inhalation Toxicology Research Institute
Lovelace Foundation for Medical Education and Research
P.O. Box 5890
Albuquerque, NM 87115

No. of Copies

Dr. William E. Marlatt
Environmental Climatology
Dept. of Watershed Sciences
Colorado State University
Fort Collins, CO 80521

H. Moses
Carbon Dioxide and Climate Research Program
Office of Health and Environmental Research
Mail Stop E-201, Germantown
Washington, DC 20545

W. R. Ney
Executive Director
National Council on Radiation Protection and Measurements
7910 Woodmont Avenue
Suite 1061
Washington, DC 20014

David Rall, Director
NIEHS
P.O. Box 12233
Research Triangle Park, NC 27709

R. C. Srivastava
University of Chicago
Laboratory for Atmospheric Probing
Geophysical Sciences
5734 S. Ellis Avenue
Chicago, IL 60637

Dr. John H. Seinfeld
Chemical Engineering
California Institute of Technology
Pasadena, CA 91125

R. G. Semonin
Illinois State Water Survey
Box 232
Urbana, IL 61801

J. Shapiro
Department of Environmental Health Sciences
School of Public Health
Harvard University
Boston, MA 02115

W. Singlevich
Air Force Technical Application Center/TD-4
Patrick AFB, FL 32925

No. of Copies

Technical Information Service
Room 773A
Savannah River Laboratory
E. I. DuPont de Nemours and Company
Aiken, SC 29801

J. E. Tillman
University of Washington
Department of Atmospheric Sciences
Seattle, WA 98195

B. W. Von Zellen
Department of Biological Sciences
Northern Illinois University
Dekalb, IL 60115

J. W. Winchester
Florida State University
Department of Oceanography
Tallahassee, FL 32306

M. A. Wolf
Air Resources Center
Oregon State University
Corvallis, OR 97331

R. C. Yoder
Rockwell International
P.O. Box 888
Golden, CO 80401

ONSITE

7 DOE Richland Operations Office

T. Austin
P. F. Dunigan
R. W. Newlin
H. E. Ransom
F. R. Standerfer
M. W. Tiernan
M. White

3 Hanford Environmental Health Foundation

B. D. Breitenstein
D. G. Quilici
B. D. Reinert

No. of Copies

2 Rockwell Hanford Operations

P. G. Lorenzini
Betty King, Librarian
Rockwell Hanford Operations
Basalt Waste Isolation Program
People's Bank Building
P.O. Box 800
Richland, WA 99352

1 UNC Nuclear Industries

T. E. Dabrowski

2 Westinghouse Hanford Company

R. O. Budd
D. E. Simpson

5 Battelle Memorial Institute

N. E. Carter
L. German
R. S. Paul
D. B. Shipler
Librarian

3 Battelle Columbus

A. H. Adelman
A. D. Barker
F. J. Milford

No. of Copies

3 Battelle-Washington D.C.

G. Johnson
S. Stryker
C. Vest

8 Battelle-Seattle

S. M. Nealey
E. B. Perrin
J. E. Rasmussen
A. H. Schilling
C. R. Schuller
R. Shikiar
M. E. Walsh
M. T. Wood

208 Pacific Northwest Laboratory

W. J. Bair (20)
N. E. Ballou
K. R. Chase
D. B. Cearlock
J. P. Corley
R. L. Drake (50)
C. E. Elderkin (40)
J. W. Finnigan
J. C. Fox
J. J. Fuquay
A. G. Gibbs
R. K. Hadlock (10)

No. of Copies

J. M. Hales (10)
A. J. Haverfield
D. L. Hessel
M. F. Johnson (3)
J. V. Larson
J. D. Ludwick
S. Marks
R. P. Marshall
J. M. Nielsen
R. E. Nightingale
D. E. Olesen
J. F. Park
H. M. Parker
R. W. Perkins
M. R. Peterson
P. M. Potter (10)
L. C. Schwendiman
C. L. Simpson
J. R. Sletager
R. A. Stokes (15)
W. L. Templeton
R. C. Thompson
C. M. Unruh
B. E. Vaughan
E. C. Watson
L. L. Wendell (10)
W. R. Wiley
R. K. Woodruff
J. A. Young
Biology Library (2)
Technical Information (5)
Publishing Coordination (2)